Stony Brook University

Semicircular Canal Morphology as Evidence of Locomotor Environment in Amniotes

A Dissertation Presented

by

Justin Avery Georgi

to

The Graduate School

in Partial Fulfillment of the

Requirements

for the Degree of

Doctor of Philosophy

in

Anatomical Sciences

Stony Brook University

May 2008

Stony Brook University

The Graduate School

Justin Avery Georgi

We, the dissertation committee for the above candidate for the Doctor of Philosophy degree, hereby recommend acceptance of this dissertation.

Dr. Catherine Forster – Advisor
Associate Professor, Department of Biological Sciences, George Washington University

Dr. Nathan Kley – Co-Advisor
Assistant Professor, Department of Anatomical Sciences

Dr. William Jungers – Chairperson of Defense
Chairman, Department of Anatomical Sciences

Dr. James Clark – Outside Member
Chairman, Department of Biological Sciences, George Washington University

This dissertation is accepted by the Graduate School

Lawrence Martin
Dean of the Graduate School

Abstract of the Dissertation

Semicircular Canal Morphology as Evidence of Locomotor Environment in Amniotes

by

Justin Avery Georgi

Doctor of Philosophy

in

Anatomical Sciences

Stony Brook University

2008

The vestibular system is a critical component of the neural control of locomotion in vertebrates. In the vestibule, macular endorgans transduce linear movements of the head and the semicircular ducts transduce rotational movements. Integrated in the cerebellum with visual and proprioceptive inputs, the vestibular signals provide vital information about movement relative to the environment, and drive stabilization reflexes.

The semicircular ducts leave distinct canals through the bones of the posterior braincase. These bony semicircular canals preserve some of the morphologies that determine the functional parameters of the semicircular ducts: *e.g.*, response time, signal gain and frequency range. Thus, the semicircular canals represent the function of a neurological system via discrete bony correlates. Therefore, because the semicircular

ducts have morphologies that determine the functional response of the system, and because some of these morphologies can be determined by examination of the semicircular canals, it has been previously hypothesized that there are correlations between semicircular canal morphology and locomotion. Semicircular canals represent a possible way, independent of post-cranial morphology, to verify hypotheses about locomotion in extinct vertebrates.

To test some of the underlying assumptions of this hypothesis of semicircular canal adaptation, the semicircular canals of a broad array of amniotes were examined using Computed Tomography (CT). Shape analysis of the semicircular canals in carnivoran mammals, turtles, varanids and crocodilians shows that despite phylogenetic shape differences, there is a consistent pattern of shape change that correlates with the terrestrial-to-aquatic locomotor transition. This pattern is most observable in the anterior semicircular canal where the height of the common crus and the height of the peak of the canal adjacent to the common crus are reduced in aquatic taxa. It is further demonstrated that this change in anterior semicircular canal shape is strongly tied to factors of limb morphology that correlate with locomotion and not with other factors of skull morphology, thus supporting the hypothesis that this is adaptive change in the system and not coincidental change. On the basis of this highly correlated, adaptive change, the results of this study then are shown to be applicable to the prediction of locomotor environment in extinct organisms via examination of the semicircular canals preserved in fossil crocodilians.

Table of Contents

List of Figures

List of Tables

Acknowledgements

As with any study of this size, this one is not just the work of one person; numerous people have assisted me throughout and deserve recognition for their efforts. I hope the following acknowledgments are exhaustive, but I know there will be some who are, inadvertently, omitted.

This project would never have gotten off the ground, let alone reached completion without the constant aid and guidance of the members of my dissertation committee, past and present. Dr. Catherine Forster, my advisor, has given me the encouragement and freedom to pursue a project unlike anything with which she had any previous experience. Dr. Nathan Kley, my co-advisor, has been a cornucopia of practical advice both professional and personal. Dr. William Jungers' recommendations and assistance on the more esoteric statistical methods of this study have been invaluable. Dr. James Clark, my external committee member, has provided useful and thought-provoking suggestions from the very beginning of this project. Lastly, Dr. Callum Ross, formerly a member of the committee, was not only a constant advocate of this project but one of its greatest challengers, always holding me and my work to the highest expectations, and helping me reach them.

This project would also have floundered without the constant assistance, and generosity of numerous different specimen repositories. Faculty, staff, and students at the American Museum of Natural History's Reptile and Amphibian, and Mammal divisions of the Vertebrate Zoology Department as well as the Vertebrate Paleontology Department, The Vertebrate Paleontology Departments of the Museum of Comparative Zoology, The Yale Peabody Museum, and The Science Museum of

Minnesota have spent countless hours in aiding my project with the loan of specimens for CT scanning as well as permitting me constant access to the collections for specimen measurement.

The bulk of the data collection for this project was done via the CT scanning of specimens, and this would not have been possible without all the time and understanding of people of the CT division of the Radiology Department at the Stony Brook Medical Center. The patience and hard work they have committed to this project have given me the ability to assemble an unprecedented dataset of digital information on the internal structure of amniote skulls.

All the members of the Anatomical Sciences Department at Stony Brook University not previously mentioned also helped bring this project to life. From encouragement and constant comments to a wonderful atmosphere conducive to learning, research, and friendship, the family of faculty, staff, and students of this department have made the time spent producing this work pleasant and memorable.

Lastly, my family, of course, deserves special thanks. My mother, father, and brother have been encouraging my scientific curiosity my whole life; they were, truly, supporting this project long before it was even conceived. My wife, Melissa, has put up with more throughout the course of this work than any other individual and, despite this, has been my most ardent supporter.

To all of these people, and to any I may have missed, I offer my sincerest gratitude, and I hope that you are also proud of this work that you have helped create.

New York, 2008

Chapter 1
Introduction

INTRODUCTION

The vestibular system is a critical component of the neural control of locomotion in vertebrates. In the vestibule, macular endorgans transduce linear movements of the head and the semicircular ducts transduce rotational movements. Integrated in the cerebellum with visual and proprioceptive inputs, the vestibular signals provide vital information about movement relative to the environment, and drive reflexes that stabilize the eyes, head and trunk.

The semicircular ducts leave distinct canals through the bones of the posterior braincase. These bony semicircular canals preserve some of the morphologies that determine the functional parameters of the semicircular ducts: *e.g.*, response time, signal gain, and frequency range. Thus, the semicircular canals represent the function of a neurological system via discrete bony correlates. Therefore, because the semicircular ducts may have morphologies that attune the system parameters to specific qualities and modes of locomotion and because some of these morphologies can be determined by examination of the semicircular canals, it has been hypothesized that there are correlations between semicircular canal morphology and locomotion.

Working from this hypothesis, a number of previous studies have investigated the relationship between aspects of the morphology of the bony labyrinth and aspects of locomotion within various amniote clades (Alonso *et al.*, 2004; Hadžiselimović and Savković, 1964; Lindenlaub *et al.*, 1995; Matano *et al.*, 1985; McVean, 1999; Spoor *et al.*, 2002; Spoor *et*

al., 2007; Spoor and Thewissen, 2008; Spoor *et al.*, 1994, 1996; Walker *et al.*, 2003). Many of these (Alonso *et al.*, 2004; Spoor *et al.*, 2002; Spoor *et al.*, 2007; Spoor *et al.*, 1994, 1996; Walker *et al.*, 2003) have even made predictions about the locomotion of fossil taxa, based on the work of Jones and Spells (1963) and others (Jones, 1974; Mayne, 1965), from the semicircular canal morphology. All of these studies have, in one way or another, observed a relationship between locomotion and the size of the semicircular canals (or ducts) relative to body mass. Those of the most quantitative nature have even managed correlations sufficient for bivariate prediction of locomotor attributes based on some feature of vestibular morphology.

What these studies, particularly those that include fossil taxa, do not do, however, is properly use or further elucidate the theoretical connection between the vestibular system and locomotion. This leaves their results and conclusions open to some doubt (Graf and Vidal, 1996; Hullar, 2006).

Use of the theoretical connection, in this case, refers to the process of examining the semicircular canals (or the ducts themselves) via morphologies that are explicitly involved in the determination of the functional response of these complicated sensors. For example, all of the studies listed above that derive from the work of Jones and Spells (1963) suffer from an historical assumption of modeling the circuit of the canal (or duct) as a circle. Using the geometric formulae for circles, these studies rely upon the radius of curvature of the circuit as a proxy for the actual functional parameter, the area enclosed by the circuit. because the structures in question, however, are never truly circular, before its use continues, an examination of the model is required.

The second failure of these studies, failure to elucidate the

theoretical locomotion-vestibular connection, stems from the treatment of this hypothesis as an assumption rather than a testable hypothesis that must be supported before it can be used as the basis of further work. There are two primary results that derive from this failure. First, limited taxonomic utility; no matter how strong the reported correlation between semicircular canal morphology and locomotion, without an understanding of the nature of the underlying connection, any attempts to use the correlation for prediction on taxa beyond those in the initial study will be weakened and, justifiably, open to doubt. Second, limited functional utility; without an understanding of the nature of the underlying connection, any functional conclusion drawn from a simple correlation is fully unsupported and, again, justifiably open to doubt.

This study seeks to answer the doubts about using vestibular morphology as a method for reconstructing the locomotion of extinct vertebrates. As a first step, the use of the radius of curvature model will be considered in a theoretical framework and a replacement model, semicircular canal shape, which addresses the deficiencies of the former will be proposed. This semicircular canal shape model will first be used to investigate whether there are changes in semicircular canal shape in growing *Alligator mississippiensis*. This will serve to give the semicircular canal shape model a feasibility test and, more importantly, indicate if taxa with indeterminate growth need to be size-matched adults in further studies to avoid any body size related effects on semicircular canal shape.

After a survey of general semicircular canal shapes in varanoid squamates, mammalian carnivores, turtles and crocodilians, the semicircular canal shape model will be used in these groups to determine if there is a correlation between changes in canal shape and the difference between terrestrial, semi-aquatic, and aquatic locomotion. The taxonomic

breadth of this study already provides any reported correlation with broader predictive applicability than previous studies, however, in an effort to avoid the weakness of those studies and to further increase predictive applicability, the adaptive nature of the change in canal shape will be investigated. Finally, if a change in semicircular canal shape corresponds with the locomotor transition regardless of phylogenetic position and it shows to be of a truly adaptive nature, then the predictive power of the semicircular canal shape model will be tested by attempting to reconstruct the locomotor environment of fossil crocodilians.

The semicircular canal shape model cannot address the difficulties of interpreting the functional changes in the semicircular duct system. This study, however, is intended to determine if the model can address the theoretical concerns that derive from using the radius of curvature model and provide an outline for future studies that attempt to understand the locomotion of fossil vertebrates on the basis of semicircular canal morphology.

Chapter 2

Morphology and Mechanics of Semicircular Ducts and Associated Vestibular Structures

INTRODUCTION

Vertebrates sense motion in several different ways. Proprioception detects movement of portions of an organism relative to an internal frame of reference, the organism itself. Vision, orientation and balance senses are used to perceive motion relative to an external frame of reference, the environment. Synthesizing this information at a very basic neurological level, a vertebrate constructs a complete three-dimensional representation of its moving body in its environment.

With the sense of balance integral, at a neurological level, to a vertebrate's ability to move in its environment (locomote), it is reasonable to hypothesize that the system responsible for the sensation of balance is adapted to the specific demands of both the type of movement and the environment through which the organism moves. This work will investigate the connection between the sense of balance and movements amniote vertebrates use while navigating their environment.

In the chapters that follow, the biophysics of the sense of balance will be described and related to the morphology of the system. These morphological correlates will be surveyed across a wide array of amniote groups with both terrestrial and aquatic representatives. The vestibular morphologies of the terrestrial and aquatic taxa will be compared within each group to determine if differences exist between these functional groups and between groups to determine if those differences are universal across amniotes that exhibit this functional distinction. Differences between terrestrial and aquatic groups, if any, will be compared to the

morphology of several regions of cranial and postcranial morphology to test if the changes in vestibular morphology are functional in nature and correlated with locomotor function or are a result of some other pressure such as space requirements or simple allometry. Lastly, these findings will then be applied in a paleontological framework to demonstrate the viability of using vestibular morphology to reconstruct the locomotor behavior or environment of extinct vertebrates.

VESTIBULAR MICROANATOMY

To sense orientation and balance vertebrates utilize a suite of endorgans located within the inner ear region of the head. In the bony housing of the postero-lateral braincase wall, the soft tissue structures of the vestibular apparatus consist of interconnected membranous sacs and ducts filled with a fluid called endolymph. Within each section of the membranous inner ear one or more vestibular endorgans, patches of sensory epithelia, can be found.

In the case of the vestibular system, the vernacular description, 'balance and orientation,' does not convey the full complexity of the signals provided by the vestibular endorgans. The non-auditory sensory epithelia of the inner ear can be divided into two primary types: maculae and cristae. Maculae detect linear motions including the orientation with respect to the line of gravity. The cristae of the semicircular ducts detect rotational motions. Some specialized epithelial regions (*e.g.* the papilla neglecta) even detect combinations of these factors (Brichta and Goldberg, 1998, 2000). Despite the differentiation of task, these endorgans all function along a similar principle: deflection of hair cells resulting from the motion of the surrounding fluid relative to some stable or motionless point.

Each subdivision of the vestibule contains one or more endorgans. The cells of these epithelial regions are the main functional unit of all of balance, orientation and acoustic transduction; these are the hair cells. Within all the non-acoustic sensory epithelia, two different morphotypes of hair cell are recognized, termed Type I and Type II, but the differences in structure do not influence the mechanism by which these cells transduce movement of the head. Rather the types are distinguished based on the shape of the cell and the morphology of the contact with the vestibular afferent nerve.

Hair cells, regardless of type, derive their name from the numerous hair-like projections that emerge from the apical surface of the cell body. These projections are termed stereocilia and are arranged in rows of increasing height as they approach a single longest projection called the kinocilium. The distal ends of each of the stereocilia and the kinocilium of each hair cell are embedded in a gelatinous mass that moves freely relative to the structure to which the hair cells bodies are anchored. Thus, movement of this mass, by whatever means, bends or shears the stereocilia and kinocilium.

Because of the location of the kinocilium to one side of the apical surface of the hair cell, and the placement of stereocilia all to one side of the kinocilium, each hair cell has an axis of orientation (running from shortest stereocilia to kinocilium). Any deflection of the stereocilia and kinocilium, therefore, has a direction component along this axis. That is, either the stereocilia are being deflected toward the kinocilium or away from it.

This asymmetry of deflection is reflected in asymmetric changes to ion channels in the membrane of the cell. Deflection of the stereocilia in the direction of the kinocilium causes the opening of potassium ion (K^+)

channels in the cellular membrane and a dramatic increase in the transportation of K^+ from the surrounding fluid into the cell (depolarization). Deflection away from the kinocilium causes the closure of these K^+ channels and a reduction or complete cessation of the K^+ transport (hyperpolarization). The state of polarization of the hair cell membrane determines the state of calcium ion (Ca^{++}) channels, whose transport of Ca^{++} into the cell promotes the release of neurotransmitters across the synapse with the vestibular afferent axon. Thus, a depolarized membrane increases the transport of Ca^{++} and therefore increases the release of neurotransmitters while a hyperpolarized membrane closes Ca^{++} channels and slows the release of neurotransmitters to the vestibular afferent axon.

A typical vestibular afferent axon that synapses with a hair cell maintains a resting frequency of activity when its hair cell is not under the effects of deflection. This resting discharge changes with changes in the rate of neurotransmitter release by the hair cell. Thus, a hyperpolarized hair cell (releasing fewer neurotransmitters) slows the frequency of activity, and the afferent nerve is said to be inhibited. In contrast, a depolarized hair cell (releasing more neurotransmitters) increases the frequency of activity, and the nerve is said to be excited.

Despite sharing the basic unit of the hair cell, the two primary kinds of sensory epithelia, the maculae and the cristae, differ in general form. The maculae are planar arrangements of hair cells with varying orientations. All of the stereocilia and kinocilia from these hair cells are embedded in a single gelatinous mass that covers the whole area of the epithelium called the otolith membrane. This otolith membrane is covered by a layer of calcium carbonate crystals called otoconia. Otoconia are sufficiently dense that flow within the endolymph that surrounds this otolith membrane/otoconia complex does not act to move the mass (and thus

does not deflect the hair cells) in any appreciable fashion. Rather, movement of the otoconia is accomplished by linear acceleration in a plane parallel to the epithelium. The variable orientation of the hair cells within the maculae allow for the maximum sensation of any in-plane acceleration rather than a reconstruction of that acceleration based on any orthogonal axes. That is, for any orientation of an acceleration vector, some afferents from the macula are maximally excited while others are maximally inhibited and those from hair cells with orientations oblique to the accelerations showing varying degrees of excitation and inhibition accordingly.

In contrast to the maculae, the cristae are neither planar nor multidirectional. A crista is an epithelial region commonly described as an inverted saddle-shape or as a hill. The hair cells of the crista are all arranged in a single direction, and the stereocilia and kinocilia are embedded in a gelatinous mass called the cupula. The cupula has a density similar to that of the surrounding endolymph, and, in contrast to the otolith membrane, has no supporting structure of higher density to decouple its movement from that of the endolymph. Instead, the cupula stretches across nearly the entire endolymphatic space where is it found. This morphology means that any endolymph flow in the space closed off by the cupula pushes against the cupula deforming it and deflecting the embedded stereocilia and kinocilia. The single orientation of the crista hair cells results in endolymph flow being registered only in a positive (excitatory) or negative (inhibitory) direction along a single axis.

VESTIBULAR MEMBRANOUS ANATOMY

The membranous labyrinth is a complex series of interconnected sacs and ducts filled with a fluid called endolymph and surrounded by a

fluid called perilymph. These fluids are distinct, not only in position relative to the membranous labyrinth, but also in composition; perilymph has a high concentration of sodium ions (Na^+), similar to extracellular fluid, and endolymph has a high concentration of K^+, similar to intracellular fluid (McKinley and O'Loughlin, 2006; Wang and Freeman, 1987). Endolymph surrounds the apical surfaces of the hair cells, the stereocilia and kinocilia and the cupulae and otolith membranes with their otoconia. Its high concentration of K+ is, as discussed above, critical to the activity of the hair cells, whereas the perilymph, which bathes the basal aspects of the sensory epithelia, is the Ca^{++} reservoir which helps drive the neurotransmitter release. These fluids also differ in the mechanical role they play. Perilymph, outside the labyrinth, plays a passive role supporting and cushioning the delicate membranous structures. Endolymph, on the other hand, plays an active role in the function of the system; in the cristae, movement of the endolymph causes displacement of the gelatinous mass affixed to the hair cells and this is the first step of the signal transduction pathway of the semicircular ducts.

All of the membranous inner ear is divided into three parts; the auditory organ, the vestibule and the semicircular ducts. Each of these regions is highly conserved throughout vertebrate evolution and an understanding of the functional differences must be based on a understanding of the generalized conserved form and the influence of that form on the function. The acoustic function of the inner ear, while sharing many properties with the vestibular function, is not considered in this work and therefore the morphology of the auditory regions of the membranous labyrinth will not be emphasized[1], while the other two regions will be

[1] Much work has been dedicated to the differences in the hearing and the morphology of the auditory organ. Some of this work has even addressed the specific differences in

examined in detail.

The membranous vestibule is subdivided into two major regions; the utricle and the saccule. Each is an irregularly shaped vesicle, though the utricle trends more towards a tubular shape and the saccule tends to be more bulbous. The utricle is considered to have anterior and posterior portions with a dilation at the anterior end, the utricular recess. On the floor of the utricular recess is found the utricular macula. This position locates the utricular maculae in an approximately horizontal plane, and thus, this endorgan is suited for sensing linear accelerations parallel to the horizontal (*e.g.* backwards/forwards or left/right). The utricle is confluent with the typically more lateral saccule through a small utriculosaccular duct.

The more bulbous saccule is also confluent with the acoustic region of the membranous labyrinth, and also gives rise to the endolymphatic duct which passes from the labyrinth into the cranial cavity where, most frequently, it ends in an endolymphatic sac. On the medial wall of the saccule is found the saccular macula. This position means that the saccular maculae are suited for sensing linear accelerations parallel to the sagittal plane (*e.g.* up/down or forwards/backwards). Vertical linear accelerations are, of course, a special case because this describes the acceleration of gravity and thus in most vertebrates oriented naturally relative to earth horizontal and vertical, the saccular maculae detect the line of gravity and define 'up' for the organism.

The other region of the membranous vestibule is the semicircular ducts. The three ducts are thin tubes that emanate from the utricle and

---

terrestrial and aquatic organisms. See Senses on the Threshold, (2008, J. G. M. Thewissen and S. Nummela eds., University of California Press) for a complete review of these differences in both mammalian and non-mammalian amniotes.

curve around (take a semicircular path) to join up with a different portion of the utricle. The three ducts are termed the anterior duct, the posterior duct (these combined are often referred to as the vertical ducts for they lie in vertical planes approximately 45° from sagittal open anteriorly and posteriorly, respectively) and the horizontal, or lateral, duct (lying approximately parallel to the horizontal plane, though there is tremendous variability of this orientation across vertebrates (Hullar, 2006)). At one end of each duct, where it originates from the utricle, is a dilated region called the ampulla, wherein can be found the crista for that duct.

The anterior duct's ampulla is confluent with the anterior-most end of the utricle and the duct curves superiorly, postero-medially and then inferiorly again to rejoin the utricle around its midpoint. The posterior duct's ampulla is confluent with the posterior-most end of the utricle and the duct curves superiorly, antero-medially, and then joins the inferiorly directed portion of the anterior duct to course to the utricle. This shared portion of the courses of the anterior and posterior ducts is the common crus, and it joins the utricle at the separation between its anterior and posterior divisions. The lateral duct's ampulla is confluent with the anterior end of the utricle; it is laterally adjacent to (but not directly confluent with) the ampulla of the anterior duct. The lateral duct curves laterally, posteriorly and then turns medially again to join the posterior division of the utricle near the junction of utricle and common crus. It should now be clear that the three semicircular ducts lie in planes approximately orthogonal to each other and that bilaterally, each duct lies in a plane approximately parallel to the plane of the complimentary duct on the other side (Fig. 1).

As noted above, the crista of each duct detects flow of endolymph only in an excitatory or inhibitory direction. With each crista located

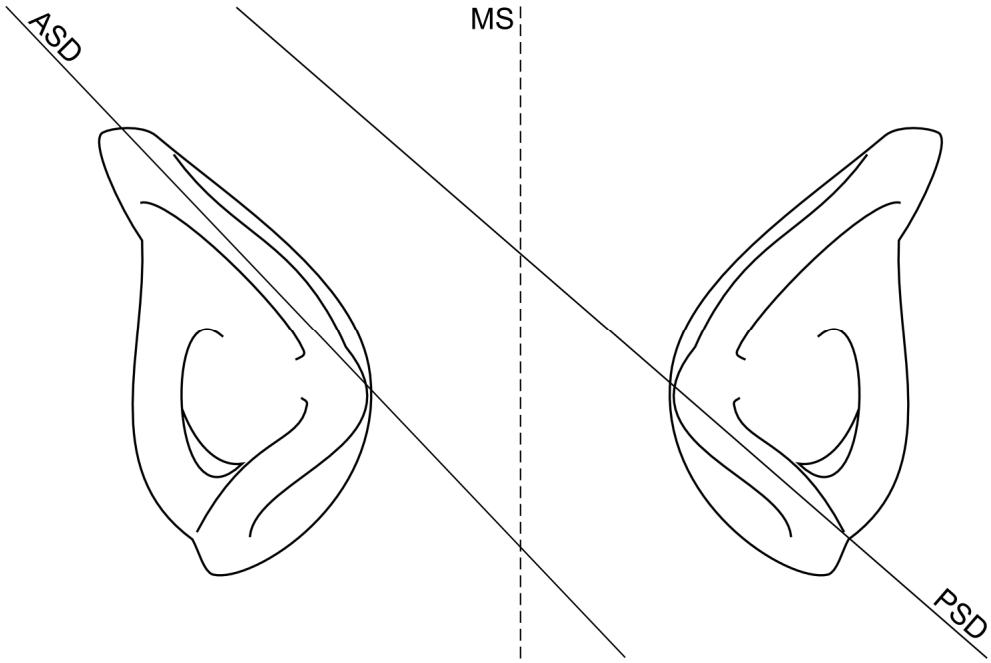

Figure 1: Planar relationships between semicircular ducts. As a result of the symmetrical arrangement across the midsagittal plane (MS), the semicircular ducts of the left and right vestibular systems are arrayed in three approximately coplanar pairs. The anterior semicircular duct (ASD) of the left system and the posterior semicircular duct (PSD) of the right system lie in approximately the same plane. The reverse is true for the anterior duct on the right and the posterior duct on the left. Lastly, the two lateral canals lie in approximately the same horizontal plane. It should be noted, however, that the planar coincidences are rarely perfect.

between the duct and the utricle, excitatory flow for each duct must either be from the direction of the utricle or from the direction of the duct. The cristae of the vertical ducts are arranged such that flow from the direction of the utricle is excitatory whereas the lateral duct is the opposite and flow from the duct is excitatory. Naturally, in each case flow in the opposite direction is inhibitory.

Flow into or out of the duct is brought about by angular accelerations of the head. The orthogonal nature of the canals combined with the positive/negative sensation of flow direction permits the crista of the ducts to decompose any 3-dimensional angular acceleration into three

component axes. The details, mechanics, and implications of this arrangement will be discussed in detail below.

VESTIBULAR BONY ANATOMY

The membranous labyrinth is surrounded by a space filled with perilymph and that perilymphatic space is, in turn, contained within the bones of the otic region: the prootic anteriorly, the supraoccipital superiorly, and the opisthotic posteriorly[2]. The perilymphatic space and the location of the membranous labyrinth within that space, however, are not consistent. Thus, while the cavities within these otic bones (the bony labyrinth) can be separated into the same three general compartments as the membranous labyrinth, the correlations of morphologies between the two labyrinths is not perfect. The aspects of membranous morphology that can be reliably inferred from the bony morphology differ between the different regions and sometimes even between organisms. Like the membranous description, the acoustic region of the bony labyrinth will not be elaborated on here; the focus will be on the bony vestibule, the region containing the membranous vestibule, and the semicircular canals, the channels in the bone through which pass the semicircular ducts.

The three otic bones contribute subequally to the bony vestibule. This bony vestibule is an irregularly shaped vacuity which preserves little or no specific information regarding the relationships and morphologies of the utricle and saccule. In taxa where the medial wall of the bony vestibule is completely ossified, it is formed by all three bones. In some

[2] This is the basic morphology throughout the tetrapods where these elements remain unfused. In some lineages, one or more of these bones will fuse to surrounding bones (*e.g.* crocodilians, where the opisthotic fuses to the exoccipital, the opisthotic portion of this fused bone still contributes to the walls of the bony labyrinth) or to each other (*e.g.* mammals where the bony labyrinth is found within the single petrous portion of the temporal bone).

taxa, *e.g.* Testudines (turtles and tortoises), a significant portion of the medial wall is not ossified.

In general, several foramina can be found in the medial wall of the bony vestibule communicating between this space and the cranial cavity. These foramina transmit the endolymphatic duct, the various divisions of vestibulocochlear nerve (CN VIII) and, variably, blood vessels. In taxa with a complete, but unfused, medial wall, the foramen for the endolymphatic duct is found where each of three contributions to the wall converge. Where the medial wall is fully fused, this foramen is still found in an analogous position, that is, approximately in the mid point of the wall. The nerve and vascular foramina are, typically, found more inferiorly and in variable numbers depending on the location of the branches of CN VIII.

In contrast to the bony vestibule, the semicircular canals reveal, with a reasonable measure of accuracy, the paths and planar orientations of each of the semicircular ducts. The bony canals, however, do not preserve an accurate indication of the cross-sectional area of the semicircular ducts, for it has been shown that there is not a consistent relationship across amniote taxa between bony canal and semicircular duct cross-sectional areas (Gray, 1907, 1908; Ramprashad *et al.*, 1984).

The detailed morphology of the semicircular canals will be discussed in taxa-specific descriptions in later chapters, however, a very generalized description will be made here. As stated above, the canals do preserve the path, both orientation and curvature, of the ducts they enclose. Due to the inconsistency of location of the duct within the canal the canal path is only an approximation of the duct path, but variability of location is relatively small in comparison to overall duct course (Fig. 2).

Also preserved by the bony system are the regions corresponding to the common crus and, in most cases the ampullae of each canal. The

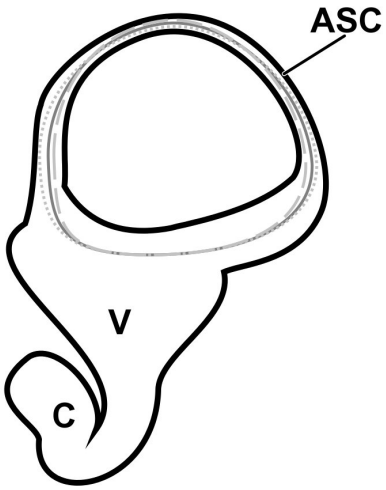

Figure 2: Schematic of a section through a typical mammalian bony inner ear in the plane of the anterior semicircular canal. Three inner ear regions are visible: the anterior semicircular canal (ASC), the bony vestibule (V), and the beginning of the cochlear spiral (C). Three possible paths of the semicircular duct through the canal are provided (solid, dashed, and dotted lines). It can been seen that, as a result of the small thickness of the canal relative to the overall path size, variation in position of the duct within the canal has little effect on the overall path. Duct position only becomes a significant factor when estimating duct path in cases where the width of the canal approaches the same order of magnitude as the overall path.

quality of the definition of the bony ampullary regions depends on numerous factors in addition to the endolymph to perilymph ratio. These confounding factors include ratio of duct size to ampulla size, life history stage, phylogenetic factors and overall organism size.

As described above, the bony vestibule preserves little to no information about the membranous labyrinth, while the semicircular canals preserve some information. Therefore, if information about the membranous system is to be obtained in situations where the membranous system is completely unknown (*i.e.* the examination of fossil taxa) the most information is obtainable from the semicircular canal system (Hullar, 2006). Thus, this study of the connection between the vestibular system and locomotion in modern and fossil amniotes, will focus

on the semicircular canals.

SEMICIRCULAR DUCT BIOPHYSICS

An understanding of the connection between the vestibular organs and an organism's ability to balance goes back to the early 19th century (Flourens, 1828). The basic mechanics of the vestibular system, however, were not understood until the end of the 19th century when Ernst Mach and Josef Breuer independently hypothesized that movement of the endolymph relative to the membranes displaces the cupulae and bends the hair cells resulting in the neuronal activation (Breuer, 1891; Mach, 1875). In the years that followed, many researchers tested and tried to model the Max-Breuer theory of semicircular duct function (*e.g.*, Lee, 1893; Maxwell, 1921). It was not until 1933, however, when Wilhelm Steinhausen put forth a model of the flow of endolymph inside the semicircular ducts, that a robust understanding of the duct mechanics was possible (Steinhausen, 1933). Steinhausen's model of endolymph flow as a heavily damped torsion pendulum remains, to this day, the foundation of further semicircular duct biophysics models.

In its mechanically simplest form, a torsion pendulum is a mass suspended by a string. If, instead of setting this mass into motion swinging side-to-side, torque is applied to the mass (*i.e.* if it is spun in place), the mass will continue to spin, twisting the string, until the elastic force of the twisted string is enough to slow and eventually stop the rotational momentum of the spinning mass. At this point, the string will begin to untwist, causing the mass to spin in the opposite direction it started. The system will continue in this manner, converting rotational kinetic energy (the spinning mass) into rotational potential energy (the elasticity of the twisted string) and back again, until, as a result of friction,

all of the energy in the system has slowly bled out. The damping of the system is simply a measure of the amount of energy that is lost, due primarily to friction, with each iteration of the energy transfer.

Each piece of the damped torsion pendulum has a simple analog within the semicircular duct. The rotating mass is the endolymph flowing around the circular system. The springy, gelatinous cupula provides the elastic restoring force by first being deformed by the flowing endolymph and then pushing back on the endolymph as it returns to its resting shape and position. The friction in the system is found at the boundary between the endolymph and the membrane wall.

Steinhausen's analogy of the semicircular duct flow to a torsion pendulum allows a simple identification of the morphological factors that determine the various parameters for flow. Mass of the endolymph inside the duct is simply the product of the density of endolymph and the volume of the duct, which is, in turn, related to the length and the cross sectional area. The elastic force provided by the cupula is related its material properties and its volume. The damping force, by far the most complicated in this system, is related to the viscosity of the endolymph and the cross-sectional area of the tube it is flowing through (the duct) and the length of that tube. From these relationships, it is clear that the cross sectional area of the duct as well as the length of duct are the primary morphological factors that are driving the function of this system, though cupular size and shape also play a role.

Over the decades since Steinhausen's initial proposal of the torsion pendulum model, many researchers have validated, refined and further generalized the equations of semicircular duct function (Lowenstein and Sand, 1940; Muller, 2000; Oman *et al.*, 1987; Van Buskirk *et al.*, 1976; van Egmond *et al.*, 1949). Despite all this work, an exact, simple answer

doesn't exist. At the root of the problem is the mathematics of fluid flow. All fluids that flow in a Newtonian fashion (*i.e.* any substance that flows as a homogenous fluid) can have their motion described by the basic tenet of fluid dynamics, the Navier-Stokes equation (Navier, 1823; Stokes, 1845). However, when applied to a system as complicated as a semicircular duct, the Navier-Stokes equation produces mathematical structures that cannot readily be solved directly (Elshehawey *et al.*, 2001; Van Buskirk *et al.*, 1976) and resolution of this problem requires the addition of simplifying assumptions or iterative complex calculations to produce reasonable approximations. These methods have proven successful and today, several biophysical properties of canals are recognized and frequently discussed, and their dependence on the morphology of the system firmly established.

Of first importance in this study is the force or pressure effect of rotation of the system on the fluid inside. This is not the metric of sensitivity, the amount of fluid rotation produced per unit of externally applied rotation, commonly found in models of semicircular canal function (McVean, 1999; Muller, 1994; Oman *et al.*, 1987). Rather, this is one half of that concept; this is only the inertial response of the fluid, it does not take resultant flow into account, that factor will be considered subsequently. Rabbit and colleagues (2004) approximate this "inertial forcing coefficient" as

$$g \approx 2\pi\rho\overline{R}^2\cos(\theta) \tag{1}$$

where ρ is the density of the endolymph (which is usually considered a constant across amniote taxa), $\overline{R}$ is the average distance from the centroid of the duct to the centerline path (average radius) and θ is the angle

a	b	R_e	A_e	A_c	P_e	P_c	R_{gm}	R_m
3	3	3.000	28.274	28.274	18.849	18.849	3.000	3.0
6	3	4.625	56.548	67.226	29.065	29.065	4.242	4.5
9	3	6.381	84.823	127.927	40.093	40.094	5.196	6.0
9	6	7.575	169.646	180.275	47.596	47.596	7.348	7.5
12	3	8.191	113.097	210.817	51.465	51.470	6.000	7.5
12	9	10.553	339.292	349.908	66.310	66.310	10.392	10.5

Table 1: Comparison of perimeters and average radii between circles and ellipses. The perimeter (P_e) and average radius (R_e) are calculated for a series of sample ellipses with semiaxes *a* and *b*. The perimeter of a circle with the same average radius as each ellipse (P_c) shows that regardless of ratio of the semiaxes, the perimeters of the ellipse and circle are the same within the error of the method for approximating the perimeter of the ellipse. The radius approximated by the geometric mean (R_{gm}) and arithmetic mean (R_m) are shown to highlight the discrepancies in value between these methods of approximation and the calculated R_e.

between the plane of rotation and the plane of the canal[3].

Equation 1, though a common approximation for mammalian ducts (Ten Kate *et al.*, 1970), is not sufficiently generalized to apply to ducts with circuit shapes that are broadly divergent from circular. The problem arises because $\overline{R}^2$ is a surrogate measurement; the more appropriate measurement is the area enclosed by the canal circuit (McVean, 1999; Muller, 1994, 1999; Oman *et al.*, 1987; Ten Kate *et al.*, 1970). Thus, in equation 1, $\pi\overline{R}^2$ represents the area of a circle with radius $\overline{R}$. It can be shown, however, that the area of an ellipse with semiaxes (half of the major axis or minor axis respectively) *a* and *b* diverges from the area of a circle with radius equal to the ellipse's $\overline{R}$.

Determining $\overline{R}$ for an ellipse is difficult. Neither the average of *a*

[3] One of the assumptions made in this simplification is that the duct does not deviate from a single plane. This assumption is false; the semicircular ducts of many taxa exhibit out of plane deformations. This discrepancy will be eliminated by further generalization below.

and *b*, nor the geometric mean of *a* and *b* accurately represent the average distance from the center of an ellipse to its perimeter as can be seen in Table 1. In order to find $\overline{R}$, it is necessary to use the parametric formulae for an ellipse,

$$x = a\cos\theta \tag{2}$$

and

$$y = b\sin\theta \tag{3}$$

to calculate the radius (distance from the origin) at any given angle θ,

$$R = \sqrt{a^2\cos^2\theta + b^2\sin^2\theta}\,. \tag{4}$$

Finding the average radius around the entire ellipse is a matter of integrating equation 4 and dividing by the range of the integration. Rearranging equation 4 to get

$$R = a\sqrt{1 - \frac{a^2 - b^2}{a^2}\sin^2\theta}\,, \tag{5}$$

the integral becomes

$$\int R = a\int \sqrt{1 - \frac{a^2 - b^2}{a^2}\sin^2\theta}\,d\theta\,. \tag{6}$$

This integral takes the form of an elliptical integral of the second kind. Thus, the direct integration from 0 to $\frac{\pi}{2}$ (*i.e.* around the first quarter of the ellipse which is symmetrical with the other three and therefore has the same $\overline{R}$ as the complete ellipse) is a complete elliptical integral of the second kind which can be expressed, in one form, as

$$a\int_0^{\frac{\pi}{2}} \sqrt{1 - \frac{a^2 - b^2}{a^2}\sin^2\theta}\,d\theta = a\frac{\pi}{2}\left(1 - \sum_{n=1}^{\infty}\left[\left(\frac{(2n-1)!!}{(2n)!!}\right)^2 \frac{\left(\frac{a^2-b^2}{a^2}\right)^n}{2n-1}\right]\right). \tag{7}$$

Dividing equation 7 by $\frac{\pi}{2}$, the range of the integration, produces the

formula for $\overline{R}$,

$$\overline{R}_e = a\left(1-\sum_{n=1}^{\infty}\left[\left(\frac{(2n-1)!!}{(2n)!!}\right)^2\frac{\left(\frac{a^2-b^2}{a^2}\right)^n}{2n-1}\right]\right). \quad (8)$$

This equation is equivalent to the elliptical "correction factor" used by Muller to approximate circular radii from elliptical canals (Muller, 1999). The series described by equation 8 converges at 3 decimal places typically by *n*=30, though for cases of larger differences between *a* and *b* it can take more iterations.

Equation 8 has been used to calculate $\overline{R}$ for several representative ellipses in Table 1. It is clear that as the eccentricity of the ellipse increases, the larger $\overline{R}$ is relative to the geometric mean of *a* and *b*. The square of the geometric mean, which reduces to *a* multiplied by *b*, is the factor for area of an ellipse,

$$A_e = \pi ab\,, \quad (9)$$

and is always smaller than the circular area factor $\overline{R}^2$. Thus, estimates of semicircular duct flow force based on $\overline{R}$, such as equation 1, overestimate. While for most mammalian ducts (*i.e.*, ducts very close to circular in circuit) this overestimation is negligible (McVean, 1999), for taxa with more elliptical ducts it can become a significant factor. For example, an average anterior semicircular canal in *Alligator mississippiensis* has a major semiaxis of 4.55 mm and a minor semiaxis of 2.85 mm. Equation 8 gives the average radius for this ellipse as 3.75mm. The area of a circle with the same average radius is 44.18 mm^2, while the true elliptical area using the given axes is 40.74 mm^2. The $\overline{R}$ flow response of this canal would be overestimated by more than 8%. This error is larger for canals with higher ratios of *a* to *b* such as can be found throughout non-

mammalian amniotes; the average ratio of *a* to *b* calculated from the anterior canals of 65 non-mammalian taxa is 1.72 which corresponds to an overestimation of 10.4%. For highly elliptical canals, such as the anterior canals in varanid lizards or birds (Gray, 1907, 1908; Hadžiselimović and Savković, 1964), ratios can range from 1.90 to 2.15 giving errors of approximately 14% to 21% between actual area and area estimated from $\overline{R}$. In the most extreme of cases, such as the anterior canal of the green anaconda (*Eunectes murinus*), the ratio of major semiaxis to minor semiaxis can be as high as 2.9 which would result in an overestimation of the "inertial forcing coefficient" by 34.9%.

Therefore, to properly calculate this "inertial forcing coefficient" the area enclosed by the duct should be approximated as an ellipse and not a circle. Thus, replacing the area factor in equation 1 with equation 9, produces a more generalized form,

$$g \approx 2\pi\rho ab\cos(\theta). \tag{10}$$

Equation 10 is, of course, equivalent to equation 1 under the special circumstance of a duct with a perfectly circular circuit.

The area enclosed by the duct circuit, *A*, is a factor that can be reliably estimated from the bony labyrinth in one of two ways. Approximating the canal circuit as an ellipse, the area can be estimated using equation 9. Alternatively, the area can be directly calculated from planar representations of the canal[4]. Regardless of the method, *A* is one morphological aspect of the semicircular duct that is preserved by the

[4] Equation 10, by taking the area enclosed by the duct into account, is now not only generalized for shape of the duct circuit, but also for any deformations of the duct circuit out of plane. Oman and colleagues (1987) show that the response of a 3-dimensional duct (*i.e.* a duct with a significant portion of its circuit out of plane) to rotation is proportional to the signed area enclosed by the projection of the duct on the plane of the rotation, By calculating or estimating the area enclosed by a 3-dimensional canal from a planar representation, that projected area is being implicitly accounted for in this study.

semicircular canals, thus, this “inertial forcing coefficient” is one part of the function of this system that can be determined from the semicircular canals.

Secondly, orientation of each duct is preserved in the bony system and, thus, direction of maximum sensitivity of each canal can be approximated as well. This direction of maximum sensitivity is only an approximation because, with the three ducts interconnected through the utricle and common crus, endolymph flow scenarios become much more complicated and the actual direction of maximum sensitivity is not precisely in line with the orientation of the canal (Rabbitt, 1999). Furthermore, Rabbitt and colleagues predict that the direction of maximum sensitivity is less functionally important than the prime direction of a canal which they define as the orientation of rotation where flow is induced in only that canal and neither of the other two (1999). Prime direction of a semicircular duct can be approximated from the orientations of the canals because, mechanically, it is simply the unique plane that is at 90° to the other two ducts, approximated from the other two canals. Based on this definition is it clear that the prime direction, while dependent on the other two canals is completely independent of the orientation of the canal in question. Only in the special circumstance of three canals perfectly orthogonal to each other does the prime direction match the orientation of the canal.

The other aspect of semicircular duct function is what happens when the fluid moves (the properties of the fluid movement, of course, being described by the torsion pendulum model). The end result for the system to function must be deflection, or displacement, of the cupula. Thus, the other ratio of duct function is the displacement of the cupula per movement (in this case linear velocity) of the endolymph. This ratio is

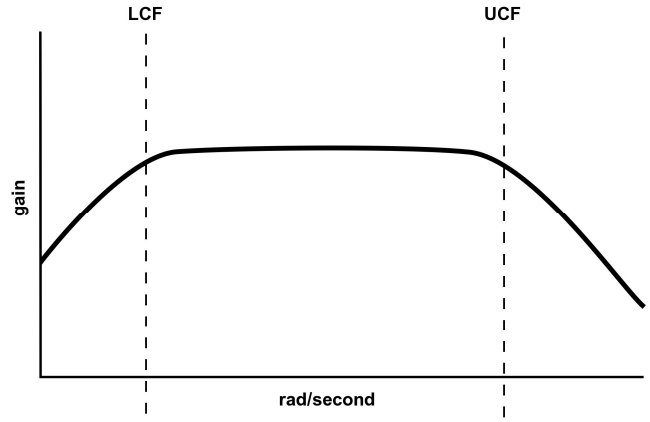

Figure 3: Theoretical semicircular duct gain across a range of rotational frequencies. The frequencies where the slope of the plot changes are the Lower Corner Frequency (LCF) and Upper Corner Frequency (UCF). These frequencies are the inverses of the long and short time constants respectively and together bracket a range of maximum gain.

called the duct's gain. The gain of a duct is not an absolute relationship, however, but one that depends on the frequency (radians per second, *i.e.* angular velocity) of the input rotation. The complex relationship is often depicted graphically as seen in Figure 3. The graphical representation emphasizes the division of this relationship into three regions: 1) starting from 0 frequency, a region of steadily increasing gain, 2) a middle plateau of maximum gain, and 3) at very high frequencies, a region of declining gain. This breakdown allows a further identification of two critical frequencies. The cutoff frequency between region 1 and region 2 is termed the lower corner frequency (LCF). The cutoff between region 2 and region 3 is termed the upper corner frequency (UCF).

These two corner frequencies and three regions represent critical aspects of the function of the system. The LCF is the inverse of a constant of semicircular duct function called the long time constant, τ_1. The UCF is the inverse of a second temporal constant, the short time constant, τ_2. These two constants derive directly from the features of the

torsion pendulum model and are approximated by Rabbit and colleagues (2004) as

$$\tau_1 \approx \frac{damping\ \ force}{elastic\ force} \tag{11}$$

and

$$\tau_2 \approx \frac{mass\ \ factor}{damping\ \ force}. \tag{12}$$

These two have direct and understandable interpretations as relates to semicircular duct function. The long time constant represents the length of time it takes for the endolymph to return to rest after movement has been induced. The short time constant represents the minimum length of time, under movement conditions, that it takes for the cupula to be maximally displaced.

It is intuitive why these two factors bracket the region of maximum duct gain. Given that maximum cupular displacement equals maximum signal output, it is impossible to achieve maximum signal output from a movement that occurs more rapidly than it is possible to attain maximum displacement. Conversely, it is impossible to achieve maximum signal output if the input movement is so slow that the endolymph can return to resting position during the course of the movement.

It is not intuitive, however, that between the corner frequencies, cupular displacement is proportional to the instantaneous angular velocity of the head rather than angular acceleration. The simple mechanics of the system dictate that it is angular acceleration that produces the relative motion between endolymph and membranous walls, and therefore, it would seem that cupular deflection should be proportional to angular acceleration. To the contrary, however, the models of duct function predict a different scenario between the LCF and UCF. In that frequency

range, the mechanics of endolymph flow will integrate the angular acceleration signal producing endolymph flow, and therefore cupular deflection, that is proportional to instantaneous angular velocity (Rabbitt *et al.*, 2004). The end result of this mechanical integration is that firing patterns in the majority of primary afferent nerves from the canals correlate with angular velocity and not acceleration (Collewijn, 1989; Highstein *et al.*, 2005).

It would seem that the LCF and UCF and their inverse time constants are behaviorally critical values, defining a range of head movement frequencies where sensation is not only maximized, but also simplified. In fact, while experimental and theoretical values for these two constants are not always consistent between or even within specific taxa, they do have consistent magnitudes which bracket the range of physiological head movements observed in most organisms; ~10-20 s for the long time constant and ~1-5 μs for the short time constant (Curthoys *et al.*, 1977b; Groen *et al.*, 1952; Muller, 1994; Oman *et al.*, 1987; Rabbitt *et al.*, 2004; Ramprashad *et al.*, 1984; Van Buskirk *et al.*, 1976).

Correlating these two important factors with semicircular canal morphology can be accomplished, as before, by reference to the torsion pendulum model. Using the assumptions and simplification presented by Rabbitt and colleagues (2004), the factors in equations 11 and 12 can be approximated as

$$mass\ factor \approx \frac{\rho \ell}{A_d} \tag{13}$$

and

$$damping\ force \approx \frac{8\pi\mu\ell}{A_d^2} \tag{14}$$

and

$$elastic\ force \approx \frac{8\pi\gamma h}{A_c^2}. \tag{15}$$

The extra terms in these formulae are: ℓ, the length of the slender duct (*i.e.*, the length of the duct circuit that does not include the utricle); A_d, the cross-sectional area of the duct; μ, the viscosity of the endolymph; γ, a factor representing the stiffness of the cupula; h, the thickness of the cupula; A_c, the cross-sectional area of the cupula. The factor of 8π in equations 14 and 15 derive from assumptions of flow patterns inside the duct and are variable depending on the flowing conditions assumed; they will have no further impact in this study. Substituting equations 13, 14, and 15 into equations 11 and 12 produces

$$\tau_1 \approx \frac{\mu\ell A_c^2}{\gamma h A_d^2} \tag{16}$$

and

$$\tau_2 \approx \frac{\rho A_d}{8\pi\mu}. \tag{17}$$

Inverting equations 16 and 17 and removing numerical, endolymph and cupular constants[5] leaves

$$LCF = \frac{1}{\tau_1} \propto \frac{hA_d^2}{\ell A_c^2} \tag{18}$$

and

$$UCF = \frac{1}{\tau_2} \propto \frac{1}{A_d}, \tag{19}$$

two equations expressing the proportional relationships of the lower and

[5] Ignoring endolymph density and viscosity and cupular stiffness in these equations is not the same as considering them constant across all vertebrates. Rather, as the focus of this work is the correlation of morphological factors with duct response, these factors are left out and only proportional effects on LCF and UCF will be considered instead of absolute values.

upper corner frequencies in terms of only semicircular duct and ampulla morphological parameters.

As discussed above, however, only some parameters of the semicircular ducts can be reliably inferred from the semicircular canals. Of the morphological parameters in equations 18 and 19, neither the cupular factors nor the cross-sectional area of the duct are viable for this study. Thus, only ℓ, the length of the slender duct, is appropriate for further consideration, and this work will focus on

$$LCF \propto \frac{1}{\ell}. \tag{20}$$

It should be noted that ℓ is not the predominant factor in equation 18. With A_c and A_d raised to the second power in that formula, changes in these variables have a greater influence on the LCF than do changes in ℓ. Nonetheless, changes in ℓ still influence LCF and may represent either adaptations tuning the LCF to some particular frequency or compensations to maintain a specific frequency when the other factors are changing. With only ℓ available, there is insufficient information to distinguish between these two options, however, in either situation, ℓ, if it varies, is still a functionally meaningful parameter.

To understand variation in ℓ, the perimeter of an ellipse must be examined. Again, modeling a canal as an ellipse with major radius *a* and minor radius *b*, the perimeter of an ellipse,

$$P_e = \pi(a+b)\sum_{n=0}^{\infty}\binom{\frac{1}{2}}{n}^2\left(\left(\frac{a-b}{a+b}\right)^2\right)^n, \tag{21}$$

gives a first approximation of the complete circuit length of the canal. Equation 21 is, however, ungainly and with an infinite sum requires expansion using an infinite series. Unlike equation 8, a slightly more

tractable approximation for the perimeter of an ellipse is available,

$$P_e \approx \pi\left(3(a+b)-\sqrt{(a+3b)(3a+b)}\right), \quad (22)$$

which for ratios of a:b within the range observed in the semicircular canals of amniotes has an error of less than 10^{-4}.

Using equations 8, 9 and 22 it is now possible to examine the relationship between the perimeter, the area, and $\overline{R}$ of elliptical canals. Table 1 shows that for an ellipse and a circle with the same $\overline{R}$, the perimeters are approximately equal. Taken by itself, this would indicate that, no matter what the shape of the duct, as long as a circular or elliptical approximation is maintained, the average radius and circuit length have an absolute relationship (specifically, the perimeter is 2π times the length of the average radius). Since the area enclosed and $\overline{R}$ do not have a direct relationship, neither do the area and the perimeter. In fact, Table 2 demonstrates that by varying the size and shape of the duct circuit, the area of an ellipse and circuit length can vary independently. This is not the whole picture, however, for the complete perimeter of a duct includes the utricular portion and the functionally significant metric is the length of the slender duct alone, ℓ. Thus, it is necessary to consider the effect the utricle has on the independence between *A* and ℓ.

Assuming, first, that the utricle accounts for a constant fraction of the overall length of the duct circuit, the independence of *A* and ℓ remains unchanged because a direct relation will exist between ℓ and the circuit length. This situation is, however, unlikely to represent the situation found in nature and, given broad morphological variation and relative independence of utricular and semicircular duct function, it is more parsimonious to assume that the fraction of the duct circuit comprised by the utricle varies according to some requirement of macular function

a	b	P_e	A_e
3.000	3.000	18.85	28.27
3.500	2.454	18.85	26.98
4.000	1.786	18.85	22.44
4.500	0.866	18.85	12.24
3.500	2.571	19.18	28.27
4.000	2.250	20.02	28.27
4.500	2.000	21.18	28.27

Table 2: Comparison of the perimeters (P_e) and areas (A_e) of ellipses with different ratios of semiaxes *a* and *b*. Ellipses of differing ratios can be selected in order to hold either the perimeter or the area constant while varying the other.

independent of semicircular duct function. With this assumption, ℓ is further decoupled from A as changes to ℓ can occur without any change to the size or shape of the duct.

Thus, three mutually independent factors have been identified as significant determinants of semicircular duct function while also available directly or approximately from the bony labyrinth: area enclosed by the canal (A), orientation of the canals, and length of the slender duct (ℓ). An examination of these factors across vertebrates is potentially informative regarding the role of semicircular duct function during different tasks and in different environments.

SEMICIRCULAR CANALS ACROSS AMNIOTES AND THE LINK TO BEHAVIOR

Regardless of the demonstration of independence between enclosed area, A, and canal length, ℓ, if the semicircular canals of all vertebrates were absolutely or even geometrically identical, then the relationship of canal length and area enclosed would also be absolutely or

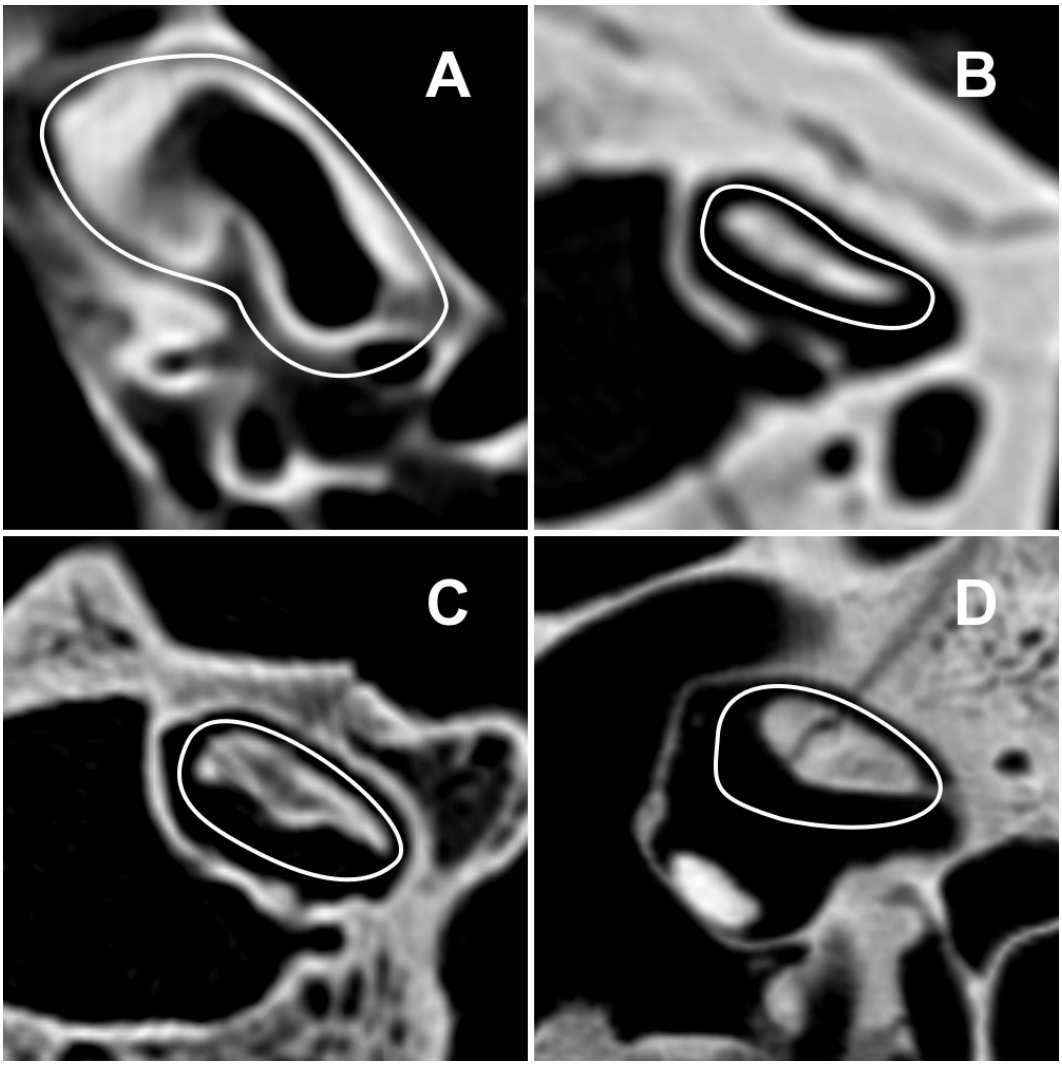

Figure 4: CT reconstructions of the anterior semicircular canals in four non-mammalian taxa: A) emperor penguin (*Aptenodytes forsteri*), B) green anaconda (*Eunectes murinus*), C) komodo dragon (*Varanus komodoensis*), D) Indian gharial (*Gavialis gangeticus*). The white paths demonstrate the approximate semicircular duct circuit for each canal. The circuits represent some of the manners in which semicircular ducts can deviate from a circular path: ranging from merely elliptical (C) to circuits with concave (A, B) or convex (D) deviations producing ovoid or cardioid circuits. Images are not to scale.

geometrically identical and all variation in one could be attributed to the other. Similarity, however, is not the case. For more than a century researches have recognized and described the variation in the semicircular ducts and canals across all classes of vertebrates (Baird,

1974; Gray, 1906; 1907; 1908; Gray, 1955; Hadžiselimović, 1968; Ramprashad *et al.*, 1986; Retzius, 1881; 1884).

Other than the basic arrangement of three ducts in roughly orthogonal planes and the connection of these ducts to each other and the utricle, most aspects of the semicircular duct system vary throughout vertebrates. At least one measure of size, $\overline{R}$, and the cross-sectional area of the duct have been shown to increase with the size of the organism (Jones and Spells, 1963). The relative size of the ducts to each other vary across taxa (Curthoys *et al.*, 1977a; Gray, 1907; 1908). The angles between each pair of ducts and the orientation of the ducts in the head vary across taxa depending on many factors such as head posture (Brichta *et al.*, 1988; Hullar, 2006) or even eyeball orientation (Ezure and Graf, 1984a). Most dramatically, as shown in Figure 4, many semicircular canals, and the ducts they contain, are hardly semicircular, deviating tremendously in shape across major vertebrate groups (Gray, 1907, 1908; Hadžiselimović and Savković, 1964; Ramprashad *et al.*, 1986); this, as has been shown, has a marked impact on the area enclosed by the duct.

Because the functional response of this system is fully dependent morphological factors, the great variety in morphology should represent a great variety in semicircular duct function. This has lead researchers to hypothesize that the semicircular ducts of an organism are morphologically adapted (and, therefore, functionally adapted) to maximize duct response to particular rotation frequencies and directions that represent the most common or important head movements the organism makes. One of the earliest examples of this hypothesis was formulated by Albert A. Gray upon noting the strange morphology of the semicircular ducts of the three-toed sloth (*Bradypus tridactylus*):

> It may be that this small size of the canals, associated with their irregular shape, may be in some way related to the sloth's clumsy and slow movements. The life which they lead, with the body inverted, as it almost continuously is, may also be connected in some way to the curious development of these organs (Gray, 1906, pg. 290).

Since that time, similar arguments have been made to connect vestibular morphology with mode of life in birds (Alonso *et al.*, 2004; Hadžiselimović and Savković, 1964), early humans (Spoor *et al.*, 1994, 1996), rodents (Lindenlaub *et al.*, 1995; Lindenlaub and Oelschläger, 1999; McVean, 1999), whales (Spoor *et al.*, 2002) and non-human primates (Matano *et al.*, 1985; Walker *et al.*, 2003).

Opponents of the semicircular canal/behavior hypothesis claim that the variation in canal morphology is strictly a result of packing the inner ear in the available space (Graf and Vidal, 1996). In some cases, this is likely true. Bissonnette and Fekete (1996), by visualizing the inner ear in a series of chicken embryos, clearly show that portions of the developing brain cause deformation in the shape of the developing semicircular ducts. In others cases, this argument is far less likely. Pre-hatchling and newly hatched alligatoroids have the anterior semicircular canal bounded by the brain on the medial side (Figure 5a), but this brain boundary does not correspond with the region where the canal deviates from circular. It is the antero-superior portion of the canal that is flattened relative to a circular shape and this region of the canal is bounded only by air-filled sinus (Figure 5b), a structure that is unlikely to have impinged the development of the canal.

The second primary argument leveled against a link between semicircular canal morphology and specifics of locomotor behavior is a standard black-box argument. In the pathway between semicircular duct response and movements of the body (either reflexive or voluntary), there is processing of the signal in the cerebellum and some of its ancillary

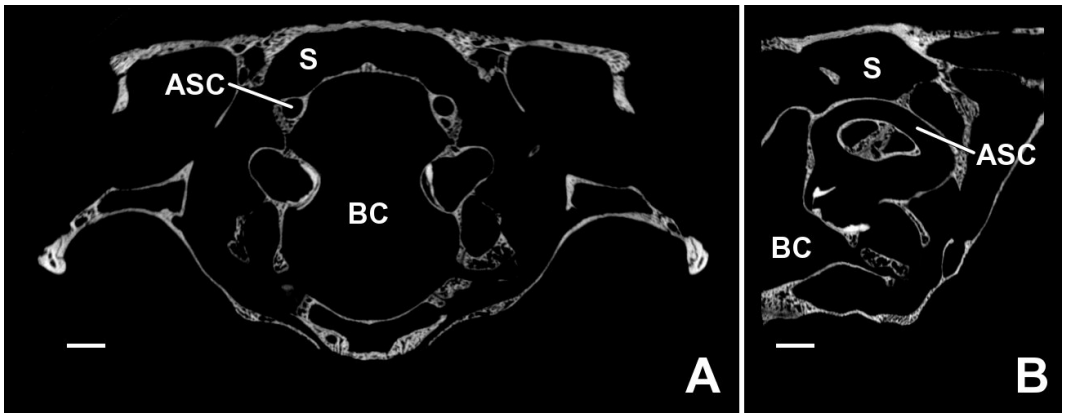

Figure 5: CT reconstructions of a hatchling dwarf caiman (*Paleosuchus palpebrosus*): A) coronal section at the level of the mid-point of the anterior semicircular canal, B) section in the plane of the anterior semicircular canal (ASC). The relatively large brain cavity (BC) is directly medial to the otic structures, however, superior to the structures is open sinus (S) confluent with the tympanic cavity.

regions, such as the flocculus and paraflocculars lobes. Thus, opponents of this hypothesis point to the complexity of this processing and how little is understood about it and say that any duct responses that vary as a result of duct morphology are neutralized via the processing pathways of the cerebellum and similarity of true functional response is maintained (Graf and Vidal, 1996). Furthermore, Hullar (2006), taking semicircular duct morphology and vestibular afferent responses from the literature claims that there is no support for a correlation between canal morphology and primary vestibular afferent nerve responses. Hullar's data, however, are few and the study includes a lengthy description of numerous sources of error, some or all of which could be masking a true relationship.

The problem of the black-box cerebellum is more difficult to discount than the spatial packing argument. Without an extensive suit of studies across all types of vertebrates, this claim of cerebellar interference cannot be addressed with positive evidence. But there is an inferential way to examine the problem that is within the bounds of what has so far

been presented. If the theory of the black-box cerebellum is correct, then there should exist no common aspect of semicircular duct morphology across a broad range of vertebrates which share particular features of locomotion. That is to say, if cerebellar processing can account for any variation in semicircular duct morphology then there should be no pattern to semicircular duct morphology in vertebrates save for what results from phylogeny. Conversely, if cerebellar processing is an insignificant factor in the response patterns of the semicircular ducts then vertebrates that share features of locomotion will share features of semicircular duct morphology.

While many of the previous studies have reported success in correlating semicircular duct or canal morphology with some aspect of behavior or locomotion they have been, by no means, conclusive. The breadth of each of these studies is limited and is insufficient to counter the black-box cerebellum argument. The use of the correlations uncovered by such studies for prediction is also limit due to the insufficient consideration and testing of the assumptions that underlie the correlation. For example, Spoor and colleagues found a significant decrease in the size of the semicircular canals of cetaceans relative to other mammals, attributing this to the stiffened cervical region of cetaceans (2002). In a later study, Spoor and Thewissen predicted a similar decrease in the size of the semicircular canals in the relatively stiff-necked phocids and an increase in the size of the semicircular canals in the flexible otariids but found the opposite pattern instead (2008).

Furthermore, these studies are also often lacking statistical support for the functional claims (Graf and Vidal, 1996), or in some cases outright contradictory in the functional interpretation (Hullar, 2006; Spoor *et al.*, 2002; Spoor *et al.*, 1996). This is most evident in the contrast between the functional interpretation of the results of Jones and Spells' original work

(1963), and some of the work derived from their methods (*e.g.*, Spoor *et al.*, 2007; Walker *et al.*, 2003). Jones and Spells concluded that the semicircular ducts of vertebrates became larger with increasing body size in order that the system be properly attuned to the slower movements of larger animals (1963). In contrast, Spoor and colleagues and Walker and colleagues maintain that comparing, when animals of the same approximate body size, the more agile or faster animal should have the larger semicircular canals (Spoor *et al.*, 2007; Walker *et al.*, 2003). To be sure, these two claims are referring to different comparison (one across the full range of vertebrate body sizes and the other across animals of a single body size), but they are still relating increase in the size of the vestibular system to two opposite locomotor classifications, slow or fast. This contradiction finds its way into these studies because there is no evidence to strength one argument over the other. This evidence does not exist because the underlying assumption of adaptive change of semicircular duct function and its connection to locomotion has never been rigorously tested.

In the chapters that follow, this work will address these deficiencies and examine the strength of the connection between semicircular duct morphology (via the proxies of semicircular canal morphology) and locomotor behavior. Examining a locomotor contrast common to most branches of the amniote tree, aquatic locomotion versus terrestrial locomotion, broader comparisons can be made than have been possible before and the basic pillars of this controversial hypothesis can be tested.

Chapter 3
Allometric Growth in the Bony Vestibule of *Alligator mississippiensis*

INTRODUCTION

The morphology of biological sensors is of interest to both functional morphologists and behaviorists. Comparing the principles by which a sensor functions and the physical properties of the sensor within an organism, researchers can make many inferences about how the organism uses that sensor.

The semicircular ducts are features of the membranous labyrinth of the inner ear. Motion of endolymph contained within the semicircular ducts relative to the surrounding membrane is transduced by hair cells into information regarding the instantaneous rotational velocity of the head. The function of the semicircular ducts as sensors of rotational movement has been understood since the early part of the 19th century (Hawkins and Schacht, 2005). Since that time, a significant body of clinical research has been produced as researchers try to understand the role of semicircular duct signals in the brain and treat the numerous common and severe vestibular maladies. Thus, much is understood about the semicircular ducts from mechanical and neurophysiological perspectives.

In 1963, Jones and Spells applied this understanding to a variety of vertebrate taxa in a functional framework (Jones and Spells, 1963). They investigated two physical parameters of the semicircular ducts that have well-understood relationships to the function of the system. This functional study uncovered a general relationship across vertebrates of increasing sensitivity of the semicircular duct system with increasing body mass of

the organism. This work provided, for the first time, evidence that the morphology of the semicircular ducts might be changing in response to changes in locomotor requirements, and Jones and Spells hypothesized that larger animals exhibited slower head movements and required an increase in the sensitivity of the semicircular ducts in order to detect these reduced movements (Jones and Spells, 1963).

Jones and Spells (1963) gathered most of their semicircular duct data from figures produced at the beginning of the 20th century by Albert Gray as part of his comprehensive investigation into the morphology of membranous labyrinths across vertebrates (Gray, 1906, 1907, 1908). However, preserving and preparing amniote membranous labyrinths is a technically and temporally prohibitive procedure. Thus, studies that seek to expand on Jones and Spells method and hypotheses in amniotes require some other method for examining the labyrinth's morphology. Advances in technology of over the last decade provide this new method.

The various features of the membranous labyrinth, including the semicircular ducts, leave distinct vacuities and channels within the bones of the otic region of the skull. The morphology of the semicircular canals, the bony channels surrounding the semicircular ducts, can be assessed using X-ray computed tomography (CT) (Spoor and Zonneveld, 1998; Van Spaendonck *et al.*, 2000). There are limitations, however, to this method; certain aspects of the membranous labyrinth cannot be illuminated by the morphology of the bony canals. For example, whereas the radius of curvature of the circular or elliptical path of the duct can be determined accurately from the radius of curvature of the canal, the internal radius and the cross-sectional area of the duct cannot be reliably determined from the bony counterparts (Ramprashad *et al.*, 1984, 1986).

CT has permitted investigators to return to some of the hypotheses

of Jones and Spells (1963) and further examine the connection between locomotion, body size and semicircular canal radius of curvature (Spoor *et al.*, 2002; Spoor *et al.*, 2007; Walker *et al.*, 2003). Along with other conclusions, these studies have verified the geometric relationship between semicircular canal radius of curvature and body mass as outlined by Jones and Spells. However, these studies have focused only on mammals. Even the original data set Jones and Spells used was primarily mammalian, consisting of measurements from 51 mammals, 18 birds, 17 fishes and 7 reptiles and amphibians (Jones and Spells, 1963).

The bones of the mammalian otic capsule are completely fused, in humans, this happens around the sixth month of development (Jeffery and Spoor, 2004), at which point the semicircular canals are already of adult size (Jeffery and Spoor, 2004; Tremble, 1929, 1978). Not all vertebrates fuse the bones of the otic capsule, however. Animals that exhibit indeterminate growth also tend to exhibit growth in the bones surrounding the membranous labyrinth and are an interesting key to understanding the nature of this canal size to organism size relationship. If this relationship has some broad import then it is reasonable to hypothesize that animals that continue to grow throughout their lifetime should continue to increase the size of the semicircular canals accordingly. In Jones and Spells' (1963) original study, only 24 of the 93 examined specimens would have exhibited continual growth, the 17 fishes and 7 reptile and amphibian specimens.

Semicircular canal growth has been examined previously in fishes (Howland and Masci, 1973a; Ten Kate, 1973; Ten Kate *et al.*, 1970). This study is the first ever to examine this phenomenon in a tetrapod taxon. *Alligator mississippiensis*, the American alligator, exhibits continual growth as do the bones of its otic capsule (the prootic, supraoccipital and fused

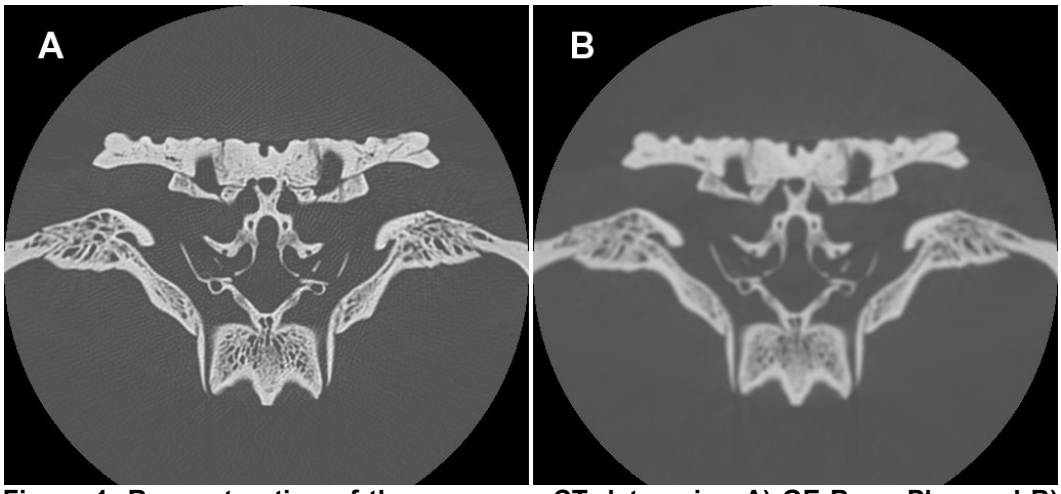

Figure 1: Reconstruction of the same raw CT data using A) GE Bone Plus and B) Standard algorithms.

opisthotic-exoccipital) and the labyrinths contained therein. Therefore, this study will examine the allometries of the alligator semicircular canal system as well as ontogenetic changes to factors such as shape and angular orientation.

MATERIALS AND METHODS

The braincase regions from 23 *Alligator mississippiensis* skulls, ranging in skull length from 51.9 to 444.0 mm, were scanned in a GE Lightspeed 16 X-Ray CT. Scanner current, power, reconstruction area, and slice thickness were adjusted for each specimen to produce optimum scan quality. Raw data from the scanner were reconstructed into individual slice images using the GE Bone Plus algorithm, which enhances the contrast in the grayscale regions corresponding to typical bone densities and increases the image sharpness at bone/tissue and bone/air boundaries (Fig. 1).

Complete CT volumes were processed using ImageJ version 1.38. Image processing included reducing the size of the data set by selecting a small volume of interest containing both right and left otic regions and

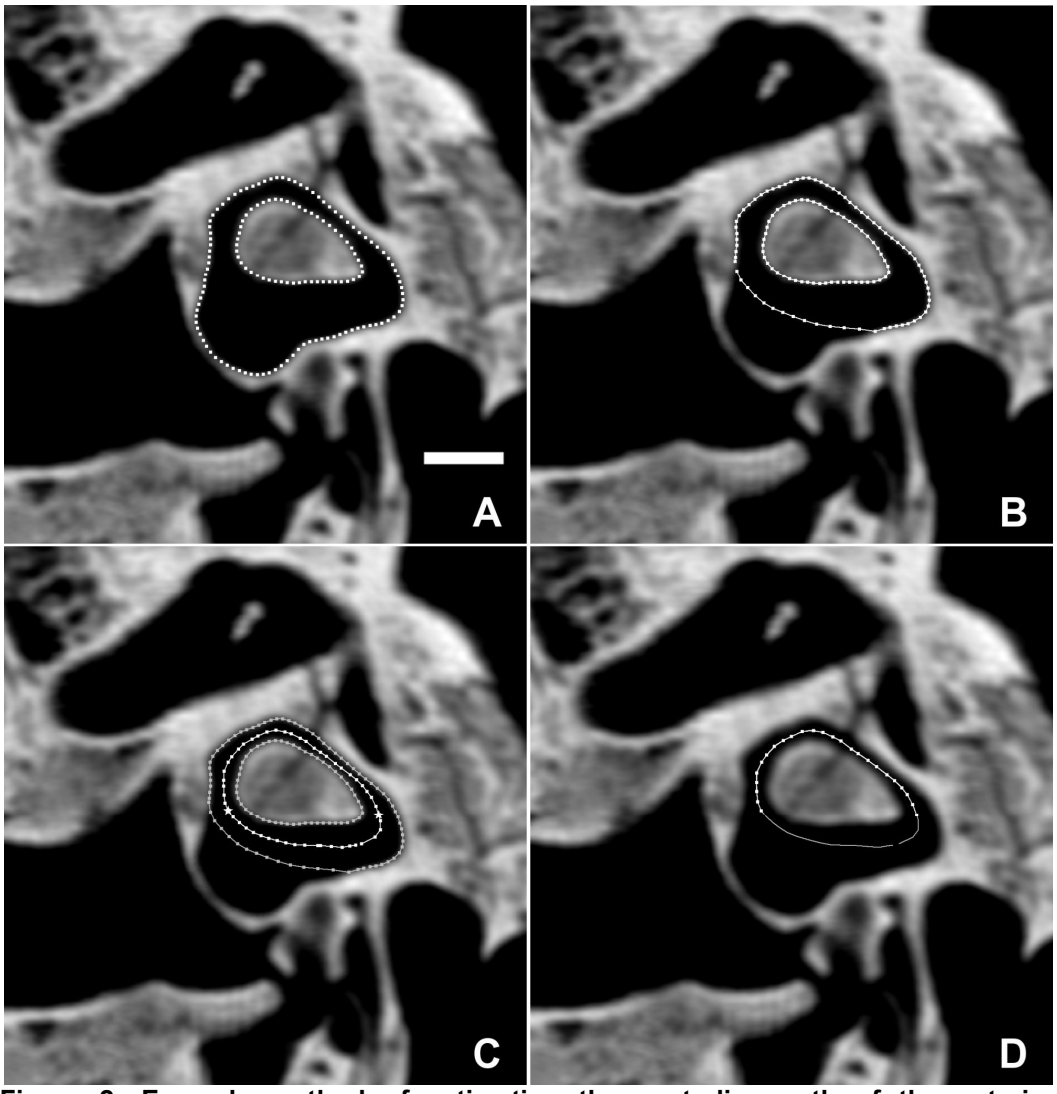

Figure 2: Example method of estimating the centerline path of the anterior semicircular duct from the anterior semicircular canal and vestibule: A) interior and exterior bony boundaries of the semicircular canal and vestibule are defined, B) exterior vestibule boundary between ampulla and common crus is replaced with equivalent segment of interior boundary, C) exterior and interior boundaries are averaged around the circuit starting from the utricular end of the ampulla, and D) the path of the slender duct – the portion of the circuit excluding ampullary and utricular contributions – is resampled at 25 points using cubic spline interpolation. Scale = 5 mm.

multiple mid-sagittal landmarks and increasing (via cubic spline interpolation) the dimensions of either the z-axis or the x- and y-axes to produce isometric voxels throughout the volume. Best-fit planes for each

of the six semicircular canals were then determined by principal component analysis of manually selected 3-dimensional coordinates along the entire center of the semicircular canal circuit, and the mid-sagittal plane was defined using the same process on multiple manually selected midline landmarks. In cases in which the complete canal circuit was not clearly visible in a single slice due to original CT quality, specimen quality or semicircular canal morphology, 3-5 parallel images were averaged to produce an accurate projection of the canal on the best-fit plane.

Angles between two planes were calculated as the inverse cosine of the dot product of the vectors normal to each plane, which were derived from the principal component method of plane fitting. For each canal system, eight angle measurements were taken: the angle between each canal and the sagittal plane; the angle between each pair of canals; the angle between the anterior canal and the posterior canal of the opposite system; and the angle between left and right lateral canals. For each specimen, angles from the left and right canal systems were averaged to produce a representative set of values for the individual.

Using SigmaScan Pro 5, scaled, two-dimensional coordinates representing the outer and inner bony borders of the semicircular canals were collected from the planar canal images (Fig. 2A). These outer and inner canal circuits were processed using Igor Pro 4.04 to calculate an average midline circuit through the semicircular canal and vestibule representing the best average approximation of the semicircular duct (Fig. 2B & 2C). From this estimated circuit, three parameters were measured: square root of the area enclosed, perimeter, and average radius from center. Defining the point along the circuit that corresponds to the boundary between the common crus and the utricle and the point between the ampulla and duct (Fig. 2C), two further parameters of the circuit can

	Mean Angle (°) ± 95% C.I.	Range of Angles (°) throughout Growth
SAG vs ASC		**33.8** - **42.4**
SAG vs PSC	**41.1** ± 5.4	
SAG vs LSC	**94.8** ± 4.6	
ASC vs PSC	**110.1** ± 6.2	
PSC vs LSC	**103.9** ± 7.9	
LSC vs ASC		**103.0** - **123.6**
ASC vs oPSC		**24.1** - **41.6**
LSC vs oLSC	**9.7** ± 9.3	

Table 1: Angles between each of the canals and the sagittal plane, between each pair of canals within one system and each canal and its compliment from the opposite system. Angles and 95% confidence intervals are given for each angle that does not significantly change during growth. For angles that do change throughout growth, minimum and maximum measured values are given.

be measured: maximum width parallel to the utricle, and maximum height perpendicular to the utricle. To provide data suitable for landmark shape analysis, the portion of the circuit representing the slender duct only (the circuit excluding the utricle and ampulla) was resampled using cubic spline interpolation to produce a consistent 25 points for each specimen (Fig. 2D).

Each of the measurements taken from the estimated canal circuit were plotted against the length of the skull (from anterior tip of the premaxillae to the posterior tip of the occipital condyle) in log-log space and the slope of the reduced major axis (RMA) regression was taken as the allometric scaling factor. The RMA regressions of all the measurements for each canal were compared for statistical similarity using the software (S)MATR (Warton *et al.*, 2006), in order to identify patterns of differential growth within a single canal. Using the same method, average semicircular canal size, taken as the mean of the three canal average radii, was plotted against the cube of skull length (the cube of a length unit equaling a volume unit and therefore a reasonable proxy for mass), was compared to the data of Spoor and colleagues (2007)[1].

[1] In order to remove the effects of taxa with highly specialized and widely divergent canal morphologies, only taxa that were classified in the "medium" agility category were used for comparison. This was the largest category in the study, 86 out of 210 specimens, and

	Anterior			Posterior			Lateral		
	Slope	Lower CI	Upper CI	**Slope**	Lower CI	Upper CI	**Slope**	Lower CI	Upper CI
Area Enclosed (square root)	**0.431**	0.404	0.459	**0.473**	0.428	0.522	**0.465**	0.439	0.493
Average radius from center	**0.434**	0.409	0.46	**0.475**	0.434	0.52	**0.460**	0.435	0.488
Axis Parallel to Utricle	**0.462**	0.439	0.487	**0.519**	0.475	0.567	**0.419**	0.394	0.445
Axis Perpendicular to Utricle	**0.431**	0.382	0.487	**0.449**	0.371	0.544	**0.525**	0.473	0.584
Length of Slender Canal	**0.451**	0.418	0.488	**0.476**	0.425	0.533	**0.514**	0.483	0.547

Table 2: Reduced major axis (RMA) slope values along with lower and upper 95% confidence values for measurements taken from the duct circuit estimate for each semicircular canal regressed against overall skull length in log-log space. These values are strongly negatively allometric relative to head size.

Average angle data were analyzed with respect to overall skull length using rank order correlation (Mosimann and James, 1979).

Procrustes analysis of the landmark data was performed using tpsRelw (Rohlf, 2005). For each set of landmarks, the first and last (the common crus/utricle boundary and the canal/ampulla boundary, respectively) were taken from the canal circuit estimation. The 23 intervening points, produced by cubic spline interpolation of the canal circuit estimation, were treated as semilandmarks, using the minimum bending energy method of sliding (Bookstein, 1997).

RESULTS

Table 1 summarizes the angles describing the orientations of the system relative to the sagittal plane and of the canals relative to each other. Only three of the measured angles have significant rank order correlations with overall skull length: the angle between the anterior

had the second broadest range of masses. Because the cube of the skull length is not a true mass measure, any significant deviations in elevations of the two regressions are not indicative of any functional or phylogenetic differences between the data. It is of interest only to compare the slopes of the regressions to determine if intraspecific changes in average semicircular canal size in *Alligator mississippiensis* relative to volume resemble the interspecific changes found across fully-grown mammals.

	Area Enclosed (square root)	Average radius from center	Axis Parallel to Utricle	Axis Perpendicular to Utricle	Length of Slender Canal
Area Enclosed (square root)	1	0.781	0.015	0.044	0.021
Average radius from center	0.781	1	0.024	0.035	0.012
Axis Parallel to Utricle	0.015	0.024	1	0.002	0.001
Axis Perpendicular to Utricle	0.044	0.035	0.002	1	0.716
Length of Slender Canal	0.021	0.012	0.001	0.716	1

Table 3: P-values for pairwise differences between lateral canal scaling factors. The only pairs that are statistically similar are area enclosed/average radius and perpendicular axis/length of slender canal.

semicircular canal and the sagittal plane (Spearman's rho, $r_s = -0.597$, $p < 0.01$), the angle between the anterior and lateral canals ($r_s = -0.506$, $p < 0.05$), and the angle between the anterior canal and the posterior canal of the opposite side ($r_s = -0.464$, $p < 0.05$). These values indicate that the orientation of the anterior semicircular canal is changing while the other two canals (and the system as a whole) remain in place.

Table 2 summarizes the allometric scaling coefficients for the five measurements for each canal. All measurements were linear (or equivalent to linear, in the case of the square root of the area) and therefore the expectation of isometric growth relative to overall skull length is 1. The maximum scaling factor observed in any of the three canals is 0.525 in the lateral canal's axis perpendicular to the utricle. Thus, all of the measurements scale with extreme negative allometry with respect to skull length (Fig. 3).

Scaling factors of each of the five measurements for the anterior semicircular are all statistically similar (Fig. 3A), ranging from 0.431 to 0.462 and with a minimum coefficient of determination of 0.933. The mean slope for anterior semicircular canal scalings is 0.442. Similarly, none of scaling factors for the posterior semicircular canal show any

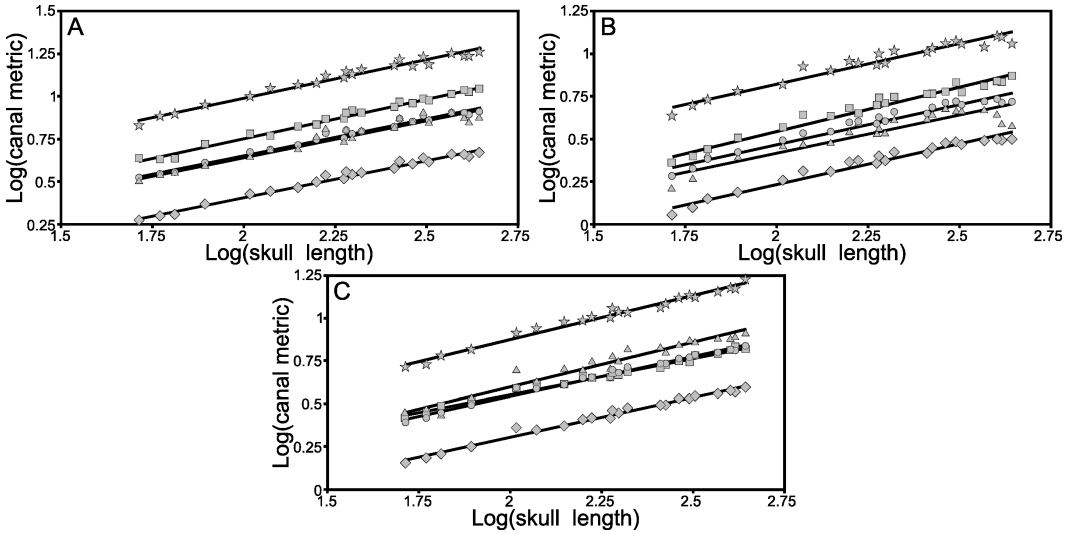

Figure 3: Relative ontogenetic growth within the A) anterior, B) posterior, and C) lateral semicircular canals of *Alligator mississippiensis*. Five variables, area enclosed (circles), average radius of curvature (diamonds), width parallel to the utricle (squares), height perpendicular to the utricle (triangles), and canal streamline length (stars), are plotted against skull length in $\log_{10}$-$\log_{10}$ space. All of the Reduced Major Axis (RMA) slopes (see Table 2) are much less than one and, therefore, indicate strong negative allometry. Within the anterior (A) and posterior (B) semicircular canals, the slopes are all statistically similar. The lateral canal however exhibits a three significant scaling groups: the axis perpendicular to the utricle and the canal length have the highest allometry; the area enclosed and average radius share an intermediate allometry; the axis parallel to the utricle has the lowest allometry.

statistical difference (Fig. 3B). The mean slope for posterior semicircular canal scalings is 0.478. This slope is significantly different from the anterior mean slope ($p < 0.05$).

In contrast to the other two canals, the lateral semicircular canal shows significant differences in the scaling of different parts (Fig. 3C). Table 3 summarizes the p-values for pairwise difference comparisons between all lateral semicircular canal scaling factors. The two largest scaling factors, the length of the slender canal and the axis perpendicular to the utricle, do not differ statistically from each other but are statistically different from each of the other three scaling factors. Similarly, the two mid-range scaling factors, the square root of the area enclosed and

average radius are not different, but are different from the other three. This makes it apparent that the smallest of the five lateral semicircular canal scaling values (and the smallest absolute scaling factor observed in any of the three canals), the axis parallel to the utricle, is statistically different from all of the other allometries of the lateral canal. An important consequence of this pattern of differential growth is a change in the overall shape of the lateral canal; the two axes describing the circularity of the canal, the axis parallel to the utricle and the axis perpendicular to the utricle, are the lowest and highest allometries, respectively, in the lateral canal system. In the smaller specimens these two values are roughly similar and thus the canal circuit they describe is roughly circular; as the perpendicular axis rapidly outgrows the lateral axis, the canal looses its circular circuit and becomes more elliptical. The mean scaling factor for the lateral semicircular canal measurements is 0.477. Although this is very close to the posterior canal mean scaling factor, as a result of its broader variance it is not statistically different from the anterior canal's mean.

Average semicircular canal size scales to the cube of skull length by a factor of 0.151. Spoor and colleagues' (2007) "medium" category mammals have an average semicircular canal scaling of 0.152 relative to body mass. These two scaling factors are statistically indistinguishable ($p = 0.801$).

Procrustes landmark analysis gives a similar but more detailed picture of shape changes in the anterior semicircular canal. Only the scores along the 4^{th} of the anterior canal's shape axes correlated with skull length ($r_s = 0.423$, $p < 0.05$). This axis describes only 4.0% of the overall shape variation (the first three axes have already accounted for 86.8% of the variation), and the variation it describes is a straightening of

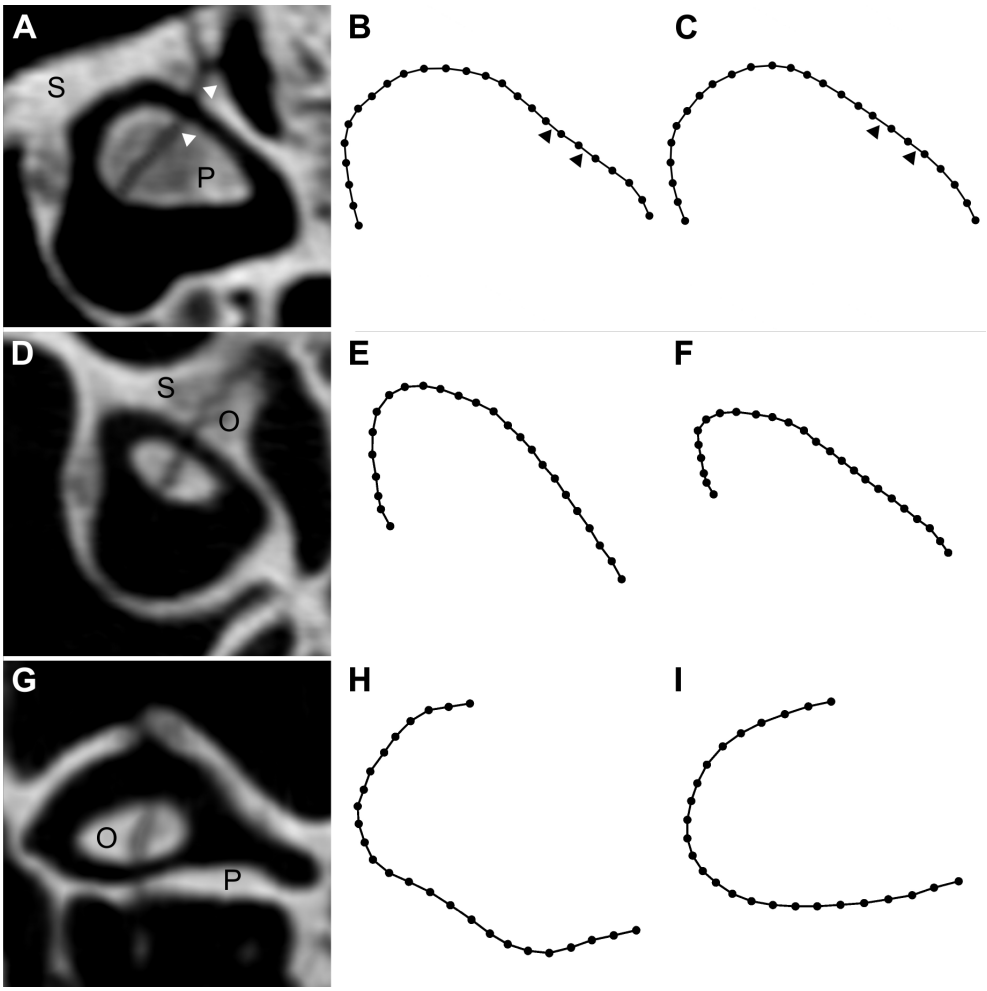

Figure 4: The only shape change in the anterior semicircular canal (A) that correlates with skull length occurs in the region of the suture (white arrows) between the prootic (P) and the supraoccipital (S) bones. In the smallest specimens (B), there is a subtle concavity (black arrows) to the canal on the prootic side of the suture. In the largest specimens (C), this concavity has disappeared (black arrows). In contrast, there is marked shape change in both the posterior (D) and lateral (G) semicircular canals that correlates with skull length. In both cases, the pronounced change is one of decreasing length along the region shared with the anterior semicircular canal. For the posterior canal, this region is the common crus and it appears to get shorter relative to the width of the canal from the smallest (E) to the largest (F) specimens. For the lateral canal the shared region is the utricle (represented by the gap between the path endpoints), and is appears to get shorter relative to an increase in width of the canal from the smallest (H) to the largest (I) specimens. In the posterior canal, shape change along the suture between the supraoccipital and the opisthotic (O) is, if present at all, overwhelmed by the overall shape change of the canal. The same is true along the suture between the prootic and the opisthotic in the lateral semicircular canal.

the canal in the region of intersection between the prootic and supraoccipital elements (Fig. 4A-C).

The landmark and scaling analyses for the posterior semicircular canal, however, do not agree. Where there was no significant difference in posterior canal scaling factors, indicating no shape change during growth, skull length correlates significantly (r_s = -0.426, $p < 0.05$) with the scores of the 1st shape axis (Fig. 4D-F). This axis corresponds to 51.4% of the shape variation and clearly describes a changing relationship between the maximum width of the slender canal path (which is the axis parallel to the utricle) and the maximum height of the path (which is related, though not identical, to the axis perpendicular to the utricle).

The landmark analysis of the lateral canal produced the same pattern of changing shape during growth as did the scaling analysis (Fig. 4G-I). The first shape axis, accounting for 65.0% of the overall variation in the lateral canals was the only axis with scores that correlated significantly with skull length (r_s = 0.787, $p << 0.01$). Like the scaling analysis, the first shape axis describes an axis perpendicular to the utricle that is growing much more rapidly than the axis parallel to the utricle and therefore producing a marked change in the eccentricity of the lateral canal path during growth.

DISCUSSION

Previous studies of intraspecific semicircular canal size have focused on fishes (Howland and Masci, 1973a; Ten Kate *et al.*, 1970). Although the average scaling factors reported in these studies are consistent with each other (once the values have been adjusted to account for differences in unit dimensions), they are not consistent with the value reported for interspecific studies of all vertebrate groups (Jones

and Spells, 1963) or the values reported for mammals alone (Jones and Spells, 1963; Spoor *et al.*, 2002; Spoor *et al.*, 2007). These intraspecific growth rates do, however, parallel interspecific growth rates reported for fishes alone (Howland and Masci, 1973b). In contrast, the scaling factor of the average semicircular canal radius in *Alligator mississippiensis* is not coincident with the growth rates reported in fishes, but is statistically identical to the scaling factors reported in interspecific mammalian studies (Spoor *et al.*, 2007).

Whether the explanation of this dichotomy in growth rates is phylogenetic (*i.e.*, a change in semicircular canal size to body mass scaling that occurs at the level of tetrapods or amniotes) or functional (*i.e.*, a change in scaling that occurs between fully aquatic species and species with some capability for terrestrial locomotion) remains unclear. Data on the size of whale semicircular canals relative to body mass is inconclusive. Although Spoor and colleagues report a higher RMA slope for whales relative to other mammals, this difference is not statistically significant (Spoor *et al.*, 2002). It is possible, however, that the lack of significance is a result of the high variance in the cetacean data, some of which is, perhaps, a result of the difficulty of matching body mass estimates to the sampled specimens. It is worth noting that, using the data from the whale study with the removal of only one outlying point (*Platanista gangetica*), when whales are compared to terrestrial mammals (*i.e.* not including the volant chiropterans, or the fully aquatic pinnipeds and sirenians), the RMA slopes are significantly different at the $p < 0.05$ level (Spoor *et al.*, 2002, computed from supplemental data).

These different growth patterns may represent a distinction in vestibular response during growth for two groups, although, whether those groups are phylogenetic or functional is unclear. Such a distinction is also

hinted at by the fact that pike do not show a change in the minimum horizontal angular acceleration required for stimulation despite changing semicircular duct size (Ten Kate *et al.*, 1970), but several species of frogs, which also exhibit ontogenetic increase in semicircular canal size (Dempster, 1930; Yamashita *et al.*, 1999), do show a decreasing minimum stimulation threshold (Yamashita *et al.*, 1999).

Ontogenetic size changes in the semicircular canal system of *Alligator mississippiensis* are not just limited to average size. Within in this overall change, there is a finer pattern of changing relative size between the canals themselves. The anterior canal grows significantly less quickly than does the posterior canal, while the rate of lateral canal growth is intermediate between the two (although it is closer to the rate of growth of the posterior canal). This pattern matches the pattern of relative growth reported in the semicircular ducts for the fish, *Lepomis gibbosus* (Howland and Masci, 1973) and is also comparable to the partial data from posterior and lateral ducts available for the pike (Ten Kate *et al.*, 1970).

Due to the presence of the overall size related pattern, be it phylogenetic or functional in nature, changes in the relative size of the semicircular canals can be interpreted in only one of two ways: 1) a historical pattern of ontogenetic change conserved to maintain the overall system relationships or 2) a compensatory change, in one or more canals, made in order to maintain overall system size relationships in response to the necessary growth pattern of a canal with more important functional responses. While the data available from this and previous studies do not distinguish between these interpretation, the evidence (including shape and orientation evidence discussed below), favors option two.

In the case of the growth of the semicircular canals in both *Lepomis*

gibbosus and *Alligator mississippiensis*, the anterior canal's growth trajectory is distinct from that of the posterior and lateral canals; specifically, it is more strongly negatively allometric. Furthermore, in both cases, the anterior semicircular canal is initially the largest of the three canals and, in *A. mississippiensis*, remains this way throughout growth[2]. Combine these two facts and the anterior semicircular canal maintains the most consistent functional response (based on its physical parameters) throughout growth.

Changes with growth also occur in the orientation of the anterior semicircular canal. In a 3-dimensional context, the three changing angles of the anterior canal sum to a rotation about an axis perpendicular to the plane of the posterior canal. This rotation brings the anterior canal to an alignment more parallel to a vertical plane throughout growth. One of the three significant orientation changes this overall movement includes is a decrease in the angle between the anterior semicircular canal and the posterior semicircular canal from the opposite system. This brings the anterior canal closer to the theoretically ideal coplanar alignment with the opposite posterior canal and increases the efficacy of the push-pull interaction between the responses of these two ducts.

Finally, ontogenetic changes also occur in the shapes of the semicircular canals of *Alligator mississippiensis*. Like the rates of growth, however, the magnitude of these shape changes is different for different canals. Of the three, the anterior semicircular canal exhibits the least change in shape. Once again, the anterior semicircular canal is the most

[2] According to the allometric formulae provided by Howland and Masci (1973b), the size of the posterior semicircular canal will overtake that of the anterior canal in *Lepomis gibbosus* of greater than 467 grams. This value is much larger than the average adult mass of these fish, but not outside of the normal range. According to the allometric formulae for *Alligator mississippiensis*, an alligator would have to reach a skull length of approximately 171 meters to have equally sized anterior and posterior canals.

conserved during these ontogenetic changes.

Shape changes in the anterior semicircular canal are too slight to be detected by simple linear measures, and the scaling factors for height and width and circumference are all statistically identical. Shape change over time is only significant, for the anterior canal, when tracking landmarks around the prootic-supraoccipital suture. Dramatic changes in canal circuit shape may have an effect on the canal's response by bending portions of the circuit out of plane or changing the circularity and therefore the proportion of functionally important parameters. This minor change in the linearity of a small section of the anterior canal is unlikely, however, to have any significant effect.

In contrast, the shape changes in the lateral and posterior semicircular canals are likely to have an effect on the response of the ducts inside. Both exhibit a change in the circularity of the canal circuit. In the lateral canal this change is sufficiently large to be detectable by simple linear measurement and is corroborated by landmark data. This shape change, however, is tied to the growth of the anterior canal. The utricular portion of the lateral semicircular canal is the same as for the anterior canal. The anterior canal, as discussed above is initially the largest of the three canals, and has the slowest growth rate overall. Therefore, it would be expected that aspects of the lateral semicircular canal that are related to the utricle (*e.g.*, the size of the canal parallel to the utricular contribution) would be initially over-sized and would grow more slowly than other portions of the lateral canal less dependent on the utricle (*e.g.*, the size of the canal perpendicular to the utricle). Furthermore, utricle-independent metrics might be expected to grow at a quicker rate to compensate for the retarded growth of the utricular portions and maintain an appropriate overall size change.

This is precisely the growth pattern observed in the lateral semicircular canal. The length of the ellipsoid axis parallel to the utricular portion of the canal exhibits the lowest scaling factor of any portion of the semicircular canal system. By contrast, the perpendicular axis exhibits the largest single scaling factor within the entire system (Table 2). This large discrepancy in growth rates produces a change in the circularity of the lateral canal circuit sufficient to potentially affect the response of the duct independent of the increase in size.

A similar pattern of coupled growth between the posterior semicircular canal and the anterior canal producing shape change is expected. The difference in this case is that the posterior canal shares the common crus with the anterior canal and this common crus is approximately perpendicular to the utricular portion of the posterior semicircular canal and, thus, the pattern expected is opposite that found in the lateral canal. That is, it is expected that the measures of the posterior canal parallel to the utricle will grow more quickly than the overall size of the canal while measures orthogonal to those (*i.e.*, parallel to the common crus) will grow more slowly.

Again, this expectation is born out in the growth pattern of the posterior semicircular canal. The largest scaling factor within the posterior canal is for the length of the axis parallel to the utricle, whereas the smallest factor is for the length of the axis perpendicular to the utricle (Table 2). These two values, however, are not statistically different. Landmark analysis, on the other hand, shows a clear and significant shape change, with an axis along the utricle increasing at a much faster rate than the axis orthogonal to it. The discrepancy in these values comes from the difficulties in applying the canal circuit estimation method to the posterior canal.

The method of calculating the canal circuit used in this study estimates the outer utricular wall based on other characteristics of the system (particularly the shape of the inner utricular wall). Thus, measurements more dependent on the position of the outer utricular wall are subject to higher rates of error. This is why for each of the three canals the relationship between skull length and the length of the axis perpendicular to the utricle has the lowest correlation coefficient. Of the canals analyzed in this study, the posterior canals were the most difficult to consistently estimate the utricular wall, and the correlation coefficient of this scaling factor is the lowest (r^2 = 0.83, next lowest r^2 = 0.93) for any scaling factor. The landmark analysis is specific to the canal-only region of the complete circuit and is not subject to the increased potential error from the utricular estimate. It is likely, therefore, that with a more accurate method of measuring the utricular portions of the canals a statistical difference between the two axes would be found that is congruent with landmark results and indicates a significant change in semicircular canal shape throughout growth.

All three of the semicircular canal shape changes indicate not only growth between the three bones of the otic capsule, but significant remodeling of the internal structure of each bone. This is in stark contrast to reports of bone remodeling in mammals. Studies in dogs (Frisch and Sørensen, 2000; Sørensen *et al.*, 1991), rats (Sørensen *et al.*, 1990a), pigs (1990b), and rabbits (1992) have shown a consistent pattern of bone remodeling in the otic capsule where bone remodeling rates are reduced to nearly zero the closer the bone is to the perilymphatic space. Whether the rate of bone remodeling in the otic capsule in *Alligator mississippiensis* is commensurate with the rates in other areas of the skull is unknown, but it is reasonable to assume that based on the changes occurring in that

area it is much higher than the rate reported in mammals.

The mammalian bone remodeling studies postulate that the unusual remodeling rates observed are, in some way, a result of the unusual physiological or electrochemical properties of the perilymph/endolymph system (Frisch and Sørensen, 2000; Sørensen *et al.*, 1990a; Sørensen *et al.*, 1990b; Sørensen *et al.*, 1991, 1992). Given the conservative nature of the physiology of the membranous labyrinth, however, and the implied difference in remodeling rates between mammals and *Alligator mississippiensis*, it is more parsimonious to assume that the explanation behind the pattern in mammals is unique to that group or, perhaps, to any organism with determinant growth.

CONCLUSIONS

Organisms such as *Alligator mississippiensis* and *Lepomis gibbosus* that exhibit growth of the semicircular canals throughout life do so with an allometry that parallels the allometry of adult specimens in similar broad interspecific groups. Whether these interspecific groups are, however, are more appropriately united by a functional or phylogenetic relationship is unclear; therefore, it is unclear whether these consistent allometries reflect responses to imposed functional demands, are simply phylogenetic baggage, or coincidence.

Furthermore, in *Alligator mississippiensis*, within the pattern of overall allometry, there is a sub-pattern of relative changes within each semicircular canal and between the different canals. The data here suggest that this sub-pattern is a result of differential importance of the canals; the anterior semicircular canal seems to hold the highest functional importance and therefore undergoes the least morphological change, while the changes in the other two canals can be explained by

their relation to the anterior canal. The importance of the anterior semicircular canal is further emphasized during growth by a realignment that occurs, moving the canal closer to its theoretical ideal position. Lastly, these data also suggest that there is an inherent difference in the bone physiology or the regulation of that physiology within the otic region in mammals and *A. mississippiensis*.

Chapter 4
Survey of Semicircular Canal Morphology across Amniotes

INTRODUCTION

A meaningful study of functional morphology has several requisite parameters. First and foremost is a functional complex that exhibits an array of morphologies (homology of the functional complex is nice, but analogous features sharing a function can suffice). A physical model that describes the link between the morphological features and the function of the complex helps explain, or, at a minimum, verifies the presence of, the functional change relative to the morphological variation. Lastly, in order for a study to be applicable in a broad context of vertebrate evolution, the morphological variations should be features that are observable in the fossil record.

The array of different morphologies observable in the vertebrate vestibular system has long been known (Gray, 1907, 1908a; Gray, 1955; Ramprashad *et al.*, 1986; Retzius, 1881, 1884). Furthermore, there is little doubt about the homology of the system across vertebrates (Maisey, 2001) [1]. The physical model of semicircular duct function, is complete and has been expressed fully via parameters that derive from the morphology and physical properties of the ducts themselves and the fluid inside (see Chapter 2).

Most previous studies of the morphology of the vestibular system that encompass a broad range of vertebrate taxa, have focused on the

[1] Hagfish are typically described as having a vestibular system with a single semicircular duct, with an ampulla at each end. This morphology does leave some question about homology; that it is homologous to other vertebrate systems is clear, but whether it represents a first appearance of a single duct, or whether it is homologous to the two duct system in lampreys, only without the common crus, is a matter of debate (Maisey, 2001).

soft tissue of the vestibule (*e.g.*, the semicircular ducts) and are, therefore, restricted to extant taxa (Curthoys *et al.*, 1977; Gray, 1906, 1907, 1908b; 1908a; Howland and Masci, 1973; Jones and Spells, 1963; Ramprashad *et al.*, 1984, 1986; Ten Kate *et al.*, 1970). More recent vestibular studies, which seek to have paleobiological significance, are limited, due to the lack of soft tissue in fossil specimens and the uncertainty of reconstructing the soft tissues of the labyrinth from the bony landmarks, to investigations of the bony labyrinth (Spoor *et al.*, 2002; Spoor *et al.*, 2007; Spoor *et al.*, 1996). None of these studies, however, have combined an examination of the shape of the semicircular canals (the features of the bony labyrinth that correspond to the semicircular duct portion of the membranous labyrinth) with an attempt at functional or behavioral correlation.

Therefore, as this study examines the shape of semicircular canals across a wide variety amniote taxa in which the canals are previously poorly studied, or completely unstudied, a comparative description of these semicircular canals and associated labyrinthine structures is undertaken here.

MATERIALS AND METHODS

Bony vestibular systems were examined across four broad amniote clades; varanoid squamates, carnivoran mammals, turtles (including tortoises), and crocodilians. All specimens were examined non-destructively through the use of a GE Lightspeed 16 X-Ray CT (see Chapter 3 for technical details). The vestibular regions were scanned bilaterally and up to three specimens of each taxon were scanned wherever available. All vestibular regions were scanned at the minimum possible pixel resolution (0.1875 mm) with 0.1 mm slice spacing.

CT images were processed using ImageJ (versions 1.36 and later,

NIH). Processing included reduction of volume to regions specific to the vestibular system, cubic spline interpolated image size increase for the smaller specimens, production of the semicircular canal planar images, and reformatting of data for production of endocasts. Digital endocasts were produced via manual segmentation of the volume data in Slicer3D (version 2.6, 2008, Brigham and Women's Hospital); post-processing of the surface volumes produced was performed in MeshLab (Cignoni *et al.*, 2007) and Blender (version 2.44, Blender Foundation, 2007).

The descriptions that follow are of a strictly qualitative nature. The reason for this is three-fold. First, subsequent aspects of this study will focus on the shape of these structures, a feature that is inherently independent of size. Secondly, many of the structures discussed in the following sections (*e.g.* volume of the vestibular cavity) are difficult or impossible to measure accurately in some specimens due to bony deficiencies, complicated morphologies and the nature of method of examination (CT imaging). Lastly, for the majority of the taxa described, the absolute size of the structures changes more with ontogeny than does the general shape (see Chapter 3).

SQUAMATES

The term 'semicircular canal' stems from of a generic mammalian view of canal morphology. Among amniotes, mammals most commonly evince a canal shape that closely approximates a circle. Among non-mammalian Amniota, however, the shape of the canals varies widely. Given this variation, it is difficult to label the morphology of any single canal system as a generalized example for all amniotes. Generalist squamates (those taxa not highly specialized for specific environments or extreme modes of locomotion), however, have a canal shape that shares

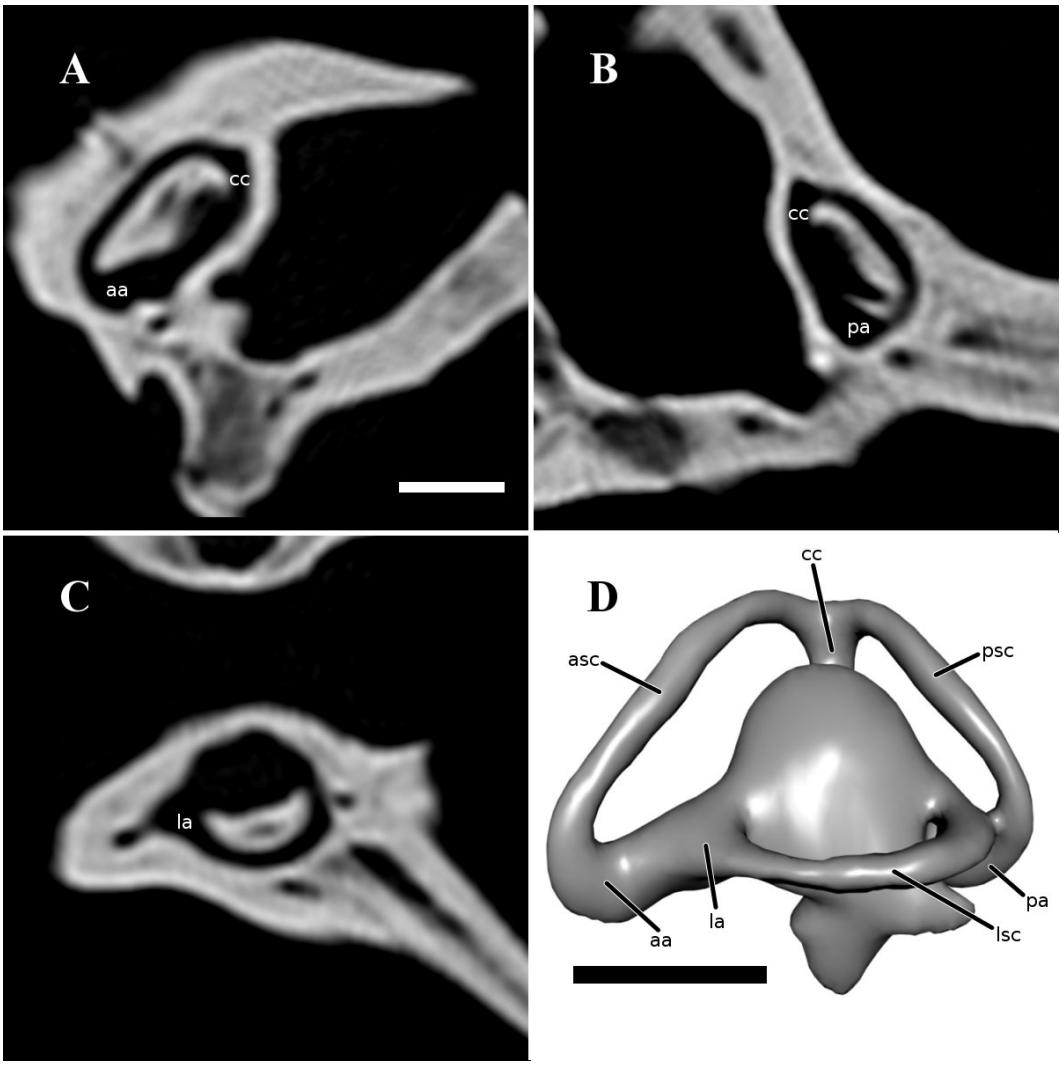

Figure 1: The semicircular canals of *Varanus salvator*. Planar images of the A) anterior, B) posterior, and C) lateral semicircular canals reformatted from CT data and D) digital endocast of the complete left bony labyrinth. Note that the direction of each planar image is roughly analogous to the canal's orientation in the endocast. aa – anterior ampulla, asc – anterior semicircular canal, cc – common crus, la – lateral ampulla, lsc – lateral semicircular canal, pa – posterior ampulla, psc – posterior semicircular canal. Scale bars = 5 mm.

at least some characteristics with most other groups. Therefore, the semicircular canal system of modern varanid lizards (Fig. 1D) will be described here as a starting point.

Varanus

In the varanid semicircular canal system, the short common crus arises from the vertically expanded bony vestibular cavity medial to the rounded peak of that cavity. The branching of the posterior canal is oriented postero-laterally along the horizontal, and that of the anterior canal is oriented at a slight angle above horizontal as it heads anterolaterally. The anterior canal (Fig. 1A) then traverses a very elongate course, the primary section of which is sub-linear and elevated only a small distance above the obliquely oriented wall of the vestibular cavity. A sharp ventral turn at the anterior end brings the anterior canal into communication with the anterior ampulla, the bony contour of which merges with the vestibular wall to form a complete anterior canal circuit.

The posterior semicircular canal (Fig. 1B), after branching from the common crus, runs a similar though less elongate path than the anterior canal. At its most posterior, where it gently bends ventrally, the bony posterior canal typically intersects, and is confluent with, the lateral canal, and its remaining course is ventral to the plane of the lateral canal. This communication is only a feature of the perilymphatic space and is not shared by the endolymph-filled membranous ducts.

The lateral semicircular canal (Fig. 1C), not including the portion of its circuit composed by the vestibular wall, is the most rounded of the three canals. The vestibular wall coplanar with the lateral canal bulges inward and produces a concave portion of the interior circuit of the lateral canal. In these cases, the interior circuit of the canal has an overall sub-circular appearance. The degree of vestibular bulge is an artifact of the relative size of the vestibule to the semicircular canal system and appears to be directly proportional to the overall size of the organism. In smaller individuals, such as a juvenile *Varanus niloticus*, this vestibular bulge can become exaggerated and produce a markedly slender, crescentic interior

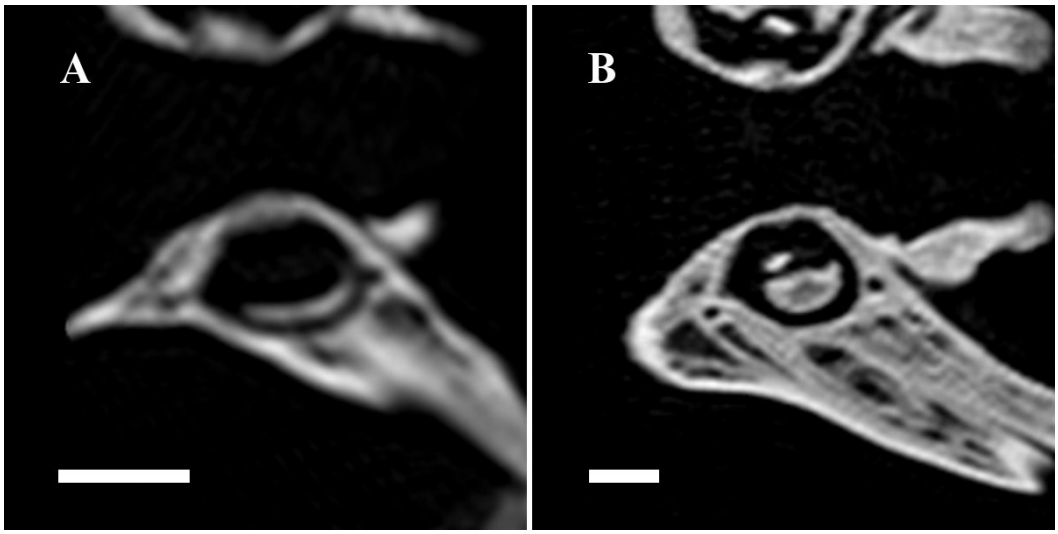

Figure 2: Planar images of the lateral semicircular canals of A) *Varanus bengalensis* and B) *V. komodoensis*. In the larger komodoensis, the vestibule is smaller relative to the lateral semicircular canal and, thus, a larger bony region is visible between the canal and the lateral vestibular wall. Scale bars = 5 mm.

circuit (Fig. 2A). In larger individuals, such as adult *V. salvator* and *V. komodoensis*, the bulge is less significant and the interior circuit of the lateral canal appears hemi-circular (Fig. 2B). It is important to note that this bulge in the vestibular wall is the contour of the saccule and not the lateral semicircular duct, which passes around the saccule to join the utricle on the medial side of the vestibular cavity.

Platecarpus

Within squamates, mosasaurs represent a fully aquatic radiation closely related to varanid lizards. In his monograph on American mosasaurs, Russell described the vestibular apparatus of mosasaurs based on the few aspects visible in disarticulated specimens and stated that, “The otic labyrinth of mosasaurs is practically identical to that of *Varanus*” (Russell, 1967, pg. 59). CT imagery of the mosasaurs *Platecarpus coryphaeus*, *P. tympaniticus* and *Tylosaurus neopaeolicus*, reveals that this, at least in the case of the semicircular canal system, is not the case.

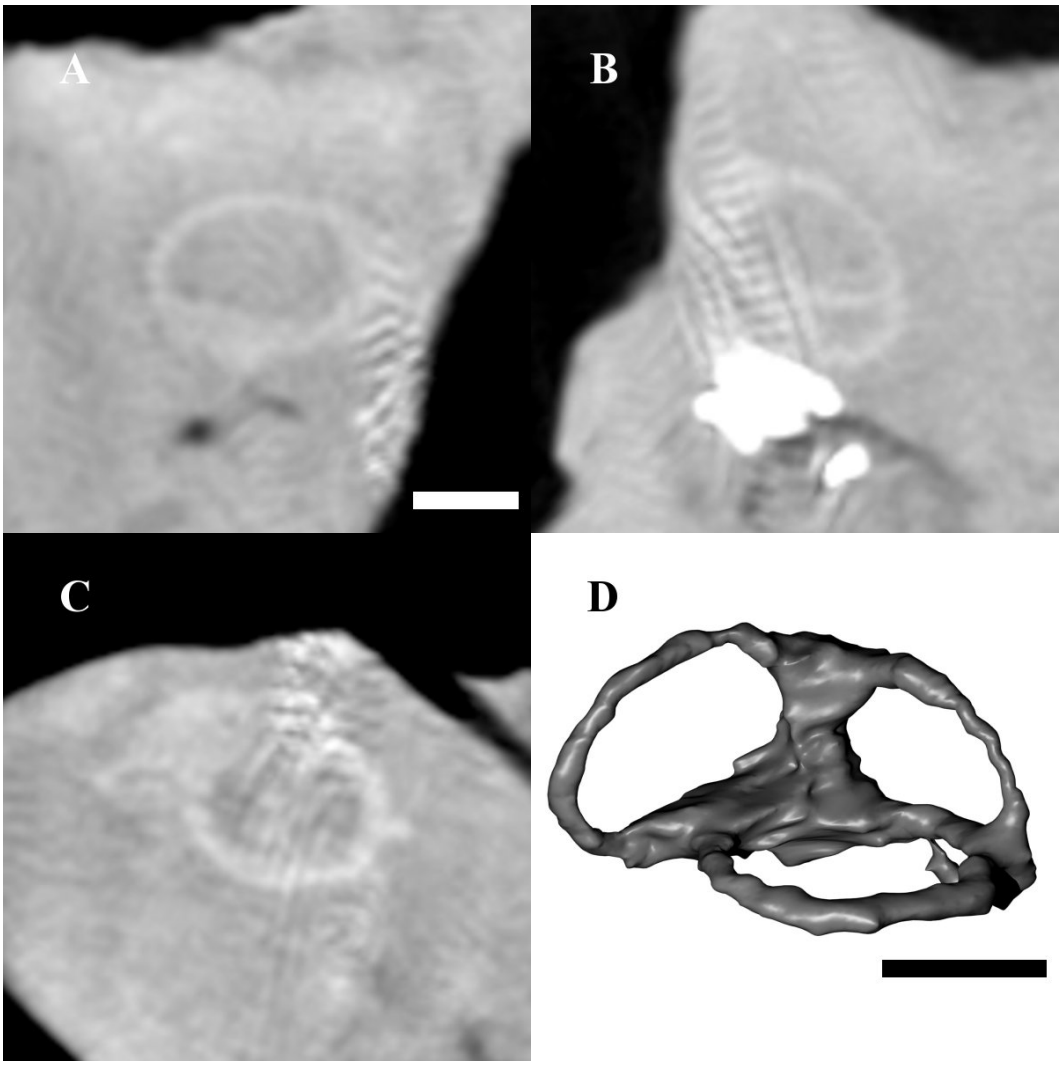

Figure 3: The semicircular canals of *Platecarpus coryphaeus*. Planar images of the A) anterior, B) posterior, and C) lateral semicircular canals reformatted from CT data and D) digital endocast of the semicircular canals and superior portion of the vestibule, partially reconstructed. Scale bars = 5 mm.

In *Platecarpus*, the posterior semicircular canal (Fig. 3B) does preserve the typical shape and conjoined relationship with the lateral canal seen in varanids. The interior circuit of the lateral canal of *Platecarpus* (Fig. 3C) does not, however, have the typical crescentic shape found in the varanid, meaning that the vestibular wall does not intrude into the approximately circular interior circuit of the canal. Most likely, this lateral

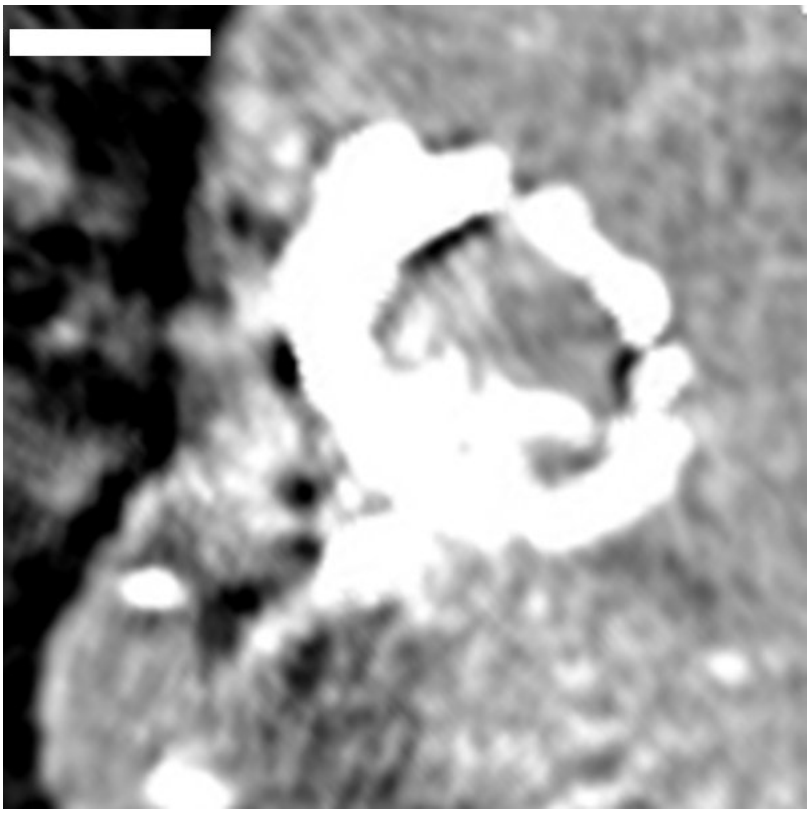

Figure 4: Planar image of the posterior semicircular canal of *Tylosaurus neopaeolicus*. Scale bar = 5 mm.

canal difference is simply a continuation of the size pattern seen among extant varanids; with a braincase nearly an order of magnitude larger than the largest modern varanid (*Varanus komodoensis*), *Platecarpus* has a semicircular canal system that has outgrown the vestibular system to such a large extent that the saccule wall barely impinges on the perceived circularity of the bony lateral canal.

The greatest difference between *Platecarpus* and the varanid condition, however, is in the anterior semicircular canal (Fig. 3A). Again, because of the large size of the canal system relative to the vestibule, the anterior canal circuit is mostly unaltered by incursion of the vestibular wall. Also, in place of the nearly linear segment of canal seen in *Varanus*, the anterior canal of *Platecarpus* maintains a gentle curve throughout its

length. Thus, in contrast to the varanid's elongate and slender anterior canal, the anterior canal of *Platecarpus* is more ovoid.

Tylosaurus

The semicircular canal system of *Tylosaurus* is generally very similar to that of *Platecarpus*. The anterior semicircular canal of *Tylosaurus* is nearly identical to that of *Platecarpus* (and therefore more ovoid and less elongate than the varanid anterior canal). The vestibular region is similarly small relative to the canal system and the saccule, therefore, does not cause the vestibular wall of the lateral canal to bulge toward the center of the canal to any great degree. The perilymphatic spaces of the lateral and posterior canals appear to be confluent. The posterior canal (Fig. 4), however, differs from both the *Varanus* and *Platecarpus* posterior canals in two ways: 1) an apparent lengthening of the posterior division of the utricle reorients the major axis of the elliptical canal path, bringing the axis into closer alignment with the horizontal; 2) while the posterior ampulla and a small section of the posterior canal are ventral to the plane of the lateral canal, much less of the overall course of the posterior canal is in this ventral position (*i.e.*, the posterior ampulla is much closer to being in the plane of the lateral canal).

MAMMALS

In the mammalian system, as stated above, the semicircular canals are generally very close to circular or elliptical in appearance[2]. This is in part due to the small size of the utricle and saccule relative to the semicircular canal system (thus, non-circular utricle or saccule

[2] The duck-billed platypus (*Ornithorhynchus anatinus*) is one example of a dramatic departure from circularity with a nearly triangular anterior semicircular duct and canal (Gray, 1908a).

contributions cause less significant deviations) and, in part, to the more inferior placement of the saccule relative to the utricle and semicircular canal systems (thus, the saccule rarely causes the vestibular wall to impinge on the path of any of the semicircular canals as it does in squamates). The semicircular canal system of mammals also shows less variation than is found across any other large amniote clade. In the majority of cases, morphological variation in mammalian semicircular canals is restricted to subtle differences in the elliptical eccentricity of the canal circuit and, occasionally, the dorsoventral location of the plane of the lateral canal relative to the vertical canals. For this reason, descriptions of the carnivoran bony labyrinth will be restricted primarily to the family level.

Canidae

The common crus of the canid semicircular canal system is tall with slight posteromedial deflection. Initially orthogonal to the superior wall of the anterior division of the utricle, the common crus rises to over half the height of the overall circuit of the anterior canal itself. The anterior semicircular canal (Fig. 5A), emanating from the superior end of the crus, curves superiorly for a significant distance before turning inferiorly again as it runs anterolaterally to the anterior ampulla. The straight and orthogonal nature of both the common crus and the anterior division of the utricle give the resultant anterior semicircular canal circuit a 'D' shaped appearance. A significant portion of the bone surrounded by the anterior canal is excavated by the opening of the subarcuate fossa.

The posterior semicircular canal in canids (Fig. 5B) takes on a different form than the anterior canal. From the top of the common crus, the posterior canal takes a course more horizontally than superiorly directed. At the end of this broad flattened curve, the canal turns inferiorly to join a sublinear common space for the posterior and horizontal

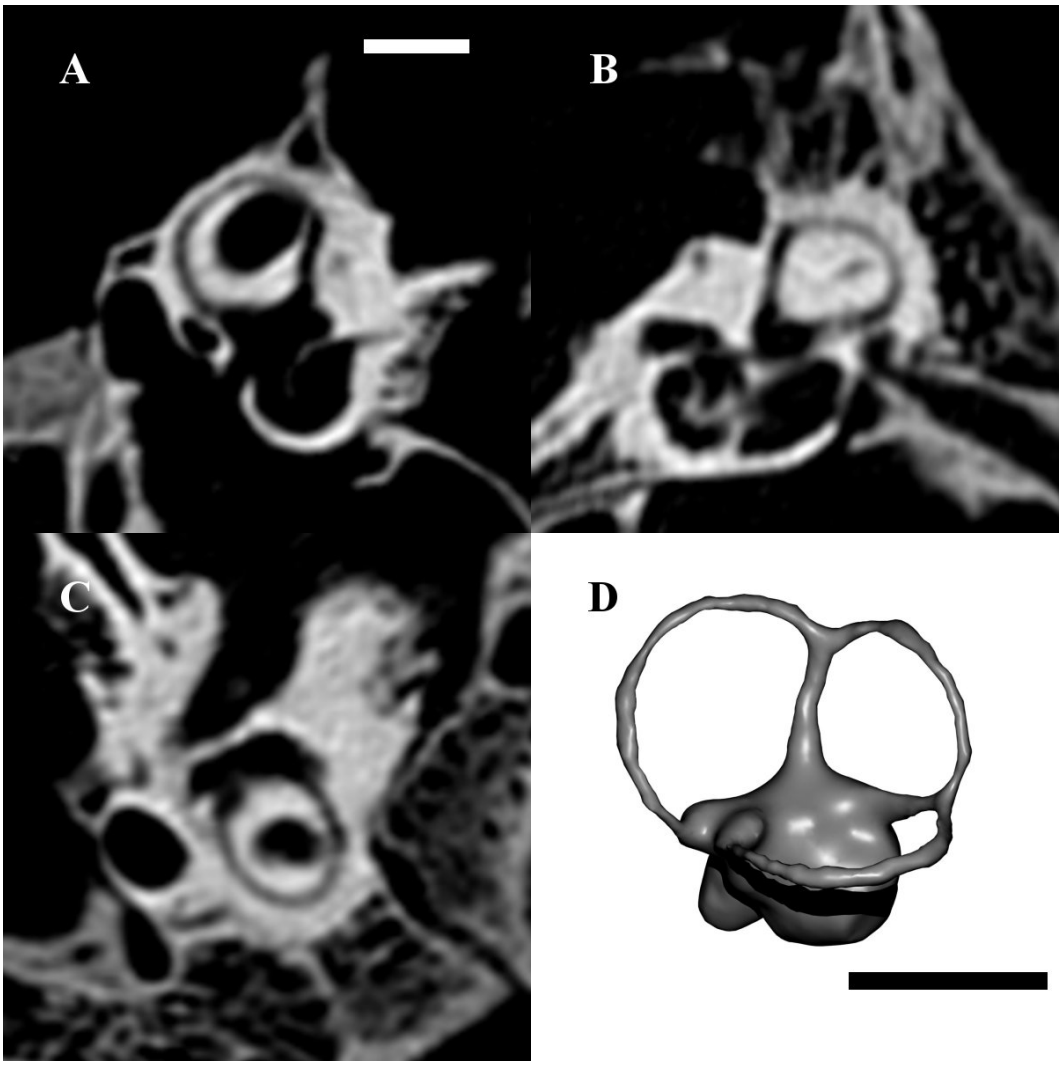

Figure 5: The semicircular canals of *Canis lupus*. Planar images of the A) anterior, B) posterior, and C) lateral semicircular canals reformatted from CT data and D) digital endocast of the complete bony labyrinth. Scale bars = 5 mm.

semicircular ducts. This narrow space passes directly anteriorly and inferomedially to join the bony posterior ampulla on the end of a very short posterior division of the utricle. The complete posterior semicircular canal circuit is, thus, longer than it is wide, with two significant sections that are approximately linear and at an acute angle to each other.

The canid lateral semicircular canal (Fig. 5C), as can be deduced

from the description of the posterior canal, lies in a plane level with the inferior portion of the posterior canal. Projecting posterolaterally from the lateral ampulla, the canal curves along a very circular course (only slightly broader along the mediolateral axis than along the anteroposterior axis) until it joins the sublinear section of common space between the lateral and posterior canals. Thus, the overall appearance of the lateral canal circuit is a very circular one with only minor posterolateral elongation and minor oblation of the posteromedial section.

The subarcuate fossa of canids is large relative to the structures of the inner ear and fills much of the space bounded by the three semicircular canals. Similar to the appearance of the anterior semicircular canal, the bone surrounded by the lateral semicircular canal is partially excavated. However, close inspection reveals that this excavation is a superior recess of the tympanic cavity that passes through the plane of the lateral canal, and not a diverticulum of the subarcuate fossa. Slightly superior to the plane of the lateral semicircular canal, this tympanic cavity recess is separated from the floor of the subarcuate fossa by a thin lamina of bone.

Mustelidae

The anterior semicircular canal of mustelids shares many characteristics with that of canids. The common crus is slender, tall, and perfectly orthogonal to the anterior division of the utricle. The course of the canal extends superiorly beyond the top of the common crus and curves gently around to join the anterior ampulla. In the otter subfamily, Lutrinae, the course of the anterior canal beyond its peak is more angular (Fig. 6A); it courses in a sublinear fashion until, just anterior to the anterior ampulla, it angles sharply to join this structure.

The posterior semicircular canals of mustelids do not differ in

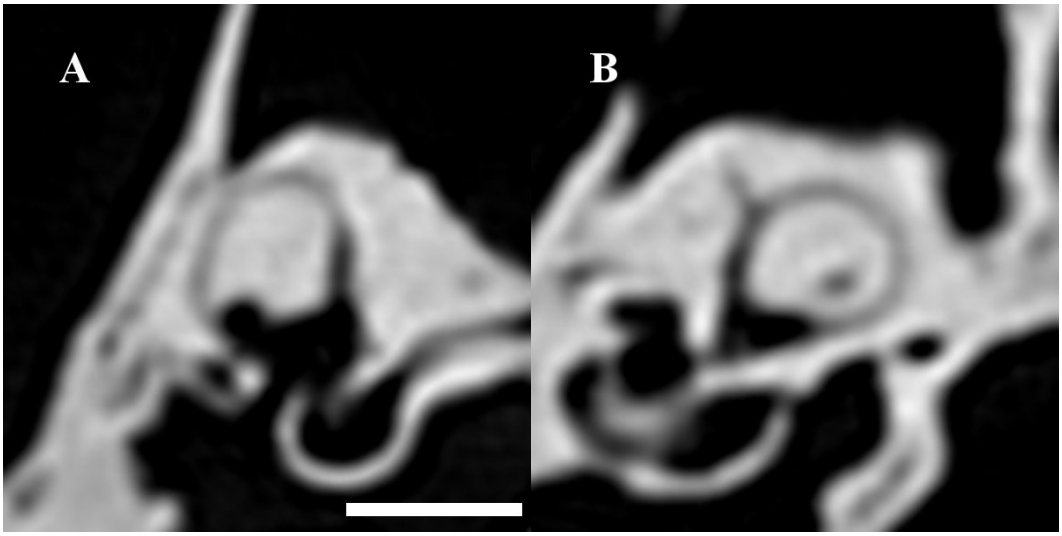

Figure 6: Planar images of the A) anterior and B) posterior semicircular canals of *Enhydra lutra*. Scale bar = 5 mm.

general from that of the canids. Minor increases in the relative robusticity of the common space for the posterior section of the lateral canal and the inferior section of the posterior canal are seen in some taxa (*e.g.*, *Taxidea* and *Pteronura*). One member of Lutrinae, however, does stand out with a distinct posterior semicircular canal morphology, *Enhydra lutris*, the sea otter. The circuit of the posterior canal of *Enhydra* (Fig. 6B) differs from the canid and mustelid templates in that the canal courses much further posterolaterally before curving inferiorly. As the posterior division of the utricle is not elongated, nor is the common space for the lateral and posterior canals, the canal must then pass anteromedially for a longer section of its inferior course to join the posterior ampulla. The end result is a posterior semicircular canal circuit that is much wider than it is tall.

The lateral semicircular canal of mustelids does not have the posterolateral expansion observed in the canid lateral canal. In general, the canal circuit is more circular, though the average smaller size of the mustelids means that frequently the circularity of the lateral canal circuit is

interrupted by the walls of the lateral ampulla and the utricular cavity, which are larger relative to the canals than in canids, particularly in the smaller forms such as the otter genus, *Aoynx*. The bone surrounded by the lateral canal, similar to the canids, exhibits some excavation by a superior recess of the tympanic cavity.

Ursidae

The anterior and lateral semicircular canals in the ursids examined are nearly identical to their counterparts in *Canis lupus*, with only minor characteristic changes in each. The posterior semicircular canal, however, resembles the ursid anterior canal more than it does the canid posterior canal.

In ursids, the common crus is taller relative to the overall height of the canal than in canids. In contrast to the canid system, however, any deviations of the common crus from linearity are in the anterolateral direction rather than the posteromedial one. Thus, rather than the 'D' shape of canids, the ursid anterior canal (Fig. 7A) is slightly more rounded. In one form, *Ursus maritimus*, the polar bear, this anterolateral deviation is more pronounced and the course of the anterior canal (Fig. 8) extends farther anterolaterally than in the canids before turning posteromedially to rejoin the ampulla. This extra curvature and longer course of the canal gives the overall circuit a wider appearance than the other ursid or canid canals. Ursids also exhibit a much larger entrance of the subarcuate fossa, which excavates most of the bone surrounded by the anterior canal, leaving only a thin wall of bone between the canal and the fossa in most places.

The posterior semicircular canal of ursids (Fig. 7B) closely resembles the anterior canal (except for *Ursus maritimus* where the difference is a result of the unusual anterior semicircular canal

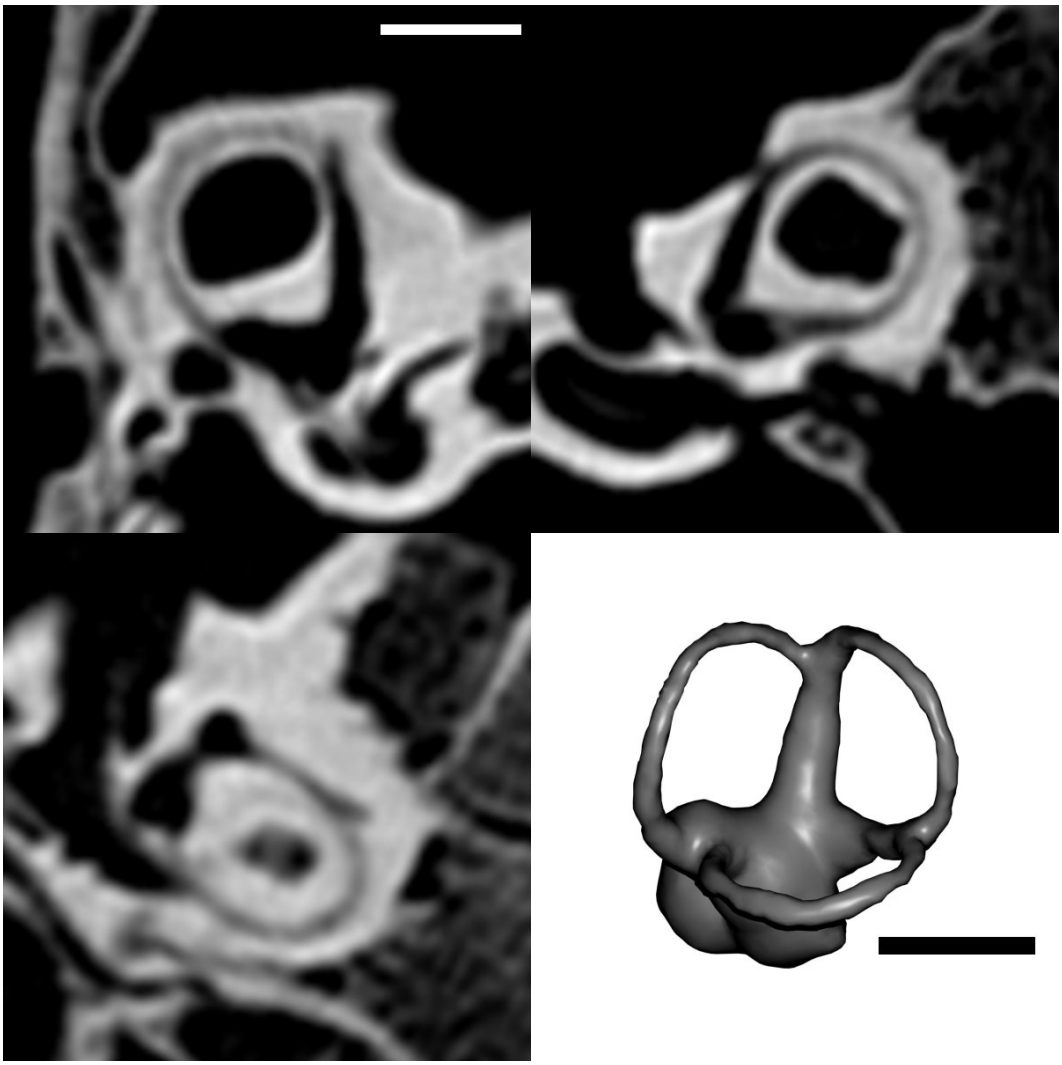

Figure 7: The semicircular canals of *Ursus americanus*. Planar images of the A) anterior, B) posterior, and C) lateral semicircular canals reformatted from CT data and D) digital endocast of the complete bony labyrinth. Scale bars = 5 mm.

morphology). A few very minor differences do exist. The common crus, in the plane of the posterior canal appears to be straighter than when viewed from the plane of the anterior canal. In this regard the ursid posterior canal resembles the anterior canal of canids. Secondly, the posterior division of the utricle is short, just as in the canids and mustelids, however, the common space for the posterior and lateral canals is also short, and

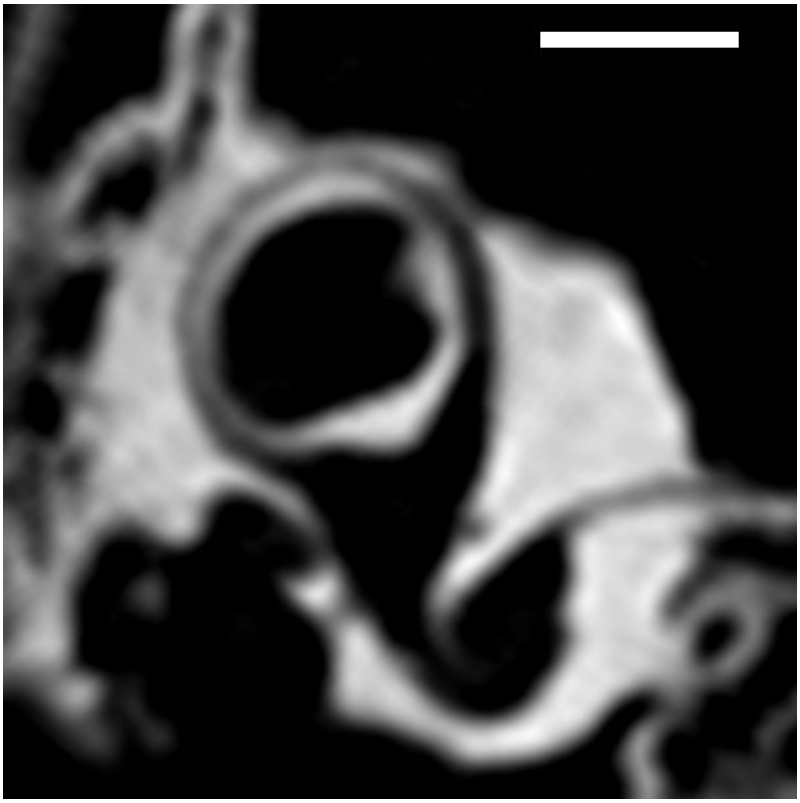

Figure 8: Planar image of the anterior semicircular canal of *Ursus maritimus*. Scale bar = 5 mm.

therefore its sublinear aspect does not interfere with the shape of the canal circuit. Thus, the posterior semicircular canal close to the ampulla curves gently superiorly, similar to the anterior canal, and does not extend in a sublinear fashion as in the canid posterior canal. Lastly, unlike in the canid, or mustelid posterior canal conditions, but similar to the ursid anterior canal condition, the ursid posterior canal surrounds bone that has been excavated by the subarcuate fossa. This posteriorly directed diverticulum of the subarcuate fossa excavates the majority of the bone surrounded by the posterior canal, though not quite to the same extreme extent as the opening to the subarcuate fossa excavates the bone of the anterior canal.

The lateral semicircular canal in ursids (Fig. 7C) is distinguishable

from that of the canids only on the basis of the amount of elongation in the postero-lateral direction. In the Ursidae, this elongation is even more pronounced than in *Canis lupus*. A small section of the bone surrounded by the canal has been excavated by the superior recess from the tympanic cavity, just as in the other mammalian lateral canals.

Otariidae

Otariidae do not show the same consistency of morphology of the semicircular canal system among taxa as is found in the other clades. Whereas the lateral and posterior semicircular canals are similar, the anterior semicircular canal of *Zalophus californianus*, deviates markedly from that of the other two otariids examined, *Arctocephalus galapagoensis* and *Callorhinus ursinus*.

The common crus in *Arctocephalus galapagoensis* is more robust than in any of the previously described systems. It rises to a height nearly one half that of the overall height of the anterior semicircular canal, as in other mammals. The appearance of the crus, however, is of a short structure due, in part, to it great thickness, but also to the overall reduction of the height of the anterior semicircular canal.

The anterior semicircular canal in *Arctocephalus* (Fig. 9A) rises from the common crus to quickly reach the canal's maximum height. Continuing anterolaterally, the canal curves only slightly and extends significantly beyond the anterior ampulla. From its most anterior point, the canal curves more sharply as it passes posteromedially to join the ampulla. The decreased overall height and greatly increased anterolateral excursion of the anterior semicircular canal gives the canal circuit an appearance that is much wider than it is tall, a marked deviation from the anterior canals previously described. There is partial excavation of the bone surrounded by the canal for an opening of the subarcuate fossa.

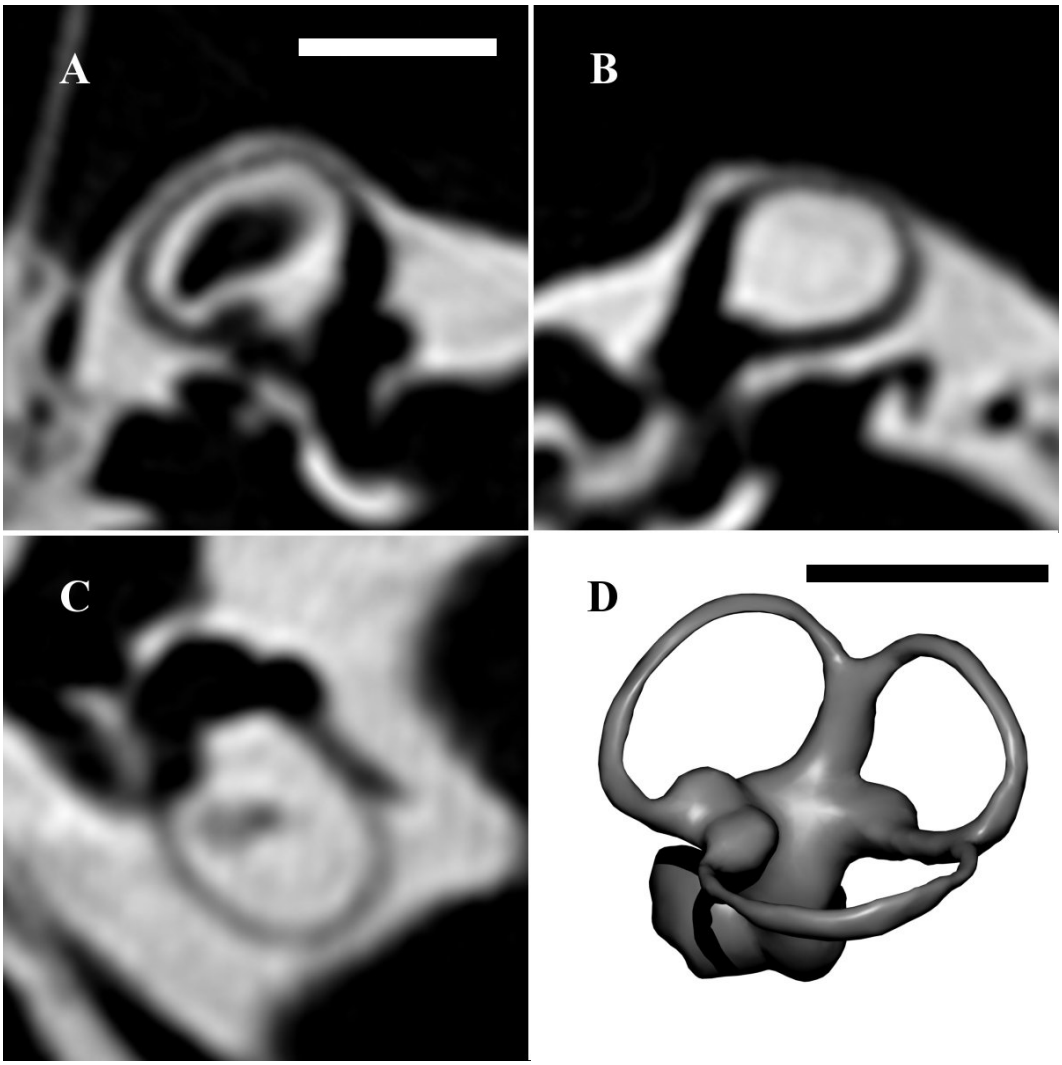

Figure 9: The semicircular canals of *Arctocephalus galapagoensis*. Planar images of the A) anterior, B) posterior, and C) lateral semicircular canals reformatted from CT data and D) digital endocast of the complete bony labyrinth. Scale bars = 5 mm.

In contrast, the anterior semicircular canal circuit of *Zalophus* (Fig. 10) appears much smaller relative to the bony vestibule than the circuit of *Arctocephalus*. The two canals share the elliptical shape with a major axis passing from anterior, lateral, and inferior to posterior, medial, and superior. As a result of the relative size differential, however, the canal circuit in *Zalophus* does not pass as far above the top of the common

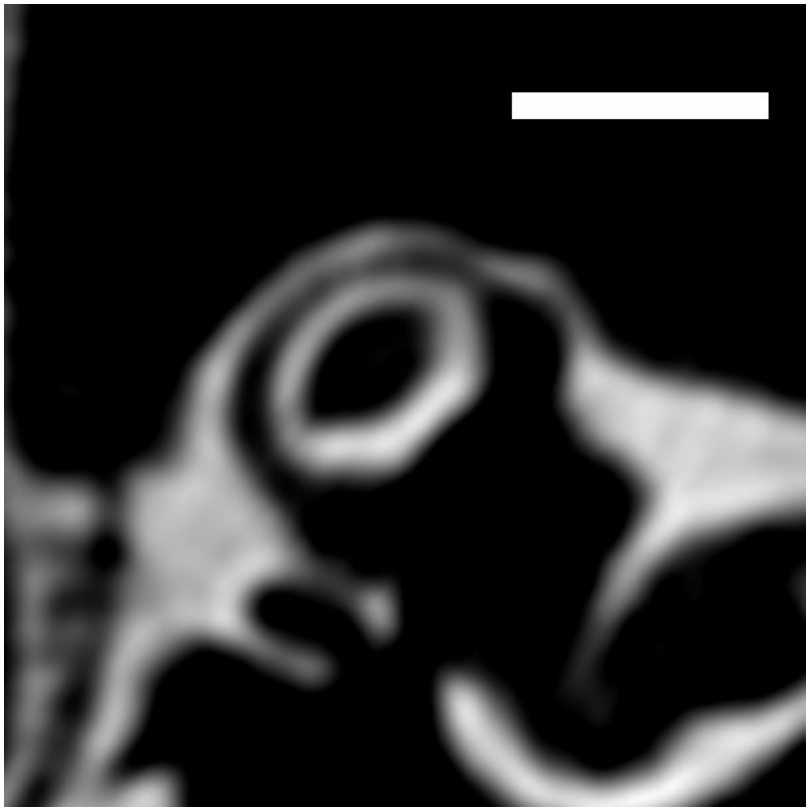

Figure 10: Planar image of the anterior semicircular canal of *Zalophus californianus*. Scale bar = 5 mm.

crus. Nor does the *Zalophus* anterior canal circuit extend significantly beyond the anterior ampulla. The difference in relative size also changes the proportion of bone excavated for the opening of the subarcuate fossa; in *Zalophus*, the opening is much larger relative to the canal size.

The posterior semicircular canal of *Arctocephalus* (Fig. 9B) more closely resembles it counterpart in other taxa than the anterior canal. Specifically, with a shortened posterior division of the utricle and posterolateral excursion greater than the overall canal height, the posterior canal closely resembles the posterior semicircular canal of canids. The primary difference between these two canals is the relationship with the cranial fossa. In canids, the posterior semicircular canal is lateral to the cranial fossa and surrounded by a significant region of dense petrous

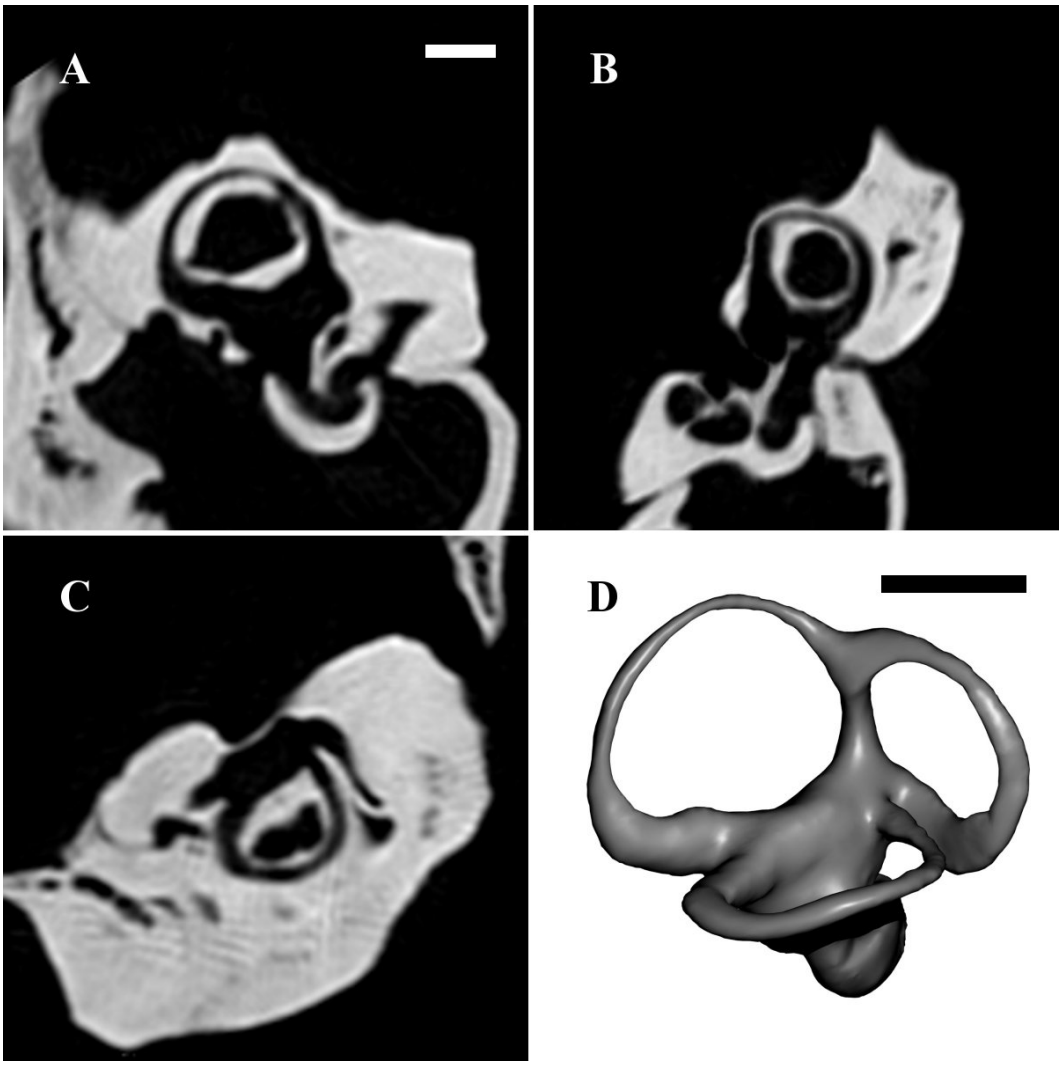

Figure 11: The semicircular canals of *Phoca vitulina*. Planar images of the A) anterior, B) posterior, and C) lateral semicircular canals reformatted from CT data and D) digital endocast of the complete bony labyrinth. Scale bars = 5 mm.

temporal bone. In *Arctocephalus*, the posterior canal is directly inferior to the cranial fossa and separated from it by only a thin lamina of bone. It is possible that this close contact of semicircular canal and cranial cavity may be driving some aspects of the canal's shape.

The lateral semicircular canal of *Arctocephalus* (Fig. 9C) is indistinguishable from that lateral canals previously described for canids and ursids. The canal circuit is elliptical in appearance with the major axis

of the ellipse oriented in a posterolateral direction. There is a significant segment along the posterior section of the circuit that is a shared space between the lateral and posterior semicircular canals.

Phocidae

Within phocidae the semicircular canal system, similar to the situation in otariids, is consistent in morphology for the posterior and lateral semicircular canals, but the anterior semicircular canal morphology is broadly divergent between phocid taxa.

The anterior semicircular canal of *Phoca* (Fig. 11A) arises from a common crus less robust than that of *Arctocephalus* and slightly anterolaterally curved. The canal curves gently superiorly before peaking at a midpoint along the anterolateral course and gently curving inferiorly until a sharp turn at the level of the elongate anterior division of the utricle brings the canal into immediate communication with the anterior ampulla. As in *Arctocephalus*, the overall impression is a canal circuit that is broader than it is tall. This is due more, however, to the straight and elongate utricular wall along the inferior portion of the circuit than to any deviations from circularity of the canal portion of the circuit. Most of the bone surrounded by the anterior canal is excavated by the entrance to the subarcuate fossa.

A second anterior semicircular canal morphology is evident in the phocid, *Hydrurga leptonyx* (Fig. 12). In *Hydrurga*, the common crus is as tall as the overall height of the anterior canal and has a slight anterolateral curve. The anterior semicircular canal itself diverges from the crus nearly horizontal and continues anterolaterally with slight inferior curvature to the course. The curvature increases as the path extends beyond, and turns back to rejoin, the ampulla. This increasing curvature results in an anterior canal with an ovoid shape, it's long axis roughly parallel to the

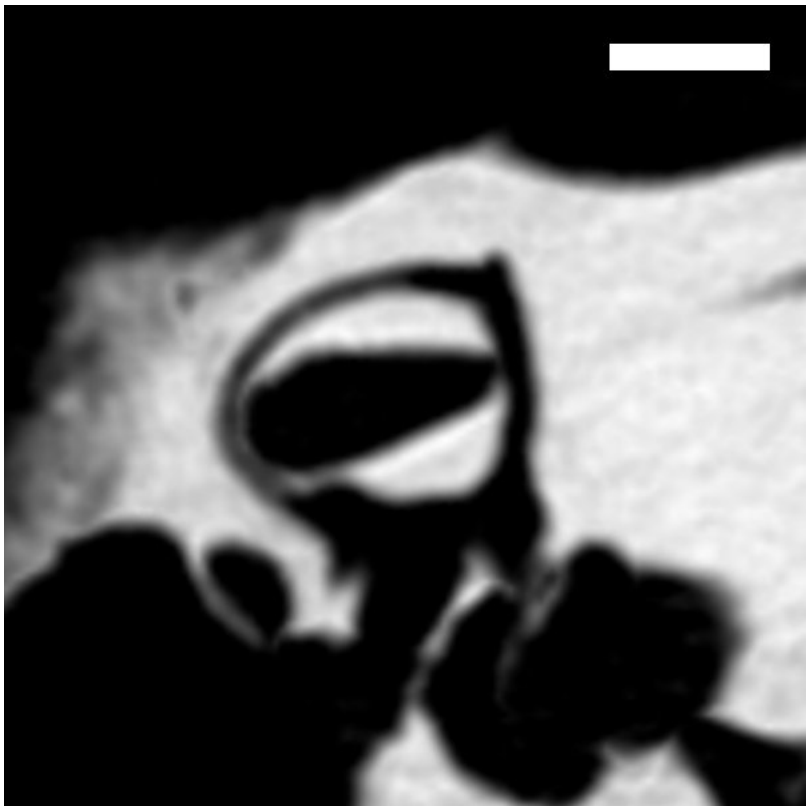

Figure 12: Planar image of the anterior semicircular canal of *Hydrurga leptonyx*. Scale bar = 5 mm.

wall of the anterior division of the utricle. The opening of the subarcuate fossa takes on a distinct shape in *Hydrurga*. It extends, horizontally across the entire space enclosed by the canal, but is vertically little more than half the height of the enclosed bone.

A third distinct anterior semicircular canal morphology is present in *Mirounga angustirostris* (Fig. 13). Unlike the previously two described anterior canals, the anterior semicircular canal in *Mirounga* appears taller than it is wide. The common crus, straight and robust, extends vertically for most of the height of the canal itself. The canal, similarly robust, rises from the common crus only slightly before turning inferiorly and continuing it anterolateral course in a gentle curve until it joins the anterior ampulla. The ampulla is elevated relative to the bony wall of the anterior division of

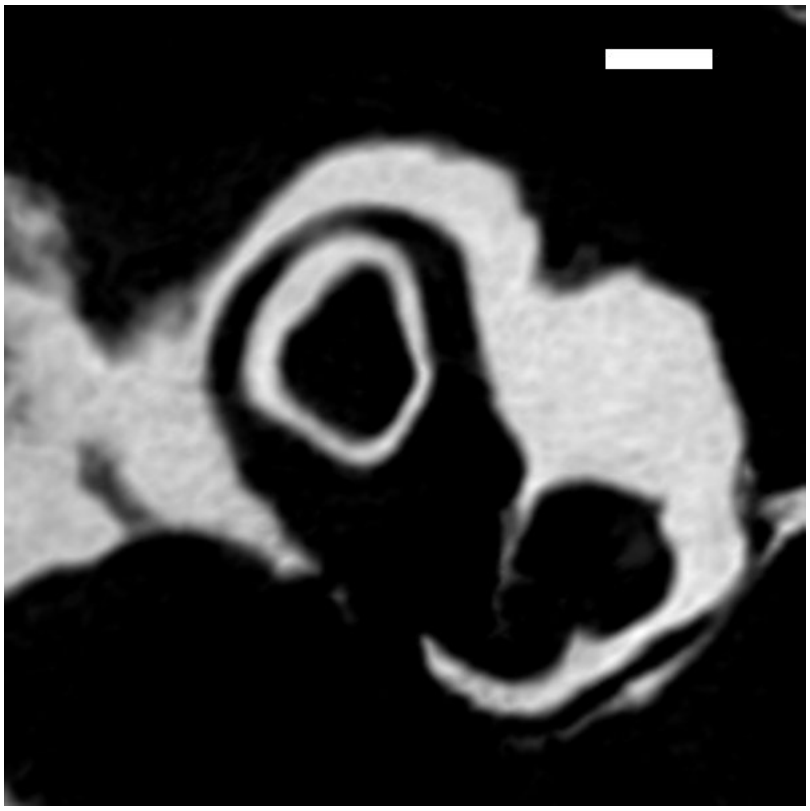

Figure 13: Planar image of the anterior semicircular canal of *Mirounga angustirostris*. Scale bar = 5 mm.

the utricle, leaving the appearance of a large depression between the ampulla and the base of the common crus. Although, without this depression the anterior canal circuit may be wider than it is tall, this deep valley in the utricular wall gives an irregular shape and a vertical appearance to the canal circuit. The opening of the subarcuate fossa, as in *Phoca*, excavates the majority of the bone surround by the canal circuit.

Despite the diversity among the anterior semicircular canals in phocids, the posterior and lateral canals show more conservation of morphology. The posterior semicircular canal in *Phoca* (Fig. 11B) emanates from the common crus horizontally before curving through an approximately 90° arc to join the posterior ampulla at the end of a robust but short posterior division of the utricle. The bone surrounded by the

posterior canal circuit is mostly excavated by a posteriorly directed diverticulum of the subarcuate fossa.

The lateral semicircular canal in phocids is distinct from the lateral canals previously described in the relationship with the posterior canal. The lateral canal remains coplanar with the inferior portion of the posterior canal, as in many of the previously described taxa; the posterior leg of the lateral canal circuit, however, is completely separated from the posterior canal by a wall of bone. There is no common space for the lateral canal and posterior canal or posterior division of the utricle. The lateral semicircular canal in *Phoca* (Fig. 11C) emerges from the lateral ampulla and curves evenly around in a posterior direction until a sharp turn medially leads to a sublinear posterior portion of the circuit. This posterior portion runs parallel to (but is not confluent with) the inferior portion of the posterior canal. The lateral canal then joins the vestibular wall near the middle where the common crus divides anterior and posterior divisions of the utricle. In *Hydrurga* and *Mirounga* the lateral canal circuit extends a little further posterolaterally before turning medially elongating the canal slightly until it resembles the lateral canals of ursids and otariids. Like the posterior canal, the bone surrounded by the lateral canal circuit is excavated by a diverticulum of the expanded subarcuate fossa. The extent of the excavation however does appear to decrease in the larger forms (*Hydrurga* shows less excavation than *Phoca*, and *Mirounga* less than *Hydrurga*).

TURTLES

Among Testudines, variations from the generalized semicircular canal description are dramatic, and several different morphologies can be found. Turtles all share a vestibular cavity that is less bulbous than that of

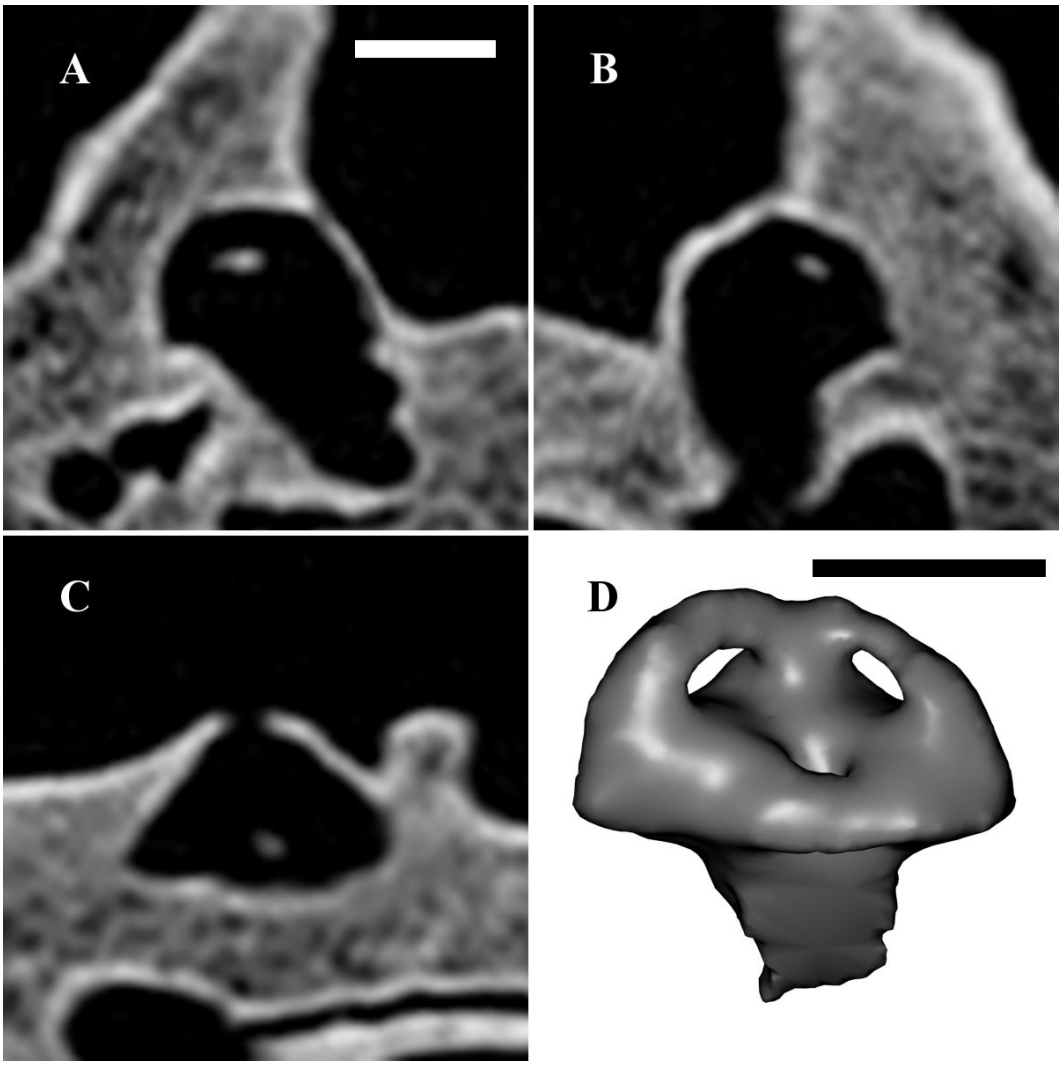

Figure 14: The semicircular canals of *Chelonoidis nigra*. Planar images of the A) anterior, B) posterior, and C) lateral semicircular canals reformatted from CT data and D) digital endocast of the complete bony labyrinth. Scale bars = 5 mm.

varanids in relation to the size of the canals. Thus, the common crus, which is as short or far shorter than in the varanid condition, arises from the very apex of the vestibular cavity.

Chelonoidis

For tortoises, such as those within the genus *Chelonoidis*, all three canals (Fig. 14) are wider relative to length than in Varanidae; also, the

anterior and posterior canals are more symmetrical. Each vertical canal (Figs. 14A & B) branches from the common crus horizontally, thus not rising above the level of the top of the common crus. Each then gently curves through an approximately 90° arc before reaching their respective ampullae. In smaller forms, such as *Chelonoidis denticulata* or *C. carbonaria*, the height of the common crus is less than the length of the of the anterior division of the utricle, giving the anterior semicircular canals a slight appearance of being longer than they are tall. In larger taxa, such as *C. nigra*, however, the common crus and the anterior division of the utricle are sub-equal in length and the anterior canal has a more circular appearance. The lateral canal (Fig. 14C) is very close in shape and thickness to the two vertical canals and also traces an even 90° arc as it passes anteriorly from its common bony space with posterior division of the utricle to the lateral ampulla.

The ampulla, utricular region and common crus are even thicker than the robust canals themselves, leaving little distinction of the boundary between ampulla and semicircular canal. Even in smaller members of *Chelonoidis*, distinction between ampulla and semicircular canals is difficult, which is in contrast to most other groups in which the smaller members have thinner semicircular canals and, as a result, greater distinction between bony canal and bony ampulla.

The robusticity of the semicircular canals in *Chelonoidis* has a second effect on the appearance of the system. The canals are so thick relative to the radius of curvature of the canal circuit, that there is almost no room for bone along the interior aspect of the canal and all that is left is a thin, gracile strut of bone.

Gopherus

In general, the gopher tortoises have a semicircular canal system

morphology indistinguishable from that of the smaller members of *Chelonoidis*. This includes the robust canals with the rounded symmetrical canal circuits and the anterior division of the utricle, slightly longer than the common crus, producing the slight longer than tall appearance of the anterior semicircular canal and the reduced bone of the interior canal circuits.

One particular member of the genus, *Gopherus polyphemus*, however, diverges from this morphology. In *G. polyphemus*, the bony vestibule has become greatly enlarged. This cavity has expanded to such an extent that the morphology of the semicircular canals surrounding it has been significantly modified. Most prominently, the bony vestibule has expanded laterally and engulfed the complete lateral semicircular canal. In a few specimens, a faint excavation on the lateral side of the vestibular cavity that represents the only remnant of the lateral canal is visible (Fig. 15A).

The hypertrophied vestibular cavity also alters the morphology of the two vertical semicircular canals. The common crus is not taller than is expected based on comparison to specimens of *Chelonoidis* or other species of *Gopherus*. The lateral expansion of the vestibular cavity, however, also includes the utricular portion and therefore, both the anterior and posterior ampullae are displaced along extended anterior and posterior divisions of the utricle. The results of this elongation of the utricular region are anterior and posterior semicircular canal circuits that are longer than they are tall. Furthermore, the circuits are not evenly rounded, but rather triangular as the canal sections course straight from the top of the common crus to the ampullary region.

The semicircular canals in *Gopherus polyphemus* themselves are less robust than in *Chelonoidis* or the other species of *Gopherus*.

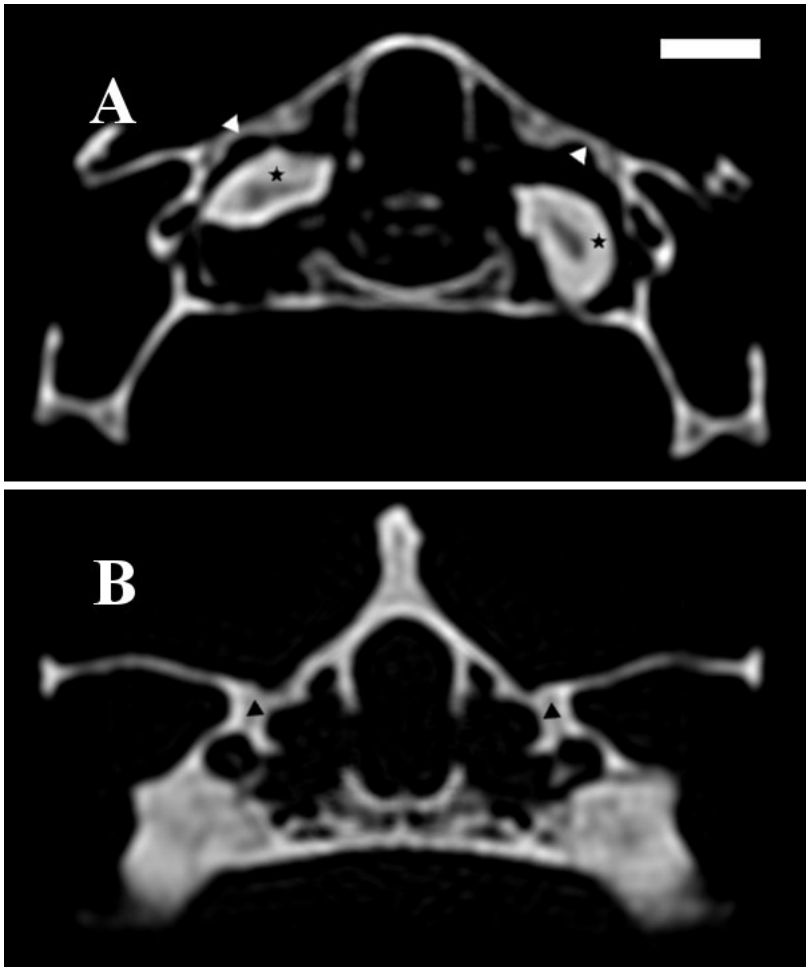

Figure 15: Coronal CT slices through the vestibule of A) *Gopherus polyphemus* and B) *G. agassizii*. In *G. polyphemus* the bony vestibule has increased in size and only a faint contour representing the lateral semicircular canal (white arrows) is visible. The expansion of the vestibule is correlated with the presence of very large otoliths (black stars). In *G. agassizii*, the bony vestibule is much smaller relative to skull size and a greater portion of the lateral canal contour (black arrows) is visible. As a result of the robusticity of the lateral canal, however, there is still no bony distinction between the medial wall of the canal and the lateral wall of the vestibule.

Nonetheless, the bony separation between canal and vestibular wall in the vertical semicircular canals is very reduced as a result of vertical expansion of the vestibular cavity. It is worth noting, however, that in *G. agassizii* the very robust nature of the semicircular canals, combined with the small average size of the skull, produces an effect similar to that seen

in *G. polyphemus*. That is, in *G. agassizii*, there is no bony distinction between the lateral wall of the vestibule and the lateral semicircular canal. Nonetheless, because this is a result of the semicircular canal and not an expansion of the vestibule, the lateral canal is clearly identifiable (Fig. 15B), unlike in *G. polyphemus*.

Carettochelys

Many members of the turtle clade are fully or partially aquatic. These aquatic groups account for many of the different morphologies found across the semicircular canal systems of turtles. The variations range from morphologies similar to that described for the genus *Chelonoidis*, with the notable difference that the system is elongated along an anteroposterior axis, to systems with slender canals and vestibular regions much more comparable to the varanid condition. An example of the former is found in the fully aquatic pig-nosed turtle, *Carettochelys insculpta*. Although certain aspects of this elongation of the vertical canals are superficially similar to that observed in *Gopherus polyphemus*, the vestibular cavity in *C. insculpta* is not hypertrophied relative to other turtles and therefore does not appear to be the primary factor driving this morphology. This anteroposterior stretching is most prominent in the shape of the anterior canal (Fig. 16A), though the posterior (Fig. 16B) also appears to be slightly lengthened relative to its height.

Neither the expansion of the vestibule nor the robusticity of the semicircular canals are as extreme in *Carettochelys insculpta* as they are in the *Chelonoidis*. Therefore, more bone is visible along the interior of each canal circuit. Furthermore, the slight reduction of the vestibular cavity causes a partial separation of the saccular portion of that cavity from the common space of the posterior utricle and posterior segment of the lateral canal. Thus, in *C. insculpta*, there is superficially a return to the

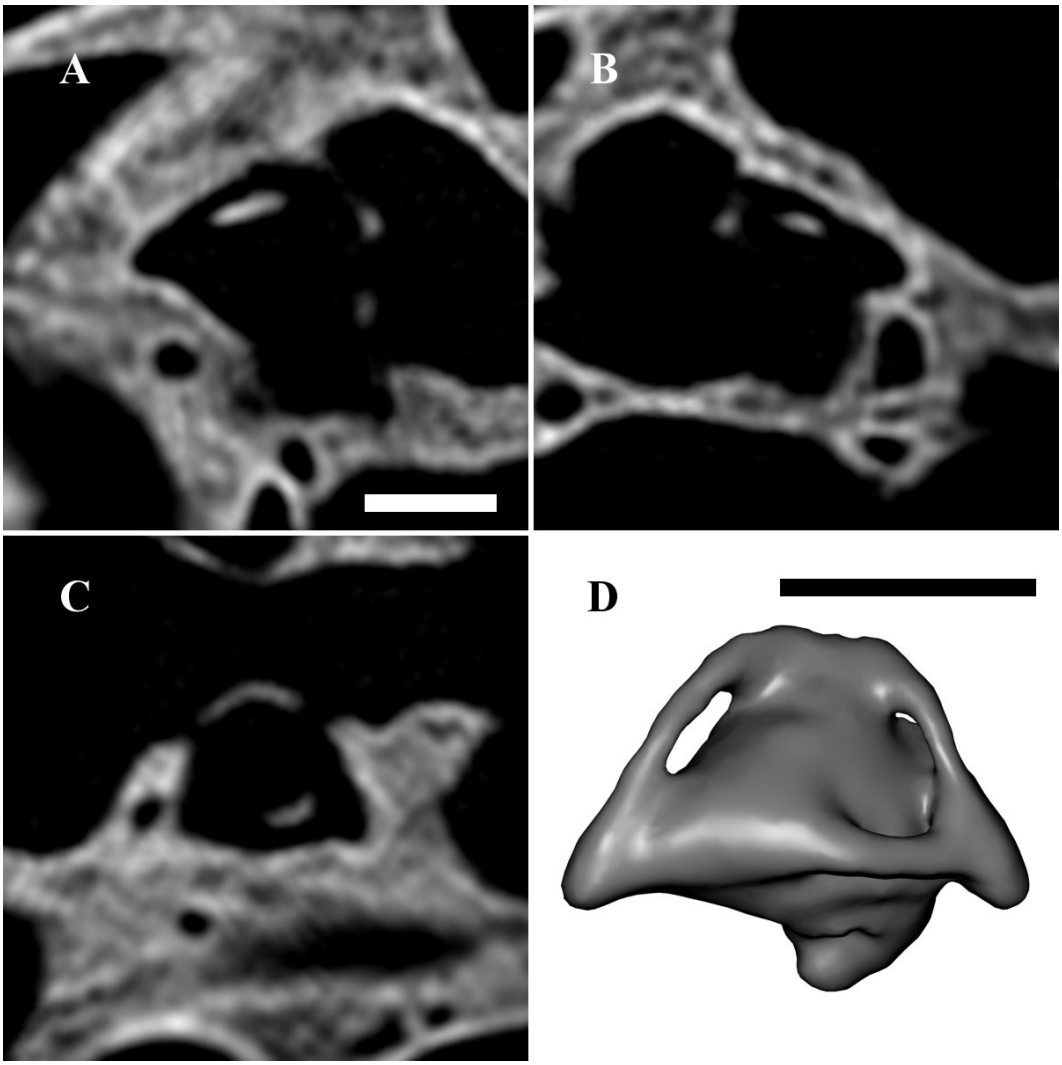

Figure 16: The semicircular canals of *Carettochelys insculpta*. Planar images of the A) anterior, B) posterior, and C) lateral semicircular canals reformatted from CT data and D) digital endocast of the complete bony labyrinth. Scale bars = 5 mm.

crescentic appearance of the lateral canal's interior circuit (Fig. 16C) exhibited by the smaller members of the genus *Varanus*. The difference in *C. insculpta* is that the interior crescentic region of bone appears to be more posterior positioned since a portion of it is found along the interior aspect of the posterior utricular cavity.

Chelydridae

The snapping turtles *Macrochelys temminckii* and *Chelydra*

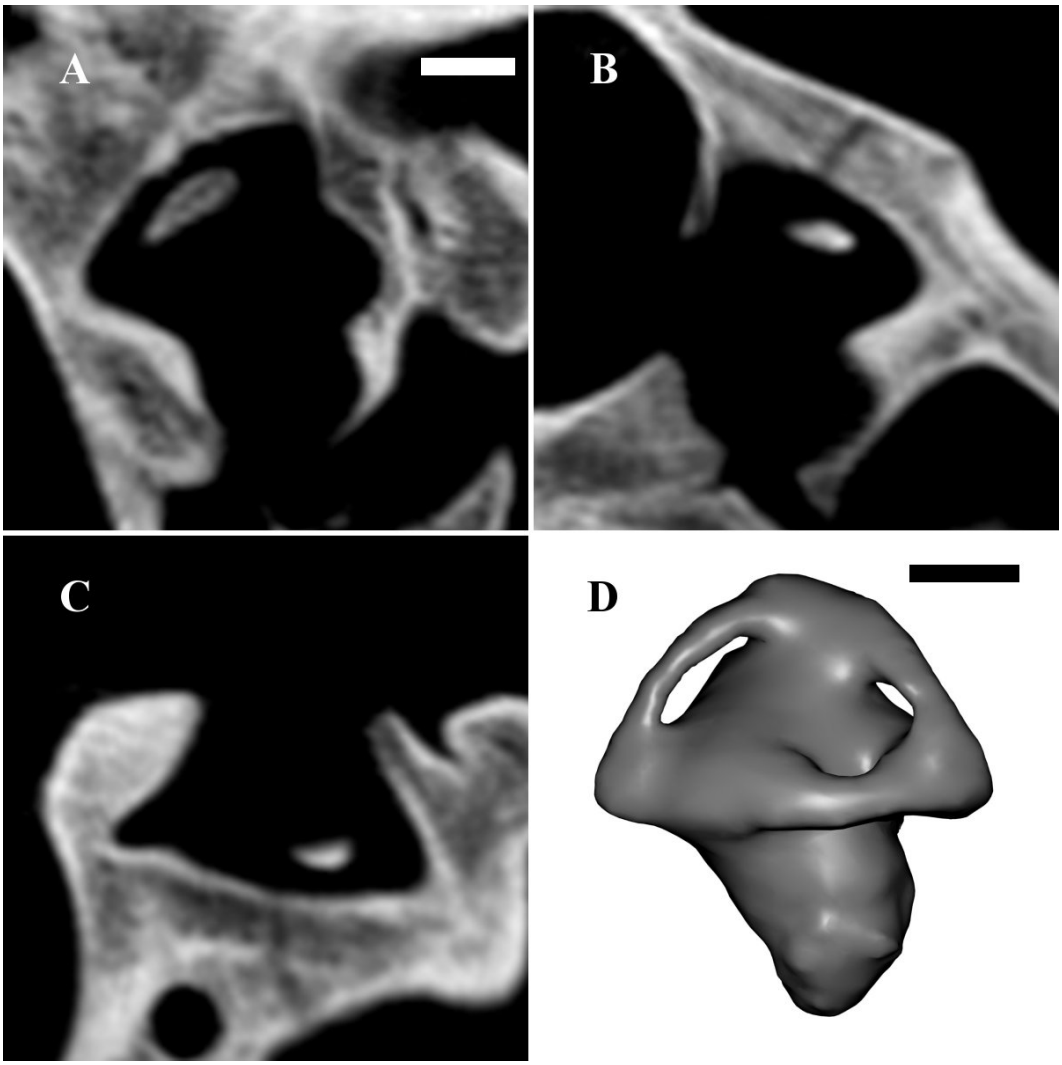

Figure 17: The semicircular canals of *Macrochelys temminckii*. Planar images of the A) anterior, B) posterior, and C) lateral semicircular canals reformatted from CT data and D) digital endocast of the complete bony labyrinth. Scale bars = 5 mm.

serpentina have semicircular canal shapes similar to those of *Carettochelys insculpta*. The anteroposterior elongation of the vertical canals relative to the rounded shape in *Chelonoidis* is more pronounced than in *Carettochelys insculpta*. The elongation of the anterior semicircular canal (Fig. 17A) has progressed to such an extent that most curvature of the canal between the common crus and the ampulla has

been obliterated. Instead, the canal takes a sub-linear course that closely parallels the vestibular wall. Thus, the interior circuit of the anterior semicircular canal has become a long, very slender sliver of bone.

The crescentic appearance of the interior of the lateral canal circuit (Fig. 17C) is lessened in Chelydridae relative to *Carettochelys*. This is likely a result of an increase in overall size (both *Macrochelys* and *Chelydra* are, on average, larger than *Carettochelys*), similar to the change in lateral canal appearance that results from increases in size in varanids.

Chelidae

In the pleurodires *Chelus fimbriatus* and *Chelodina longicollis*, the morphology of the semicircular canals deviates tremendously from that of any other turtles examined thus far. The anterior (Fig. 18A) and lateral (Fig. 18C) canals closely resemble those of varanids. The posterior canal (Fig. 18B), however, more closely resembles the typical posterior semicircular canal of other turtles than the posterior canal of varanids.

The anterior canal is elongate with a significant sublinear section of its circuit, just as in the varanid canals. The typical turtle expansion of the vestibular cavity, which is slightly exaggerated in Chelidae, produces an even more slender aspect to the interior of the circuit than in Varanidae. The lateral semicircular canal differs from the varanid lateral canal in its position near the level of the posterior ampulla rather than intersecting the course of the posterior semicircular canal more superiorly. It is similar to the varanid canal, however, in that it is as slender as the anterior and has, taking the canal only section of the circuit and the common space for the posterior utricle and posterior portion of the lateral canal into account, a very similar nearly circular overall circuit. The exaggerated expansion of the vestibular cavity, however, obliterates the majority of the bone on the

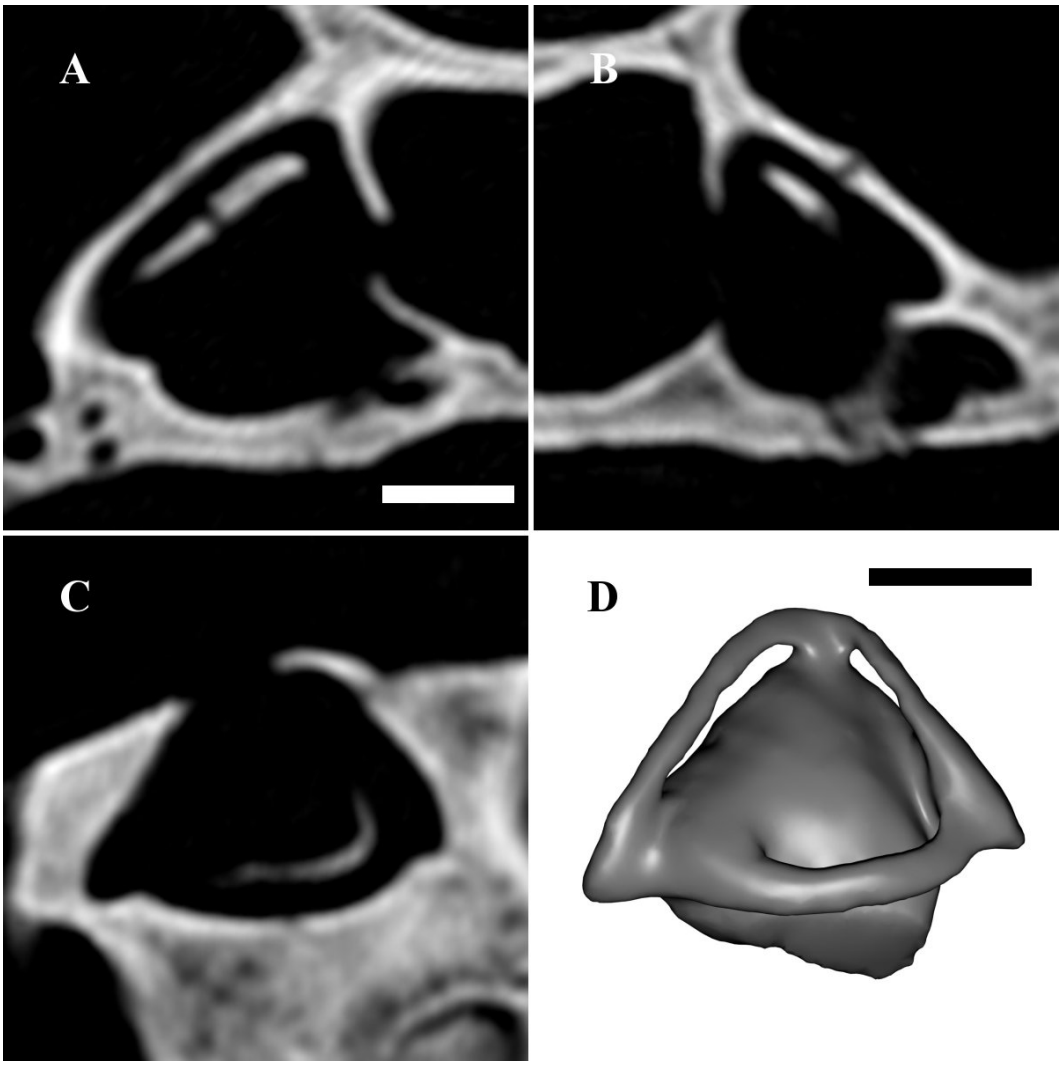

Figure 18: The semicircular canals of *Chelus fimbriatus*. Planar images of the A) anterior, B) posterior, and C) lateral semicircular canals reformatted from CT data and D) digital endocast of the complete bony labyrinth. Scale bars = 5 mm.

interior of the circuit and leaves only a very slender, crescentic, sliver of bone between the canal and the vestibular wall.

The posterior semicircular canal appears more robust than the anterior canal, however, this is due to its slightly shorter and more typical circuit. Overall, the posterior semicircular canals of these two chelids are indistinguishable from the posterior canals of the other aquatic turtles

already described.

Cheloniidae & Dermochelyidae

The morphology of the semicircular canal system in sea turtles more closely resembles the morphology observed in *Chelonoidis* and *Gopherus* than it does the other aquatic taxa already discussed (*Carettochelys*, *Chelus*, *Chelodina*, and Chelydridae). Despite these superficial similarities, however, there are numerous aspects of the semicircular canal system that give sea turtles a different typical semicircular canal morphology from all other turtle groups. The greatly larger head size of many sea turtles relative to that of tortoises means that semicircular canal and vestibular systems are also larger and therefore many effects due to size seen in the tortoises are mitigated in the sea turtles. For example, though the semicircular canals are particularly robust in sea turtles, as in *Chelonoidis*, the relative circuit diameter is large enough that there is significantly more bone circumscribed by the canal than the gracile strut seen in the tortoises.

All the semicircular canals of sea turtles share the round canal circuits and robust canals of the tortoises, but the vertical canals of Cheloniidae do show minor anteroposterior elongation, particularly in the anterior canal. This elongation is no more pronounced than that of the smaller members of *Chelonoidis*, however, these sea turtles are much larger than those small tortoises. Furthermore, this elongation of the vertical semicircular canals is found from small specimens (*Lepidochelys kempii*, and *Eretmochelys imbricata*) up to the largest in this study (*Caretta caretta*). It is unlikely, therefore, that this shape in this group is strictly a size artifact, as it may be for *Chelonoidis*.

In contrast, *Dermochelys coriacea* does not show any elongation of the vertical semicircular canals along the anteroposterior axis. Instead,

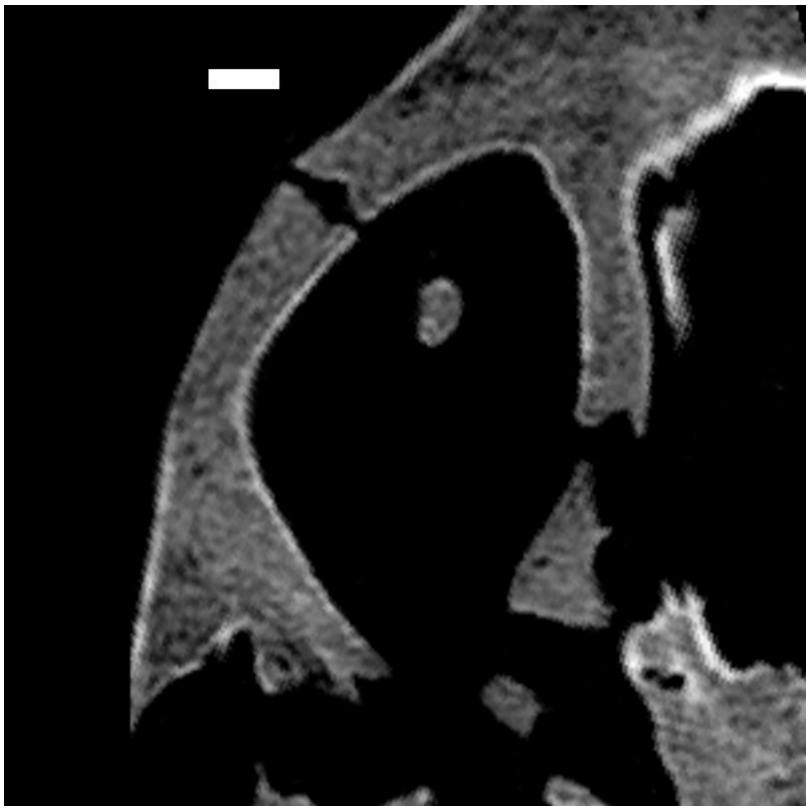

Figure 19: Planar image of the anterior semicircular canal of *Dermochelys coriacea*. Scale bar = 5 mm.

there is deviation from the circular tortoise form by superior elongation of the anterior semicircular canal (Fig. 19). This superior elongation is a result of the anterior canal continuing superiorly after it branches from the common crus before it arcs inferiorly toward the anterior ampulla. This anterior canal course is unique among the turtles examined, and gives the anterior canal a circuit shape that is taller than it is wide.

In some taxa, *Dermochelys coriacea* in particular, the lateral canal can be difficult to discern as a result of the robust canal blending with expanded ampullary and posterior utricular cavities. In overall form, however, the lateral semicircular canal of the sea turtles is indistinguishable from that of the larger tortoises, such as *Chelonoidis nigra*.

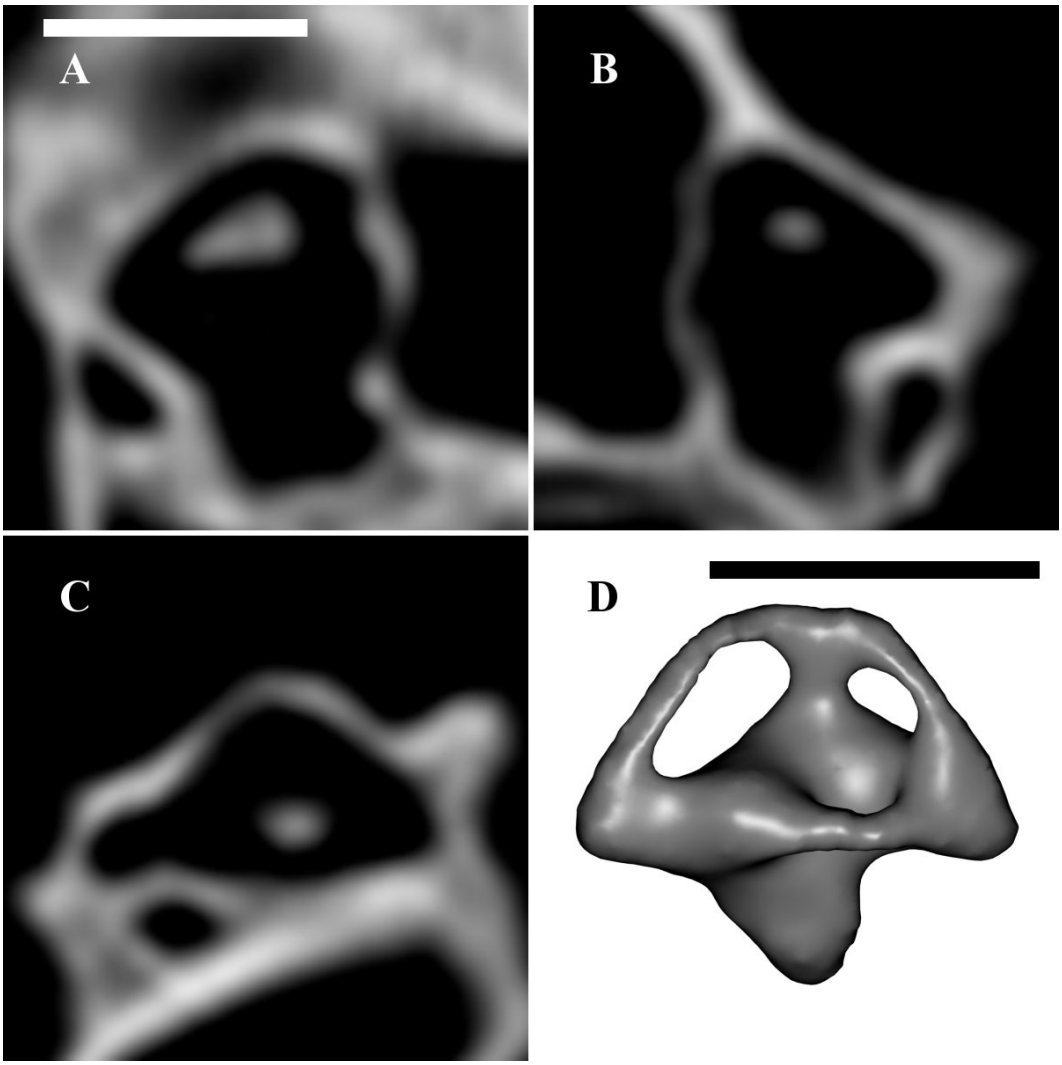

Figure 20: The semicircular canals of *Terrapene carolina*. Planar images of the A) anterior, B) posterior, and C) lateral semicircular canals reformatted from CT data and D) digital endocast of the complete bony labyrinth. Scale bars = 5 mm.

Emydidae

Within the family Emydidae there are two contrasting semicircular canal system morphotypes. The more terrestrial members, box turtles (genus *Terrapene*) and wood turtles (genus *Clemmys*), each have canals that echo the shape and the robust and symmetrical nature of the semicircular canal system seem in smaller members of *Chelonoidis*. That is, while close to circular in shape, the vertical canals (Fig. 20A & B) in

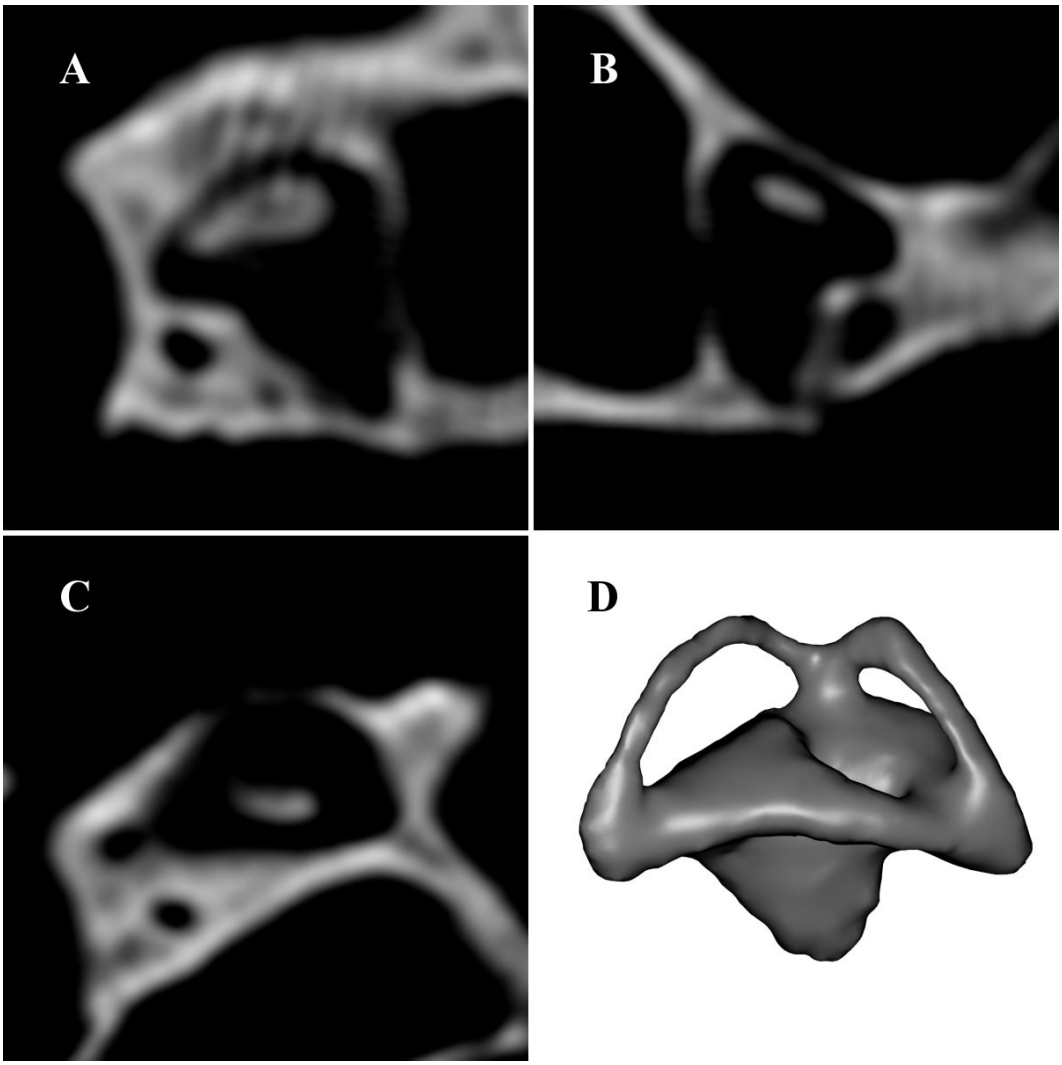

Figure 21: The semicircular canals of *Trachemys scripta*. Planar images of the A) anterior, B) posterior, and C) lateral semicircular canals reformatted from CT data and D) digital endocast of the complete bony labyrinth. Scale bars = 5 mm.

these taxa have utricular walls that are longer than the common crus is tall and therefore appear slightly elongated along an anteroposterior axis. In contrast, more aquatic emydids, such as *Trachemys scripta* and the aquatic Coahuilian box turtle *Terrapene coahuila*, show the same more pronounced anteroposterior elongation of the vertical canals (Fig. 21A & B) observed in many of the other aquatic turtle taxa.

The lateral canals of both two morphotypes, because of the general small size of these taxa, are similar to the typical small tortoise lateral canal. The only substantial difference between the two types is that in the aquatic morphotype the elongation of the vertical canals masks curvature of the lateral semicircular canal (Fig. 21C) where it joins the ampulla anteriorly and the common space with the posterior utricle.

CROCODILIANS

Within modern crocodilians each semicircular canal exhibits a common typical shape. Variation in semicircular canal shape is limited primarily to *Gavialis gangeticus*, and even in this case the change is subtle, and mostly restricted to the anterior semicircular canal.

Crocodylidae & Alligatoridae

The typical crocodilian semicircular canal is more rounded than in the generalized varanid. The common crus is taller and the branching of the two vertical canals is not equal. The anterior canal (Fig. 22A) rises more superiorly from the common crus than the posterior. In conjunction with the arced wall of the crus, the anterior canal forms a broad curve that continues its gentle contour towards the ampulla, and then terminates in a much sharper curve. This results in the typical ovoid shape of the crocodilian anterior canal (the apex of the ovoid is the ampullary end and its long axis runs from the mid point of the crus to a point just anterior to the ampulla). The posterior canal (Fig. 22B), though smaller in size than the anterior, usually shares the ovoid shape of the anterior canal. However, the shorter vertical excursion of the posterior canal from the common crus reduces the ovoid nature of the canal circuit, and, at times, produces a far more evenly elliptical course.

The lateral semicircular canal of these crocodilians (Fig. 22C) does

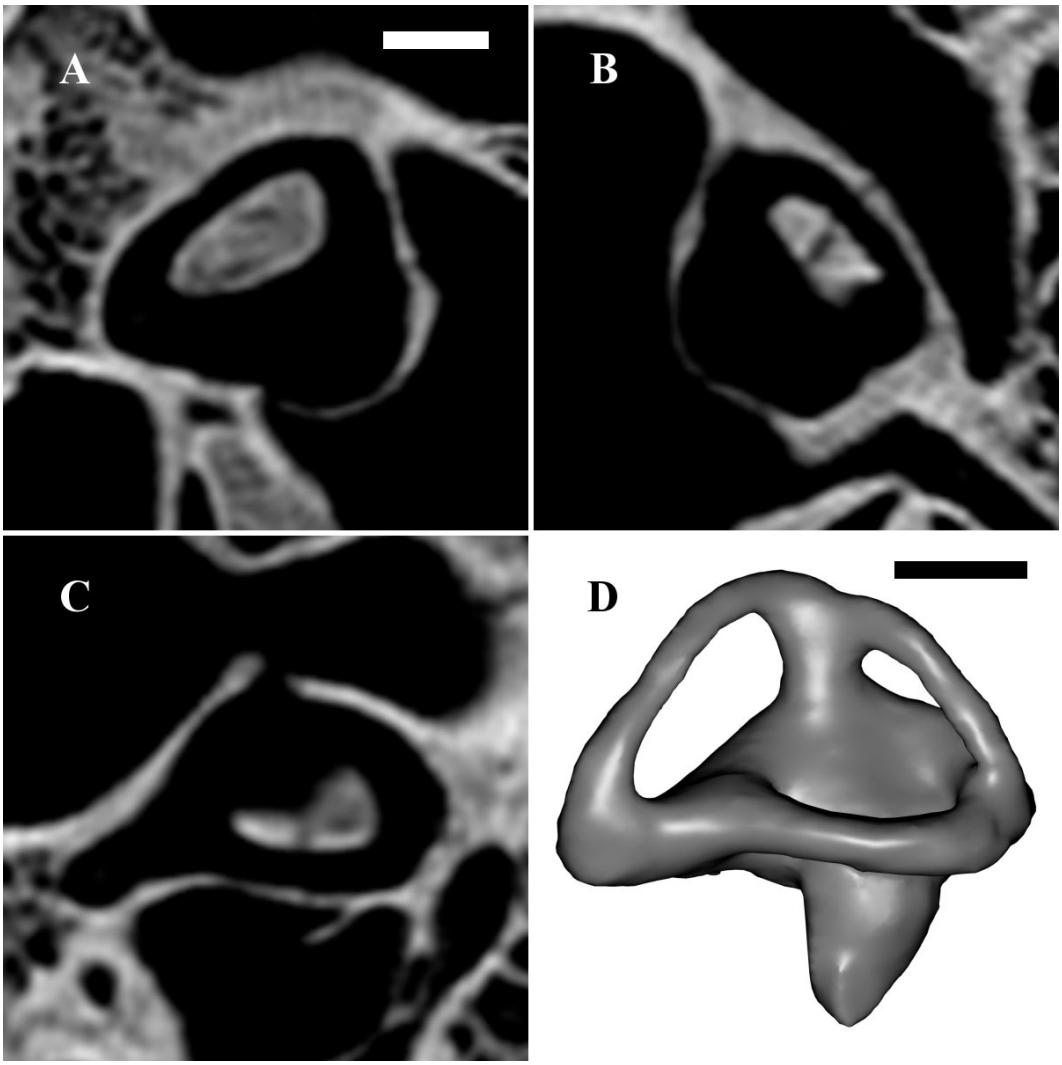

Figure 22: The semicircular canals of *Crocodylus palustris*. Planar images of the A) anterior, B) posterior, and C) lateral semicircular canals reformatted from CT data and D) digital endocast of the complete bony labyrinth. Scale bars = 5 mm.

not lie in a plane significantly superior to the posterior ampulla as it does in varanids. Similar to the condition seen in several mammals, the posterior section of the lateral canal and the posterior division of the utricle share a common bony space. In contrast to the mammalian condition, however, the greater width of the crocodilian canals in combination with the greater length of the posterior utricle create a very broad common space which

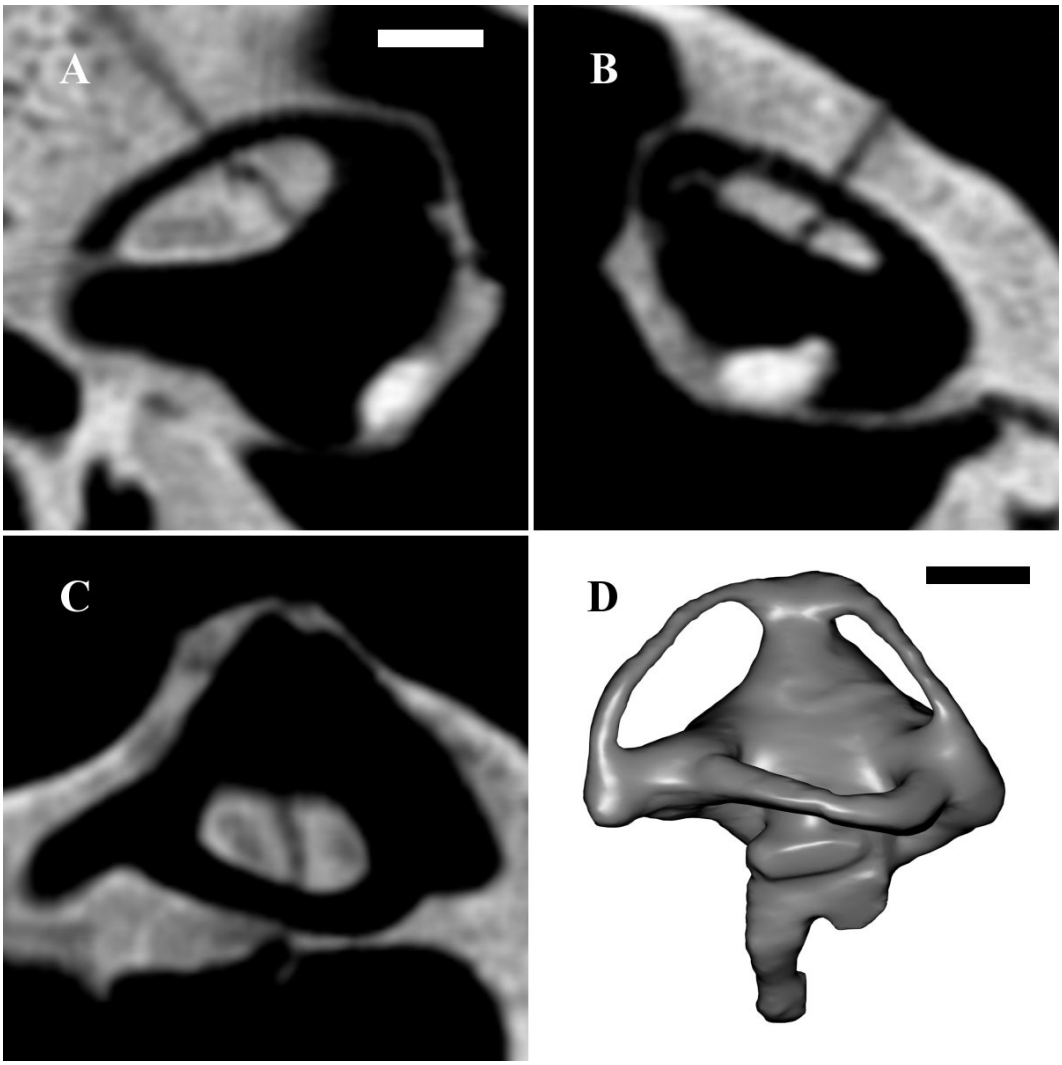

Figure 23: The semicircular canals of *Gavialis gangeticus*. Planar images of the A) anterior, B) posterior, and C) lateral semicircular canals reformatted from CT data and D) digital endocast of the complete bony labyrinth. Scale bars = 5 mm.

typically renders the bony region of the posterior ampulla indistinct. The section of lateral semicircular canal that separates from the posterior utricle and posterior semicircular canal courses anteriorly towards the lateral ampulla along a path ranging from a very gentle curve to nearly linear. The vestibular bulges in on the medial wall of the lateral canal, but to a much lesser extent than in many varanids, even in the smaller

varieties of crocodilian such as *Paleosuchus* or *Osteolaemus*.

Gavialis

The semicircular canals of the Indian gharial differ from other extant crocodilians. In *Gavialis*, the vestibular cavity is larger relative to the canals than in other crocodilians and this gives the common crus a foreshortened appearance. Furthermore, the vertical canals (Fig. 23A & B) do not continue significantly superiorly past their point of branching from the crus and they follow a straighter path towards their respective ampullary regions. These factors combined give gharials vertical semicircular canals that appear far longer than they are tall, a change from the proportions seen in other extant crocodilians. These canal shapes more closely resemble the shapes of the vertical canals in the mosasaurs, *Platecarpus* and *Tylosaurus* than they do the shape of other extant crocodilian vertical canals.

In contrast to the vertical canals, there is no significant difference between the lateral canal (Fig. 23C) of the gharial and the lateral canals of other extant crocodilians. Thus, the similarity between the gharial and mosasaur semicircular canal systems does not extend to the lateral canal.

CONCLUSIONS

These descriptions have made clear several characteristics of amniote semicircular canals systems. First, as expected, the basic arrangement of the semicircular canal system has been maintained. Secondly, there is a strong phylogenetic conservation within the larger clades. Thirdly, despite basic similarity within a phylogenetically related group, variation in semicircular canal shape is common and, in some cases, marked.

Chapter 2 lays out a theoretical justification for the expectation that

semicircular canal shape may be indicative of aspects of the function of the semicircular duct inside. In conjunction with this descriptive study, this completes the three pillars of paleobiological functional morphology outlined above. Variation in the morphology has been demonstrated on several different taxonomic levels. The shape model considered in Chapter 2, provides the link between the morphology and the function of the system. Lastly, descriptions of the semicircular canal system in mosasaurs demonstrates that, with this method, it is possible to extract this morphology from fossil vertebrates.

As we turn our attention to the numerous questions to which such a vast array of shapes in the semicircular canal system gives rise, we must, however, use caution. Although there is some theoretical justification for a functional morphological study of semicircular canal shape, due to the loss of information in going from the soft tissue to the bony system, there is no available evidence for what the specific connection may be. One responsible approach, therefore, is to treat the theoretical connection between the semicircular canals and function, not as an underlying assumption of a study, but as a first the testable hypothesis, the acceptance of which will pave the way for future detailed studies.

Under these circumstances, foremost among the many questions that can be asked is, 'Does the shape of the semicircular canals vary because of functional demands, or is the variation within clades strictly historical or a result of spatial constraints?'. The general nature of this question is important. Although these data can also lead to an overwhelming number of such specific questions as 'Does the shape of the semicircular canals vary because of the different functional demands placed on an animal that feeds on active prey versus one that forages off of stationary sources?', or 'Does the shape of the semicircular canals vary

because of the functional demands placed on an animal that moves with an erect posture versus on that moves with a sprawling posture?', until a solid connection between organism level function and semicircular canal shape can be established, answers to these more specific questions would tend to be more statistical curiosities than explainable phenomena.

Further study will, therefore, be undertaken to investigate the general nature of the link between semicircular canal shape and amniote behavior. Of course, examining semicircular canal shape relative to a completely general amniote behavior is not theoretically possible; what would a general behavior be? Thus, the following chapters will, out of necessity, examine an amniote behavior that is slightly more restrictive. Nonetheless, as this work progresses, attempts will be made to mitigate the restrictive nature of the behavior examined and relate the findings back to the validity of the general semicircular canal shape hypothesis.

Chapter 5
Canal shape and its Correlation to Locomotion in Aquatic and Terrestrial Amniotes

INTRODUCTION

The semicircular ducts of the vestibular system pose an interesting problem for functional morphologists. Superficially, the vestibular system would appear to be an ideal candidate for studying the relationship between system-level morphology and organismal-level function. As a system that draws strong interest in a clinical setting due to the numerous vestibular maladies (both severe and mild), it has been the center of intense research. Consequently, there is detailed knowledge of the morphology, histology, development, and biomechanics of the system. Furthermore, it has been known for over a century that the proper working of this system is integral for the proper functioning of posture and locomotion (Flourens, 1828; Hawkins and Schacht, 2005). Lastly, this system exhibits a wide variation in gross morphology across vertebrates (Ezure and Graf, 1984a; Gray, 1906, 1907, 1908b; 1908a; Gray, 1955; Hadžiselimović and Andelić, 1967; Hadžiselimović and Savković, 1964; Lindenlaub and Oelschläger, 1999; Ramprashad *et al.*, 1984; Spoor *et al.*, 2002), and this morphological variation should, theoretically, result in differences in the response of the system in different taxa (Curthoys *et al.*, 1977a; Curthoys *et al.*, 1977b; Howland and Masci, 1973; Jones, 1974; Jones and Spells, 1963; Mayne, 1965; Oman *et al.*, 1987; Ramprashad *et al.*, 1984). As added bait for the functional morphologist working in an evolutionary context, this soft tissue system leaves distinct bony features that are observable in some fossils. It is, therefore, possible to examine

the morphological variation of this system in extinct vertebrates. Thus, the vestibular system provides a functional morphologist with the possibility of examining a morphology, making a prediction of function based on strictly morphological grounds, correlating the functional prediction with observable behavior, and, once the morphology to function model is established, inferring the behavior of extinct organisms on the basis of morphology observable in the fossil record.

This line of reasoning has two implicit assumptions. The first assumption is, across all of the organisms examined, the relationship between vestibular function and the behavior of interest is conserved (*i.e.*, vestibular function or response A consistently produces behavior B). Of course, within works of limited scope, it is often sufficient that relationship of interest be consistent and predictable and the underlying connection is of no interest. This situation however, does not lead to a result that is generally applicable, but one that is only applicable in the specific context initially studied (see Chapter 1 for an example of specific semicircular canal relationships failing in a general context). The second assumption is that morphological changes in the vestibular system are adaptive changes in response to the requirements of the behavior of interest and not exaptations or chance similarities that result from spatial packing of the vestibular system in the space constrained skull (Graf and Vidal, 1996). These assumptions have indirect support from the numerous studies that, having accepted these assumptions, have observed correlations between vestibular morphology and behavior (Gauldie and Radtke, 1990; Georgi and Sipla, 2008; Hadžiselimović and Savković, 1964; Lindenlaub *et al.*, 1995; Matano *et al.*, 1985; McVean, 1999; Spoor *et al.*, 2002; Spoor *et al.*, 2007; Spoor and Thewissen, 2008; Spoor *et al.*, 1994). Very few studies, however, have subjected the assumptions themselves to rigorous

examination, a critical step before the study of vestibular functional morphology can continue to mature.

The assumption of conserved relationship between vestibular function and organismal action is a complicated one, given the complex nature of the system being investigated. This system is subject to a kind of "black box" phenomenon. The eighth cranial nerve carries the pulsatile discharges of the vestibular endorgans into the brain. There is a complex network of interneurons, localized centers of integration, and motor nuclei from which emerge motor neurons encoding movement responses. These are the motor neurons that drive extraocular muscles stabilizing the eyeball relative to the head (vestibuloocular reflex, or VOR), cervical muscles stabilizing the head relative the trunk (vestibulocervical reflex or VCR), and trunk muscles stabilizing the neck and trunk relative to substrate contact (vestibulospinal reflex or VSR). Any vertebrate that possesses target muscles that produce the appropriate action has a analogous reflex pathway[1] (Ezure and Graf, 1984a; 1984b) and, thus, there is the beginning of support for the assumption of conserved relationship.

There is a complication, however, called vestibular adaptation. If these simple three-neuron reflex arcs carried the vestibular signal uninterrupted, then the assumption of conserved relationship would be reasonable and easily verifiable. This, however, is not the case. In fact, the activity of this reflex arc can be modulated. The process by which short-term and long-term changes to the VOR can be effected is called

[1] Even flatfish follow this rule. The severe ontogenetic reorganization of the flatfish skull is accompanied by a reorganization of the neuromuscular reflex arcs of the vestibular system so that function is still analogous. That is, vestibular stimulation still produces contrary eye movements that stabilize the image on the retina (Graf and Baker, 1985a; 1985b).

adaptation. Vestibular adaptation is one of the primary foci of the clinical research on the vestibular apparatus as it pertains directly to the rehabilitation of patients that have suffered loss of impairment of vestibular senses and is, therefore understood to a significant degree (see Gauthier *et al.*, 2007 for review).

This vestibular adaptation is the "black box" that interferes with the assumption of conserved relationship between vestibular function and organismal behavior. If the brain can plastically modulate the vestibular reflexes, then there is no way to theoretically guarantee that if the same vestibular signal goes in, the same motor signal comes out. The uncertainty of this assumption is, therefore, one of the principal objections raised against semicircular canal functional morphology studies (Graf and Vidal, 1996; Hullar, 2006).

It is possible, however, to view this plastic adaptation as an advantageous mechanism when considering the functional evolution of the vestibular system. First, although vestibular adaptation is possible, it may not be as effective in terms of an organism's overall fitness as would a properly functional vestibular system. There would, in that case, still be evolutionary pressures to optimize the system for the organism's specific behavior. Second, vestibular adaptation is beneficial for transitional forms, both phylogenetic and functional. In the case of this study, the potential functional transitional forms, semi-aquatic organisms, could utilize vestibular adaptation to maintain some level of vestibular efficacy when entering the locomotor environment to which they were less well adapted.

Thus, although vestibular adaptation does prohibit the theoretical validation of the assumption of conserved relationship between vestibular function and organisms' behavior, it not does completely invalidate it. Nor, does it eliminate the possibility of validating this assumption

experimentally. It is still possible, via either controlled stimulation of the vestibular system or recording natural vestibular output, to investigate the connection between input vestibular signals and motor, or behavioral output and, thus, experimentally validate this assumption. This is not the aim of this study, but it is worth noting that preliminary work along these lines is being done (Yang and Hullar, 2007).

The second underlying assumption, that of adaptive change, is the focus of this study. It is similarly difficult to examine directly because of the difficulty of assessing, *in vivo*, the change in fitness resulting from a change in vestibular function. To get at this question, we must instead rely on indirect evidence. The most likely choice for indirect evidence, in this case, is a study that demonstrates a correlation between distinct vestibular morphotypes and distinct behaviors independent of phylogeny. A consistent feature of previous studies that sought to link one or more aspects of semicircular canal morphology to locomotor behavior is a study sample that focuses on a single set of closely related organisms (Gauldie and Radtke, 1990; Hadžiselimović and Savković, 1964; Lindenlaub *et al.*, 1995; Matano *et al.*, 1985; McVean, 1999; Spoor *et al.*, 2002; Spoor *et al.*, 2007; Spoor and Thewissen, 2008; Spoor *et al.*, 1994). Although these studies may offer significant evidence within the limited framework of their study groups, this is not sufficient to test a hypothesis or an assumption that is expected to apply in a broad phylogenetic context.

A second limitation of some of these previous studies is the methodology used. Hadžiselimovic and Savkoić (1964) used only qualitative descriptions of the semicircular canals of birds. Spoor and colleagues (Spoor *et al.*, 2002; Spoor *et al.*, 2007; Spoor and Thewissen, 2008; Spoor *et al.*, 1994), assess semicircular duct function on the basis of the residual distance of a specimen from a generalized semicircular

canal allometric growth line. This method is a derivative of the one originated in a landmark paper by Jones and Spells (1963), wherein they laid out a theoretical prediction and subsequently demonstrated that semicircular duct dimensions (both radius of curvature and cross-sectional area of the duct lumen) show a strongly negatively allometric relationship to body mass across vertebrates. Jones and Spells interpreted these minor increases in dimensions, lumen area as a proxy for the range of movement frequencies to which an organism is maximally sensitive, and radius of curvature as a proxy for amount of canal response per unit rotation, as an adaptive response of the semicircular ducts to the slowing of average movements as organisms increase in size (1963). These findings and interpretations were echoed in following years by additional studies (Jones, 1974; Mayne, 1965).

The problem with the way in which the more recent studies have adapted the method of Jones and Spells is two-fold. Spoor and colleagues interpret a specimen's residual variation above the general allometric line (*i.e.*, semicircular canals larger than predicted for body mass) as an indication that the organism's semicircular ducts were adapted to detect more rapid movements, and residual variation below the line (*i.e.*, smaller than predicted) as an adaptation to slower movement (Spoor *et al.*, 2002; Spoor *et al.*, 2007; Spoor and Thewissen, 2008; Spoor *et al.*, 1994). These interpretations of the functional meaning of the morphospace are opposite those that Jones and Spells put forth (see Chapter 1).

The second problem with the methods modified from Jones and Spells' work is the increase in error that results from the use of the average radius of curvature of the canal as a proxy for the duct response. Spoor and colleagues calculate the radius of curvature as the height of the

canal plus the width of the canal divided by four (Spoor *et al.*, 2002; Spoor *et al.*, 2007; Spoor and Thewissen, 2008; Spoor *et al.*, 1994). This is equivalent to the mean of the vertical radius and the horizontal radius. Although the true parameter that partially determines the duct response is the area enclosed by the complete duct circuit (Chapter 2), the use of average radius is defended because it is a simple matter to convert the radius into an area using the formula for the area of circle. Despite the name, however, semicircular canals are not perfectly circular; a canal circuit is more closely approximated by an ellipse than a circle (were a canal to be perfectly circular it could, of course, be treated as an ellipse with axes of equal length). The radial components in the formula for the area of an ellipse are the product of the major and minor radii, which is not equivalent to the average of the radii squared as would be used in a circular area formula. Using a circular formula to calculate the area of an ellipse will result in an overestimation of the area that grows larger with increasing discrepancy between the length of the axes (Fig. 1). For the taxa used in this study, if a circular area approximation were used, the calculated circular area would be an average of 10.9% larger than the true area with a maximum over-estimation of 42.1% in the case of a particularly eccentric turtle posterior semicircular canal. An elliptical area approximation reduces the average error to 3.7%.

Directly calculating the planar area enclosed by the semicircular canal eliminates the area estimation error altogether, but it also provides a secondary benefit. To calculate the area enclosed by the canal, it is sufficient to know the planar coordinates of a series of vertices around the perimeter of the shape in question. Thus, in the process of calculating the area, the length of the canal circuit (the sum of the distances between consecutive points) and true shape (the set of point coordinates) of that

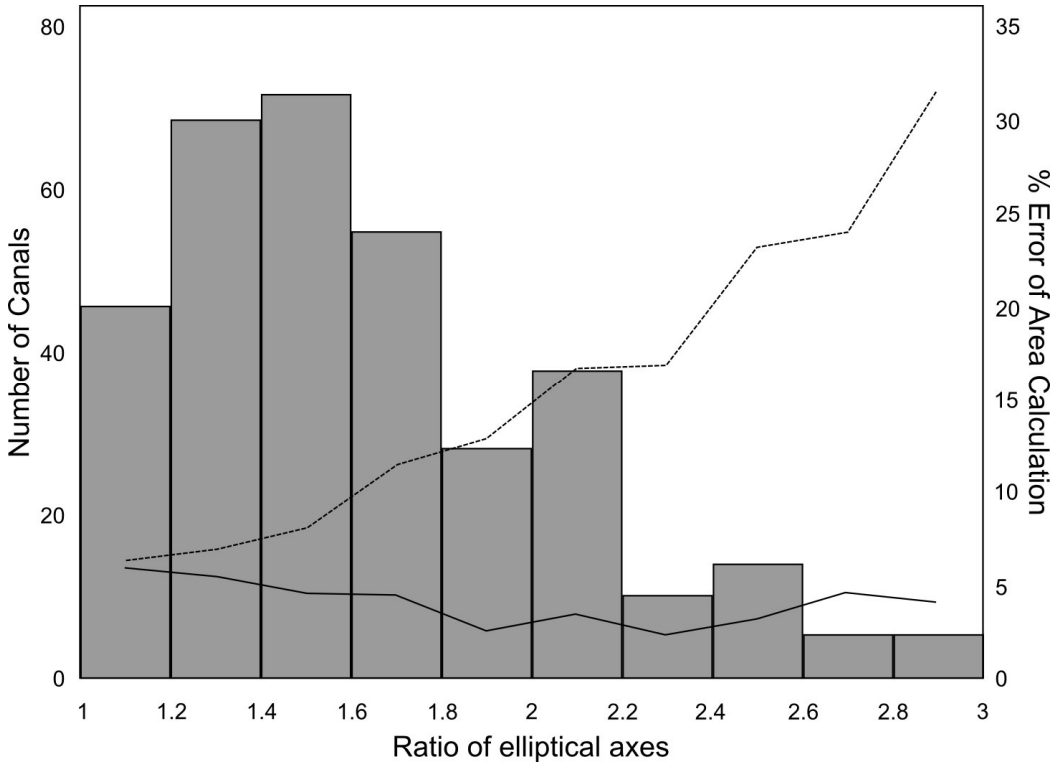

Figure 1: Distribution of axes ratios (major axis : minor axis) for all canals examined in this study (3 per specimen). The average % error of area estimations are given for each segment of the distribution: solid line – % error resulting from elliptical estimation (from product of the two radii), dashed line – % error resulting from circular estimation (square of the averaged radii). While the elliptical estimation error remains around 5%, the circular estimation error continues to increase; 169 of the 345 canals examined showed greater than 10% error by the circular approximation.

circuit are also defined. Not only is the length of the canal circuit a moderate proxy for an important semicircular duct parameter, the length of the slender portion of the duct, but the circuit length has been shown to be decoupled from the area enclosed by changing the shape (Chapter 2).

Semicircular canal circuit shape may, therefore, be a powerful measure that captures both of these independent parameters. In an adaptive context, the shape of a semicircular canal circuit can be considered representative of the balance between an animal's

requirements for semicircular duct response and range of sensitivities[2].

Having identified semicircular canal shape as the metric of interest, it is now essential to ensure a broad phylogenetic sample in order to test the assumption of adaptive change. Thus, it is necessary to find a locomotor dichotomy to examine that can be applied across a large subset of vertebrates. Furthermore, the ideal locomotor transition for this study should also encompass extremes of motion or substrate that are likely to produce significantly different patterns of head movement. The transition from terrestrial locomotion to secondarily aquatic locomotion satisfies both of these criteria.

Most large amniote clades have some members or subgroups that have returned to a partially or fully aquatic mode of existence. With this many parallel events along the vertebrate evolutionary tree, any signal that is purely functional should be easily distinguishable from one that is phylogenetic, assuming that the functional signal is a universal response.

Adoption of a secondarily aquatic locomotor behavior may induce a consistent adaptive response in the morphology of the semicircular canals for several reasons. In the simplest assessment, the density difference between the media in which the locomotion is produced is expected to have a significant effect on the movements experienced by an animal's head. During terrestrial locomotion an animal's head is surrounded by air, which does not provide much resistance to movement, whereas during aquatic locomotion, the head is surrounded by a much more viscous medium, water, which offers far more resistance to movement. Thus, it

[2] Alternatively, because this study does not take into account a third important parameter, the cross-sectional area of the duct lumen, it is also reasonable to interpret the semicircular canal circuit shape as a balance between the need to modify semicircular duct response and maintain a consistent range of sensitivities as the duct lumen changes in size (see Chapter 1).

could be expected that the head of an animal that locomotes in water will experience slower movements. Conversely, because of its higher density, movements of the water can have proportionately greater effects on the animal and, therefore, it could be expected that an aquatic animal would experience unpredictable destabilizations to its pattern of locomotion (and, thereby, unpredictable movements of the head) that are both more frequent and greater in magnitude.

In most cases, the locomotor substrate (the surface or object that the animal pushes against to produce forward movement) differs between these two environments as well. Although some vertebrates with largely or fully aquatic lifestyles "walk" along the hard substrate at the bottom of the aquatic environments (the turtle *Platysternon megacephalum* is one example used in this study), the typical aquatic animals produces forward propulsion by pushing against the water itself, whereas a terrestrial organism pushes against the ground. This difference could have several effects on movements of an animal's head. A terrestrial substrate typically will be beneath the animal as it locomotes; thus, there will be a vertical component to the substrate reaction force that pushes back on the animal. In contrast, when an animal is completely surrounded by the substrate, as in aquatic locomotion, it is possible to adopt locomotor mechanics, such as lateral undulation or laterally directed paddling, that incur little or no vertical component to the substrate reaction force. It must be noted, however, that some aquatic vertebrates utilize locomotor behaviors that do include vertical substrate reaction forces (*e.g.*, vertical undulation, subaqueous flying, or lateral undulation of an asymmetrical appendage such as a heterocercal tail).

With both surrounding medium and substrate effects, the terrestrial versus secondarily aquatic locomotion comparison provides numerous

factors that may drive multiple independent semicircular duct adaptations. The combination of these factors into a complex change in movement regime is difficult to predict, however, the semicircular ducts are a complex system with morphological parameters sensitive to many of the different components of the combined movement regime. Thus, it is reasonable to expect that the semicircular ducts (and their bony correlates, the semicircular canals) will show some adaptation attuning the response of the system to the specifics of environment.

Another benefit of using the terrestrial to secondarily aquatic locomotor transition is the ability to assess, in some way, the character of evolutionary change in the vestibular system. There are two primary possibilities for the pattern by which adaptation might occur across this functional grade. In the first scenario, gradational change, the amount of change from the terrestrial form is directly proportional to the percentage of aquatic behavior. In the second scenario, discrete change, the fully aquatic form is acquired by all organisms that engage in aquatic activity beyond a certain threshold.

Many organisms, including many examined in this study are neither fully terrestrial nor fully aquatic; this intermediate group of semi-aquatic organisms is the key to understanding whether adaptive change in the semicircular ducts is gradational or discrete. If these intermediate organisms exhibit a semicircular canal form that is intermediate between the two extremes, then a gradual change from one extreme, through the intermediate forms, to the other extreme can be hypothesized. If, on the other hand, these intermediate organisms primarily exhibit a semicircular canal form that is equivalent to either of the two extremes, then it is necessary to consider the discrete model of semicircular canal change.

MATERIALS AND METHODS

The braincases of 227 mammalian carnivores, turtles, crocodilians, and squamates were CT scanned with a GE Lightspeed 16 X-ray CT. These specimens ranged in adult size (skull length) from >5 cm to <1 m. Of the original specimens scanned, only 115, encompassing 58 species, were determined to be suitable for use in this study (Table 1). The most common reason for removal from the study sample was a vestibular morphology too small to be resolved with satisfactory detail at the minimum resolution available. Several specimens (*e.g.*, *Gopherus polyphemus*), however, were not used because extreme vestibular morphologies prevented accurate planar representation of one or more of the semicircular canals. A small number of specimens were unsuitable due to damage to the vestibular region not detectable by visual inspection. Lastly, because the aquatic squamates in this study are represented by fossil mosasaurs, some specimens were unsuitable for use due to lack of complete or distinct preservation of the vestibular region or distortion of the lateral braincase wall. In all cases, presumed adult specimens were used. Furthermore, due to potential ontogenetic changes in semicircular canal shape (see Chapter 3), within each non-mammalian taxon with indeterminate growth, specimens were size-matched as closely as possible.

Each taxon was placed into one of three locomotor categories: terrestrial, semi-aquatic, and aquatic (Table 1). Neither of the extreme categories (terrestrial or aquatic) imply an obligate locomotor mode (*i.e.*, many of the taxa categorized as terrestrial are capable of some form of aquatic locomotion and the same is true in reverse; black bears, for example, can swim and sea lions are capable of moving about on land). Rather, these categories imply that the overwhelming majority of the

Order	Genus	Species	Specimen(s)	Category
Carnivora	*Canis*	*lupus*	AMNH 98227, AMNH 98231	T
	Aonyx	*capensis*	AMNH 51850, AMNH 52104	S
	Enhydra	*lutris*	AMNH 215274, AMNH 28226	S
	Pteronura	*brasiliensis*	AMNH 77735, AMNH 30190	S
	Taxidea	*taxus*	AMNH 169988	T
	Arctocephalus	*galapagoensis*	AMNH 100319, AMNH 100341	A
	Callorhinus	*ursinus*	AMNH 71169	A
	Zalophus	*californicus*	AMNH 80293	A
	Hydrurga	*leptonyx*	AMNH 34920, AMNH 36200	A
	Mirounga	*angustirostris*	AMNH 32677, AMNH 32679, AMNH 77930	A
	Phoca	*vitulina*	AMNH 232386, AMNH 232445, AMNH 232448	A
	Melursus	*ursinus*	AMNH 22720	T
	Ursus	*americanus*	AMNH 120843, AMNH 164284, AMNH 15686	T
	Ursus	*maritimus*	AMNH 15687, AMNH 35065	T
Crocodilia	*Alligator*	*mississippiensis*	AMNH 31563, AMNH 43314	S
	Caiman	*crocodilus*	AMNH 120030, AMNH 15184	S
	Caiman	*latirostrus*	AMNH 62555	S
	Caiman	*yacare*	AMNH 97298, AMNH 97299	S
	Melanosuchus	*niger*	AMNH 110179, AMNH 97325	S
	Paleosuchus	*palpebrosus*	AMNH 137162, AMNH 97328	S
	Paleosuchus	*trigonatus*	AMNH 137175, AMNH 66391	S
	Crocodylus	*cataphractus*	AMNH 107634, AMNH 75424	S
	Crocodylus	*niloticus*	AMNH 10081, AMNH 137180	S
	Crocodylus	*palustris*	AMNH 75707, AMNH 77632	S
	Crocodylus	*rhombifer*	AMNH 57773, AMNH 77595	S
	Osteolaemus	*tetraspis*	AMNH 117801, AMNH 24740	S
	Tomistoma	*schlegelii*	AMNH 113078, AMNH 15177	A
	Gavialis	*gangeticus*	AMNH 110145, AMNH 7138, AMNH 88316	A
Squamata	†*Platycarpus*	*coryphaeus*	AMNH 1645	A
	†*Platycarpus*	*tympaniticus*	YPM 40728	A
	†*Tylosaurus*	*neopaeolicus*	MCZ 1613	A

behaviors employed by the animal are of one form and not the other. Taxa were categorized as semi-aquatic if the division between terrestrial and aquatic behaviors was more evenly split.

Although specific subcategories exist within each of the primary categories (*i.e.*, the terrestrial category contains taxa that use erect and semi-erect limb postures and are cursorial, fossorial, *etc.*) these differences in locomotor behavior were not taken into account (with the

	Varanus	*albigularis*	AMNH 47725, AMNH 47726, AMNH 47727	T
	Varanus	*bengalensis*	AMNH 117786, AMNH 29932, AMNH 71195	T
	Varanus	*exanthematicus*	AMNH 137237, AMNH 140804	T
	Varanus	*gouldii*	AMNH 82819	T
	Varanus	*komodoensis*	AMNH 37911, AMNH 37913, AMNH 74606	T
	Varanus	*niloticus*	AMNH 10085, AMNH 10500, AMNH 137116	T
	Varanus	*salvator*	AMNH 142471	S
	Varanus	*varius*	AMNH 73361	T
Testudines	*Carettochelys*	*insculpta*	AMNH 104542, AMNH 85893	A
	Elseya	*novaeguineae*	AMNH 104007, AMNH 62612, AMNH 99613	A
	Caretta	*caretta*	AMNH 129869, AMNH 7159	A
	Chelonia	*mydas*	AMNH 46909, AMNH 5912, AMNH 71597	A
	Eretmochelys	*imbricata*	AMNH 7114, AMNH 71599, AMNH 7170	A
	Lepidochelys	*kempii*	AMNH 131147, AMNH 131148	A
	Dermochelys	*coriacea*	AMNH 143174, AMNH 92959	A
	Clemmys	*insculpta*	AMNH 123800, AMNH 124941, AMNH 126586	T
	Cuora	*galbinifrons*	YPM 11854, YPM 12107	T
	Rhinoclemmys	*funerea*	YPM 12174, YPM 14340	S
	Rhinoclemmys	*punctularia*	AMNH 62584	S
	Terrapene	*carolina*	AMNH 138156, AMNH 152179	T
	Terrapene	*coahuila*	AMNH 110194	S
	Trachemys	*scripta*	AMNH 109471, AMNH 94558, AMNH 69918	A
	Platysternon	*megacephalum*	AMNH 134593, AMNH 92740	S
	Chelonoidis	*denticulata*	SUNY Rp10	T
	Chelonoidis	*nigra*	AMNH 42961	T
	Gopherus	*berlandieri*	AMNH 71616, AMNH 73816	T
	Apalone	*ferox*	AMNH 117727, AMNH 129737, AMNH 57380	A

Table 1: List of specimens examined in this study. Taxa from four orders were included and, where available, up to 3 specimens of each taxa were used to mitigate the effect of individual variation. Taxa were diagnosed as either (T) terrestrial, (S) semi-aquatic, and (A) aquatic. Collection abbreviations: AMNH – American Museum of Natural History, YPM – Yale Peabody Museum, SUNY – Stony Brook University Anatomical Sciences Collections.

exception of aquatic organisms that employ subaqueous flying) for three reasons. The primary reason for ignoring these finer scale differences in locomotion is the goal of first establishing a general link between amniote behavior and semicircular canal shape. If the general case is verified, then the potential use of this method on finer scale locomotor dichotomies

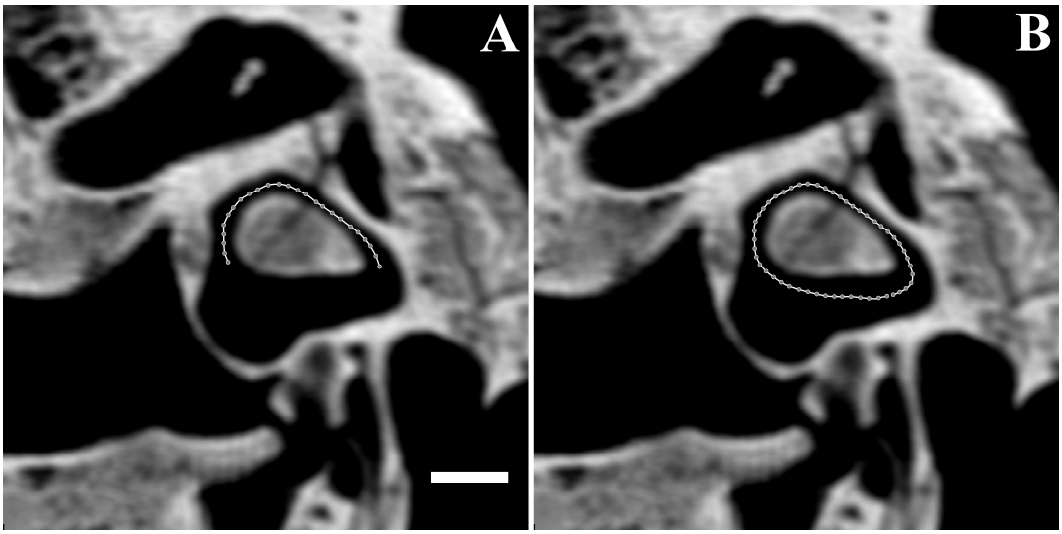

Figure 2: Representative landmark sets used for Procrustes geometric morphometric analysis. A) 25 landmark representation of the canal path without the ampulla and utricular contributions. Endpoints are fixed landmarks, all intermediate points aretreated as sliding semipoints. B) 50 landmark representation of the complete canal circuit. Endpoint defining the boundary between ampulla and utricle is a fixed landmark, all other landmarks are treated as sliding semipoints.

can be considered. The second reason is that the number of specimens required to test all of the different specific modes of locomotion found in amniotes is far beyond he possible scope of this one study. Lastly, classification of specific locomotion behavior when many of the organisms examined employ more than one type is incompatible with the method being developed here.

Planar images of each semicircular canal and canal paths composed of 25 coordinates (Fig. 2A) each were produced following previously described methods (Chapter 3). In addition, however, paths suitable for landmark shape analysis consisting of 50 coordinates (Fig. 2B) representing the complete canal circuit, including the utricle and the ampulla, were also computed from the initial mid-canal circuit estimate using cubic spline interpolation.

There are many available options for the analysis of shape of two

dimensional data sets such as the 25 point semicircular canal paths and 50 point canal circuits generated for this study. Both the canal paths and the canal circuits were aligned for geometric morphometric analysis using the Procrustes method of superimposition, with the interpolated landmarks treated as sliding semipoints using the minimum bending energy method (Bookstein, 1997). In addition to the Procrustes alignment, the 50 point canal circuit was suitable for Elliptical Fourier Analysis (Kuhl and Giardina, 1982). Elliptical Fourier Analysis (EFA) treats the x and y components of the coordinate series as separate parameterized functions and, through Fourier decomposition of these functions, produces coefficients that describe a series of harmonic ellipses that, when concatenated, sum to the original outline (Fig. 3). EFA is a useful tool for shape analyses in situations in which there are few homologous landmarks around the closed outline of the shape in question (as in the case of these semicircular canals) and requires only a single homologous starting point if, as is the case for this study, outline orientation is going to be taken into account (Ferson *et al.*, 1985; Haines and Crampton, 2000; Rohlf and Archie, 1984). In this study, outlines are all oriented such that the line which represents the intersection between the canal plane and a sagittal plane is the vertical axis of the coordinate system, therefore a single homologous landmark is used for each canal, the ampulla. Elliptical Fourier coefficients were computed for the first 10 harmonics which, in all cases, represented the original outline with a high degree of fidelity. NTSysPC version 2.11S (Applied Biostatistics Inc., 2003) was used to calculate the Elliptical Fourier coefficients.

Haines and Crampton (2000), however, cite several potential drawbacks to EFA, the most significant of which is that the coefficients produced are not “computationally independent” and are, therefore, less

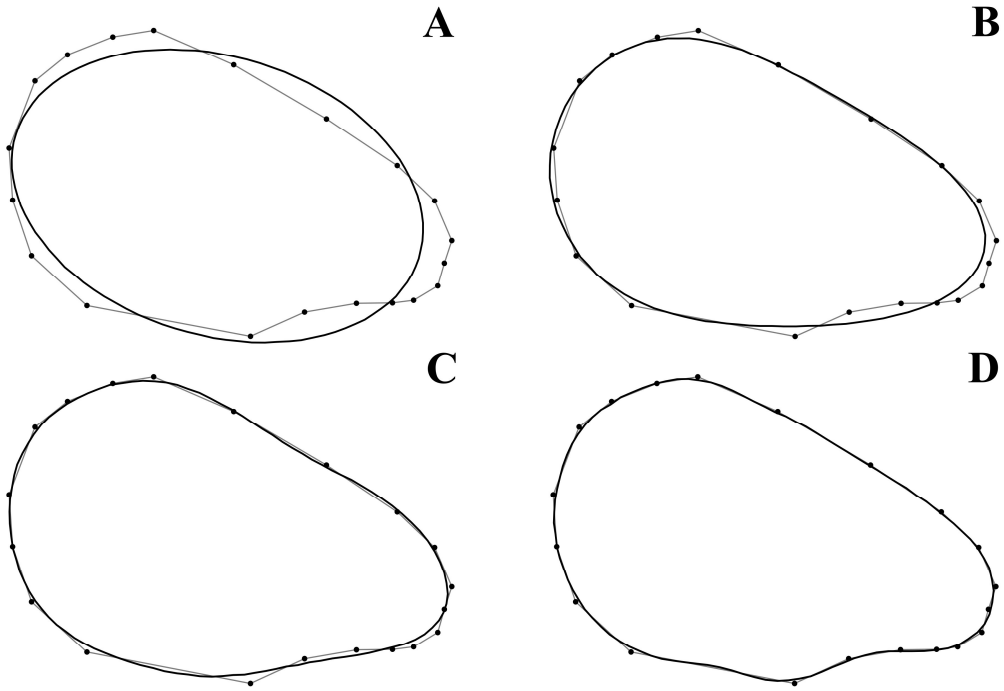

Figure 3: Example of reconstructing (black lines) a semicircular canal circuit (grey lines) via Elliptical Fourier Analysis (EFA). A) first harmonic ellipse, B) concatenation of 3 harmonic ellipses, C) 5 harmonic ellipses, D) 10 harmonic ellipses. In this study, improvements to the reconstruction fidelity beyond 10 harmonics are inconsequential.

appropriate for further statistical analysis. In this study, this drawback also applies to the Procrustes analysis of the outlines. Significant but small-scale deviations from the smooth contour of the canal are rare and, therefore, with an arbitrary number of points (25 and 50) used to describe the contour, it is expected that the position of each point is not completely independent of its neighbor (*i.e.*, if point *n* is higher in one form than the others, it is expected that points *n-1* and *n+1* will also be higher, though not necessarily to the same extent). This problem of non-independence of data will be addressed by the selection of the statistical analysis method.

As the goal of this study is to use semicircular canal morphology to distinguish between three explicitly defined groups within the data set,

discriminant function analysis (DFA) is the most suitable method for analyzing these data. DFA, however, requires that there be fewer variables than subjects. In the case of the Procrustes aligned outlines and the Fourier coefficients, particularly if all three canals are to be combined into a single analysis, there is an overwhelming amount of data (150, 300, and 120 variables per specimen for the canal path, canal circuit, and Fourier analyses, respectively).

The typical approach under these circumstances would be to apply a principal components transformation to the data and to reduce the number of variables being investigated to a few principal axes that describe the majority of the variation in the data. Principal axes are, by definition, orthogonal (*i.e.*, the composite variables would be independent of one another); this would remedy the non-independence objection to Fourier coefficients raised by Haines and Crampton (2000) as well as the hypothesized non-independence of the Procrustes landmarks. Principal axes, however, are possibly less ideal for this analysis because of the magnitude of shape variance in the data set that is independent of the functional relationship being investigated. As evidenced by the previous morphological descriptions (Chapter 4), deviations in the shape of the semicircular canal circuits across this broad a sample of amniotes are most prominently phylogenetic in nature. Phylogenetic differences in semicircular canal shape are sufficiently large that they would be expected to dominate most of the composite axes produced by principal component transformation.

A phylogenetic comparative method, however, is difficult to apply in this case. Any attempt to remove autocorrelation derived from historical relatedness, suffers from the particular aspects of this dataset. Moen (2006) outlines a concise review of why data with characteristics like this

dataset are resistant Generalized Least-Squares (GLS) regression methods. The problem lies with fitting an appropriate model of character change to this data set. With distance from the root of the tree to each tip being the correlate of the character being investigated, a tree in which all or most of the tips have the same distance from the root (*i.e.*, a tree where all or most of the tips are contemporaneous, such as would encompass all the taxa in this study, which are mostly extant, save for the mosasaurs, calibrated to divergence time) prohibits proper GLS calculation. Moen recommends either of two different character models that can alleviate this difficulty (2006). First, a speciation model where the all branch lengths of the tree are equal. This model, however, assumes that the tree in questions has consistent representation of nodes all the way from the root to the tips. That is, if the character change is modeled based on speciation events then even the fossil intermediates representing all or most of the speciation events between the root and the tip taxa are required to get an accurate result from this model. Clearly, this dataset which would have its tree rooted at the divergence between synapsid and diapsid amniotes does not represent even a small fraction of the speciation events that occur between the root and the tip taxa. The other character change model that Moen cites, if the first two don't work, is a model of genetic change where branch lengths are characterized by numbers of genetic substitutions between nodes. Obviously, this approach is not viable for any study that includes fossils, as this one does.

Data variable reduction is further complicated by an inability to predict localized semicircular canal changes. If, for example, a model of semicircular canal modification predicted change in the length of the common crus or a decrease in the utricular contribution to the posterior canal circuit, the data set could be pared down to focus on only these

areas. Because of the nature of what is being investigated, overall shape data, no one area can, *a priori*, be assumed to be of higher functional significance than any other. What is required, therefore, is an analysis that reduces a large data set by selecting the most appropriate variables for the classification of interest.

A solution to the difficulties of non-independence, the inability to reduce the number variables, and the lack of *a priori* knowledge of the most functionally informative variables is found by using DFA with stepwise inclusion of variables. Stepwise variable inclusion iteratively selects for inclusion in the final DFA the single variable that produces the most significant (above an arbitrary threshold value) increase in group separation. Furthermore, additional threshold criteria can be stipulated such that, after the inclusion of a new variable, previously added variables can be removed if they no longer significantly contribute to group separation. The reduction of the larger data set is now achieved through criteria-based selection of all the variables that significantly inform the classification of interest. This reduced data set now satisfies the requirements for DFA. Furthermore, if two or more variables are interrelated then addition of a second is not likely to significantly increase the group distinction, and therefore only one of each highly interdependent group is likely to be included in the analysis. SPSS version 8.0 (SPSS Inc., 1997) was used to perform the stepwise DFA analyses in this study.

In this study, Wilks' lambda significances were used with a value of $p < 0.05$ for the variable inclusion threshold and $p > 0.10$ set for the variable removal threshold. The Wilks' lambda method was chosen over the alternatives for this study for two reasons: it takes into account both group separation (distance between the group centroids) and group coherence (variance around the group centroid), and it does not tend to

force equal separation between the groups (Klecka, 1980) and thus does not favor the gradational model of evolutionary change discussed below.

Using stepwise DFA helps mitigate the problem of phylogenetic control by focusing on functional rather than phylogenetic differences. As long as there is little or no phylogenetic bias within the three functional groups, this method will identify variables that have the highest functional to phylogenetic signal ratio. To limit the phylogenetic bias within each of the classification groups, it is sufficient to ensure that each classification group has representatives from each clade. The mammalian, turtle, and squamate groups in this study all satisfy this criterion, but there are no extant crocodilians that can be classified as fully terrestrial in locomotor behavior, thus, only the semi-aquatic and aquatic groups contain crocodilian members. The effects of this distribution will be examined by running the same analysis with and without the crocodilian specimens.

DFA derives a number of discriminating axes equal to one less than the number of groups being examined; in this case, a maximum of two discriminant axes will be produced. Thus, the final morphospace that will be described by this analysis will be at most two dimensional. Furthermore, because DFA maximizes variation between groups along the first axis and will, in this two-axis case, leave the smaller residual variation along the second axis, there are only a small number of arrangements of the three groups within the morphospace that are possible (Fig. 4). Three non-collinear points (and unless the residual variation between the groups is 0, the group centroids will not be collinear) are constrained to have a triangular relationship. It must be expected, therefore, that two of the groups will define the primary axis and the only thing that is going to determine the nature of the triangular relationship of the three groups is the location of the third.

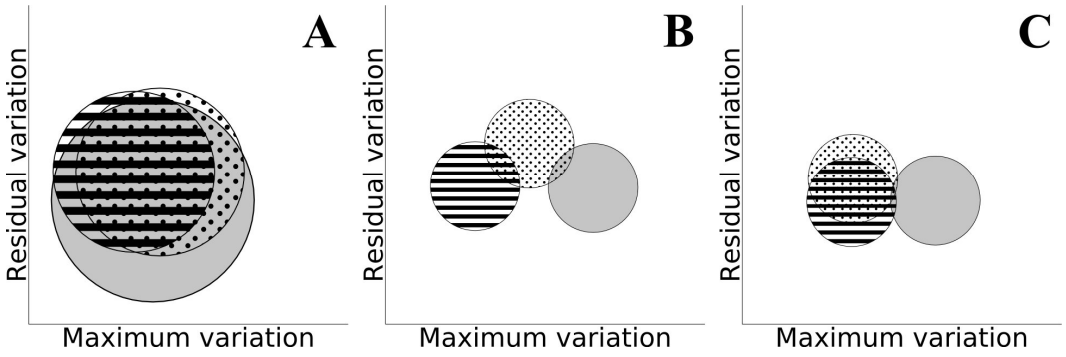

Figure 4: Potential outcomes of a three group discriminant function analysis. A) No distinction between terrestrial (grey), semi-aquatic (dots) and aquatic (stripes) groups. B) The axis of maximum variation between groups represents a gradual model of semicircular canal adaptive change with the semi-aquatic organisms exhibiting and intermediate state along the axis between the terrestrial and aquatic organisms. C) The axis of maximum variation represents a discrete model of semicircular canal adaptive change with the semi-aquatic organisms sharing a common morphotype with aquatic organisms and both distinct from the terrestrial morphotype (the reverse is also possible with the semi-aquatic group and terrestrial group indistinguishable from each other but distinct from the aquatic group). The functional axis is not restricted to the primary axis in these cases, it is possible that the functional signal accounts for less of the variation between the groups than some other factor; under this circumstance, the same patterns of change may be seen along the residual variation axis.

There is, of course, the possibility that no functional relationship exists that is universal to the four phylogenetic groups being investigated. In this case, although the group centroids must still have a triangular relationship, the within-group variances will be so large that no significant difference between functional groups will exist on either axis (Fig. 4A). On the other hand, if at least one of the two axes does produce significant discrimination between functional groups, it is expected that the arrangement of groups along that axis will reflect either of the two evolutionary models laid out for semicircular canal change, gradational, or discrete. Gradational change (*i.e.*, the expectation that a semi-aquatic organism shows adaptations that balance the demands of both types of locomotion and, therefore, exhibits an intermediate morphology) would be represented by terrestrial and aquatic groups defining the extreme of the

functional axis with the semi-aquatic group in the region between them (Fig. 4B). Discrete change (*i.e.* the expectation that adaptations for either of the extreme locomotion modes supersede the adaptations for the other and that, therefore, semi-aquatic organisms will have the adaptations of only the dominant form) would be represented by terrestrial and aquatic groups, again, forming the extremes of the functional axis but with the semi-aquatic group indistinguishable, along that axis, from one of the two extremes (Fig. 4C).

Lastly, it will be informative to examine which, if any, taxa are misclassified by the DFA. This will help in two areas. First, it will allow some estimate of the overall success of the classification and the success of each individual classification group. Second, it may also expose any patterns of taxonomic bias that are hidden by the general results. If, for example, the overall discrimination is significant, but most or all of the incorrectly classified specimens are mammals then this would cast doubt on the overarching nature of the detected shape change.

RESULTS

Elliptical Fourier Analysis (EFA) of each semicircular canal circuit produces 42 coefficients to describe the first 10 harmonics. The first two coefficients represent size and are typically not used for further analysis (Kuhl and Giardina, 1982); all the others are grouped four coefficients per harmonic. Thus, for this shape study, the first two coefficients are ignored, and the remaining 40 from each of the three canals are combined into a single 120-variable analysis. Discriminant Function Analysis (DFA) with stepwise inclusion of variables reduces this to 17 variables (Table 2).

One sample Kolmogorov-Smirnov tests of normality on each of the 17 variables included shows that within each classification group all the

Variable included in Analysis	Function 1 Coefficient	Function 2 Coefficient
ASC 1b	1.112	-1.070
ASC 1d	1.665	-1.037
ASC 4a	-0.508	-0.024
ASC 8a	-0.337	-0.039
ASC 8d	-0.032	0.481
ASC 9b	-0.346	0.258
PSC 1b	-0.166	0.721
PSC 3b	1.037	0.610
PSC 4c	-0.516	-0.326
PSC 5b	0.210	0.599
PSC 6c	0.177	-0.474
PSC 9d	-0.574	-0.516
PSC 10a	0.043	-0.351
LSC 1a	-0.368	1.151
LSC 3d	0.976	0.802
LSC 4b	-0.221	-0.420
LSC 4d	-0.349	0.732

Table 2: Standardized canonical discriminant function coefficients of Elliptical Fourier coefficients. 17 variables significantly informed the analysis, 6 from the anterior semicircular canal (ASC), 7 from the posterior semicircular canal (PSC), and 4 from the lateral semicircular canal (LSC). In the variable designations (*e.g.*, 1b) the number refers to the elliptical harmonic and the letter refers to one of the four coefficients within that harmonic. The issue of non-independence of Elliptical Fourier coefficients raised by Haines and Crampton (2000) refers to pairs of coefficients a and b or c and d within a single harmonic. No such pair appears in this variable list due to the stepwise inclusion of variables.

variables can be considered as being derived from a normally distributed population with one exception (in the aquatic group, the fourth coefficient in the first harmonic, 1D, for the anterior canal is not normally distributed). Thus, although the assumption of multivariate normality for the discriminant variables is not maintained, the violation is minor. As a result, only significance values for the discriminant functions very close to the threshold of $p = 0.05$ will be called into question (Klecka, 1980).

These data also do not satisfy the recommendation of homogeneity or equal group covariance matrices (Box's Test of covariance matrix inequality, $p << 0.01$). The primary ramification of this violation is less

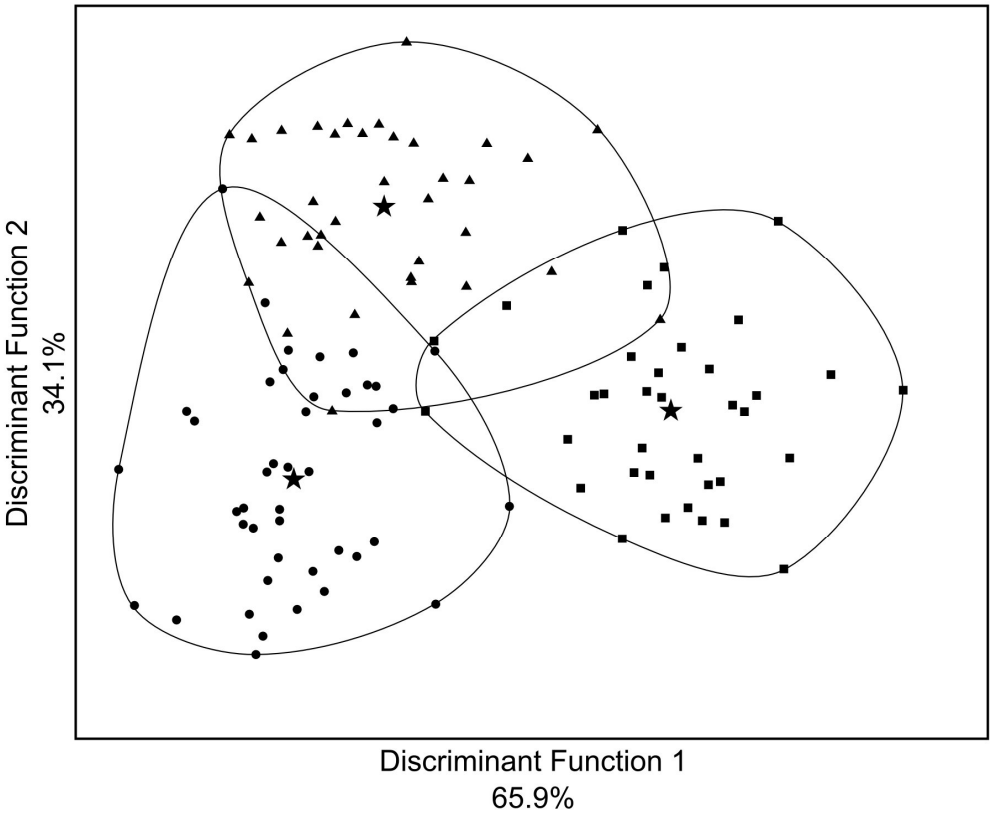

Figure 5: Discriminant function plot of locomotor groups based on Elliptical Fourier Analysis of the semicircular canal circuits. Circles are aquatic, triangles are semi-aquatic, squares are terrestrial, and stars represent the centroids for each of the groups. Axis 1 explains 65.9% of the variation between the groups and axis 2 the remaining 34.1%. Both axes exhibit significant discrimination ($p << 0.01$).

separation between the classification groups than might be achieved otherwise (Klecka, 1980). This, as long as there is significant discrimination between the groups, is of minimal concern. It does, however, increase the likelihood of misclassification of specimens that fall on the border between groups as these borders are less computationally distinct.

The discriminant functions produced explain 65.9% and 34.1% of the variation between the groups and both produce significant separation between at least two groups (as the significance is strong, $p << 0.01$, the

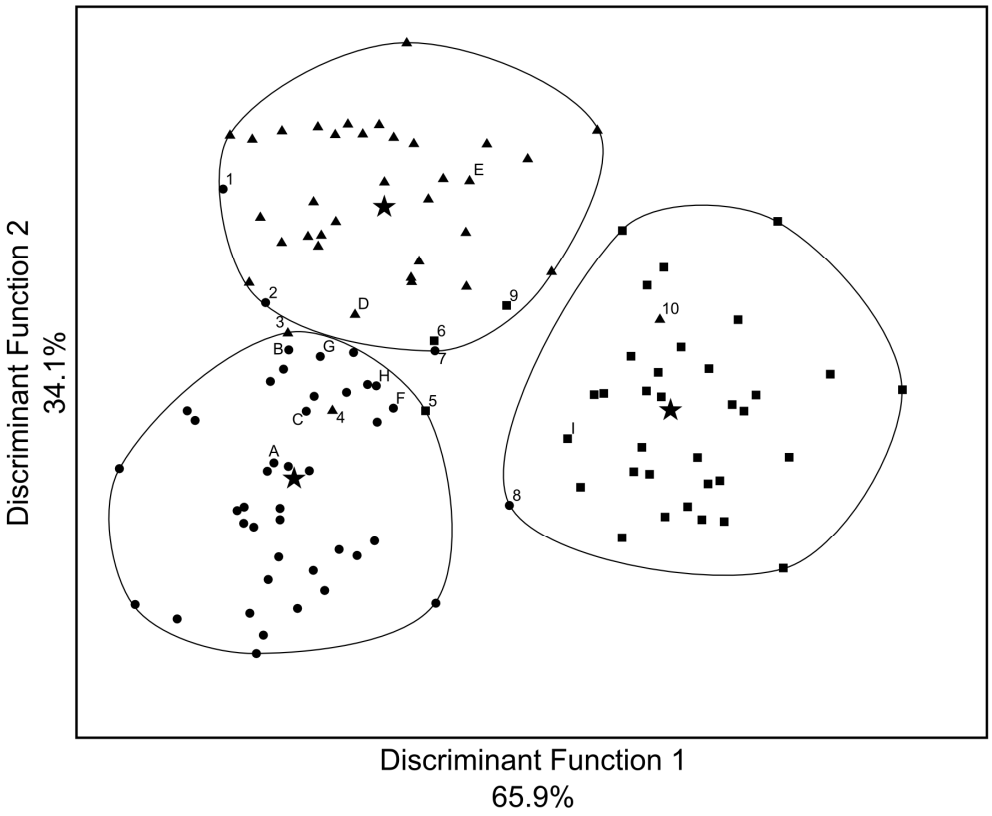

Figure 6: Classification territories for the Discriminant Function plot based on the Elliptical Fourier Analysis. Circles are aquatic, triangles are semi-aquatic, squares are terrestrial, and stars represent the centroids for each of the groups. Only 10 of the 115 specimens are misclassified: 1) *Tomistoma schlegelii*, 2) *Gavialis gangeticus*, 3) *Enhydra lutris*, 4) *Platysternon megacephalum*, 5) *Taxidea taxus*, 6) *Chelonoidis nigra*, 7) *Arctocephalus galapagoensis*, 8) *Trachemys scripta*, 9) *Gopherus berlandieri*, 10) *Varanus salvator*. In 7 of the 10 cases of misclassification, there is at least one other member of the same species in the dataset that is properly classified: A) *Tomistoma schlegelii*, B & C) *Gavialis gangeticus*, D) *Enhydra lutris*, E) *Platysternon megacephalum*, F) *Arctocephalus galapagoensis*, G & H) *Trachemys scripta*, I) *Gopherus berlandieri*.

minor violation of normal distribution does not alter the interpretation of these functions as providing distinction between the classification groups). As can be seen on Figure 5, a plot of the specimens in the morphospace defined by the two functions shows a distinct separation of the three classification groups.

A plot of the data from this discriminant analysis with the calculated

classification territories highlighted (Fig. 6) shows that 10 of the 115 cases are misclassified (only 8.7%). Of those 10, only two, *Taxidea taxus* and *Trachemys scripta*, are misclassified between the two extreme classification categories (*i.e.*, *Taxidea taxus* is terrestrial but misclassified as aquatic, and the reverse is true for *Trachemys scripta*). It should be noted, however, that the specimen of *Trachemys scripta* that is misclassified is only one of three members of that species in this analysis; the other two individuals are properly classified as fully aquatic. The other eight misclassifications are between one of the extreme groups and the intermediate groups. Again, six of the eight specimens that are misclassified between the intermediate group and one extreme have conspecific specimens in the analysis that are properly classified.

Procrustes landmark analysis of the same semicircular canal circuit data produces similar results (Fig. 7). In this case, the initial data set contains 300 variables (3 canals circuits each composed of 50 two-dimensional coordinates) and stepwise DFA finds 6 variables with significant contributions to group separation. The resulting discriminant functions explain 63.4% and 36.6% of the variation between the groups and, again, both produce significant separation between at least two groups ($p << 0.01$). Examination of the morphospace produced by these two functions shows that the first function exhibits a distribution of specimens very similar to that of the first DFA (correlation between the scores of the first discriminant functions is strong, Spearman's rho 0.673, $p << 0.01$).

Procrustes landmark analysis of the canal-only portion of the semicircular canal circuit does not produce the same results as in the first two analyses. Stepwise DFA reduces a data set of 150 variables (3 canals only paths each composed of 25 two-dimensional landmarks) to 9

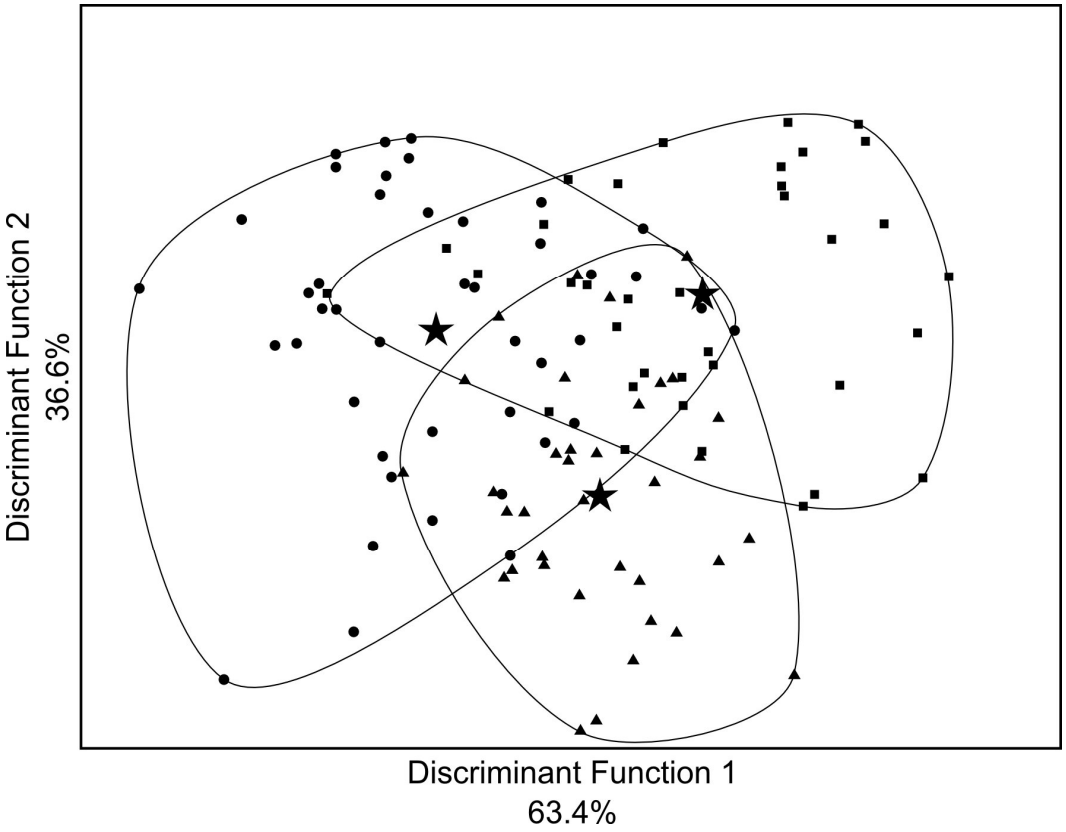

Figure 7: Discriminant function plot of locomotor groups based on Procrustes aligned landmark analysis of the semicircular canal circuits. Circles are aquatic, triangles are semi-aquatic, squares are terrestrial, and stars represent the centroids for each of the groups. Axis 1 explains 63.4% of the variation between the groups and axis 2 the remaining 36.6%. Both axes exhibit significant discrimination ($p << 0.01$).

variables. The distribution of specimens in the morphospace defined by these two functions is not the same as seen in the previous analyses (Fig. 8). The discriminant functions produced account for 60.0% and 40.0% of the variation between the groups, similar to the ranges in the previous two analyses, and both axes describe significant separation between at least two groups ($p << 0.01$). The two axes, however, are reversed relative to the first two morphospaces. That is, whereas the axis that separates the semi-aquatic group from the terrestrial and aquatic groups is the primary axis in the case of this analysis, it is the residual variation axis in the case

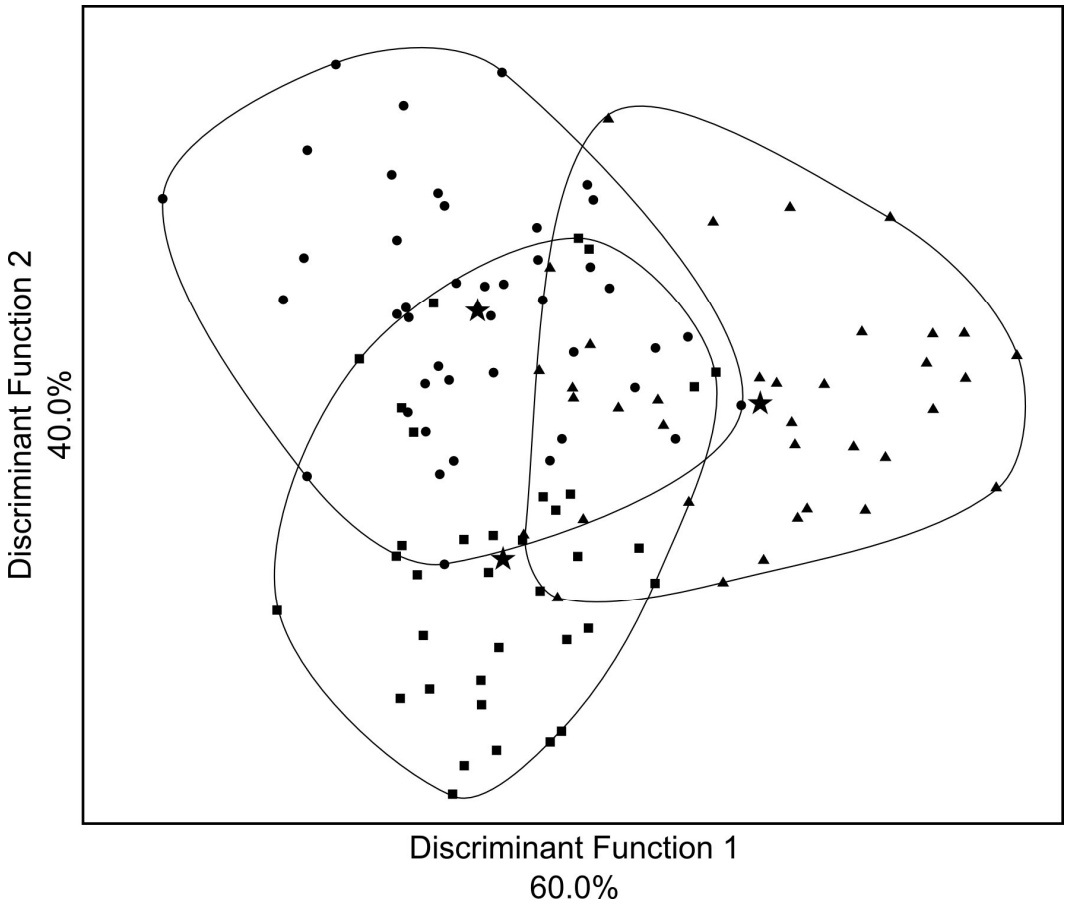

Figure 8: Discriminant function plot of locomotor groups based on Procrustes aligned landmark analysis of only the canal portion of the semicircular canal circuits. Circles are aquatic, triangles are semi-aquatic, squares are terrestrial, and stars represent the centroids for each of the groups. Axis 1 explains 60.0% of the variation between the groups and axis 2 the remaining 40.0%. Both axes exhibit significant discrimination ($p << 0.01$). The distribution of specimens along the second axis of this morphospace is similar to that found along the first axes of the Elliptical Fourier and complete canal circuit morphospaces.

of the first two analyses. Similarly, the distribution that appears on the primary axes of the first two analyses has been demoted to the residual variation axis in this analysis (correlation of the second function scores with the scores of the first discriminant function from the Fourier data is strong, Spearman's rho = -0.616, $p << 0.01$).

Whether or not the strong phylogenetic signal within the data set

has an effect on the results obtained by this method is examined by analyzing the semicircular canal circuit landmark data without the crocodilian specimens. Stepwise DFA of this reduced data set produces a pair of discriminant axes very similar to the discriminant axes of the entire data set. The nonparametric correlation between the specimen location along the primary axes of the two analyses is strong and significant (correlation with scores from the first discriminant function of the full circuit Procrustes analysis is strong, Spearman's rho = -0.851, $p << 0.01$). Both axes maintain significant separation of groups; the primary axis does, however, increase in the amount of variation explained, accounting for 79.5% of the variation in this smaller data set.

Similarly, when an entire sub-group, independent of phylogeny, is removed from the dataset (all aquatic organisms that utilize sub-aqueous flying) the result of the DFA remains consistent with previous analyses (correlation with scores from the first discriminant function of the full circuit Procrustes analysis is strong, Spearman's rho = 0.830, $p << 0.01$). In this instance, however, the primary axis exhibits a decrease in variation explained, accounting for only 56.7% of the variation between the groups.

DISCUSSION

The two tests of this method with the reduced data sets (one without crocodilians, and one without sub-aqueous flyers) demonstrate that this method is both robust and sensitive. Not surprisingly, removal of the crocodilian data increases the proportion of primary signal in the data set by reducing the phylogenetic disparity; nonetheless, presence or absence of the crocodilian data does not significantly alter the overall morphospace defined by the discriminant functions, indicating that an appropriate level of independence from phylogenetic shape has been

achieved. Furthermore, although removal of an entire locomotor group, organisms that utilize sub-aqueous flying, reduces the proportion of the primary signal, it also does not significantly alter the general morphospace. Thus, this method appears to produce a primary axis of discrimination sensitive to the functional discrepancy in semicircular canal shape.

The strength of this method for classifying amniote locomotor behavior is also considerable. The initial DFA on the Elliptical Fourier data has a 91.3% success rate on classifications (Fig. 6). Furthermore, only two of the 10 misclassified cases are off by two steps along the classification scale (*i.e.*, misclassified between the two extreme locomotor categories), whereas the other eight misclassifications are more 'minor', being between one of the extreme groups and the intermediate group. Seven of the 10 misclassified specimens have conspecific specimens in the analysis that are correctly classified (*Taxidea taxus*, *Varanus salvator*, and *Chelonoidis nigra* are the only single representatives that are misclassified). Increasing the sample size of these taxa, and of the dataset overall, may help further reduce these misclassifications that appear to result from individual variation. It is also worth noting that, as stated above, the minor violation of homogeneity was expected to result in a slight increase in the misclassification of specimens on the very borders of group territories. Thus, a sufficient increase in sample size that also balances the group homogeneity could substantially improve the classification success.

Two of the cases of misclassification appear to be a direct result of the strength of the crocodilian phylogenetic signal along the secondary axis. One specimen of both *Gavialis gangeticus* and *Tomistoma schlegelii* are each classified as semi-aquatic rather than the initial aquatic

designation. It is possible that with these taxa that have locomotor behaviors on the margin between two categories (see Chapter 7 for a discussion of the justification for the aquatic classification of these two taxa). Both these misclassified specimens, however, are found on the very margin of the semi-aquatic group, whereas the correctly classified members of these groups are more certainly within the aquatic territory. Furthermore, if just the primary axis, that with the locomotor signal, is considered, these two specimens fall nearly in line with the centroid for the aquatic group. Taking these considerations into account, the most likely explanation for the misclassification of these two specimens is their displacement along the secondary axis, which is probably a result of their crocodilian affinity.

Lastly, the distributions of misclassifications between the four clades examined is encouraging for the success of this method. No particular clade can claim a disproportionate number of the misclassified cases and at least one member of each of the clades is misclassified (Squamates 1, Mammals 3, Turtles 4, and Crocodilians 2 misclassifications). Thus, it seems, again, this method may be appropriately generalized, and not treat any of the specimens with a significant phylogenetic bias.

All but one of the discriminant analyses, regardless of shape variables used or specimen subsets produced the same pattern of specimen distribution along the primary axis of variation (the one exception to this, the canal path landmark data, produced the same pattern but along the residual variation axis). This is a pattern that matches the expected distribution of groups based on the gradual evolutionary change model. That is, terrestrial and aquatic morphotypes define the extremes along these axes, and the semi-aquatic morphotypes

are found in a region intermediate between the two extremes. This gradual distribution, as it occurs in all of the clades examined in this study, supports the hypothesis that there is adaptive change in semicircular canal shape in response to the demands of an aquatic habitat.

What adaptive change is occurring? Examination of the variables included in the stepwise discriminant analyses and the structure matrices from each analysis can begin to answer this question. When the Elliptical Fourier coefficients are treated to discriminant analysis, the structure matrix shows that the two anterior canal first harmonic coefficients that were not used in the analysis (because they were not independent of the two that were included) also have relatively high correlations with this data axis (all 4 of the anterior canal first harmonic coefficients are within the highest 21, out of 120, absolute correlations with the first function, no other harmonic from any of the canal circuits shows as high an average absolute correlation with the first discriminant function). Thus, on the whole, the anterior canal first harmonic, which is a measure of the overall ellipsoid ratio, dominates the discriminant function that corresponds to the locomotion signal.

Dominance of the anterior canal in the functional signal is consistent with the patterns of ontogenetic change in semicircular canal shape seen in the American alligator, *Alligator mississippiensis* (Chapter 3). In the alligator, the anterior semicircular canal shows little ontogenetic variation in shape, whereas the other two canals show significant ontogenetic variation. The changes exhibited by the posterior and lateral canals, however, are primarily driven by growth of the associated portions of the anterior canal. This pattern of development is indicative of a system in which the importance of the functional response of the anterior semicircular canal is weighted more highly than that of the other two

canals. According to the Elliptical Fourier coefficients, the shape changes are most prominent in the anterior canal, indicative of a system in which, again, the function of the anterior semicircular canal is prioritized.

There are also large contributions to this discriminant function from the third harmonics of the posterior and lateral semicircular canals. As the third harmonic, these coefficients represent shape changes that are on the order of one third of the overall circuit length, that is, smaller, more localized changes than are seen in the shape of the anterior semicircular canal. Again, this is possibly parallel to the pattern of ontogenetic growth in *Alligator mississippiensis*, in which shape changes do occur ontogenetically in the posterior and lateral canals, but these changes are localized to the regions of each canal that are related to the anterior canal.

A drawback to the Elliptical Fourier analysis is that interpreting the shape changes represented by the correlations between the harmonic coefficients and the discriminant function is difficult. Thus, in order to understand what changes are occurring, it is necessary to look at a different shape method.

A better understanding of the actual morphological changes that occur in the semicircular canals may be possible via examination of the landmark analyses. In these analyses, morphological interpretation of variables is straightforward. Discriminant analysis of the Procrustes aligned landmark data for the complete canal circuit produces a very similar distribution as the Fourier data (the functions in the two analyses also describe very similar proportions of the overall variation). The interpretation of the first discriminant function, therefore, remains the same. The structure coefficients, however, do not seem to tell the same story as the Fourier variables. Notably, the highest anterior canal structure correlation is ranked 69th and only four anterior canal structure

coefficients appear in the highest 100. In contrast to the pattern observed in Fourier structure coefficients, the posterior and lateral semicircular canals dominate this analysis.

One potential explanation for this discrepancy is the Procrustes alignment of the canal circuits, in particular, the rotation that is applied to each circuit in order to achieve least-squared landmark deviations. In the Fourier analysis, the strongest discriminating variables were for the first harmonic of the anterior semicircular canal, which describes the overall ellipsoid appearance of the circuit, including the orientation of the major axis of the ellipse. During superposition for Generalized Procrustes Analysis, each canal circuit is rotated independently and therefore the rotational deviation from the fixed Fourier alignment (each canal is oriented such that the vertical axis of the coordinate space corresponds to the line of intersection between the canal plane and the sagittal plane) is different for each canal. This appears to be bringing the morphological characters that produce strong functional discrimination in the Fourier analysis out of alignment. It is, therefore, not surprising that this landmark analysis underemphasizes the functional significance of the anterior semicircular canal.

An examination of the aligned data relative to the original unaligned data demonstrates how the Procrustes alignment differentially affects the functional signal within the anterior semicircular canal data relative to the posterior and lateral canals. It is not the amount of Procrustes rotation each group of canal circuits undergoes, it appears to be a matter of which subsets get rotated. With a circular standard deviation (Fisher, 1993) of 0.461 the spread of Procrustes rotations for the posterior canals is greater than for either the anterior or lateral canals (circular standard deviations of 0.391 and 0.278, respectively), yet, the functional signal attributable to the

posterior canal is not the most reduced by the Procrustes alignment. Reconstructing an average terrestrial mammalian anterior semicircular canal circuit, however, it becomes apparent that these circuits have been turned nearly 90° relative to their original (sagittal plane vertical) orientation and the common crus, which previously had been approximately parallel to the vertical axis, now lies along the horizontal axis. In contrast, the average non-mammalian anterior semicircular canal and all the posterior and lateral canal circuits do not appear to have been rotated significantly relative to the original orientation. Thus, the functional signal in the anterior semicircular canal circuits has been reduced because the Procrustes rotation misaligns the mammalian anterior canals.

It seems that this differential rotation results from the location of the ampulla (the starting location of the point series used to describe the circuits) within the mammal canals. In the non-mammalian taxa, with a more extended anterior division of the utricle, the ampulla is more laterally placed and there is rarely any significant course of the canal lateral to the ampulla. In contrast, many mammalian anterior semicircular canals have less expanded anterior divisions of the utricle and more medially located ampullae. With all the other landmarks in the circuit designated as sliding semi-landmarks, there is no secondary fixed point preventing the 90° rotation from bringing the medially placed ampulla in line with the laterally placed one.

Despite the difficulty with the anterior semicircular canal data, it is still possible to extract functionally significant results from the posterior and lateral semicircular canal circuits. Furthermore, it is possible to see how these results do, in fact, correspond with the results derived from the Fourier data. Examining the structure coefficients from the stepwise discriminant analysis, a pattern appears, similar in both cases. The

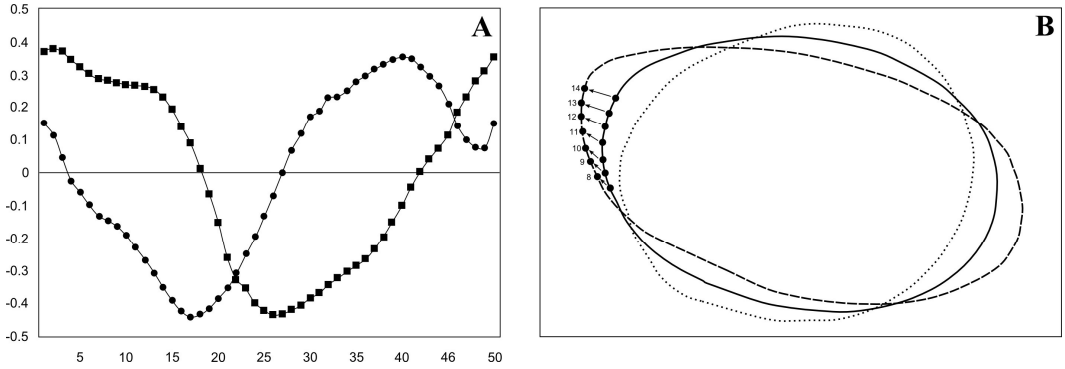

Figure 9: Pattern of landmark change in the posterior semicircular canal circuit. A) The pattern of structure coefficients for the X (circles) and Y (squares) is that of basic sinusoidal trigonometric functions. B) The result of applying these structure coefficients to the average posterior canal circuit (solid line) when scaled along the positive or terrestrial portion of the functional axis results in a canal circuit (dashed line) that is shorter and wider than the average. This change appears to be driven by the reorientation and elongation of the area of the common crus (partially represented by points 8 – 14). Similarly altering the average circuit by the structure coefficients scaled along the negative or aquatic portion of the functional axis results in the opposite change in circuit shape (dotted line).

structure coefficients for each corresponding set of data (X coordinates and Y coordinates for each canal circuit) have a maximum and minimum value and a smooth transition from one to the other and back again (Fig 9A). These maxima and minima are out of phase with each other between the X and Y coordinate series (thus producing patterns very similar to the cosine and sine trigonometric functions). Combining these results (Fig. 9B) produces patterns of change that are primarily changes in the eccentricity (the ratio of the major axis to the minor axis) of the ellipsoidal circuit. In the posterior semicircular canal one of the places where this change becomes most prominent is in the area of the common crus (*i.e.*, the region of the posterior semicircular canal that is in common with the anterior semicircular canal). This area of the posterior canal is increasing in height at the terrestrial end of the functional axis, implying that the anterior semicircular canal my be changing in a parallel manner, that is, increasing in height (with an accompanying decrease in width) in

the more terrestrial organisms.

If this parallel change in the anterior semicircular canal is, in fact, the case, then it should also be detectable in the lateral semicircular canal as a decrease in the length of common region between these two canals, the anterior division of the utricle. Examining the lateral semicircular canal structure coefficients, this prediction is upheld. In the case of the lateral semicircular canal circuit, the anterior division of the utricle is represented by the end of the coordinate series and its length is more closely parallel to the horizontal axis. This region of the canal circuit is where the structure coefficients for the X coordinates change from positive correlation with the first discriminant function to negative correlation. That is, the lower X values in this region increase and the larger X values decrease with increasing values of the first discriminant function. This results in a shortening of the horizontal component of this region with increasing terrestriality, as predicted, thus supporting the hypothesis that the changes described by this analysis in the posterior and lateral semicircular canals are just derivatives of changes in the anterior canal not detected because of the extreme Procrustes rotation.

When the ampullary and utricular contributions to the canal circuit are removed and shape of the slender portion of the canal alone is considered, the functional significance of the analysis appears to be reduced. The functionally informative axis of the morphospace transitions from the primary axis (as in the first two analyses) to the secondary axis and accounts for only 40.0% of the variation between the groups. Nonetheless, some discrimination between the functional groups is possible. Furthermore, the pattern of distribution along this second axis is still highly correlated with the functional distribution from the first analysis.

The decrease in the strength of the functional signal in this last

analysis is not at all surprising. By eliminating the utricular and ampullary portions of the semicircular canal circuit the shapes being considered no longer capture the complete area enclosed by the canal and thus this biophysically important factor is no longer informing the analysis to the same extent as before. Nonetheless, these canal-only shapes, with two (broadly spaced) non-sliding endpoints should mitigate the problem of the previous Procrustes analysis with the rotation of the anterior semicircular canal, and there should be a resulting increase in the contribution of the anterior canal morphology to the functionally informative discriminant axis.

The structure coefficients, as expected, lend further support for the emerging pattern of anterior semicircular canal importance. Anterior semicircular canal variables exhibit, in this analysis, the highest absolute structure coefficient on the functional axis of any of the analyses, 0.629, and the highest mean absolute structure coefficient (ANOVA; $p < 0.05$) of the canals in this analysis.

When the structure coefficients are applied to the anterior semicircular canal path data, a similar pattern to that proposed in the previous analysis is found (Fig. 10). That is, the more terrestrial the organism (in this case the lower the score along the second discriminant function) the taller the anterior semicircular canal is, particularly in the region of the common crus; this results in an overall appearance of a taller semicircular canal relative to its width. Aquatic organisms exhibit a corresponding decrease in the height of the anterior canal in the area of the common crus and, therefore, appear wider relative to their height.

Changes in the posterior and lateral semicircular canal paths parallel the patterns seen in the previous analysis and the patterns expected based on their relationships to the changing anterior semicircular canal, though in the lateral canal path the observed change is minor as

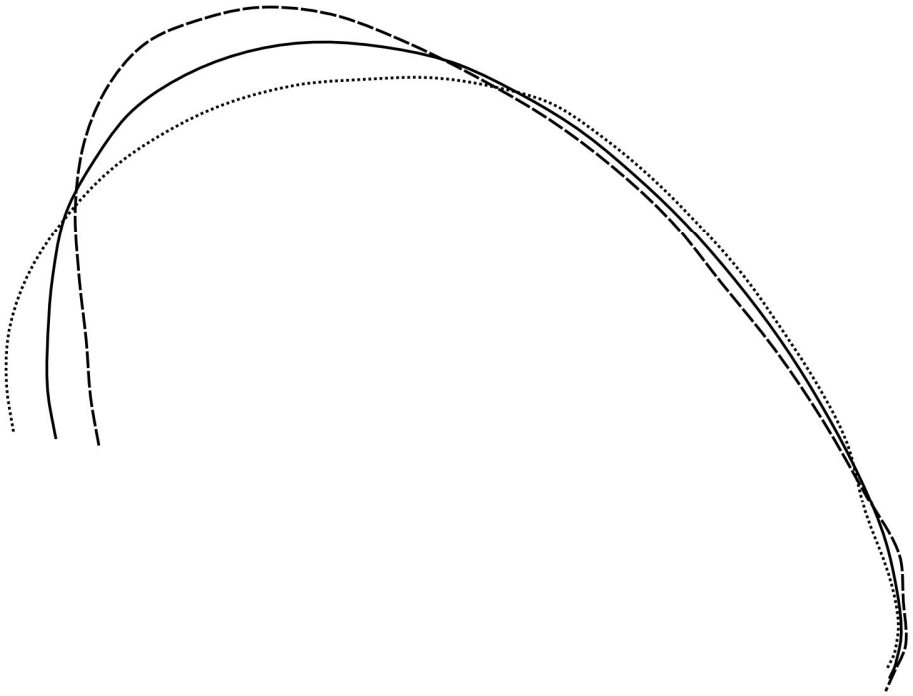

Figure 10: Structure coefficient based changes in the anterior semicircular canal path. The more terrestrial the organism (dashed line) the taller the region of the common crus and the thinner the canal path relative to its height. The changes observed in the posterior and lateral semicircular canals can both be attributed to the changes observed in the anterior semicircular canal. The posterior canal also exhibits an increase in the height of region of the common crus, and the lateral canal exhibits a decrease in the length of the anterior division of the utricle (the region shortened by the decrease in width of the anterior canal path).

the utricular portion of the circuit is not included in this path data. The posterior semicircular canal path exhibits a corresponding increase in the height of the common crus area, and the lateral semicircular canal exhibits a tendency toward minor decreases in the lengths of the (not included) utricular region.

CONCLUSIONS

Regardless of the phylogenetic differences in semicircular canal shape, this parameter, which implicitly encodes a ratio between the two

functionally important variables, area enclosed and streamline length of the canal, contains functionally important information about the locomotion of an organism. The majority of the shape change exhibited by the semicircular canals between terrestrial and aquatic organisms seems to be in the anterior semicircular canal, an idea consistent with the findings about changing canal shape in growing *Alligator mississippiensis* (Chapter 3). Shape changes also occur in the posterior and lateral semicircular canals, but these seem to be driven by the shape changes in the associated regions of the anterior semicircular canal.

In terrestrial organisms, there is an increase in the height of the anterior semicircular canal circuit (particularly in the region of the common crus) and corresponding decrease in its relative width relative to a closely related semi-aquatic organism. Conversely, in aquatic organisms, there is a decrease in the height of the anterior semicircular canal circuit and the common crus with the appropriate increase in circuit width relative to semi-aquatic organisms.

The consequences of this change in shape for the function of the semicircular canal are not entirely clear because this analysis only captures two of the biophysically important variables. These data cannot address whether this is a change driven by the semicircular canals themselves or a response of the canals to some other spatial factor changing in the skull. However, the presence of this change in four broadly divergent groups of amniotes with terrestrial and secondarily aquatic members suggests that this represents some form of change that is an adaptation to the invasion of an aquatic environment.

Chapter 6
The Correlation between Semicircular Canal Morphology and Cranial and Post-Cranial Skeletal Morphology

INTRODUCTION

It has been demonstrated that the anterior semicircular canal evinces a consistent change in shape in amniotes that reinvade an aquatic habitat (Chapter 5). There are several possible explanations for this observation. The first is that this represents the anterior semicircular canal being packed into the available space in the braincase and the size and shape of that space are adapting, in a consistent manner, to the demands of the change in environment. For example, hydrodynamic streamlining would be expected to reduce the overall height of the skull, which could, in turn, cause a reduction in the height of the semicircular canal system. The second possible explanation is that the canals themselves are adapting, independent of spatial packing requirements, to the changes in movement regime imposed by the changes in locomotor medium and substrate. Beyond either of those two hypotheses, it is also possible that the semicircular canals, because of the complicated nature of the system, are responding to changes in any number of other systems that are independent of locomotion such as the visual system or the oral cavity (feeding and oral prey capture unquestionably impose particular head movement regimes, particularly such behaviors as inertial feeding or lateral striking).

Several previous studies have observed differences in semicircular canal morphology across a variety of taxa with varying strategies for locomotion and, as a result, postulated a connection between semicircular

canal morphology and locomotor behavior (Georgi and Sipla, 2008; Hadžiselimović and Savković, 1964; Matano et al., 1985; Spoor et al., 2002; Spoor et al., 2007; Spoor and Thewissen, 2008; Spoor et al., 1994). Because of the sole focus on the vestibular system, however, none of these have been able to demonstrate that the observed change in the semicircular canal morphology is, itself, the adaptation and not an exaptation related to some other true adaptive change. Thus, the question of whether or not semicircular canal morphology changes in response to changes in locomotor behavior is still debatable.

It is not surprising, therefore, that the functional interpretations of some of these studies have been challenged. Graf and Vidal (1996) argued against locomotion-based adaptation of the semicircular canals in their response to Spoor and colleagues' (1994) observation that the vertical semicircular canals[1] in bipedal apes (*e.g.*, humans) had a larger radius of curvature than the lateral semicircular canal. Hullar (2006) assumed that if size-based semicircular canal adaptation hypotheses were true then vestibular afferent activity would be altered appropriately with canal size changes but found no support for this from literature values. More recently, however, Yang and Hullar (2007) experimentally determined that there is support for the relationship between canal size and vestibular afferent activity.

This study seeks to address the adaptive semicircular canal change hypothesis by examining a change in the circular canal morphology observed to correlate with a change in locomotor behavior and comparing it to morphological changes outside the semicircular canal system that are

[1] The anterior and posterior semicircular canals are typically described as being oriented parallel to the earth normal vector (*i.e.*, the gravity vector or vertical). Thus, they are frequently referred to in combination as the vertical canals.

known to be adaptive responses to the locomotor change of interest. In this case, the semicircular canal change being examined is the decrease in anterior semicircular canal height (particularly in the area of the common crus) relative to its width in secondarily aquatic tetrapods. The broad phylogenetic prevalence of this morphological change (demonstrated in carnivoran mammals, turtles, varanoid squamates, and crocodilians; Chapter 5) lends circumstantial evidence to the adaptive nature of this change by ruling out a phylogenetic basis for it. This is not, however, actual evidence in favor of adaptive change as it is still possible to argue that, for example, the space-constrained vertical semicircular canals are decreasing in height in response to a decrease in skull height that is an adaptive change to hydrodynamics of locomoting in an aquatic medium.

Furthermore, numerous hypotheses can be put forth that explain morphological changes in the semicircular canals as adaptations to non-locomotion related factors. The neurological connection between the semicircular ducts and the extraocular muscles is well known (the vestibuloocular reflex, or VOR) and it could, therefore, be hypothesized that changes in semicircular canal morphology are merely in response to changes in visual demands that may or may not accompany a locomotor transition. Alternatively, it could be hypothesized that the semicircular canals are adaptively changing in response to head rotations that are not related to locomotion, but, instead, result from rapid movements related to prey capture or inertial transport of food items within the oral cavity.

MATERIALS AND METHODS

37 amniote specimens from the study in Chapter 5 had sufficiently complete skeletal representation for this study (Table 1). The semicircular

Order	Genus	Species	Specimen
Carnivora	*Canis*	*lupus*	AMNH 98231
	Enhydra	*lutris*	AMNH 215274
	Pteronura	*brasiliensis*	AMNH 30190
	Arctocephalus	*galapagoensis*	AMNH 100341
	Callorhinus	*ursinus*	AMNH 71170
	Melursus	*ursinus*	AMNH 22720
	Ursus	*americanus*	AMNH 164284
	Ursus	*maritimus*	AMNH 15686
Crocodilia	*Alligator*	*mississippiensis*	AMNH 43314
	Caiman	*crocodilus*	AMNH 120030
	Caiman	*latirostrus*	AMNH 62555
	Caiman	*yacare*	AMNH 97299
	Melanosuchus	*niger*	AMNH 97325
	Paleosuchus	*palpebrosus*	AMNH 97328
	Paleosuchus	*trigonatus*	AMNH 66391
	Crocodylus	*niloticus*	AMNH 137180
	Crocodylus	*palustris*	AMNH 77632
	Crocodylus	*rhombifer*	AMNH 57773
	Osteolaemus	*tetraspis*	AMNH 117801
	Gavialis	*gangeticus*	AMNH 110145
Squamata	*Varanus*	*exanthematicus*	AMNH 137237
	Varanus	*gouldii*	AMNH 82819
	Varanus	*komodoensis*	AMNH 37913
	Varanus	*niloticus*	AMNH 10085
	Varanus	*salvator*	AMNH 141155
Testudines	*Carettochelys*	*insculpta*	AMNH 85893
	Caretta	*caretta*	AMNH 129868
	Chelonia	*mydas*	AMNH 5912
	Eretmochelys	*imbricata*	AMNH 7170
	Lepidochelys	*kempii*	AMNH 131148
	Dermochelys	*coriacea*	AMNH 92959
	Clemmys	*insculpta*	AMNH 126586
	Terrapene	*carolina*	AMNH 151408
	Terrapene	*coahuila*	AMNH 110194
	Trachemys	*scripta*	AMNH 94558
	Platysternon	*megacephalum*	AMNH 92740
	Apalone	*ferox*	AMNH 129737

Table 1: List of specimens used in this study. Representatives from four diverse clades of amniotes were used in order to capture the strengths of any functional signal relative to the strong phylogenetic differences between the groups. Collection abbreviations: AMNH – American Museum of Natural History.

canals of each specimen were imaged using a GE Lightspeed 16 X-Ray CT scanner. Previously outlined methods (Chapter 3) were followed in the production of 25 point (2 homologous and 23 sliding semipoint landmarks) semicircular canal path landmark sets for the anterior semicircular canals.

Due to the varied nature of amniote morphology, selecting a suite of metrics that utilize features consistently present across all the specimens is difficult. As a result, the available measurements in this study are limited. From the cranial and postcranial skeleton, 20 measurements were taken representing 5 different regions or functional modules.

Of the 20 metrics used (see Table 2 for definitions), 10 were derived from the cranium. The three measurements representing overall skull shape were skull length, skull height, and maximum skull width. For comparison with the orbits and general neural elements, three measurements were used, foramen magnum size, minimum interorbital width, and maximum interorbital width. Representing the oral cavity were four measurements, oral cavity length, oral cavity width, mandibular articulation size and mandibular articulation width. The other 10 metrics were derived from appendicular elements of the postcranium. From the forelimb, five measurements were taken: humerus length, humerus midshaft width, humerus midshaft height, humerus distal width, and radius length. An equivalent series of five measurements was taken from the hind limb: femur length, femur midshaft width, femur midshaft height, femur distal width, and tibia length. In order to remove the effects of overall size, each specimen's variables were scaled to the geometric mean of that specimen, producing a matrix of size independent (dimensionless) metrics.

Each of the hypotheses correlating a region or functional module

Group	Measurement	Definition
Skull Shape	1. Skull length	Distance along base of skull from anterior-most midline point on the premaxillae to the posterior tip of the occipital condyle
	2. Skull height	Perpendicular distance of midline frontal-parietal suture from line defined by measurement 1
	3. Maximum skull width	Distance across skull at the widest point
Neural Region	4. Foramen magnum size	Square root of the area of the foramen, approximated as an ellipse using the height and width of the opening
	5. Minimum interorbital width	Minimum distance between the medial margins of the orbits
	6. Maximum interorbital width	Maximum distance between the lateral margins of the orbits
Oral Region	7. Oral cavity length	Length of the tooth row from the anterior midline to posterior margin of posterior tooth element*
	8. Oral cavity width	Distance between the posterior-most tooth row elements*
	9. Mandibular articulation size	Distance across the articular surface between the cranium and the mandible (measured on the cranium)
	10. Mandibular articulation width	Distance between the lateral margins of the cranium-mandibular articulation (measured on he cranium)

with the morphology of the semicircular canals can be evaluated in a single analysis that examines the covariance in the semicircular canal measurements and metrics representing the different regions, Partial Least Squares Analysis (PLSA). Similar to generalized multiple regression analysis, PLSA (specifically the two-block PLSA that will be used here) finds a relationship between two sets of measurements. Unlike multiple regression, however, which treats one of the two sets of variables as dependent and the other as independent, PLSA treats both sets symmetrically (Rohlf and Corti, 2000) and, thus, requires no hypothesis of directional causation.

Two-block PLSA will result in a series of paired variable sets (one half of each pair representing the data from one of the different data sets)

Forelimb	11. Humerus length	Maximum length of the humeral shaft without the humeral head
	12. Humerus midshaft width	Diameter of the humeral shaft at its midpoint and parallel to the plane of the humeral condyles
	13. Humerus midshaft height	Diameter of the humeral midshaft at is midpoint and perpendicular to the plane of the humeral condyles
	14. Humerus distal width	Diameter of the humeral shaft proximal to and in the plane parallel to the humeral condyles
	15. Radius length	Maximum length of the radius along its shaft
Hind Limb	16. Femur length	Maximum length of the femoral shaft without the femoral head
	17. Femur midshaft width	Diameter of the femoral shaft at its midpoint and parallel to the plane of the femoral condyles
	18. Femur midshaft height	Diameter of the femoral midshaft at is midpoint and perpendicular to the plane of the femoral condyles
	19. Femur distal width	Diameter of the femoral shaft proximal to and in the plane parallel to the femoral condyles
	20. Tibia length	Maximum length of the tibia along its shaft

Table 2: Definitions of the measurements used in this study listed according to the module (*i.e.*, functional or non-functional hypothesis) they represent. *- In the case of edentulous taxa, tooth and tooth row elements were replaced with analogous measurements of the keratinous beak.

that describe shared covariation between the two data sets. The new PLSA variables are linear combinations of the original variables and, thus, the combination coefficients represent the relative contribution of each variable to the covariation of the two sets represented by that variable pair. In the specific case of this study, should one of the canal shape PLSA variables correspond to the previously reported functional shape change, then the coefficients for the paired PLSA variables derived from the regional metrics will represent the amount of covariation each regional metric undergoes with respect to the functional semicircular canal shape change.

The software tpsPLS (Rohlf, 2006) was used to perform this analysis. This program first converts the shape landmarks into partial

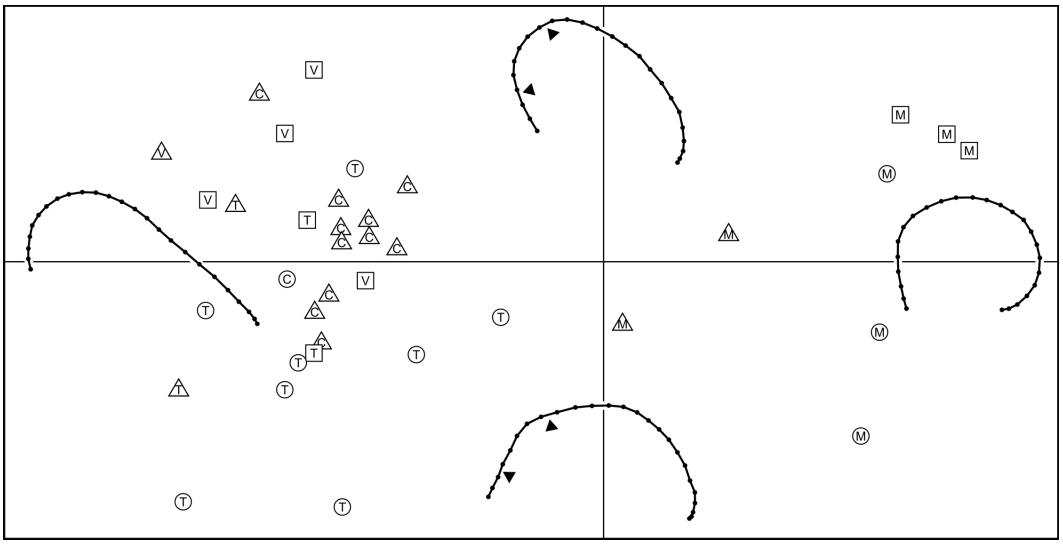

Figure 1: Projected specimen canal shape distribution along the two significant covariation axes derived from Partial Least-Squares analysis. The first axis (horizontal) describes 92.5% of the covariation between the datasets but is driven by phylogenetic differences between all of the mammals (M) on the right and the crocodilians (C), varanids (V), and turtles (T) on the left. The second axis (vertical) describes only 6.8% of the covariation between the datasets but does produce a locomotion based specimen distribution with terrestrial (squares) taxa at the top, aquatic (circles) taxa at the bottom, and most semi-aquatic taxa (triangles) in an intermediate position. The shape change in the anterior semicircular canal along the second axis corresponds very closely to the reported shape change between locomotor modes. In particular, the shape change is localized to the region of the common crus and the course of the canal as it emerges from the crus (black arrows), with the terrestrial taxa showing a higher crus and taller canal.

warp values before performing the PLSA. This software also provides functionality for randomized permutation tests that assist in assessing the statistical strength of the results. Standardization was not required for these data prior to PLSA as, within each data set, all variables had identical dimensions.

RESULTS

Only the first two PLSA variable pairs describe more than a fraction of a percent of the covariation between the two data sets. This first pair of variables accounts for a large majority of the covariation, 92.5%, and the

second variable pair only accounts for 6.8%. A randomized permutation test (100 permutations) indicates that these two variable pairs have moderate statistical support (in most cases, the summed squared covariance explained and the correlations between the variables of the data sets were higher in the observed data than in the permutation sets).

Rank order correlation of the shape scores along the PLSA variables with the specimens' scores along the functionally significant shape change axis in the first analysis from Chapter 5 show only a single significant correlation. PLSA variable 2 (Spearman's rho $p < 0.01$) appears to capture a shape change in the anterior semicircular canal that is similar to the reduction of height in the area of the common crus as taxa become more aquatic (Fig. 1). The reconstructed shapes along this axis confirms this pattern. In contrast, visual inspection of the specimen score distribution along the first PLSA variable shows a clear pattern of phylogenetic differentiation with the mammalian specimens distinct from all the other groups. Table 3 shows the first two sets of PLSA variable coefficients for the linear metric data.

DISCUSSION

The difference in magnitude between the covariance explained by Variable 1, which carries phylogenetic significance, and Variable 2, which carries functional significance, is consistent with expectations based on previously examined patterns. That is, between all these diverse amniote organisms there is a very strong difference in both semicircular canal shape and general cranial and postcranial factors based on phylogenetic affinity. Underneath that phylogenetic difference, however, there is a detectable functional signal that is also significant, both in the cranial and postcranial factors and in the semicircular canal shape.

Measurement	Variable 1	Variable 2
Skull length	0.42444	0.43595
Skull height	-0.07124	-0.09041
Maximum skull width	0.17382	0.03795
Foramen magnum size	0.00632	-0.02462
Minimum interorbital width	-0.2806	-0.1623
Maximum interorbital width	0.12316	-0.05528
Oral cavity length	0.41794	0.26426
Oral cavity width	0.42887	-0.12258
Mandibular articulation size	-0.02348	0.0157
Mandibular articulation width	0.22106	0.07491
Humerus length	-0.08689	0.11144
Humerus midshaft width	0.00715	-0.08334
Humerus midshaft height	-0.07282	-0.0274
Humerus distal width	-0.06001	0.0146
Radius length	-0.37848	0.37864
Femur length	-0.01072	0.57074
Femur midshaft width	-0.00701	-0.01082
Femur midshaft height	0.016	0.01465
Femus distal width	-0.00393	-0.00157
Tibia length	-0.34988	0.43571

Table 3: Coefficients for the linear metric data set from the first two PLSA variables. Variable 1 accounts for 92.5% of the covariation between the two data sets. Variable 2 accounts for 6.8% of the covariation. Specimen scores along variable 2 for this data set show a decrease in magnitude from terrestrial to aquatic locomotion, thus, positive coefficients represent elements that decrease in relative length and negative coefficients represent elements that increase in relative length as taxa become more aquatic.

By examining the magnitudes of the PLSA coefficients for the second variable (Table 3) it is possible to determine which of the linear metrics show the most similar change to the functional change in semicircular canal shape. The highest magnitude coefficient is for the length of the femur. Only three other coefficients are larger than half the magnitude of this largest one, the length of the tibia, the length of the radius and the length of the skull.

Three of the four coefficients with the largest magnitudes describe the relationship of the change in the semicircular canal system with aspects of limb morphology. The direction of these correlations corresponds with the expected limb changes commensurate with a transition from terrestrial to aquatic locomotion; that is, each of these limb

elements grows relatively shorter with increasing aquatic behavior. Thus, the changes in the anterior semicircular canals that correlate with locomotor mode show the greatest dependence on that locomotion specific morphology and not secondary dependence on some other, non-locomotor, trait that is changing adaptively.

The occurrence of the large-magnitude coefficient for skull length is likely just an artifact of specimen distribution. The direction of this correlation indicates that the relative length of the skull is decreasing with an increase in aquatic behavior. From a functional interpretation, this finding is counterintuitive as aquatic amniotes often exhibit more hydrodynamicaly suitable elongate and narrow skulls. This contrary finding is a possible result of the aquatic specimens in this data set being represented by a larger percentage of turtles (which have foreshortened skulls relative to other aquatic taxa) than the other phylogenetic groups.

It seems, therefore, that the amniote anterior semicircular canal is adaptively changing in response to different sensory demands that occur upon the reinvasion of an aquatic environment. The hypothesis that this change may be an exaptation driven by purely spatial demands (in particular the height of the skull) is not supported by the PLSA. The overall height of the skull is not a strong contributor to either covariation axis; it is nearly an order of magnitude less influential to the locomotor axis than the length of the femur.

Similarly, non-locomotor adaptive hypotheses of canal shape change being driven by prey capture and manipulation requirements might be indicated by large coefficients in the oral cavity metrics along the second axis. This is not the case. Although, the length of oral cavity has a larger coefficient than many other metrics, the sign is the same as the sign on the skull length coefficient and, likely, this oral cavity length is

giving an elevated signal because of its close relation to the overall skull length. For the same reasons, visual system hypotheses are also not supported. The orbital metrics show very weak negative coefficients along the second axis.

The suit of measurements used in this study was hampered by the requirement of identifying metrics that could consistently be found across the very broad variety of taxa included. Like the general shape method of Chapter 5, however, this first attempt produces some significant answers and opens some promising doors for improving the technique. A slightly different set of taxa might allow the identification of metrics that more precisely convey functional information regarding the various different hypotheses. More interestingly, perhaps, just as the possibility exists that the general canal shape method can be applied to other locomotor regimes, it is also possible that this method can be applied to any of the same finer scale locomotor dichotomies for which non-canal morphological correlates have been identified, for example, erect versus sprawling terrestrial locomotion (Beck et al., 2000).

CONCLUSIONS

Lastly, although this study demonstrates the adaptive nature of shape change in the anterior semicircular canals, it cannot address the functional significance of that change. The primary shortcoming, in this regard, is the inability to assess changes in all of the parameters that determine semicircular membranous duct function (these data do not address either the cross-sectional areas of the semicircular duct lumina nor the mechanical properties of the ducts' cupulae). Thus, it is not possible to derive what changes occur in the function of the semicircular ducts.

Chapter 7
Using Semicircular Canal Morphology to Reconstruct Locomotion in Extinct Amniotes: A Crocodylomorph Case Study

INTRODUCTION

From an evolutionary perspective, a common primary goal of functional morphological study is to identify a series of factors, observable in the fossil record, that have known functional correlates, in order to predict the function in organisms only observable in the fossil record. This study of the functional morphology of the shape of the semicircular canals is no different. The functional correlates of semicircular canal shape, with regards to whether an organism employs terrestrial or aquatic locomotion, have been established; now, it is necessary to determine if this information can be used in a predictive manner for fossil organisms with unknown or indeterminate modes of locomotion.

In terrestrial amniotes, the anterior semicircular canal has a different characteristic feature to its shape than in aquatic amniotes, independent of the typical shape found in members of its clade (Chapter 5). This shape change is centralized in the area of the common crus and the portion of the anterior canal that emerges from this structure. In terrestrial amniotes, the common crus is straight and long and the anterior semicircular canal continues to rise, usually steeply, towards a peak in its path beyond the area of the crus. In contrast, in aquatic amniotes, the common crus is shorter and often less straight; the anterior canal in these aquatic forms does not continue in as steeply a vertical direction after branching from the common crus, if it rises at all. The resultant overall

shape of these anterior canals is, in terrestrial amniotes, a canal that is tall relative to its width and, in aquatic amniotes, one that is wide relative to its height. Intermediate forms, semi-aquatic amniotes that balance terrestrial and aquatic behaviors, have an intermediate canal shape.

The question remains, however, whether or not this functional adaptation is sufficiently distinct to be used to identify terrestrial, semi-aquatic or aquatic locomotor behaviors in an extinct organism on the basis of semicircular canal morphology alone. To address this question, this study will examine a group of organisms with both extant and extinct members that exhibit a variety of locomotor behaviors across the spectrum from fully terrestrial to fully aquatic. Crocodylomorphs are, today, represented by members of three clades of crocodilians, the Alligatoridae (alligators and caimans), the Crocodylidae (crocodiles, dwarf crocodiles and the false gharial), and Gavialidae (the Indian gharial). The fossil history of the Crocodylomorpha however extends back to the late Triassic (Clark et al., 2004).

Modern crocodilians are predominately semi-aquatic. They are all well adapted to aquatic lifestyles (ranging from fresh to saline habitats) and employ a combination of lateral undulatory swimming and paddling. They are also, however, capable of utilizing numerous different terrestrial locomotor behaviors, ranging from the typical crocodilian semi-erect 'high-walk' to a sprawling belly-slide, and in some instances a bounding gallop. Despite these general patterns, there is a wide range of terrestrial capabilities in modern crocodilians, from the gharial which, as an adult, is incapable of utilizing the 'high-walk' (Bustard and Singh, 1978) and, with its piscivorous nature, is nearly fully aquatic, to some caimans which are capable of long distance overland migration between watering holes during dry seasons (Campos et al., 2003) and juvenile Australian

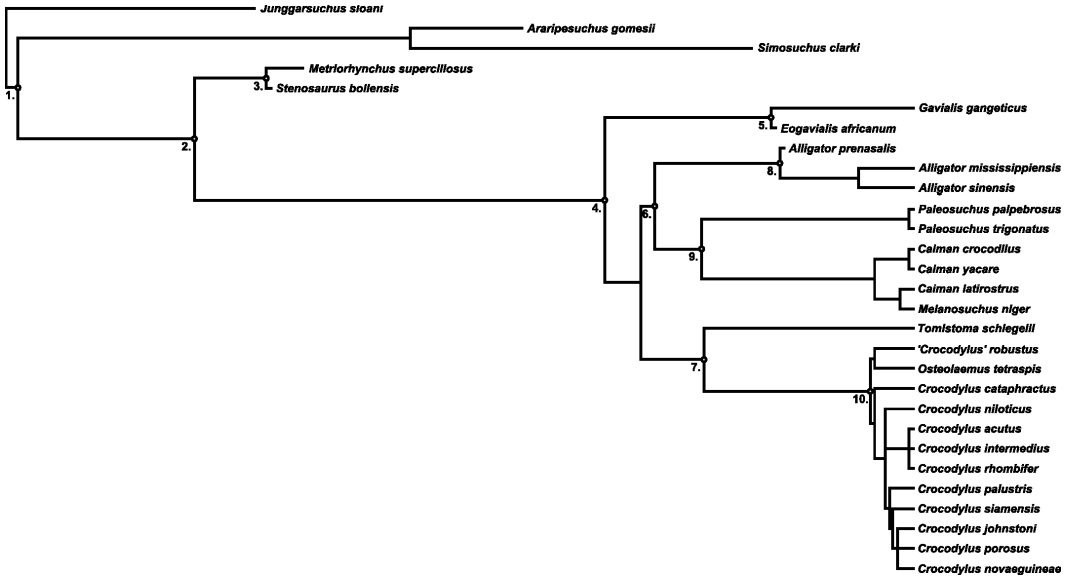

Figure 1: Phylogenetic relationships of fossil and extant taxa used in this analysis (Compostie from Brochu, 2006; Buckley et al., 2000; Clark et al., 2004; Gasparini et al., 2006; Pol and Apesteguia, 2005). 1. Mesoeucrocodylia 2. Neosuchia 3. Thalattosuchia 4. Crocodylia 5. Gavialidae 6. Alligatoridae 7. Crocodylidae 8. Alligatorinae 9. Caimaninae 10. Crocodylinae.

freshwater (*Crocodylus johnstoni*) and saltwater (*C. porosus*) crocodiles which can use a bounding gallop at high speeds (Renous et al., 2002). This gallop has also been reported in the American alligator (*Alligator mississippiensis*) moving at higher speeds (Reilly and Elias, 1998).

The range of locomotor behaviors becomes even broader when the fossil members of Crocodylomorpha (Walker, 1970) are considered (Fig. 1). Early members of this clade were fully terrestrial, utilizing a parasagittal limb posture, whereas some taxa became fully aquatic and adapted to marine environments. The 'shenosuchians', a paraphyletic group at the base of the Crocodylomorpha (Clark and Sues, 2002; Clark et al., 2004; Walker, 1990), maintain a suite of characters that clearly indicate terrestrial locomotor adaptation inherited from their early archosauromorph ancestors (Parrish, 1987; Walker, 1970). More deeply nested within Crocodylomorpha is Mesoeucrocodylia (Benton and Clark,

1988; Whetstone and Whybrow, 1983). Though there is some debate about the phylogenetic relationships of the basal mesoeucrocodylians and the placement of the genus *Araripesuchus* (Candeiro and Martinelli, 2006; Ortega et al., 2000; Pol and Apesteguia, 2005; Turner, 2006), there is no dispute about the terrestrial habits of this long-limbed, small-bodied crocodyliform (Ortega et al., 2000; Pol and Apesteguia, 2005).

Within Neosuchia, a clade of crocodyliforms that also has an unresolved position within Mesoeucrocodylia (Clark, 1994; Gasparini et al., 2006; Ortega et al., 2000; Pol and Apesteguia, 2005), another radiation, the thalattosuchians, derived numerous specializations for fully aquatic locomotion in a marine habitat. Less derived members of this clade (*e.g.*, *Steneosaurus*) exhibit moderate aquatic adaptations such as a reduction of dermal armor and mild dorsoventral flattening of the forelimbs (Buffetaut, 1980, 1982). Whereas more derived thalattosuchians, such as members of the genus *Metriorhynchus*, developed broad dorsoventrally flattened paddle-like limbs and an inferiorly directed bend of the caudalmost vertebrae indicating support for a heterocercal tail.

Just outside of Thalattosuchia, a group of marine crocodyiforms, the dyrosaurs, did not develop the paddle-like limbs or the heterocercal tail, but instead maintained robust limbs and a straight, but slightly dorsoventrally expanded, caudal vertebral column. Dyrosaurs, however, are not included in this analysis because they have an unusual vestibular morphology that makes accurate calculation of the semicircular canal shape impossible. Furthermore, this unusual morphology may indicate a non-swimming aquatic locomotor behavior (bottom walking) in these taxa (Georgi, 2006).

Two of the fossil taxa are embedded deep within crown clade Crocodylia: *Alligator prenasalis* and *'Crocodylus' robustus*. With two

exceptions, *Gavialis gangeticus* and *Tomistoma schlegelii*, all extant crocodilians are semi-aquatic. Thus, these relatively recent fossils are diagnosed as semi-aquatic based on both phylogenetic parsimony and extreme morphological similarity to all the closely related semi-aquatic forms.[1]

In two of the fossil taxa, mode of locomotion is questionable and will be tested by examination of the shape of the anterior semicircular canal. *Eogavialis africanum*, a fossil gavialoid, is not as easily classified as its sister group in this analysis, *Gavialis gangeticus*. *Gavialis gangeticus* is classified as aquatic in this study due not only to its piscivorous nature, but also to the fact adult gharials can not employ the crocodilian 'high-walk'. Thus, although *E. africanum* exhibits a morphology that suggests a similar piscivorous nature, no evidence exists as to its capacity for the 'high-walk', and it must be classified, for the purposes of this analysis, as having indeterminate locomotor behavior.

The other fossil taxon in this study with an unknown locomotor behavior is the mesoeucrocodylian, *Simosuchus clarki*. The original description of *Simosuchus* notes that it does not have the dorsally directed nares or orbits of aquatic crocodilians, and that it shares many skull characteristics with the closely related and supposedly fossorial *Malawisuchus* (Buckley et al., 2000; Gomani, 1997). Furthermore, analysis of limb proportions allies *Simosuchus* more closely with tetrapods that employ terrestrial locomotion than those that employ aquatic or semi-aquatic locomotion (J. Groenke, Unpublished Data). There is, however,

[1] Traditional phylogenetic hypotheses keep *Tomistoma* closely allied to Crocodylidae and leave *Gavialis* outside as a sister group to Alligatoridae and Crocodylidae (Brochu, 2003). Early molecular studies, on the other hand, strongly supported moving *Gavialis* inside of Crocodylidae sister to *Tomistoma* (Brochu, 2003). More recent molecular studies, however, have become more congruent with the morphological studies (McAliley et al., 2006), leaving *Tomistoma* as the only fully aquatic modern crocodilian within either Crocodylidae or Alligatoridae.

also evidence that *Simosuchus* was semi-aquatic. The hexagonally arranged foramina on the maxilla and mandible of *Simosuchus* are potentially sites for pressure transducing organs that are only found in semi-aquatic crocodilians whether extant or extinct (Soares, 2002). The two fossil taxa classified as semi-aquatic in this study, *'Crocodylus' robustus* and *Alligator prenasalis* both share this feature. Thus, there is conflicting evidence regarding whether *Simosuchus* was semi-aquatic or terrestrial and it must be considered to have an indeterminate locomotor mode.

These two indeterminate taxa are fortuitously arrayed to test both possible functional contrasts in this data set. *Eogavialis africanum* will test if this analysis can distinguish between semi-aquatic and aquatic locomotor modes. *Simosuchus clarki* will test if this analysis can distinguish between terrestrial and semi-aquatic locomotor modes.

MATERIALS AND METHODS

The semicircular canals of 61 crocodylomorph specimens representing 29 taxa (Table 1) were imaged using a GE Lightspeed 16 X-ray CT. Specimens were size-matched in order to minimize any ontogenetic shape effects (Chapter 3). Anterior semicircular canal shape was quantified using previously described methods (Chapter 3) to produce 50 point landmark representations of the shape of the complete semicircular canal circuit.

A series of analyses performed on the semicircular canal shape in a broad array of amniotes showed that an Elliptical Fourier Analysis (EFA) of the circuit shape produced the best discrimination between the classification groups of terrestrial, semi-aquatic, and aquatic amniotes (Chapter 5). It was further demonstrated in the same study, that of the

Taxa	Specimens
†*Jungarrsuchus sloani*	IVPP V14010
†*Araripesuchus gomesii*	AMNH 24450
†*Simosuchus clarki*	UA 8679
†*Metriorhynchus superciliosus*	AMNH 997
†*Stenosaurus bollensis*	MCZ 1063
†*Gavialis gangeticus*	AMNH 110145, AMNH 7138, AMNH 88316
†*Eogavialis africanum*	AMNH 5073
†*Alligator prenasalis*	MCZ 1014
Alligator mississippiensis	AMNH 31563, AMNH 9043, AMNH 43316
Alligator sinensis	AMNH 23898, AMNH 23899, AMNH 23900
Paleosuchus palpebrosus	AMNH 137162, AMNH 97328
Paleosuchus trigonatus	AMNH 137174, 137175, AMNH 66391
Caiman crocodilus	AMNH 120030, AMNH 15184, AMNH 58137, SN
Caiman yacare	AMNH 97298, AMNH 97299
Caiman latirostrus	AMNH 62555
Melanosuchus niger	AMNH 101419, AMNH 110179, AMNH 97325
Tomistoma schlegelii	AMNH 113078, AMNH 15177
†*'Crocodylus' robustus*	MCZ 1006
Osteolaemus tetraspis	AMNH 117801, AMNH 24740
Crocodylus cataphractus	AMNH 10074, AMNH 107634, AMNH 75424
Crocodylus niloticus	AMNH 10081, AMNH 137180, AMNH 71192
Crocodylus acutus	AMNH 15175, AMNH 15182, AMNH 9659
Crocodylus intermedius	NMNH 211281
Crocodylus rhombifer	AMNH 141073, AMNH 57773, AMNH 77595
Crocodylus palustris	AMNH 75707, AMNH 77632, AMNH 96134
Crocodylus siamensis	AMNH 28358, AMNH 49231, AMNH 72640
Crocodylus johnstoni	AMNH 86540, SN
Crocodylus porosus	AMNH 58015, AMNH 6581, AMNH 7131
Crocodylus novaeguineae	AMNH 64425

Table 1: List of taxa examined in this study. Institutional abbreviations: AMNH – American Museum of Natural History, IVPP – Institute of Vertebrate Paleontology and Paleoanthropology, MCZ – Museum of Comparative Zoology, NMNH – National Museum of Natural History, SN – Personal Collection of Stephen Nash, UA – University of Antananarivo.

coefficients produced by EFA, those from the first and third harmonics of the anterior canal circuit were responsible for the strongest discrimination. Therefore, EFA was applied to this set of crocodylomorph anterior semicircular canal circuits and the first 4 elliptical harmonics were extracted (see Chapter 5 for a discussion of the problems with EFA and the solutions employed in this study). For each taxon represented by more than a single individual, a species average of the Fourier coefficients was calculated and all further statistical treatment was done on this reduced set of 29 specimens.

All of the modern taxa were classified as having semi-aquatic

locomotor behavior except for *Gavial gangeticus* and *Tomistoma schlegelii*, which were classified as utilizing aquatic behavior. Of the 29 represented taxa, 8 were fossils and therefore have only inferred or indeterminate locomotor behavior. For those fossil taxa in which the locomotor inference is well supported, they were categorized accordingly (*Junggarsuchus sloani* and *Araripesuchus gomesii* as terrestrial; *Alligator prenasalis* and *'Crocodylus' robustus* as semi-aquatic; *Metriorhynchus superciliosus* and *Steneosaurus bollensis* as fully aquatic). The two fossil taxa with indeterminate locomotor mode, *Eogavialis africanum* and *Simosuchus clarki*, were left unclassified for the analysis.

A phylogenetic independent contrast analysis was performed in order to assess the amount of phylogenetic autocorrelation inherent to the data (Maddison and Maddison, 2007; Midford et al., 2007) based on the phylogenetic hypothesis in Figure 1. Four different methods of branch length estimation were utilized, minimum time of divergence, natural log of minimum time of divergence, arbitrary length based on node depth (Pagel, 1992), and all branch lengths equal to 1. Under each of the four conditions, the magnitude of the contrast at each node was compared in bivariate space with the standard deviation of that contrast to insure independence of the contrast values (Garland Jr. et al., 1992).

Following the methods of Chapter 5, Discriminant Function Analysis (DFA) with stepwise inclusion of variable was performed in order to identify those variables that maximized the differentiation between the functional groups. In this case, however, the two taxa with indeterminate locomotor habit were each treated as separate categories in the analysis (for a total of 5 categories). In order to test the robusticity of this method for determining locomotor behavior in fossil taxa, after *Simosuchus* and *Eogavialis* have been classified in an overall analysis, each fossil taxon

will be excluded one case at a time and subjected to DFA analysis with just the Fourier coefficients identified in the stepwise DFA.

RESULTS

Under each of the four of the branch length hypotheses, Phylogenetic Independent Contrast methods failed to actually produce contrast sets free from autocorrelation. In each case, at least 2 of the 16 variables produced significant correlations between the contrast magnitudes and the contrast standard deviations. The variables that produced the most strongly significant correlations were the variables that, in the overall analysis of Chapter 5, had the highest correlations with the functional axis.

Stepwise DFA on the non-contrast dataset produces only a single significant discriminant function (Fig. 2). This function describes 91.0% of the separation between the 5 groups. Consistent with the results from Chapter 5, this function describes a gradient with aquatic and terrestrial locomotion at the extremes and semi-aquatic locomotion in between these. Second highest group classification based on the squared Mahalanobis Distance to the centroids groups *Simosuchus clarki* with the terrestrial crocodylomorphs and *Eogavialis africanum* with the aquatic ones.

The stepwise DFA selected three variables for inclusion in the analysis, two from the 3rd harmonic and one from the 1st harmonic. Examination of the structure matrix shows two other variables that have a correlation with as large a magnitude as the three included variables. Of those, one is a second variable from the first harmonic and the other is a third variable from the third harmonic. This parallels the results from the overall amniote analysis of Chapter 5 in which the structure matrix

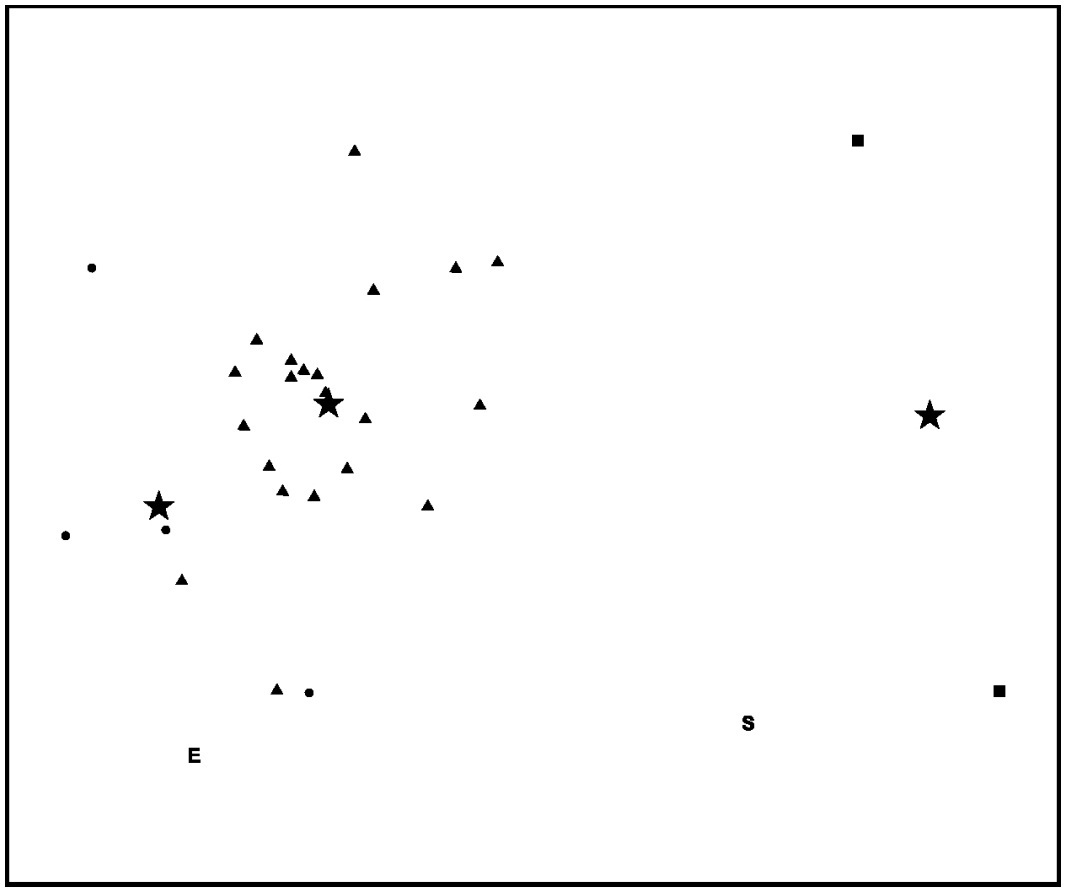

Figure 2: Bivariate plot of the scores of the first two discriminant functions resulting from a stepwise Discriminant Function Analysis of the Elliptical Fourier coefficients from the first 4 harmonics of the anterior semicircular canal in 29 fossil and extant crocodylomorph taxa. The first function describes 91.0% of the variance between the 5 groups, none of the other functions produced statistically significant distinction. The first discriminant function describes a functional gradient from more aquatic taxa on the left to more terrestrial taxa on the right. Three Elliptical Fourier variables contribute to this function, 1 from the first harmonic and 2 from the third. Circles – aquatic, triangles – semi-aquatic, squares – terrestrial, E – *Eogavialis africanum*, and S – *Simosuchus clarki*. Categorization of the two separate taxa based on the squared Mahalanobis distances to group centroids classifies *Simosuchus* as terrestrial and *Eogavialis* as fully aquatic.

indicated that anterior canal 1st and 3rd harmonics played a large role in the functionally significant discriminant function.

With the locomotion of *Simosuchus* and *Eogavialis* assigned to the appropriate groups, casewise testing of the other six fossils properly

assigned each to the initially inferred group. Of the six analyses, 5 produced only a single significant discriminant function with a minimum described variance between the groups of 93.5%. The sixth, *Araripesuchus gomesii*, produces two significant discriminant functions. The first of the two functions (which remains the functionally important one) still describes an overwhelming majority of the variation between the groups, 84.5%.

DISCUSSION

The Phylogenetic Independent Contrast (PIC) method was unable to produce contrast values for the internal phylogenetic nodes that were independent of their evolutionary position. In this case, however, this does not indicate that these data are strictly phylogenetic in nature and therefore not viable for functional analysis. Rather, this is a reflection of the nature of Crocodylomorph evolutionary history.

The analysis of all amniotes from Chapter 5 demonstrated that the signal being detected is independent of broad phylogenetic trends and this analysis uncovered the same pattern of functionally significant variables. The Partial Least-Squares analysis from Chapter 6 demonstrated that this particular shape change is, in fact, adaptive in nature relative to the change in locomotion that the organism is undergoing. In light of these two facts, it is reasonable to assume that, despite the results indicating phylogenetic correlation from the PIC analysis, that the indicated shape change in these crocodylomorphs is functional and not simply a phylogenetic artifact.

PIC analysis is returning consistently phylogenetically correlated data because of the historical transformation of basal, terrestrial crocodylomorphs into more derived, aquatic or semi-aquatic forms.

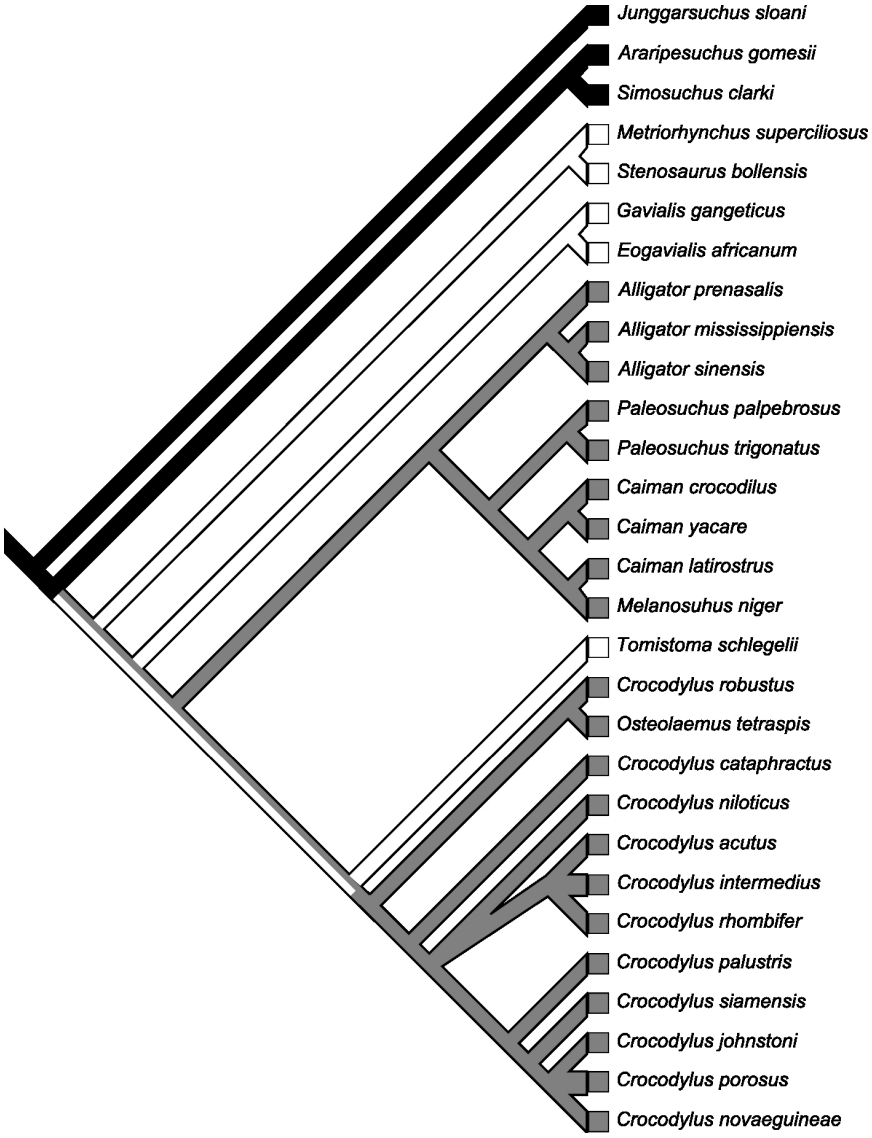

Figure 3: Parsimony reconstructed hypothesis of the evolution of locomotor behavior (treated as an ordered state from terrestrial to semi-aquatic to aquatic) through the Crocodylomorpha. Terrestrial lineages are in black, semi-aquatic in grey and aquatic lineages are in white. Only the more basal members of the clade are terrestrial. As of the Neosuchia, there are no more terrestrial members and the stem lineage becomes ambiguous between semi-aquatic and aquatic locomotion. The classification of *Simosuchus clarki* as terrestrial fixes the state of the early stem lineage as terrestrial (if it were semi-aquatic, the stem lineage would be ambiguous all the way to the root) which accurately reflects the terrestrial locomotion of the archosauromorph ancestors of this clade. The classification of *Eogavialis africanum* as aquatic only serves to fix the Gavialidae as aquatic and does not reduce or increase the ambiguity of the stem Crocodylia.

Evolving from terrestrial archosauromorphs, basal crocodylomorphs are primarily terrestrial. The only three terrestrial taxa in the analysis are the three species at the base of the tree (Fig. 3). No extant crocodilian is fully terrestrial, so there is no good way to balance this phylogenetic disparity. Nonetheless, the striking agreement of this analysis with the overall amniote analysis lends strong support to the idea that these results are phylogenetically correlated only because of the particular historical trends in crocodylomorph locomotion.

The assignment of *Simosuchus clarki* to the group of terrestrial locomotors agrees, to a certain extent, with the diagnosis of the original description (Buckley et al., 2000). Although, it must be noted this does not address the type of terrestrial locomotion so the fossorial hypothesis remains untested. Soares' (2002) hypothesis about the presence of the multiple foramina on the maxillae and mandible indicating a semi-aquatic lifestyle is not supported. This hypothesis is interesting as it is based on neurosensory morphology and is, theoretically, independent of axial or appendicular morphology. Semicircular canal shape, however, is similarly a neurosensory morphology and also independent of these other factors. These two neurosensory arguments do not, however, agree. There are two most parsimonious functional explanations regarding this discrepancy (non-functional explanations such as phylogenetic inertia are, of course, also a possibility). It is possible that *Simosuchus* utilized these pressure receptors for a different purpose than water surface disturbance detection. On the other hand, there is also the possibility that *Simosuchus* employed some specialized behavior that requires no adaptation for aquatic locomotion but still results in a significant amount of time spent with the head in the water (*e.g.*, shore wading).

The indeterminate nature of the locomotion of *Eogavialis africanum*

was based on a lack of evidence (unknown capacity for crocodilian 'high-walk'), not conflicting evidence as in the case of *Simosuchus*. Thus, the assignment of *Eogavialis* to the aquatic group does not resolve any evidence-based hypotheses, nor does it, due to the nature of negative evidence, actually imply that *Eogavialis* was incapable of the 'high-walk'. It does however remove character state ambiguity from the stem lineage of Gavialidae as represented in this study. It must be noted, that more basal gavialoids, the 'thoracosaurs', may reintroduce ambiguity at the base of Gavialoidea as they are exclusively found in marginal marine sediments (Brochu, 2004) and therefore might have been either semi-aquatic or fully aquatic. A thoracosaur braincase was scanned for this study, but the vestibular preservation was insufficient for accurate rendering of the semicircular canals.

Accurate casewise assignment of the remaining six fossil specimens into their inferred locomotor groups lends much strength to the confident use of this analysis to predict the locomotor behaviors of extinct organisms based solely on vestibular morphology. Looking at the score distribution along the first discriminant function, it is not surprising that the two terrestrial taxa, *Junggarsuchus sloani* and *Araripesuchus gomesii*, are accurately assigned as there is a notable gap between these taxa and the semi-aquatic taxa. Whether this gap represents a more significant functional divide between terrestrial taxa and those that use semi-aquatic locomotion than is found between semi-aquatic and aquatic locomotors, or whether it just represents a sampling bias due to the paucity of terrestrial data points cannot be determined. It is, however, worth noting that, in the overall amniote analysis (Chapter 5), there doesn't appear to be nearly the same gap between terrestrial and semi-aquatic regions of the morphospace.

Even more encouraging is the correct assignment of both of the inferred aquatic taxa, *Steneosaurus bollensis* and *Metriorhynchus superciliosus*, and of the two inferred semi-aquatic taxa, *Alligator prenasalis* and *'Crocodylus' robustus*. The scores of these two functional groups are much more closely related along the first discriminant function (even to the point of some overlap) but, nonetheless, there is still sufficient information in just the three elliptical coefficients used for this analysis to correctly parse these four fossil taxa.

This shape-based method also seems to have several advantages over previous attempts to use vestibular morphology to examine the locomotor behavior of extinct organisms (Spoor et al., 2007; Spoor et al., 1994, 1996; Walker et al., 2003). The two primary differences between this new method and older ones are a matter of scaling and phylogenetic correction. Previous studies, based on the initial comparative work of Jones and Spells (Jones, 1974; Jones and Spells, 1963; Mayne, 1965), require that a size variable be compared to the body mass of the organism. In fossil studies, body mass is an estimated measure of questionable reliability that will always add error to the analysis. Secondly, having demonstrated that the critical morphological character suite for this method is, in all likelihood, an adaptive change (Chapter 6) and independent of phylogenetic baseline shape (Chapter 5) the need for precise knowledge of the phylogenetic position of the organism in question and complicated transformations designed to removed phylogenetic correlation is reduced.

It is also notable that the locomotor distinctions of this study are more specific than in previous studies. Past work has focused on vague terms such as 'agile' and 'slow' (Spoor et al., 2007; Spoor and Thewissen, 2008; Walker et al., 2003). Although it could be argued that the locomotor

categories of terrestrial, semi-aquatic, and aquatic are also, to a certain extent, vague, this is only a first attempt with this method and finer scale locomotor determinations may yet be possible as this method matures. For example, it is notable that within the semi-aquatic category, *Crocodylus johnstoni* (capable of employing a terrestrial gallop), *Paleosuchus trigonatus* (nocturnal forest floor hunter with a high percentage of small terrestrial vertebrates and invertebrates in is diet), and *Crocodylus palustris* (capable of traveling long distances between water in dry season and digs and utilizes extensive burrows) are the three closest to the terrestrial discriminant scores. Similarly, within the aquatic group, *Tomistoma schlegelii* (more capable of terrestrial locomotion than is the gharial) and *Steneosaurus bollensis* (fossil aquatic crocodilian with limbs not yet modified into paddles) are the two points that most closely overlap with the semi-aquatic range of discriminant scores.

CONCLUSIONS

Examining extant and extinct members of the archosaurian clade Crocodylomorpha, it has been shown that the shape of the anterior semicircular canal is functionally distinct. Using Elliptical Fourier coefficients from the first and third harmonic ellipse, separation of these taxa into groups based on the terrestrial, semi-aquatic, and aquatic locomotor behavior of these organisms is possible. Furthermore, this analysis is sufficiently robust as to permit the classification of extinct organisms whose locomotor mode may be unknown or indistinct. *Simosuchus clarki*, a mesoeucrocodylian with morphological evidence that points to both terrestrial and semi-aquatic behavior, is found to have a semicircular canal system adapted for terrestrial locomotion. In contrast, *Eogavialis africanum*, a gavialoid with insufficient evidence to distinguish

between aquatic and semi-aquatic modes of life, is found to have a semicircular canal system adapted for aquatic locomotion.

This is only the beginning for this method. The refinement the analytical methods and the addition of more data may permit even more discrimination of the amount of aquatic or terrestrial locomotion employed by extinct organisms, and maybe even distinguish between different modes within a single locomotor lifestyle (*i.e.*, lateral undulation versus limb paddling).

Chapter 8
Concluding Remarks

CONCLUDING REMARKS

The success of this study does not, in my opinion, lie with the specific results obtained with regards to specific amniotes and their preferred locomotor environment. Rather, it has more to do with the demonstrated efficacy of the methods developed for the examination of semicircular canal morphology in the context of functional morphology and the fossil record. Beyond that specific success, any study that proves fertile for new questions and avenues of research should be considered successful; this work, as a result of the methods employed, has, I believe, achieved this fertile state.

At a glance, Chapter 5 of this study presents evidence that, in mammalian carnivores, turtles, crocodilians and some squamate lizards, the common crus is taller and the anterior semicircular canal continues higher beyond the top of the crus in terrestrial forms (with a corresponding shortening of the crus and decrease in height of the anterior semicircular canal in aquatic forms). Although this is an interesting find, it is, taken in isolation, of only moderate importance. Moreover, without further context, the utility of this result is limited, even though the reported correlation between shape and locomotor environment is strong, because there is no evidence that the correlation can be applied in a predictive nature beyond the clades covered in the study.

Chapter 6 addresses this specific issue by demonstrating that the change in the semicircular canal shape covaries with changes in the locomotor modules (limbs) of the specimens examined and not with

features of the surrounding skull morphology. This is taken as strong evidence of an adaptive change in the system (*i.e.*, one that is occurring directly as a result of changes in the locomotion and not as a result non-locomotor changes in the skull). Now the results of Chapter 5 have theoretical justification for application in a broader context. As an adaptive change, it is reasonable to hypothesize that the identified change in semicircular canal shape can be found in any amniote clade, not just those covered in Chapter 5.

It should be emphasized, again, that there is no way, based on the data available in this study, to determine the actual effect on the function of the semicircular ducts brought about by this reported change in semicircular canal function, and numerous different hypotheses are equally justifiable. Speculating on the nature of the differences between a terrestrial and an aquatic environment, however, may favor one of the possible explanatory hypotheses. In particular, it is notable that, due to its higher density, an aquatic environment can be expected to impose slower general movements on locomoting animals (in order to maintain a similar Reynolds number with respect to changing environment, an organism should move over an order of magnitude more slowly in water than in air).

The change from terrestrial to aquatic locomotion is accompanied by an overall increase in the elliptical nature of the anterior semicircular canal. An ellipse of the same area as a circle will have a longer perimeter. In semicircular duct terms, an elliptical duct that encloses the same area as a circular one will have a longer duct length. Identical areas mean the two differently shaped ducts will have the same inertial force response to rotation, but the longer elliptical canal length will lower the minimum rotational velocity to which the duct is maximally sensitive. That is, all other factors being equal, the elliptical duct will have the same strength of

response, as the circular duct, but be sensitive to slower rotations (such as would be expected in an aquatic environment).

This study grew out of a desire to construct a tool to aid in the reconstruction of the locomotor behaviors of fossil vertebrates. With Chapters 5 and 6 demonstrating a theoretical rationale for expecting semicircular canal shape differences in terrestrial and aquatic amniotes, Chapter 7 finally shows that this model does permit a robust reconstruction of locomotor environment in fossil crocodilians. These specific results, however, are only the beginning. Not all questions of locomotion in fossil taxa are restricted to whether mammalian carnivores, turtles, varanids, and crocodilians prefered to move about on land or in water. The success of this method is that it need not be restricted solely to the locomotor transition nor to the taxa considered in this study. The method outlined herein makes the study of semicircular canal morphology available to answer a broad array of questions regarding locomotion.

The full potential and limits of this method are, as yet, unknown. It will be instructive to examine other broad ranges of locomotion (*e.g.*, Is there a change in semicircular canal shape between terrestrial taxa and flying taxa?), or even fine scale locomotor differences (*e.g.*, Is there a difference in semicircular canal shape between terrestrial taxa that use a sprawled posture and those that walk with erect limbs?).

Questions besides those that deal specifically with semicircular canal morphology are also raised by the results presented here. Knowing that the semicircular canals (and therefore the semicircular ducts within the canals) are changing adaptively in response to locomotor changes speaks only to the fact there must be differences in the movements experienced by the head of terrestrial and aquatic amniotes; it cannot, because of the impossibility of reconstructing a complete picture of

semicircular duct function, provide a full description of what the movement differences are. An important next step in understanding the connection between the vestibular system and locomotion will be the experimental determination of the movement profiles of the heads of terrestrial and aquatic amniotes or, for that matter, any organisms that this method is applied to in the future.

Bibliography

Alonso PD, Milner AC, Ketcham RA, Cookson MJ, Rowe TB. 2004. The Avian Nature of the Brain and Inner Ear of *Archaeopteryx*. Nature 430:666-669.

Baird IL. 1974. Some Aspects of the Comparative Anatomy and Evolution of the Inner Ear in Submammalian Vertebrates. Brain Behav Evol 10:11-36.

Beck AL, Blob RW, Hopson JA. 2000. Interpreting Limb Posture in Fossil Tetrapods: Morphological Indicators of Sprawling and Non-Sprawling Locomotion. J Vert Paleo 20(3 Supp):20A.

Benton MJ, Clark JM. 1988. Archosaur Phylogeny and the Relationships of the Crocodylia. Benton MJ, editor. Oxford: Clarendon Press.

Bissonnette JP, Fekete DM. 1996. Standard Atlas of the Gross Anatomy of the Developing Inner Ear of the Chicken. J Comp Nerol 368(4):620-630.

Bookstein FL. 1997. Landmark Methods for Forms Without Landmarks: Morphometrics of Group Differences in Outline Shape. Med Im Anal 1(3):225.

Breuer J. 1891. Ueber die Function der Otolithen-Apparate. Pflügers Archiv European Journal of Physiology V48(1):195.

Brichta AM, Acuna DL, Peterson EH. 1988. Planar Relations of Semicircular Canals in Awake, Resting Turtles, *Pseudemys Scripta*. Brain Behav Evol 32(4):236-245.

Brochu CA. 2003. Phylogenetic Approaches Toward Crocodylian History. Ann Rev Earth Planet Sci 31(1):357-397.

Brochu CA. 2004. A New Late Cretaceous Gavialoid Crocodylian From

Eastern North America And The Phylogenetic Relationships Of Thoracosaurs. J Vert Paleo 24(3):610-633.

Brochu CA. 2006. A New Miniature Horned Crocodile from the Quaternary of Aldabra Atoll, Western Indian Ocean. Copeia 2006(2):149-158.

Buckley GA, Brochu CA, Krause DW, Pol D. 2000. A pug-nosed crocodyliform from the Late Cretaceous of Madagascar. Nature 405(6789):941-944.

Buffetaut E. 1980. Teleosauridae et Metriorhynchidae: l 'évolution de deux familles de Crocodiliens mésosuchiens marins du Mésozoïque. 105e Congrès National des Sociétés Savantes:pp.1-12.

Buffetaut E. 1982. Radiation évolutive, paléoécologie at biogéographie des crocodiliens mésosuchiens. Mémoires de la Société Géologique de France 60(142):1-88.

Bustard HR, Singh LAK. 1978. Studies on the Indian Gharial *Gavialis gangeticus* (Gmelin) (Reptilia, Crocodilia). Change in Terrestrial Locomotory Pattern with Age. J Bombay Nat Hist Soc 74:534-536.

Campos Z, Coutinho M, Magnusson WE. 2003. Terrestrial Activity of Caiman in the Pantanal, Brazil. Copeia 3(3):628-634.

Candeiro CRA, Martinelli AG. 2006. A review of paleogeographical and chronostratigraphical distribution of mesoeucrocodylian species from the upper Cretaceous beds from the Bauru (Brazil) and Neuquén (Argentina) groups, Southern South America. Journal of South American Earth Sciences 22(1-2):116-129.

Cignoni P, Cerisoli E, Corsini M, Fiorin V, Gfrei A, Gangemi G, Latronico M, Mazzanti F, Mochi A, Pirosu F, Ponchio F, Portelli D, Ranzuglia G, Vacca D, Vannini F, Venturi A, Vergauwen M. 2007. MeshLab Visual Computing Lab - ISTI - CNR http://meshlab.sourceforge.net/. Version 1.0.0.

Clark JM. 1994. Patterns of Evolution in Mesozoic Crocodyliformes. Fraser NC, Sues H-D, editors. Cambridge: Cambridge University Press.

Clark JM, Sues H-D. 2002. Two new basal crocodylomorph archosaurs from the Lower Jurassic and the monophyly of the Sphenosuchia. Zool J Linn Soc 136(1):77-95.

Clark JM, Xu X, Forster CA, Wang Y. 2004. A Middle Jurassic `sphenosuchian' from China and the origin of the crocodylian skull. Nature 430(7003):1021-1024.

Collewijn H. 1989. The Vestibulo-ocular Reflex: an Outdated Concept? In: Allum JHJ, Hulliger M, editors. Prog Brain Res: Elsevier Science Publishers.

Curthoys IS, Blanks RHI, Markham CH. 1977a. Semicircular Canal Radii of Curvature (R) in Cat, Guinea Pig and Man. J Morph 151(1):1-15.

Curthoys IS, Markham CH, Curthoys EJ. 1977b. Semicircular Duct and Ampulla Dimensions in Cat, Guinea Pig and Man. J Morph 151(1):17-34.

Dempster WT. 1930. The Morphology of the Amphibian Endolymphatic Organ. J Morph 50(1):71-126.

Elshehawey EF, Elbarbary EME, Afifi NAS, El-Shahed M. 2001. An Exact Solution of the Endolymph Equation. App Math Comp 124(3):331.

Ezure K, Graf W. 1984a. A Quantitative Analysis of the Spatial Organization of the Vestibulo-ocular Reflexes in Lateral- and Frontal-eyed Animals – I. Orientation of Semicircular Canals and Extraocular Muscles. Neuroscience 12(1):85-93.

Ezure K, Graf W. 1984b. A Quantitative Analysis of the Spatial Organization of the Vestibulo-ocular Reflexes in Lateral- and Frontal-eyed Animals – II. Neuronal Networks Underlying Vestibulo-

oculomotor Coordination. Neuroscience 12(1):95-109.Flourens M. 1828. Experiences sur les canaux semi-criculaires de l'oreille, dans les mammifères. Lues à l'Académie royale des Sciences.

Ferson S, Rohlf FJ, Koehn RK. 1985. Measuring Shape Variation of Two-Dimensional Outlines. Syst Zool 34(1):59-68.

Flourens M. 1828. Experiences sur les canaux semi-criculaires de l'oreille, dans les mammifères. Lues à l'Académie royale des Sciences.

Fisher NI. 1993. Statistical Analysis of Circular Data. Cambridge: University of Cambridge.

Frisch T, Sørensen MS. 2000. Estimation of Volume Referent Bone Turnover in the Otic Capsule after Sequential Point Labeling. Ann Otol Rhinol Laryngol 109(1):33-39.

Garland Jr. T, Harvey PH, Ives AR. 1992. Procedures for the Analysis of Comparative Data Using Phylogenetically Independent Contrasts. Syst Biol 41(1):18-32.

Gasparini Z, Pol D, Spalletti LA. 2006. An Unusual Marine Crocodyliform from the Jurassic-Cretaceous Boundary of Patagonia. Science 311(5757):70-73.

Gauldie RW, Radtke RL. 1990. Using the Physical Dimensions of the Semicircular Canal as a Probe to Evaluate Inner Ear Function in Fishes. Comparative Biochemistry and Physiology Part A: Physiology 96(1):199-203.

Gauthier GM, Blouin J, Bourdin C, Vercher J-L. 2007. Adaptive Control: a Review of the Ability to Acquire and Maintain High Sensorimotor Performance. Computers in Biology and Medicine 37(7):989-1000.

Georgi JA. 2006. Dyrosaurid Inner Ear Morphology as Evidence for Locomotor Behavior. J Vert Paleo 26(3 Sup):66A.

Georgi JA, Sipla JS. 2008. Balance: Comparative and Functional Anatomy

in Aquatic Reptiles and Birds. In: Thewissen JGM, Nummela S, editors. Sensory Evolution on the Threshold: Adaptations in Secondarily Aquatic Vertebrates: University of Californa Press.

Gomani EM. 1997. A crocodyliform from the Early Cretaceous dinosaur beds, northern Malawi. J Vert Paleo 17:280-294.

Graf W, Baker R. 1985a. The Vestibuloocular Reflex of the Adult Flatfish. I. Oculomotor Organization. J Neurophysiol 54(4):887-899.

Graf W, Baker R. 1985b. The Vestibuloocular Reflex of the Adult Flatfish. II. Vestibulooculomotor Connectivity. J Neurophysiol 54(4):900-916.

Graf W, Vidal P-P. 1996. Semicircular Canal Size and Upright Stance Are Not Interrelated. J Hum Evol 30(2):175-181.

Gray AA. 1906. Observations on the Labyrinth of Certain Animals. Proc Roy Soc Lond B 78(525):284-296.

Gray AA. 1907. The Labyrinth of Animals, Vol 1. London: Churchill.

Gray AA. 1908a. The Labyrinth of Animals, Vol 2. London: Churchill.

Gray AA. 1908b. An Investigation on the Anatomical Structure and Relationships of the Labyrinth in the Reptile, the Bird, and the Mammal. Proc Roy Soc Lond B 80(543):507-528.

Gray O. 1955. A Brief Survey of The Phylogenesis of the Labyrinth. J Laryngol Otol 69:151-179.

Groen JJ, Lowenstein O, Vendrik JH. 1952. The Mechanical Analysis of the Responses from the End-organs of the Horizontal Semicircular Canal in the Isolated Elasmobranch Labyrinth. J Physiol (Lond) 117:329-346.

Hadžiselimović H. 1968. Contribution to Knowledge of the Bony Labyrinth and Interfenestral Axis in Certain Mammals and Man. Acta Anat 70(1):54-65.

Hadžiselimović H, Savković LJ. 1964. Appearance of Semicircular Canals

in Birds in Relation to Mode of Life. Acta Anat 57:306-315.

Haines AJ, Crampton JS. 2000. Improvements To The Method Of Fourier Shape Analysis As Applied In Morphometric Studies. Palaeontology 43(4):765-783.

Hawkins JE, Schacht J. 2005. Sketches in Otohistory -- Part 8: The Emergence of Vestibular Science. Audiol Neurotol 10(4):185-190.

Highstein SM, Rabbitt RD, Holstein GR, Boyle RD. 2005. Determinants of Spatial and Temporal Coding by Semicircular Canal Afferents. J Neurophysiol 93(5):2359-2370.

Howland HC, Masci J. 1973a. The Functional Allometry of Semicircular Canals, Fins and Body Dimensions in the Juvenile Centrarchid Fish, *Lepomis gibbosus* (L.). J Embryol Exp Morph 29(3):721-743.

Howland HC, Masci J. 1973b. The Phylogenetic Allometry of the Semicircular Canals of Small Fishes. Zoomorphology 75(4):283-296.

Hullar TE. 2006. Semicircular Canal Geometry, Afferent Sensitivity, and Animal Behavior. Anat Rec A 288A(4):466-472.

Jeffery N, Spoor F. 2004. Prenatal Growth and Development of the Modern Human Labyrinth. J Anat 204(2):71-92.

Jones GM. 1974. Chapter II. The Functional Significance of Semicircular Canal Size. In: Kornhuber HH, editor. Vestibular System Part 1: Basic Mechanisms. Berlin: Springer-Verlag.

Jones GM, Spells KE. 1963. A Theoretical and Comparative Study of the Functional Dependence of the Semicircular Canal upon Its Physical Dimensions. Proc Roy Soc Lond B 157(968, A Discussion on Photosynthesis):403-419.

Klecka WR. 1980. Discriminant Analysis. Lewis-Beck MS, editor. Newbury Park, CA: Sage Publications.

Kuhl FP, Giardina CR. 1982. Elliptic Fourier Features of a Closed Contour. Computer Graphics and Image Processing 18:236-258.

Lee FS. 1893. A Study of the Sense of Equilibrium in Fishes. J Physiol (Lond) 15(4):311-348.

Lindenlaub T, Burd H, Nevo E. 1995. Convergent Evolution of the Vestibular Organ in the Subterranean Mole-rats, *Cryptomys* and *Spalax*, as Compared With the Aboveground Rat, *Rattus*. J Morph 224(3):303-311.

Lindenlaub T, Oelschläger HA. 1999. Morphological, Morphometric, and Functional Differences in the Vestibular Organ of Different Breeds of the Rat (*Rattus norvegicus*). Anat Rec 255:15-19.

Lowenstein O, Sand A. 1940. The Mechanism of the Semicircular Canal. A Study of the Responses of Single-Fibre Preparations to Angular Accelerations and to Rotation at Constant Speed. Proc Roy Soc Lond B 129(855):256-275.

Mach E. 1875. Grundlinien der Lehre von den Bewegungsempfindungen. Leipzig.

Maddison WP, Maddison DR. 2007. Mesquite: A Modular System or Evolutionary Analysis. Version 2.01: http://mesquiteproject.org.

Maisey JG. 2001. Remarks on the Inner Ear of Elasmobranchs and Its Interpretation from Skeletal Labyrinth Morphology. J Morph 250(3):236-264.

Matano S, Kubo T, Niemitz C, Günther M. 1985. Semicircular Canal Organ in Three Primate Species and Behavioral Correlations. Fortschr Zool 30:677-680.

Maxwell SS. 1921. The Equilibrium Functions of the Internal Ear. Science 53(1375):423-429.

Mayne R. 1965. The "Match" of the Semicircular Canals to the Dynamic

Requirements of Various Species. The Role of the Vestibular Organs in the Exploration of Space. NASA SP-77: NASA. p 57-67.

McAliley LR, Willis RE, Ray DA, White PS, Brochu CA, Densmore Iii LD. 2006. Are crocodiles really monophyletic?--Evidence for subdivisions from sequence and morphological data. Molecular Phylogenetics and Evolution 39(1):16-32.

McVean A. 1999. Are the Semicircular Canals of the European Mole, *Talpa Europaea*, Adapted to a Subterranean Habitat? Comp Biochem Physiol A 123(2):173.

Midford PE, Garland Jr. T, Maddison WP. 2007. PDAP:PDTREE Package for Mesquite. Version 1.1: http://mesquiteproject.org/pdap_mesquite/.

Mosimann JE, James FC. 1979. New Statistical Methods for Allometry with Application to Florida Red-Winged Blackbirds. Evolution 33(1):444-459.

Muller M. 1994. Semicircular Duct Dimensions and Sensitivity of the Vertebrate Vestibular System. J Theor Biol 167(3):239-256.

Muller M. 1999. Size Limitations in Semicircular Duct Systems. J Theor Biol 198(3):405-437.

Muller M. 2000. Biomechanical Aspects Of The Evolution Of Semicircular Duct Systems. Neth J Zool 50(2):279-288.

Navier CLMN. 1823. Mémoire sur les lois du mouvement des fluides. Mem Acad R Sci (Paris) 6:389-416.

Moen DS. 2006. Cope's Rule in Cryptodiran Turtles: Do the Body Sizes of Extant Species Reflect a Trend of Phyletic Size Increase? J Evol Biol 19(4):1210-1221.

Oman CM, Marcus EN, Curthoys IS. 1987. The Influence of Semicircular Canal Morphology on Endolymph Flow Dynamics. Acta Otolaryngol

103(1):1-13.

Ortega F, Gasparini Z, Buscalioni AD, Calvo JO. 2000. A New Species Of *Araripesuchus* (Crocodylomorpha, Mesoeucrocodylia) From The Lower Cretaceous Of Patagonia (Argentina). J Vert Paleo 20(1):57-76.

Pagel MD. 1992. A Method for the Analysis of Theoretical Data. J Theor Biol 156:431-442.

Parrish JM. 1987. The Origin of Crocodilian Locomotion. Paleobiology 13(4):396-414.

Pol D, Apesteguia S. 2005. New Araripesuchus Remains from the Early Late Cretaceous (Cenomanian;Turonian) of Patagonia. Amer Mus Nov 3490(1):1-38.Rabbitt RD. 1999. Directional Coding of Three-dimensional Movements by the Vestibular Semicircular Canals. Biol Cybern 80(6):417-431.

Rabbitt RD, Damiano ER, Grant JW. 2004. Biomechanics of the Semicircular Canals and Otolith Organs. In: Highstein SM, Fay RR, Popper AN, editors. The Vestibular System. New York: Springer.

Ramprashad F, Landolt JP, Money KE, Laufer J. 1984. Dimensional Analysis and Dynamic Response Characterization of Mammalian Peripheral Vestibular Structures. Am J Anat 169(3):295-313.

Ramprashad F, Landolt JP, Money KE, Laufer J. 1986. Comparative Morphometric Study of the Vestibular System of the Vertebrata: Reptilia, Aves, Amphibia, and Pisces. Acta Otolaryngol Suppl 427:1-42.

Reilly SM, Elias JA. 1998. Locomotion in alligator mississippiensis: kinematic effects of speed and posture and their relevance to the sprawling-to-erect paradigm. J Exp Biol 201(18):2559-2574.

Renous S, Gasc J-P, Bels VL, Wicker R. 2002. Asymmetrical gaits of

juvenile *Crocodylus johnstoni*, galloping Australian crocodiles. J Zool Lond 256(3):311-325.

Retzius G. 1881. Das Gehörorgan der Wirbeltiere. I. Stockholm: Samson and Wallin.

Retzius G. 1884. Das Gehörorgan der Wirbeltiere. II. Das Gehörorgan der Reptilien, der Vogel und der Saugethiere. Stockholm: Samson and Wallin.

Rohlf FJ. 2005. tpsRelw, Relative Warp Analysis. Version 1.42.

Rohlf FJ. 2006. tpsPLS, partial least-squares. Version 1.18: Department of Ecology and Evolution, Stony Brook University.

Rohlf FJ, Archie JW. 1984. A Comparison of Fourier Methods for the Description of Wing Shape in Mosquitoes (Diptera: Culicidae). Syst Zool 33(3):302-317.

Rohlf FJ, Corti M. 2000. Use of Two-Block Partial Least-Squares to Study Covariation in Shape. Syst Biol 49:740-753.

Russell DA. 1967. Systematics and Morphology of American Mosasaurs. Peaboby Mus Nat Hist Bull 23:1-241.

Soares D. 2002. An ancient sensory organ in crocodilians. Nature 417(6886):241-242.

Sørensen MS, Bretlau P, Jørgensen MB. 1990a. Bone Modeling in the Otic Capsule of the Rat. Acta Otolaryngol 110((5-6)):374-378.

Sørensen MS, Bretlau P, Jørgensen MB. 1990b. Quantum Type Bone Remodeling in the Otic Capsule of the Pig. Acta Otolaryngol 110((3-4)):217-223.

Sørensen MS, Jørgensen MB, Bretlau P. 1991. Remodeling Patterns in the Bony Otic Capsule of the Dog. Ann Otol Rhinol Laryngol 100(9 Pt 1):751-758.

Sørensen MS, Jørgensen MB, Bretlau P. 1992. Distribution of Bone

Remodeling Units in the Otic Capsule of the Rabbit. Acta Otolaryngol 112:462-469.

Spoor F, Bajpai S, Hussain ST, Kumar K, Thewissen JGM. 2002. Vestibular Evidence for the Evolution of Aquatic Behaviour in Early Cetaceans. Nature 417(6885):163-166.

Spoor F, Garland T, Jr., Krovitz G, Ryan TM, Silcox MT, Walker A. 2007. The Primate Semicircular Canal System and Locomotion. PNAS 104(26):10808-10812.

Spoor F, Thewissen JGM. 2008. Comparative and Functional Anatomy of Balance in Aquatic Mammals. In: Thewissen JGM, Nummela S, editors. Sensory Evolution on the Threshold: Adaptations in Secondarily Aquatic Vertebrates: University of California Press.

Spoor F, Wood B, Zonneveld F. 1994. Implications of Early Hominid Labyrinthine Morphology for Evolution of Human Bipedal Locomotion. Nature 369(6482):645-648.

Spoor F, Wood B, Zonneveld F. 1996. Evidence for a Link Between Human Semicircular Canal Size and Bipedal Behaviour. J Hum Evol 30(2):183-187.

Steinhausen W. 1933. Über die Beobachtung der Cupula in den Bogengangsampullen des Labyrinths des lebenden Hechts. Pflügers Archiv European Journal of Physiology 232(1):500-512.

Stokes GG. 1845. On the Theorie of Internal Friction of Fluids in Motion. Trans Cambridge Phil Soc 8:287-305.

Ten Kate JH. 1973. The Mechanics of the Growing Semicircular Canal. J Exp Biol 58(2):351-366.

Ten Kate JH, Van Barneveld HH, Kuiper JW. 1970. The Dimensions and Sensitivities of Semicircular Canals. J Exp Biol 53(2):501-514.

Tremble GE. 1929. The Bony Labyrinth of the New-born and of the Adult.

Arch Otolaryngol 9:175-180.

Tremble GE. 1978. Size of Bony Labyrinth of Human Infant and Adult Compared to that in Certain Animals. Ann Otol Rhinol Laryngol 87(3):351-355.

Turner AH. 2006. Osteology and phylogeny of a new species of *Araripesuchus* (Crocodyliformes: Mesoeucrocodylia) from the Late Cretaceous of Madagascar. Hist Biol 18(3):255 - 369.

Van Buskirk WC, Watts RG, Liu YK. 1976. The Fluid Mechanics of the Semicircular Canals. J Fluid Mech 78(1):87-98.

Van Egmond AAJ, Groen JJ, Jongkees LBW. 1949. The Mechanics of the Semicircular Canal. J Physiol (Lond) 110:1-17.

Van Spaendonck MP, Cryns K, Heyning PHVD, Scheuermann DW, Camp GV, Timmermans JP. 2000. High Resolution Imaging of the Mouse Inner Ear by Microtomography: a New Tool in Inner Ear Research. Anat Rec 259(2):229-236.

Walker A, Silcox MT, Bloch JI, Spoor FS, Krovitz GE. 2003. The Semicircular Canals of Plesiadapiform Primates and Their Functional Significance. J Vert Paleo 23(Suppl 3):107A.

Walker AD. 1970. A Revision of the Jurassic Reptile Hallopus victor (Marsh), with Remarks on the Classification of Crocodiles. Phil Trans R Soc Lond B 257(816):323-372.

Walker AD. 1990. A Revision of Sphenosuchus acutus Haughton, a Crocodylomorph Reptile from the Elliot Formation (Late Triassic or Early Jurassic) of South Africa. Phil Trans: Biol Sci 330(1256):1-120.

Warton DI, Wright IJ, Falster DS, Westoby M. 2006. Bivariate Line-Fitting Methods for Allometry. Biol Rev 81(2):259-291.

Whetstone K, Whybrow P. 1983. A “cursorial” crocodilian from the Triassic

of Lesotho (Basutoland), Southern Africa. Occasional Papers of the Natural History Museum, The University of Kansas 106:1-37.

Yamashita M, Naitoh T, Kashiwagi A, Kondo Y, Wassersug RJ. 1999. Allometry in Vestibular Responses of Anurans. Adv Space Res 23(12):2083-2086.

Yang A, Hullar TE. 2007. Relationship of Semicircular Canal Size to Vestibular-Nerve Afferent Sensitivity in Mammals. J Neurophysiol 98:3197-3205.

Appendix A

Custom Macros for Igor Pro version 4

This macro and it's functions calculate the best fit plane for each of the six semicircular canals based on manually selected points selected in the program VoxBlast 3D (input as X, Y, and Z coordinates and an index specifying which canal the point defines). Output is in the form of six three variable vectors; these are the normal vectors for the best fit planes. (All text following "//"s is comment text and not part of the action of the macro or functions.)

```
Macro CanalFindVB (Xwave,Ywave,Zwave,Iwave)
	String Xwave,Ywave,Zwave,Iwave
	Prompt Xwave,"X points",popup,Wavelist("*",";","")
	Prompt Ywave,"Y points",popup,Wavelist("*",";","")
	Prompt Zwave,"Z points",popup,Wavelist("*",";","")
	Prompt Iwave,"Index wave",popup,Wavelist("*",";","")
	PauseUpdate; Silent 1

	Variable/G gPixelSize
	Variable/G gSliceSize
	if(gPixelSize==0)
		gPixelSize=.1875
		gSliceSize=.31
	endif

	FindCanalCalc($Xwave,$Ywave,$Zwave,$Iwave)
EndMacro

Function FindCanalCalc (Xwave,Ywave,Zwave,Iwave)
	Wave Xwave,Ywave,Zwave,Iwave
	Variable PixelSize,SliceSize,VBlastScale
	NVAR gPixelSize
```

```
	NVAR gSliceSize
	PixelSize=gPixelSize
	SliceSize=gSliceSize
	Prompt PixelSize, "Pixel Spacing"
	Prompt SliceSize, "Slice Spacing"
	DoPrompt "Scan Parameters", PixelSize,SliceSize
	gPixelSize=PixelSize
	gSliceSize=SliceSize
//Initialize
Make /D /O /N=6 IndexCount,IndexStart                    //Create wave to count number of each color in index wave,
                                                                and wave to record starting place for each
	Variable i                                           //Create short term variables
//Calculate VoxBlast Z scaling factor
	VBlastScale=0                                        //Initialize Scale variable to 0
	Do                                                   //Loop begin
		VBlastScale+=1                               //Increment scale variable
	While(SliceSize-PixelSize*VBlastScale>0)             //Continue to loop if the calculated factor is positive
	Printf "Z scale = "+num2str(VBlastScale)+"\r\r"      //Output the scale factor to be used
//Parse
	For(i=numpnts(Iwave)-1;i>=0;i-=1)                    //Loop through the index wave
		IndexStart[Iwave[i]]=i                       //Record posiiton of value, overwriting previous and counting
                                                                down to start of that color
		IndexCount[Iwave[i]]+=1                      //Increment the appropriate color counter
	EndFor
	Make /D /O /N=(IndexCount[0]-1) wvRedX,wvRedY,wvRedZ    //Create storage waves for Red X,Y,Z coordinates
                                                                (named for VoxBlast colors)
	wvRedX=Xwave[p+IndexStart[0]]*PixelSize              //Fill & scale RedX wave
	wvRedY=Ywave[p+IndexStart[0]]*PixelSize              //Fill & scale RedX wave
	wvRedZ=Zwave[p+IndexStart[0]]*SliceSize/VBlastScale  //Fill & scale RedZ wave
	Make /D /O /N=(IndexCount[1]-1) wvGreenX,wvGreenY,wvGreenZ      //Create storage waves for Green coordinates
                                                                (named for VoxBlast colors)
	wvGreenX=Xwave[p+IndexStart[1]]*PixelSize            //Fill & scale GreenX wave
	wvGreenY=Ywave[p+IndexStart[1]]*PixelSize            //Fill & scale GreenY wave
	wvGreenZ=Zwave[p+IndexStart[1]]*SliceSize/VBlastScale       //Fill & scale GreenZ wave
```

```
		Make /D /O /N=(IndexCount[2]-1) wvBlueX,wvBlueY,wvBlueZ	//Create storage for Blue coordinates (VoxBlast colors)
		wvBlueX=Xwave[p+IndexStart[2]]*PixelSize			//Fill & scale BlueX wave
		wvBlueY=Ywave[p+IndexStart[2]]*PixelSize			//Fill & scale BlueY wave
		wvBlueZ=Zwave[p+IndexStart[2]]*SliceSize/VBlastScale	//Fill & scale BlueZ wave
		Make /D /O /N=(IndexCount[3]-1) wvCyanX,wvCyanY,wvCyanZ	//Create storage for Cyan coordinates (VoxBlast colors)
		wvCyanX=Xwave[p+IndexStart[3]]*PixelSize			//Fill & scale CyanX wave
		wvCyanY=Ywave[p+IndexStart[3]]*PixelSize			//Fill & scale CyanY wave
		wvCyanZ=Zwave[p+IndexStart[3]]*SliceSize/VBlastScale		//Fill & scale CyanZ wave
		Make /D /O /N=(IndexCount[4]-1) wvMagentaX,wvMagentaY,wvMagentaZ		//Create storage for Magenta
		wvMagentaX=Xwave[p+IndexStart[4]]*PixelSize		//Fill & scale MagentaX wave
		wvMagentaY=Ywave[p+IndexStart[4]]*PixelSize		//Fill & scale MagentaY wave
		wvMagentaZ=Zwave[p+IndexStart[4]]*SliceSize/VBlastScale	//Fill & scale MagentaZ wave
		Make /D /O /N=(IndexCount[5]-1) wvYellowX,wvYellowY,wvYellowZ	//Create storage waves for Yellow coordinates
		wvYellowX=Xwave[p+IndexStart[5]]*PixelSize		//Fill & scale YellowX wave
		wvYellowY=Ywave[p+IndexStart[5]]*PixelSize		//Fill & scale YellowY wave
		wvYellowZ=Zwave[p+IndexStart[5]]*SliceSize/VBlastScale		//Fill & scale YellowZ wave
//Calculate
		Make /D /O /N=(3,3) CovarMat				//Create storage wave for covariance matrix
		Make /D /O /N=1 CovarStore				//Create storage wave for covariance calculation
		Make /D /O /N=(6,3) MeanMat				//Create wave for output of the canal plane coordinates
		Make /D /O /N=18 VectorOutput				//Create wave for storage of final output data
		WaveStats /Q wvRedX					//Calculate waves statistics
		MeanMat[0][0]=V_avg					//Store the average of the VoxBlast points
		WaveStats /Q wvRedY					//Calculate waves statistics
		MeanMat[0][1]=V_avg					//Store the average of the VoxBlast points
		WaveStats /Q wvRedZ					//Calculate waves statistics
		MeanMat[0][2]=V_avg					//Store the average of the VoxBlast points
		WaveStats /Q wvGreenX					//Calculate waves statistics
		MeanMat[1][0]=V_avg					//Store the average of the VoxBlast points
		WaveStats /Q wvGreenY					//Calculate waves statistics
		MeanMat[1][1]=V_avg					//Store the average of the VoxBlast points
		WaveStats /Q wvGreenZ					//Calculate waves statistics
		MeanMat[1][2]=V_avg					//Store the average of the VoxBlast points
		WaveStats /Q wvBlueX					//Calculate waves statistics
```

```
	MeanMat[2][0]=V_avg 	//Store the average of the VoxBlast points
	WaveStats /Q wvBlueY 	//Calculate waves statistics
	MeanMat[2][1]=V_avg 	//Store the average of the VoxBlast points
	WaveStats /Q wvBlueZ 	//Calculate waves statistics
	MeanMat[2][2]=V_avg 	//Store the average of the VoxBlast points
	WaveStats /Q wvCyanX 	//Calculate waves statistics
	MeanMat[3][0]=V_avg 	//Store the average of the VoxBlast points
	WaveStats /Q wvCyanY 	//Calculate waves statistics
	MeanMat[3][1]=V_avg 	//Store the average of the VoxBlast points
	WaveStats /Q wvCyanZ 	//Calculate waves statistics
	MeanMat[3][2]=V_avg 	//Store the average of the VoxBlast points
	WaveStats /Q wvMagentaX 	//Calculate waves statistics
	MeanMat[4][0]=V_avg 	//Store the average of the VoxBlast points
	WaveStats /Q wvMagentaY 	//Calculate waves statistics
	MeanMat[4][1]=V_avg 	//Store the average of the VoxBlast points
	WaveStats /Q wvMagentaZ 	//Calculate waves statistics
	MeanMat[4][2]=V_avg 	//Store the average of the VoxBlast points
	WaveStats /Q wvYellowX 	//Calculate waves statistics
	MeanMat[5][0]=V_avg 	//Store the average of the VoxBlast points
	WaveStats /Q wvYellowY 	//Calculate waves statistics
	MeanMat[5][1]=V_avg 	//Store the average of the VoxBlast points
	WaveStats /Q wvYellowZ 	//Calculate waves statistics
	MeanMat[5][2]=V_avg 	//Store the average of the VoxBlast points
//ASC1 CALCULATION
	Redimension /N=(IndexCount[0]-1) CovarStore 	//Resize the wave used for calculating covariance
	CovarStore=(wvRedX[p]-MeanMat[0][0])*(wvRedX[p]-MeanMat[0][0])	//Calculate pointwise covariance
	WaveStats /Q CovarStore 	//Calculate waves statistics
	CovarMat[0][0]=V_avg 	//Store average covariance in matrix
	CovarStore=(wvRedX[p]-MeanMat[0][0])*(wvRedY[p]-MeanMat[0][1])	//Calculate pointwise covariance
	WaveStats /Q CovarStore 	//Calculate waves statistics
	CovarMat[0][1]=V_avg 	//Store average covariance in matrix
	CovarMat[1][0]=V_avg 	//Store average covariance in matrix
	CovarStore=(wvRedX[p]-MeanMat[0][0])*(wvRedZ[p]-Meanmat[0][2])	//Calculate pointwise covariance
	WaveStats /Q CovarStore 	//Calculate waves statistics
```

```
	CovarMat[0][2]=V_avg 	//Store average covariance in matrix
	CovarMat[2][0]=V_avg 	//Store average covariance in matrix
	CovarStore=(wvRedY[p]-MeanMat[0][1])*(wvRedY[p]-MeanMat[0][1])	//Calculate pointwise covariance
	WaveStats /Q CovarStore 	//Calculate waves statistics
	CovarMat[1][1]=V_avg 	//Store average covariance in matrix
	CovarStore=(wvRedY[p]-MeanMat[0][1])*(wvRedZ[p]-MeanMat[0][2])	//Calculate pointwise covariance
	WaveStats /Q CovarStore 	//Calculate waves statistics
	CovarMat[1][2]=V_avg 	//Store average covariance in matrix
	CovarMat[2][1]=V_avg 	//Store average covariance in matrix
	CovarStore=(wvRedZ[p]-MeanMat[0][2])*(wvRedZ[p]-Meanmat[0][2])	//Calculate pointwise covariance
	WaveStats /Q CovarStore 	//Calculate waves statistics
	CovarMat[2][2]=V_avg 	//Store average covariance in matrix
	MatrixEigenV /L CovarMat 	//Extract Eigen values and vectors
	Wave W_eigenValues,M_L_eigenVectors 	//Declare names of waves created by MatrixEigenV
	Redimension /R W_eigenValues 	//Convert eigen values from imaginary to real numbers
	WaveStats /Q W_eigenValues 	//Calculate waves statistics
	VectorOutput[0,2]=M_L_eigenVectors[p][V_minloc]	//Store final vectors
//PSC1 CALCULATION
	Redimension /N=(IndexCount[1]-1) CovarStore 	//Resize the wave used for calculating covariance
	CovarStore=(wvGreenX[p]-MeanMat[1][0])*(wvGreenX[p]-MeanMat[1][0])//Calculate pointwise covariance
	WaveStats /Q CovarStore 	//Calculate waves statistics
	CovarMat[0][0]=V_avg 	//Store average covariance in matrix
	CovarStore=(wvGreenX[p]-MeanMat[1][0])*(wvGreenY[p]-MeanMat[1][1])//Calculate pointwise covariance
	WaveStats /Q CovarStore 	//Calculate waves statistics
	CovarMat[0][1]=V_avg 	//Store average covariance in matrix
	CovarMat[1][0]=V_avg 	//Store average covariance in matrix
	CovarStore=(wvGreenX[p]-MeanMat[1][0])*(wvGreenZ[p]-MeanMat[1][2])//Calculate pointwise covariance
	WaveStats /Q CovarStore 	//Calculate waves statistics
	CovarMat[0][2]=V_avg 	//Store average covariance in matrix
	CovarMat[2][0]=V_avg 	//Store average covariance in matrix
	CovarStore=(wvGreenY[p]-MeanMat[1][1])*(wvGreenY[p]-MeanMat[1][1])//Calculate pointwise covariance
	WaveStats /Q CovarStore 	//Calculate waves statistics
	CovarMat[1][1]=V_avg 	//Store average covariance in matrix
	CovarStore=(wvGreenY[p]-MeanMat[1][1])*(wvGreenZ[p]-MeanMat[1][2])//Calculate pointwise covariance
```

```
	WaveStats /Q CovarStore 	//Calculate waves statistics
	CovarMat[1][2]=V_avg 	//Store average covariance in matrix
	CovarMat[2][1]=V_avg 	//Store average covariance in matrix
	CovarStore=(wvGreenZ[p]-MeanMat[1][2])*(wvGreenZ[p]-MeanMat[1][2])//Calculate pointwise covariance
	WaveStats /Q CovarStore 	//Calculate waves statistics
	CovarMat[2][2]=V_avg 	//Store average covariance in matrix
	MatrixEigenV /L CovarMat 	//Extract Eigen values and vecotrs
	Wave W_eigenValues,M_L_eigenVectors 	//Declare names of waves created by MatrixEigenV
	Redimension /R W_eigenValues 	//Convert eigen values from imaginary to real numbers
	WaveStats /Q W_eigenValues 	//Calculate waves statistics
	VectorOutput[3,5]=M_L_eigenVectors[p-3][V_minloc] 	//Store final vectors
//LSC1 CALCULATION
	Redimension /N=(IndexCount[2]-1) CovarStore 	//Resize the wave used for calculating covariance
	CovarStore=(wvBlueX[p]-MeanMat[2][0])*(wvBlueX[p]-MeanMat[2][0])	//Calculate pointwise covariance
	WaveStats /Q CovarStore 	//Calculate waves statistics
	CovarMat[0][0]=V_avg 	//Store average covariance in matrix
	CovarStore=(wvBlueX[p]-MeanMat[2][0])*(wvBlueY[p]-MeanMat[2][1])	//Calculate pointwise covariance
	WaveStats /Q CovarStore 	//Calculate waves statistics
	CovarMat[0][1]=V_avg 	//Store average covariance in matrix
	CovarMat[1][0]=V_avg 	//Store average covariance in matrix
	CovarStore=(wvBlueX[p]-MeanMat[2][0])*(wvBlueZ[p]-MeanMat[2][2])	//Calculate pointwise covariance
	WaveStats /Q CovarStore 	//Calculate waves statistics
	CovarMat[0][2]=V_avg 	//Store average covariance in matrix
	CovarMat[2][0]=V_avg 	//Store average covariance in matrix
	CovarStore=(wvBlueY[p]-MeanMat[2][1])*(wvBlueY[p]-MeanMat[2][1])	//Calculate pointwise covariance
	WaveStats /Q CovarStore 	//Calculate waves statistics
	CovarMat[1][1]=V_avg 	//Store average covariance in matrix
	CovarStore=(wvBlueY[p]-MeanMat[2][1])*(wvBlueZ[p]-MeanMat[2][2])	//Calculate pointwise covariance
	WaveStats /Q CovarStore 	//Calculate waves statistics
	CovarMat[1][2]=V_avg 	//Store average covariance in matrix
	CovarMat[2][1]=V_avg 	//Store average covariance in matrix
	CovarStore=(wvBlueZ[p]-MeanMat[2][2])*(wvBlueZ[p]-MeanMat[2][2])	//Calculate pointwise covariance
	WaveStats /Q CovarStore 	//Calculate waves statistics
	CovarMat[2][2]=V_avg 	//Store average covariance in matrix
```

```
        MatrixEigenV /L CovarMat                                    //Extract Eigen values and vecotrs
        Wave W_eigenValues,M_L_eigenVectors                         //Declare names of waves created by MatrixEigenV
        Redimension /R W_eigenValues                                //Convert eigen values from imaginary to real numbers
        WaveStats /Q W_eigenValues                                  //Calculate waves statistics
        VectorOutput[6,8]=M_L_eigenVectors[p-6][V_minloc]           //Store final vectors
//ASC2 CALCULATION
        Redimension /N=(IndexCount[4]-1) CovarStore                 //Resize the wave used for calculating covariance
        CovarStore=(wvMagentaX[p]-MeanMat[4][0])*(wvMagentaX[p]-MeanMat[4][0])     //Calculate pointwise covariance
        WaveStats /Q CovarStore                                     //Calculate waves statistics
        CovarMat[0][0]=V_avg                                        //Store average covariance in matrix
        CovarStore=(wvMagentaX[p]-MeanMat[4][0])*(wvMagentaY[p]-MeanMat[4][1])     //Calculate pointwise covariance
        WaveStats /Q CovarStore                                     //Calculate waves statistics
        CovarMat[0][1]=V_avg                                        //Store average covariance in matrix
        CovarMat[1][0]=V_avg                                        //Store average covariance in matrix
        CovarStore=(wvMagentaX[p]-MeanMat[4][0])*(wvMagentaZ[p]-MeanMat[4][2])     //Calculate pointwise covariance
        WaveStats /Q CovarStore                                     //Calculate waves statistics
        CovarMat[0][2]=V_avg                                        //Store average covariance in matrix
        CovarMat[2][0]=V_avg                                        //Store average covariance in matrix
        CovarStore=(wvMagentaY[p]-MeanMat[4][1])*(wvMagentaY[p]-MeanMat[4][1])     //Calculate pointwise covariance
        WaveStats /Q CovarStore                                     //Calculate waves statistics
        CovarMat[1][1]=V_avg                                        //Store average covariance in matrix
        CovarStore=(wvMagentaY[p]-MeanMat[4][1])*(wvMagentaZ[p]-MeanMat[4][2])     //Calculate pointwise covariance
        WaveStats /Q CovarStore                                     //Calculate waves statistics
        CovarMat[1][2]=V_avg                                        //Store average covariance in matrix
        CovarMat[2][1]=V_avg                                        //Store average covariance in matrix
        CovarStore=(wvMagentaZ[p]-MeanMat[4][2])*(wvMagentaZ[p]-MeanMat[4][2])     //Calculate pointwise covariance
        WaveStats /Q CovarStore                                     //Calculate waves statistics
        CovarMat[2][2]=V_avg                                        //Store average covariance in matrix
        MatrixEigenV /L CovarMat                                    //Extract Eigen values and vecotrs
        Wave W_eigenValues,M_L_eigenVectors                         //Declare names of waves created by MatrixEigenV
        Redimension /R W_eigenValues                                //Convert eigen values from imaginary to real numbers
        WaveStats /Q W_eigenValues                                  //Calculate waves statistics
        VectorOutput[9,11]=M_L_eigenVectors[p-9][V_minloc]          //Store final vectors
//PSC2 CALCULATION
```

```
	Redimension /N=(IndexCount[5]-1) CovarStore		//Resize the wave used for calculating covariance
	CovarStore=(wvYellowX[p]-MeanMat[5][0])*(wvYellowX[p]-MeanMat[5][0])		//Calculate pointwise covariance
	WaveStats /Q CovarStore		//Calculate waves statistics
	CovarMat[0][0]=V_avg		//Store average covariance in matrix
	CovarStore=(wvYellowX[p]-MeanMat[5][0])*(wvYellowY[p]-MeanMat[5][1])		//Calculate pointwise covariance
	WaveStats /Q CovarStore		//Calculate waves statistics
	CovarMat[0][1]=V_avg		//Store average covariance in matrix
	CovarMat[1][0]=V_avg		//Store average covariance in matrix
	CovarStore=(wvYellowX[p]-MeanMat[5][0])*(wvYellowZ[p]-MeanMat[5][2])		//Calculate pointwise covariance
	WaveStats /Q CovarStore		//Calculate waves statistics
	CovarMat[0][2]=V_avg		//Store average covariance in matrix
	CovarMat[2][0]=V_avg		//Store average covariance in matrix
	CovarStore=(wvYellowY[p]-MeanMat[5][1])*(wvYellowY[p]-MeanMat[5][1])		//Calculate pointwise covariance
	WaveStats /Q CovarStore		//Calculate waves statistics
	CovarMat[1][1]=V_avg		//Store average covariance in matrix
	CovarStore=(wvYellowY[p]-MeanMat[5][1])*(wvYellowZ[p]-MeanMat[5][2])		//Calculate pointwise covariance
	WaveStats /Q CovarStore		//Calculate waves statistics
	CovarMat[1][2]=V_avg		//Store average covariance in matrix
	CovarMat[2][1]=V_avg		//Store average covariance in matrix
	CovarStore=(wvYellowZ[p]-MeanMat[5][2])*(wvYellowZ[p]-MeanMat[5][2])		//Calculate pointwise covariance
	WaveStats /Q CovarStore		//Calculate waves statistics
	CovarMat[2][2]=V_avg		//Store average covariance in matrix
	MatrixEigenV /L CovarMat		//Extract Eigen values and vecotrs
	Wave W_eigenValues,M_L_eigenVectors		//Declare names of waves created by MatrixEigenV
	Redimension /R W_eigenValues		//Convert eigen values from imaginary to real numbers
	WaveStats /Q W_eigenValues		//Calculate waves statistics
	VectorOutput[12,14]=M_L_eigenVectors[p-12][V_minloc]//Store final vectors
//LSC2 CALCULATION
	Redimension /N=(IndexCount[3]-1) CovarStore		//Resize the wave used for calculating covariance
	CovarStore=(wvCyanX[p]-MeanMat[3][0])*(wvCyanX[p]-MeanMat[3][0])	//Calculate pointwise covariance
	WaveStats /Q CovarStore		//Calculate waves statistics
	CovarMat[0][0]=V_avg		//Store average covariance in matrix
	CovarStore=(wvCyanX[p]-MeanMat[3][0])*(wvCyanY[p]-MeanMat[3][1])	//Calculate pointwise covariance
	WaveStats /Q CovarStore		//Calculate waves statistics
```

```
	CovarMat[0][1]=V_avg                                    //Store average covariance in matrix
	CovarMat[1][0]=V_avg                                    //Store average covariance in matrix
	CovarStore=(wvCyanX[p]-MeanMat[3][0])*(wvCyanZ[p]-MeanMat[3][2])   //Calculate pointwise covariance
	WaveStats /Q CovarStore                                 //Calculate waves statistics
	CovarMat[0][2]=V_avg                                    //Store average covariance in matrix
	CovarMat[2][0]=V_avg                                    //Store average covariance in matrix
	CovarStore=(wvCyanY[p]-MeanMat[3][1])*(wvCyanY[p]-MeanMat[3][1])   //Calculate pointwise covariance
	WaveStats /Q CovarStore                                 //Calculate waves statistics
	CovarMat[1][1]=V_avg                                    //Store average covariance in matrix
	CovarStore=(wvCyanY[p]-MeanMat[3][1])*(wvCyanZ[p]-MeanMat[3][2])   //Calculate pointwise covariance
	WaveStats /Q CovarStore                                 //Calculate waves statistics
	CovarMat[1][2]=V_avg                                    //Store average covariance in matrix
	CovarMat[2][1]=V_avg                                    //Store average covariance in matrix
	CovarStore=(wvCyanZ[p]-MeanMat[3][2])*(wvCyanZ[p]-MeanMat[3][2])   //Calculate pointwise covariance
	WaveStats /Q CovarStore                                 //Calculate waves statistics
	CovarMat[2][2]=V_avg                                    //Store average covariance in matrix
	MatrixEigenV /L CovarMat                                //Extract Eigen values and vectors
	Wave W_eigenValues,M_L_eigenVectors                     //Declare names of waves created by MatrixEigenV
	Redimension /R W_eigenValues                            //Convert eigen values from imaginary to real numbers
	WaveStats /Q W_eigenValues                              //Calculate waves statistics
	VectorOutput[15,17]=M_L_eigenVectors[p-15][V_minloc]//Store final vectors

//Cleanup
	Killwaves IndexCount,IndexStart,wvRedX,wvRedY,wvRedZ,wvGreenX,wvGreenY,wvGreenZ
	Killwaves wvBlueX,wvBlueY,wvBlueZ,wvCyanX,wvCyanY,wvCyanZ,wvMagentaX,wvMagentaY
	Killwaves wvMagentaZ,wvYellowX,wvYellowY,wvYellowZ
	KillWaves CovarMat,CovarStore,MeanMat,W_eigenValues,M_L_eigenVectors
End
```

This macro and it's functions provide all of the tools required to calculate the average (midline) path of the semicircular canal starting from a pair of coordinate series that describe the internal and external margins of the bony canal. Output is 10 variables describing various properties of canal shape as well as coordinate series describing the average complete circuit and the average path of the canal not including the utricle.

```
Macro CanalMultiPath (InternXwave,InternYwave,ExternXwave,ExternYwave,OutString)
	String InternXwave,InternYwave,ExternXwave,ExternYwave,OutString
	Prompt InternXwave,"Internal X points",popup,Wavelist("*",";","") //If not preinput use dialog to promt user for Inner X
                                                                        wave
	Prompt InternYwave,"Internal Y points",popup,Wavelist("*",";","") //If not preinput use dialog to promt user for Inner Y
                                                                        wave
	Prompt ExternXwave,"External X points",popup,Wavelist("*",";","")       //If not preinput use dialog to promt user for
                                                                        Outer X wave
	Prompt ExternYwave,"External Y points",popup,Wavelist("*",";","")       //If not preinput use dialog to promt user for
                                                                        Outer Y wave
	Prompt OutString,"Seed for Output String"       //If not preinput use dialog to promt user for name seed
	PauseUpdate; Silent 1           //Delay graph update until end of macro, supress display of the command line
	Display /K=1 $InternYwave vs $InternXwave       //Graph internal Y versus internal X no confim on killing on graph
	AppendToGraph $ExternYwave vs $ExternXwave      //Add external Y versus external X to graph
	ShowInfo                        //Add cusor/status bar to bottom of graph
	ControlBar 40                   //Add a control bar to top of graph
	Button $Outstring,disable=2,pos={10,10}, size={100,20},proc=MultiPathTrim,title="Trim"   //Add trim button to control bar
	Button $Outstring+"Undo",disable=2,pos={120,10}, size={100,20},proc=MultiPathUndo,title="Undo"       //Add undo
                                                                        button to control bar
	Button $Outstring+"CalcP",disable=2,pos={230,10}, size={100,20},proc=MultiPathCalcP,title="Calc Path"  //Add button to
                                                                        control bar
	Button $Outstring+"CalcO",disable=2,pos={340,10}, size={100,20},proc=MultiPathCalcO,title="Calc Outline"        //Add
                                                                        button to control bar
	Button $Outstring+"Stats",disable=2,pos={450,10}, size={100,20},proc=MultiPathStatCalc,title="Statistics"//Add button to
                                                                        control bar
//PREPROCESSING
```

```
	String  IXwaveAdj,IYwaveAdj,EXwaveAdj,EYwaveAdj	//Create name strings for manipulation of the origional data
	IXwaveAdj=Outstring+"IX"		//Create name of working IX wave
	IYwaveAdj=Outstring+"IY"		//Create name of working IY wave
	EXwaveAdj=Outstring+"EX"		//Create name of working EX wave
	EYwaveAdj=Outstring+"EY"		//Create name of working EY wave
	Make /D /O /N=(numpnts($InternXwave)) $IXwaveAdj	//Create working IX wave
	Make /D /O /N=(numpnts($InternYwave)) $IYwaveAdj	//Create working IY wave
	Make /D /O /N=(numpnts($ExternXwave)) $EXwaveAdj	//Create working EX wave
	Make /D /O /N=(numpnts($ExternYwave)) $EYwaveAdj	//Create working EY wave
	$IXwaveAdj=$InternXwave[p]	//Populate working IX wave
	$IYwaveAdj=$InternYwave[p]	//Populate working IYwave
	$EXwaveAdj=$ExternXwave[p]	//Populate working EX wave
	$EYwaveAdj=$ExternYwave[p]	//Populate working EY wave
	Smooth /E=1 1,$IXwaveAdj,$IYwaveAdj,$EXwaveAdj,$EYwaveAdj		//Perform binomial smoothing on both the
external and internal paths
	AppendToGraph $IYwaveAdj vs $IXwaveAdj		//Add new internal path to the graph
	AppendToGraph $EYwaveAdj vs $EXwaveAdj		//Add new external path to the graph
	ModifyGraph lsize($IYwaveAdj)=3,rgb($IYwaveAdj)=(0,12800,52224)		//Change size and color of output path
	ModifyGraph mode($IYwaveAdj)=4,marker($IYwaveAdj)=19		//Change style of output path
	ModifyGraph lsize($EYwaveAdj)=3,rgb($EYwaveAdj)=(0,12800,52224)		//Change size and color of output path
	ModifyGraph mode($EYwaveAdj)=4,marker($EYwaveAdj)=19		//Change style of output path
//INITIALIZE UNDO ARCHITECHTURE
String  UndoWaveName,UndoDataWaveName //Create name string for undo storage waves for manipulation of the origional
                                                                                                                data
	UndoWaveName=Outstring+"Undo"		//Initialize name of Undo wave
	UndoDataWaveName=Outstring+"UndoData"		//Initialize name of Undo data wave
	Make /D /O /N=(numpnts(CsrWaveRef(A)),2,1) $UndoWaveName		//Create Undo wave
	Make /D /O /N=(4,1) $UndoDataWaveName		//Create Undo data wave
EndMacro

Function MinPointDeviation (Xfwave,Yfwave)
	Wave Xfwave,YfWave		//Declare function parameter variables
//NON-PARAMETER DECLARATIONS
	Make /D /O /N=(numpnts(Xfwave)-2) TempDistWave		//Create a storage wave for the distance values
```

```
	Variable i				//Create loop variable
//MAIN CALCULATIONS
		For(i=1;i<numpnts(Xfwave)-1;i+=1)	//Iterate from the 2nd point through the second to last point
		TempDistWave[i-1]=abs((Xfwave[i+1]-Xfwave[i-1])*(Yfwave[i-1]-Yfwave[i])-(Xfwave[i-1]-Xfwave[i])*(Yfwave[i+1]-
Yfwave[i-1]))*(((Xfwave[i+1]-Xfwave[i-1])^2+(Yfwave[i+1]-Yfwave[i-1])^2)^.5)	//Calculate ditance of i from line i-1 to i+1
		endfor
	WaveStats /Q TempDistWave	//Calculate Wave Statistics
	Killwaves TempDistWave		//Cleanup Temp waves
	Return V_minloc+1		//Return position of point of minimum distance
End

Function ExternalNormalPoint(EXfwave,EYfwave,IXfwave,IYfwave,Position)
	Wave EXfwave,EYfwave,IXfwave,IYfwave	//Declare function parameter variables
	Variable Position		//Declare function parameter variables
//NON-PARAMETER DECLARATIONS
	Variable Leg1Len,Leg2Len,Leg1X,Leg1Y,Leg2X,Leg2Y,AvX,AvY,StartX,StartY,i  //Create Variable for temporary strage
							of calculation values
	Make /D /O /N=(3,2) Points	//Create storage wave for working points
	Make /D /O /N=5 workPos		//Create a storage for points surrounding point of interest
//CREATE  3 WORKING POINTS
		For(i=-2;i<3;i+=1)	//Loop from 2 points before to two points after
		workPos[i+2]=PointCheck(Position+i,IXfwave)	//Populate wave with termination of wave sensitive values
							around point of interest
		Endfor
	Points[0][0]=(IXfwave[workPos[0]]+IXfwave[workPos[1]])/2	//Set first point X coordinate equal to averge of X
							coordinates from two preceeding points
	Points[0][1]=(IYfwave[workPos[0]]+IYfwave[workPos[1]])/2	//Set first point Y coordinate equal to averge of Y
							coordinates from two preceeding points
	Points[1][0]=IXfwave[workPos[2]]	//Set middle point X coordinate equal to X coordinate of point of interest
	Points[1][1]=IYfwave[workPos[2]]	//Set middle point Y coordinate equal to Y coordinate of point of interest
	Points[2][0]=(IXfwave[workPos[3]]+IXfwave[workPos[4]])/2//Set last point X coordinate equal to average X coordinates
							from two follow points
```

```
	Points[2][1]=(IYfwave[workPos[3]]+IYfwave[workPos[4]])/2//Set last point Y coordinate equal to average Y coordinates
	                                                        from two follow points
//FIND ANGLE BISECTION POINT
	Leg1Len=((Points[0][0]-Points[1][0])^2+(Points[0][1]-Points[1][1])^2)^.5    //Calculate distance between first point and
	                                                        point of interest
	Leg2Len=((Points[2][0]-Points[1][0])^2+(Points[2][1]-Points[1][1])^2)^.5    //Calculate distance between third point and
	                                                        point of interest
	Leg1X=Points[1][0]+(Points[0][0]-Points[1][0])*(5/Leg1Len)      //Find X coordinate for point distance Leg1Len along
	                                                        Leg2
	Leg1Y=Points[1][1]+(Points[0][1]-Points[1][1])*(5/Leg1Len)      //Find Y coordinate for point distance Leg1Len along
	                                                        Leg2
	Leg2X=Points[1][0]+(Points[2][0]-Points[1][0])*(5/Leg2Len)      //Find X coordinate for point distance Leg1Len along
	                                                        Leg2
	Leg2Y=Points[1][1]+(Points[2][1]-Points[1][1])*(5/Leg2Len)      //Find Y coordinate for point distance Leg1Len along
	                                                        Leg2
	AvX=(Leg1X+Leg2X)/2          //Average leg endpoints to find X coordinate of bisection point
	AvY=(Leg1Y+Leg2Y)/2          //Average leg endpoints to find Y coordinate of bisection point
	StartX=Points[1][0]          //Store value in variable
	StartY=Points[1][1]          //Store value in variable
	Killwaves workPos,Points                //Cleanup Temp waves
	Return MinPointLineDistance(EXfwave,EYfwave,StartX,StartY,AvX,AvY) //Return an answer
End

Function MinPointLineDistance(Xwave,Ywave,X1,Y1,X2,Y2)
	Wave Xwave,Ywave             //Declare function parameter variables
	Variable X1,Y1,X2,Y2         //Declare function parameter variables
//NON-PARAMETER DECLARATIONS
	Make /D /O /N=(numpnts(Xwave)) TempDistWave         //Create wave for storage of distance values
	Make /D /O /N=0 DistFromPoint,PointLocation    //Create waves for parsing multiple minimum values on the basis of
	                                                        distance from X1,Y1
	Variable i,j,FinalPoint      //Declare for loop variable and position variable for DistFromPoint and PointLocation
	                                                        waves
//PERFORM CALCULATIONS
	j=0                          //Initialize position variable
```

```
	TempDistWave[0]=((X2-X1)*(Y1-Ywave[0])-(X1-Xwave[0])*(Y2-Y1))/(((X2-X1)^2+(Y2-Y1)^2)^.5)   //Calculate ditances at
                                                                point zero
		For(i=1;i<numpnts(Xwave);i+=1)
		TempDistWave[i]=((X2-X1)*(Y1-Ywave[i])-(X1-Xwave[i])*(Y2-Y1))/(((X2-X1)^2+(Y2-Y1)^2)^.5)      //Calculate
                                                                ditance at point i
			if(sign(TempDistWave[i])!=sign(TempDistWave[i-1]))      //Check if new point is on opposite side of line
                                                                from previous point
			Redimension /n=(j+2) DistFromPoint, PointLocation       //Make room in storage waves
			DistFromPoint[j]=((Xwave[i-1]-X1)^2+(Ywave[i-1]-Y1)^2)^.5       //Store distance: previous external
                                                                point to normal origin
			PointLocation[j]=i-1      //Store location of external point
			j+=1              //Increment position variable
			DistFromPoint[j]=((Xwave[i]-X1)^2+(Ywave[i]-Y1)^2)^.5   //Store distance of current external point from
                                                                normal point of origin
			PointLocation[j]=i        //Store location of external point
			j+=1              //Increment position variable
			Endif
		Endfor
	WaveStats /Q DistFromPoint     //Calculate wave statistics
	FinalPoint=PointLocation[V_minloc]      //Store value in variable
	Killwaves TempDistWave,DistFromPoint,PointLocation    //Cleanup Temp waves
	Return FinalPoint                 //Return location of minimum distance point
End

Function PointCheck(Position,RefWave)
	Wave RefWave                      //Declare function parameter variables
	Variable Position                 //Declare function parameter variables
//NON-PARAMETER DECLARATIONS
	Variable waveLen=numpnts(RefWave)   //Create and initialize wave length variable
//POSITION CHECK CALCULATION
		if(Position>=waveLen)   //Check if position is past end of wave
		return Position-waveLen//Return adjusted value, i.e. wrap position around to beginning of wave
		elseif(Position<0)        //Check if position is before beginning of wave
```

```
		return waveLen+Position		//Return adjusted value, i.e. wrap position around to end of wave
		endif
	return Position			//Return unadjusted value
end

Function PositionDistance(FromPos, ToPos,RefWave)
	Wave RefWave			//Declare function parameter variables
	Variable FromPos,ToPos		//Declare function parameter variables
	Variable Length			//Create length storage variable
	Length=ToPos-FromPos+1		//Calculate Length
		if(length<=0)		//Check Length value for direction
		Length+=numpnts(RefWave)	//Adjust length value
		endif
	Return Length			//Return proper length
End

Function TrueMaxPos(RefWave)
	Wave RefWave			//Declare function parameter variables
	Variable MaxVal,PosTotal,PosNumber,i	//Create variables
	WaveStats /Q Refwave		//Calculate wave stats for processed wave
	MaxVal=V_max			//Store max value
	PosTotal=0			//Initialize variable to 0
	PosNumber=0			//Initialize variable to 0
		For(i=0;i<numpnts(RefWave);i+=1)	//Loop through wave
			if(RefWave[i]==MaxVal) //Is this an instance of the maximum wave value
			PosTotal+=i	//Add this position to the total
			PosNumber+=1 //Increment the number of positions recorded
			endif
		Endfor
	Return round(PosTotal/PosNumber)	//Return Position integer closest to average of all maximum value positions
End

Function MultiPathTrim(ctrlName) : ButtonControl
```

```
	String ctrlName
	Printf "Trimming...\r"		//Indicate on control window status of proceedure
	String BaseName=ctrlName	//Create and initialize string variable for the seed string which will be the basis for all
								permanent names based on the name of the Trim
button which stores the value entered in the macro initialization
	Button $ctrlName+"Undo",disable=0	//Enable Undo button
	String  IXwaveAdj,IYwaveAdj,EXwaveAdj,EYwaveAdj	//Create name strings for waves for manipulation of the
origional data
	IXwaveAdj=BaseName+"IX"	//Create name of working IX wave
	IYwaveAdj=BaseName+"IY"	//Create name of working IY wave
	EXwaveAdj=BaseName+"EX"	//Create name of working EX wave
	EYwaveAdj=BaseName+"EY"	//Create name of working EY wave
	Wave IXout=$IXwaveAdj		//Create working IX wave reference
	Wave IYout=$IYwaveAdj		//Create working IY wave reference
	Wave EXout=$EXwaveAdj		//Create working EX wave reference
	Wave EYout=$EYwaveAdj		//Create working EY wave reference
	Variable Circuit, UndoNum	//Create Undo variables
	String  UndoWaveName,UndoDataWaveName	//Create name string for undo storage waves for manipulation of the
origional data
	UndoWaveName=BaseName+"Undo"	//Initialize name of Undo wave
	UndoDataWaveName=BaseName+"UndoData"	//Initialize name of Undo data wave
	Wave UndoWave=$UndoWaveName	//Create Undo wave reference
	Wave UndoDataWave=$UndoDataWaveName	//Create Undo data wave reference
		if(DimSize(UndoWave,2)>0)	//Check if UndoWave previously exists
		UndoNum=DimSize(UndoWave,2)	//Set Number of undo layers equal to Layers in UndoWave
		else
		UndoNum=0		//Initialize number of undo layers to 0
		endif
		if(cmpstr(CsrWave(A),nameofwave(EYout))==0) //Check if cursor A is on the External wave
		Circuit=0		//Set Circuit variable to 0 (External)
		else
		Circuit =1		//Set Circuit variable to 1 (Internal)
		endif
```

```
	UndoNum+=1			//Increment the number of undo layers
	Redimension /N=(4,UndoNum) UndoDataWave  //Add a layer to the Undo data wave
	Redimension /N=(max(DimSize(UndoWave,0),numpnts(CsrWaveRef(A))),2,UndoNum) UndoWave //Add a layer to the
Undo wave
	UndoDataWave[0][UndoNum-1]=numpnts(CsrWaveRef(A))	//Store length of wave pair to be altered
	UndoDataWave[1][UndoNum-1]=pcsr(A)//Store cursor A position
	UndoDataWave[2][UndoNum-1]=pcsr(B)//Store cursor B position
	UndoDataWave[3][UndoNum-1]=Circuit  //Store Circuit variable
	UndoWave[][0][UndoNum-1]=CsrXWaveRef(A)[p]		//Store Xwave to be altered
	UndoWave[][1][UndoNum-1]=CsrWaveRef(A)[p] //Store Ywave to be altered
//MAKE ALTERATION
		if(Circuit==1)		//Check whether circuit to be altered is internal or external
		WallCopy(IXout,IYout,EXout,EYout,pcsr(A),pcsr(B))	//If internal call Wall copy function with these settings
		else
		WallCopy(EXout,EYout,IXout,IYout,pcsr(A),pcsr(B))	//If external call Wall copy function with these settings
		endif
End

Function WallCopy(Xtrim,Ytrim,Xsource,Ysource,pStart,pEnd)
	Wave Xtrim,Ytrim,Xsource,Ysource	//Declare waves passed to function
	Variable pStart,pEnd		//Declare variables passed to function
	Rotate -(pEnd),Xtrim,Ytrim	//Reorder waves such that the end of the trimmed section is the end of the waves
	Redimension /N=(numpnts(YTrim)-PositionDistance(pStart,pEnd,Ytrim)+2) Xtrim,Ytrim	//Remove the trimmed section
	pStart=numpnts(Ytrim)-1		//Reset the pStart value
	pEnd=0				//Reset pEnd value
	Variable pSourceStart,pSourceEnd,pSourceAX,pSourceAY,SourceWallLen	//Declare variables to define endpoints
							of working area on the Source waves and center of
							source circuit, and position length of target area
	WaveStats /Q Xsource		//Calculate wave statistics for source X coordinates wave
	pSourceAX=V_avg			//Store X coordinate of center point
	WaveStats /Q Ysource		//Calcualte wave statistics for source Y coordinates wave
	pSourceAY=V_avg			//Store Y coordinate of center point
	pSourceStart=MinPointLineDistance(Xsource,Ysource,Xtrim[pStart],Ytrim[pStart],pSourceAX,pSourceAY)//Find start of
							the region to copy
```

```
pSourceEnd=MinPointLineDistance(Xsource,Ysource,Xtrim[pEnd],Ytrim[pEnd],pSourceAX,pSourceAY)    //Find the end
                                                                                                of the region to be copied
Variable TrimM,TrimB,SourceM,SourceB,TempX,TempY//Declare variables used in end point adjustment
        Do                          //Start loop
        SourceM=(pSourceAY-Ysource[pSourceStart])/(pSourceAX-Xsource[pSourceStart])        //Calculate slope from
                                                                                                start of source to center point
        SourceB=Ysource[pSourceStart]-Xsource[pSourceStart]*SourceM          //Calculate intercept of line from start of
                                                                                                source to center point
        TrimM=(Ytrim[pStart]-Ytrim[PointCheck(pStart-1,YTrim)])/(Xtrim[pStart]-Xtrim[PointCheck(pStart-1,YTrim)])
                                        //Calculate slope of line from trim start to previous point on wave
        TrimB=Ytrim[pStart]-Xtrim[pStart]*TrimM//Calculate intercept from trim start to previous point on wave
                if(Xtrim[pStart]==Xtrim[PointCheck(pStart-1,YTrim)])       //If trim line is vertical
                TempX=Xtrim[pStart]     //Set a temporary X coordinate storage variable
                TempY=SourceM*TempX+SourceB       //Set a temporary Y coordinate storage variable
                elseif(Xsource[pSourceStart]==pSourceAX)       //Else if source line is vertical
                TempX=pSourceAX       //Set a temporary X coordinate storage variable
                TempY=TrimM*TempX+TrimM   //Set a temporary Y coordinate storage variable
                else
                TempX=(SourceB-TrimB)/(TrimM-SourceM)       //Set a temporary X coordinate storage variable
                TempY=TrimM*TempX+TrimB   //Set a temporary Y coordinate storage variable
                endif
                if(((TempX-Xtrim[PointCheck(pStart-2,YTrim)])^2+(TempY-Ytrim[PointCheck(pStart-
2,YTrim)])^2)^.5>((Xtrim[PointCheck(pStart-1,YTrim)]-Xtrim[PointCheck(pStart-2,YTrim)])^2+(Ytrim[PointCheck(pStart-
1,YTrim)]-Ytrim[PointCheck(pStart-2,YTrim)])^2)^.5)      //Check for correct positioning of new point
                Xtrim[pStart]=TempX     //Set X point
                Ytrim[pstart]=TempY     //Set Y point
                Break               //Break out of loop
                endif
        pSourceStart=PointCheck(pSourceStart+1,YSource)       //Move source starting point
        While(1)                    //Loop
        Do
        SourceM=(pSourceAY-Ysource[pSourceEnd])/(pSourceAX-Xsource[pSourceEnd])          //Calculate slope of
                                                                                                line from end of source to center point
```

```
		SourceB=Ysource[pSourceEnd]-Xsource[pSourceEnd]*SourceM //Calculate intercept of line from end of source
									to center point
		TrimM=(Ytrim[pEnd]-Ytrim[PointCheck(pEnd+1,YTrim)])/(Xtrim[pEnd]-Xtrim[PointCheck(pEnd+1,YTrim)])
					//Calculate slope of line from trim end to previous point on wave
		TrimB=Ytrim[pEnd]-Xtrim[pEnd]*TrimM  //Calculate slope of line from trim end to previous point on wave
			if(Xtrim[pEnd]==Xtrim[PointCheck(pEnd+1,YTrim)])	//If trim line is vertical
			TempX=Xtrim[pEnd]	//Set a temporary X coordinate storage variable
			TempY=SourceM*TempX+SourceB	//Set a temporary Y coordinate storage variable
			elseif(Xsource[pSourceEnd]==pSourceAX)	//Else if source line is vertical
			TempX=pSourceAX	//Set a temporary X coordinate storage variable
			TempY=TrimM*TempX+TrimM  //Set a temporary Y coordinate storage variable
			else
			TempX=(SourceB-TrimB)/(TrimM-SourceM)	//Set a temporary X coordinate storage variable
			TempY=TrimM*TempX+TrimB  //Set a temporary Y coordinate storage variable
			endif
			if(((TempX-Xtrim[PointCheck(pEnd+2,YTrim)])^2+(TempY-
Ytrim[PointCheck(pEnd+2,YTrim)])^2)^.5>((Xtrim[PointCheck(pEnd+1,YTrim)]-
Xtrim[PointCheck(pEnd+2,YTrim)])^2+(Ytrim[PointCheck(pEnd+1,YTrim)]-Ytrim[PointCheck(pEnd+2,YTrim)])^2)^.5)
	//Check for correct positioning of new point
			Xtrim[pEnd]=TempX	//Set X point
			Ytrim[pEnd]=TempY	//Set Y point
			Break		//Break out of loop
			endif
		pSourceEnd=PointCheck(pSourceEnd-1,YSource)	//Move source ending point
		While(1)		//Loop
	SourceWallLen=PositionDistance(pSourceStart,pSourceEnd,Ysource)	//Calculate the length, in points, of the region to
									be copied
	Redimension /N=(numpnts(YTrim)+SourceWallLen-2) Xtrim,Ytrim	//Add the length of the region to be copied to
									end of trimmed wave (exclusive of endpoints)
	Variable TotalAngle,TempAngle,TempDist,RealDist,TempHypo,i,pCurrent,StartRatio,EndRatio,UseRatio  //Declare
									required variables for copying calculations
	EndRatio=((pSourceAX-Xtrim[0])^2+(pSourceAY-Ytrim[0])^2)^.5/((pSourceAX-Xsource[pSourceEnd])^2+(pSourceAY-
Ysource[pSourceEnd])^2)^.5 //Calculate the ratio of the distances between the center point and the two ending points
```

```
        StartRatio=((pSourceAX-Xtrim[pStart])^2+(pSourceAY-Ytrim[pStart])^2)^.5/((pSourceAX-
Xsource[pSourceStart])^2+(pSourceAY-Ysource[pSourceStart])^2)^.5                //Calculate ratio of the distances between the
                                                                                center point and the two starting points
        TotalAngle=asin(abs(((pSourceAX-Xsource[pSourceStart])*(Ysource[pSourceStart]-Ysource[pSourceEnd])-
(Xsource[pSourceStart]-Xsource[pSourceEnd])*(pSourceAY-Ysource[pSourceStart]))/((pSourceAX-
Xsource[pSourceStart])^2+(pSourceAY-Ysource[pSourceStart])^2)^.5)/((pSourceAX-Xsource[pSourceEnd])^2+(pSourceAY-
Ysource[pSourceEnd])^2)^.5)  //Calculate angle: starting point to center point to end point
        TempHypo=((pSourceAX-Xsource[pSourceStart])^2+(pSourceAY-Ysource[pSourceStart])^2+(pSourceAX-
Xsource[pSourceEnd])^2+(pSourceAY-Ysource[pSourceEnd])^2)^.5                    //Calculate a theoretical third leg of triange
        RealDist=((Xsource[pSourceEnd]-Xsource[pSourceStart])^2+(Ysource[pSourceEnd]-Ysource[pSourceStart])^2)^.5
        //Calculate the actual line distance between start point and end point
                if(RealDist>TempHypo) //Compare theoretical and actual distances
                TotalAngle=Pi-TotalAngle          //Adjust angle to correct internal measure
                endif
                For(i=1;i<SourceWallLen-1;i+=1)           //Loop through the points along the source region to be copied
                pCurrent=PointCheck(pSourceStart+i,Ysource)   //Set the point to investigate
                TempAngle=asin(abs(((pSourceAX-Xsource[pSourceStart])*(Ysource[pSourceStart]-Ysource[pCurrent])-
(Xsource[pSourceStart]-Xsource[pCurrent])*(pSourceAY-Ysource[pSourceStart]))/((pSourceAX-
Xsource[pSourceStart])^2+(pSourceAY-Ysource[pSourceStart])^2)^.5)/((pSourceAX-Xsource[pCurrent])^2+(pSourceAY-
Ysource[pCurrent])^2)^.5)        //Calc angle: start point to center to current
                TempDist=((pSourceAX-Xsource[pCurrent])^2+(pSourceAY-Ysource[pCurrent])^2)^.5      //Calculate the
                                                                distance from the center to the current point on the source
                                                                region
                TempHypo=((pSourceAX-Xsource[pSourceStart])^2+(pSourceAY-Ysource[pSourceStart])^2+TempDist^2)^.5
                                                //Calculate a theoretical third leg of triange
                RealDist=((Xsource[pCurrent]-Xsource[pSourceStart])^2+(Ysource[pCurrent]-Ysource[pSourceStart])^2)^.5
//Calculate the actual distane between starting point and and current point on the source region
                if(RealDist>TempHypo) //Compare theoretical and actual distances
                TempAngle=Pi-TempAngle        //Adjust angle to correct internal measure
                endif
                UseRatio=StartRatio+(EndRatio-StartRatio)*(TempAngle/TotalAngle)      //Base the distance ratio to be used on
                                                                the ratio of the current angle to the total angle
                Xtrim[pStart+i]=pSourceAX-UseRatio*(pSourceAX-Xsource[pCurrent])     //Calculate new x coordinate on altered
                                                                wave
```

```
		Ytrim[pStart+i]=pSourceAY-UseRatio*(pSourceAY-Ysource[pCurrent])	//Calculate new y coordinate on altered
                                                                                wave
		EndFor
End

Function MultiPathUndo(ctrlName) : ButtonControl
	String ctrlName
	Printf "Undoing...\r"			//Indicate on control window status of proceedure
	String BaseName				//Create a string variable for the seed which will be the basis for all permanent names
	BaseName=ctrlName[0,strlen(ctrlName)-5]		//Initialize to the name of the Undo button which stores the value
                                                                entered in the macro initialization
	String  UndoWaveName,UndoDataWaveName	//Create name string for undo storage waves for manipulation of the
                                                                origional data
	UndoWaveName=BaseName+"Undo"	//Initialize name of Undo wave
	UndoDataWaveName=BaseName+"UndoData"	//Initialize name of Undo length wave
	Wave UndoWave=$UndoWaveName	//Create Undo wave reference
	Wave UndoDataWave=$UndoDataWaveName	//Create Undo data wave reference
	Variable UndoNum			//Create Undo variables
	UndoNum=DimSize(UndoWave,2)		//Set number of undo layers
	String  XResetAdj,YResetAdj	//Create name strings for manipulation of the origional data
		If(UndoDataWave[3][UndoNum-1]==1)	//Check if layer to undo is internal circuit
		XResetAdj=BaseName+"IX"		//Set working X wave reference to internal X
		YResetAdj=BaseName+"IY"		//Set working Y wave reference to Internal Y
		else
		XResetAdj=BaseName+"EX"		//Set working X wave reference to external X
		YResetAdj=BaseName+"EY"		//Set working Y wave reference to external Y
		endif
	Wave XReset=$XResetAdj		//Create working IX wave reference
	Wave YReset=$YResetAdj		//Create working IY wave reference
	Redimension /N=(UndoDataWave[0][UndoNum-1]) XReset,YReset		//Set working waves to length stored in Undo
                                                                data wave
	XReset=UndoWave[p][0][UndoNum-1]	//Populate working x wave
	YReset=UndoWave[p][1][UndoNum-1]	//Populate working Y wave
```

```
	Cursor /P A $nameofwave(YReset) UndoDataWave[1][UndoNum-1]	//Move cursor A to the new external wave keeping the point location
	Cursor /P B $nameofwave(YReset) UndoDataWave[2][UndoNum-1]	//Move cursor B to the new external wave keeping the point location
	UndoNum-=1			//Decrement number of undo layers
	Redimension /N=(4,UndoNum) UndoDataWave  //Remove a layer from the Undo data wave
	Redimension /N=(DimSize(UndoWave,0),2,UndoNum) UndoWave //Remove a layer from the Undo wave
		if(UndoNum==1)		//Check if last undo layer used up
		Button $ctrlName,disable=2	//Disable Undo button
		endif
End

Function MultiPathCalcP(ctrlName) : ButtonControl
	String ctrlName
	Printf "Calculating...\r"		//Indicate on control window status of proceedure
	String BaseName			//Create a variable for the seed string which will be the basis for all permanent names
	BaseName=ctrlName[0,strlen(ctrlName)-6]	//Initialize string to the trimmed name of the Undo  button which stores the value entered in the macro initialization
	String  IXwaveAdj,IYwaveAdj,EXwaveAdj,EYwaveAdj	//Create name strings for manipulation of the origional data
	IXwaveAdj=BaseName+"IX"	//Create name of working IX wave
	IYwaveAdj=BaseName+"IY"	//Create name of working IY wave
	EXwaveAdj=BaseName+"EX"	//Create name of working EX wave
	EYwaveAdj=BaseName+"EY"	//Create name of working EY wave
	Wave IXout=$IXwaveAdj		//Create working IX wave reference
	Wave IYout=$IYwaveAdj		//Create working IY wave reference
	Wave EXout=$EXwaveAdj		//Create working EX wave reference
	Wave EYout=$EYwaveAdj		//Create working EY wave reference
	Rotate -(pcsr(A)),EXout,EYout	//Reorder external waves
	Rotate -(pcsr(B)),IXout,IYout	//Reorder internal waves
	Variable AveLen			//Create storage variable for length of average output
	AveLen=50			//Initialize to 50
	String  AXwaveAdj,AYwaveAdj	//Create name strings for average path waves average
	AXwaveAdj=BaseName+"AX"	//Create name of average X wave
```

```
	AYwaveAdj=BaseName+"AY"	//Create name of average Y wave
	Make /D /O /N=(numpnts(IYout)) IntCircumDist,IntDiffDist		//Make waves to store total internal circuit distances
									and distance comparison
	Make /D /O /N=(AveLen) $AXwaveAdj,$AYwaveAdj	//Make average waves
	Make /D /O /N=(numpnts(EYout)) ExtCircumDist,ExtDiffDist	//Make waves to store total external circuit distances
									and distance comparison
	Wave AXout=$AXwaveAdj	//Set average X wave reference
	Wave AYout=$AYwaveAdj	//Set average Y wave reference
//CALCULATE DISTANCES
	Variable IntLoc,ExtLoc,i	//Declare variables for the location of points to be used on internal and external points
	IntCircumDist[0]=0		//Set first cumulative distance point to 0
	ExtCircumDist[0]=0		//Set first cumulative distance point to 0
		for(i=1;i<numpnts(IYout);i+=1)	//Loop from second point to end of internal circuit
		IntCircumDist[i]=((IXout[i]-IXout[i-1])^2+(IYout[i]-IYout[i-1])^2)^.5+IntCircumDist[i-1]		//Set cumulative
									distance equal to distance between last two points plus
									previous cumulative distance
		endfor
	IntCircumDist/=IntCircumDist[numpnts(IYout)-1]	//Divide all distances by total to produce fractional distances
		for(i=1;i<numpnts(EYout);i+=1)	//Loop from second point to end of external circuit
		ExtCircumDist[i]=((EXout[i]-EXout[i-1])^2+(EYout[i]-EYout[i-1])^2)^.5+ExtCircumDist[i-1]	//Set cumulative
									distance equal to distance between last two points plus
									previous cumulative distance
		endfor
	ExtCircumDist/=ExtCircumDist[numpnts(EYout)-1]		//Divide all distances by total to produce fractional distances
//CALCULATE AVERAGE PATH
	AXout[0]=(IXout[0]+EXout[0])/2	//Set first point of average X wave
	AYout[0]=(IYout[0]+EYout[0])/2	//Set first point of average Y wave
	AXout[AveLen-1]=(IXout[numpnts(IYout)-1]+EXout[numpnts(EYout)-1])/2	//Set last point of average X wave
	AYout[AveLen-1]=(IYout[numpnts(IYout)-1]+EYout[numpnts(EYout)-1])/2	//Set last point of average Y wave
		for(i=1;i<(AveLen-1);i+=1)		//Loop from 2nd to 2nd to last point of average waves
		ExtDiffDist=abs(ExtCircumDist-(i/AveLen))		//Populate difference wave with the differeence between
									fractional distances and fractional position
		WaveStats /Q ExtDiffDist		//Calculate wave statistics
```

```
		ExtLoc=V_minloc		//Store location of minimum distance differernce
		IntDiffDist=abs(IntCircumDist-(i/AveLen))		//Populate difference wave with the differeence between
									fractional distances and fractional position
		WaveStats /Q IntDiffDist//Calculate wave statistics
		IntLoc=V_minloc		//Store location of minimum distance differernce
		AXout[i]=(IXout[IntLoc]+EXout[ExtLoc])/2		//Set current average X point to average of X coordinates at
										minimum locations
		AYout[i]=(IYout[IntLoc]+EYout[ExtLoc])/2		//Set current average X point to average of X coordinates at
										minimum locations
		endfor
		for(i=0;i<AveLen-1;i+=1)//Loop through whole average waves
			if(AXout[i]==AXout[i+1] && AYout[i]==AYout[i+1])		//Check for consecutive identical points
			printf "Warning: Duplicate Points on Average Wave!!\r"	//Print warning
			endif
		endfor
	Killwaves ExtCircumDist,IntCircumDist,IntDiffDist,ExtDiffDist	//Cleanup temporary waves
	Button $(BaseName+"Stats"), Disable=0//Enable 'Stats' button
	Cursor /P A $nameofwave(EYout) 0	//Move cursor A to the point corresponing to its original location
	Cursor /P B $nameofwave(IYout) 0	//Move cursor B to the point corresponing to its original location
	if(cmpstr(nameofwave(WaveRefIndexed("",4,1)),nameofwave(AYout))!=0 &&
cmpstr(nameofwave(WaveRefIndexed("",5,1)),nameofwave(AYout))!=0) //Check graph status of path wave
	AppendToGraph $nameofwave(AYout) vs $nameofwave(AXout) //Display path waves on graph
	ModifyGraph lsize($nameofwave(AYout))=2,rgb($nameofwave(AYout))=(39168,0,31232) //Change size and color of
									average wave
	ModifyGraph mode($nameofwave(AYout))=4,marker($nameofwave(AYout))=19  //Change style of average wave
	endif
End

Function MultiPathCalcO(ctrlName) : ButtonControl
	String ctrlName
	Printf "Calculating...\r"		//Indicate on control window status of proceedure
	String BaseName			//Create a variable for the seed string which will be the basis for all permanent names
```

```
BaseName=ctrlName[0,strlen(ctrlName)-6]          //Initialize string to the trimmed name of the Undo  button which stores
                                                                the value entered in the macro initialization
String  IXwaveAdj,IYwaveAdj,EXwaveAdj,EYwaveAdj     //Create name strings for manipulation of the origional data
IXwaveAdj=BaseName+"IX"       //Create name of working IX wave
IYwaveAdj=BaseName+"IY"       //Create name of working IY wave
EXwaveAdj=BaseName+"EX"    //Create name of working EX wave
EYwaveAdj=BaseName+"EY"    //Create name of working EY wave
Wave IXout=$IXwaveAdj          //Create working IX wave reference
Wave IYout=$IYwaveAdj          //Create working IY wave reference
Wave EXout=$EXwaveAdj         //Create working EX wave reference
Wave EYout=$EYwaveAdj         //Create working EY wave reference
Rotate -(pcsr(A)),EXout,EYout    //Reorder external waves
Rotate -(pcsr(B)),IXout,IYout      //Reorder internal waves
Variable EOutLen,IOutLen,i        //Create length variable for output wave creation
Variable EFinalLen=30,IFinalLen=20      //Create and initiaize variables that determine the ultimate length of the output
String  OXwaveAdj,OYwaveAdj  //Create name strings for average path waves average
OXwaveAdj=BaseName+"OX"   //Create name of average X wave
OYwaveAdj=BaseName+"OY"   //Create name of average Y wave
Make /D /O /N=(EFinalLen+IFinalLen) $OXwaveAdj,$OYwaveAdj            //Make average waves
Wave OXout=$OXwaveAdj        //Set average X wave reference
Wave OYout=$OYwaveAdj        //Set average Y wave reference
        If(numpnts(EYout)<EFinalLen)   //Check the length of the calculated external wall
        printf "Error: Insufficient resolution on external wall!\r"      //Yell at me
        Return 0                                //Exit the function
        endif
Make /D /O /N=(numpnts(EYout)) OEXtemp,OEYtemp    //Make temporary manipulation waves
OEXtemp=EXout                     //Populate external canal wall X coordinate wave
OEYtemp=EYout                     //Populate external canal wall Y coordinate wave
        Do
                If(numpnts(OEYtemp)==EFinalLen)       //Check if the length of the calculated external wall has reached
                                                                the desired length
                break              //Exit the loop
                endif
```

```
		Deletepoints MinPointDeviation(OEXtemp,OEYtemp),1,OEXtemp,OEYtemp		//Remove the point containing
									the least contour information
		while (1)			//Loop indefinately
		If(numpnts(IYout)<IFinalLen)	//Check the length of the calculated internal wall
		printf "Error: Insufficient resolution on internal wall!\r"	//Yell at me
		Return 0			//Exit the function
		endif
	Make /D /O /N=(numpnts(IYout)) OIXtemp,OIYtemp		//Make temporary manipulation waves
	OIXtemp=IXout			//Populate internal canal wall X coordinate wave
	OIYtemp=IYout			//Populate internal canal wall Y coordinate wave
		Do
			If(numpnts(OIYtemp)==IFinalLen)		//Check if the length of the calculated external wall has reached
									the desired length
			break		//Exit the loop
			endif
		Deletepoints MinPointDeviation(OIXtemp,OIYtemp),1,OIXtemp,OIYtemp //Remove the point containing the least
									contour information
		while (1)			//Loop indefinately
		For(i=0;i<EFinalLen;i+=1)		//Loop through external canal points
		OXout[i]=OEXtemp[i]	//Populate the first part of final X output wave
		OYout[i]=OEYtemp[i]	//Populate the first part of final Y output wave
		Endfor
		For(i=0;i<IFinalLen;i+=1)		//Loop through internal canal points
		OXout[EFinalLen+i]=OIXtemp[IFinalLen-i-1]	//Populate the second part of final X output wave
		OYout[EFinalLen+i]=OIYtemp[IFinalLen-i-1]	//Populate the second part of final Y output wave
		Endfor
	Killwaves OIXtemp,OIYtemp,OEXtemp,OEYtemp		//Cleanup temporary waves
	Cursor /P A $nameofwave(EYout) 0	//Move cursor A to the point corresponing to its original location
	Cursor /P B $nameofwave(IYout) 0	//Move cursor B to the point corresponing to its original location
	if(cmpstr(nameofwave(WaveRefIndexed("",4,1)),nameofwave(OYout))!=0 &&
cmpstr(nameofwave(WaveRefIndexed("",5,1)),nameofwave(OYout))!=0)		//Check graph status of outline wave
	AppendToGraph $nameofwave(OYout) vs $nameofwave(OXout)//Display outline wave on graph
	ModifyGraph lsize($nameofwave(OYout))=2,rgb($nameofwave(OYout))=(0,65280,0)	//Change size and color of
									outline wave
```

```
	ModifyGraph mode($nameofwave(OYout))=4,marker($nameofwave(OYout))=19  //Change style of outline wave
	endif
	Killvariables /A/Z			//Clean up all the variables
End

Function CursorMovedHook(info)		//Internally defined Function
	String info				//Declare variables passed to function
	String bTrim,bCalcP,bCalcO		//Declare String variables to store names of buttons to be altered
	bTrim=StringFromList(0,ControlNameList("",",",","),",")		//Set string to name of first button (Trim)
	bCalcP=StringFromList(2,ControlNameList("",",",","),",")		//Set string to name of third button (Calc path)
	bCalcO=StringFromList(3,ControlNameList("",",",","),",")		//Set string to name of fourth button (Calc outline)
		if(cmpstr(CsrWave(A),nameofwave(WaveRefIndexed("",2,1)))==0 &&
cmpstr(CsrWave(B),nameofwave(WaveRefIndexed("",2,1)))==0)		//Test if cursor A and B are on the internal working
									wave
		Button $bTrim, Disable=0		//Enable 'Trim' button
		Button $bCalcP, Disable=2		//Disable 'Calc Path' button
		Button $bCalcO, Disable=2		//Disable 'Calc Outline' button
		elseif(cmpstr(CsrWave(A),nameofwave(WaveRefIndexed("",3,1)))==0 &&
cmpstr(CsrWave(B),nameofwave(WaveRefIndexed("",3,1)))==0)		//Test if cursor A and B are on the external working
									wave
		Button $bTrim, Disable=0		//Enable 'Trim' button
		Button $bCalcP, Disable=2		//Disable 'Calc Path' button
		Button $bCalcO, Disable=2		//Disable 'Calc Outline' button
		elseif(cmpstr(CsrWave(A),nameofwave(WaveRefIndexed("",3,1)))==0 &&
cmpstr(CsrWave(B),nameofwave(WaveRefIndexed("",2,1)))==0)		//Test if cursor A is on the external and B is on the
									internal working wave
		Button $bTrim, Disable=2		//Disable 'Trim' button
		Button $bCalcP, Disable=0		//Enable 'Calc Path' button
		Button $bCalcO, Disable=0		//Enable 'Calc Outline' button
		else
		Button $bTrim, Disable=2		//Disable 'Trim' button
		Button $bCalcP, Disable=2		//Disable 'Calc Path' button
		Button $bCalcO, Disable=2		//Disable 'Calc Outline' button
		endif
```

```
Function MultiPathStatCalc(ctrlName) : ButtonControl
	String ctrlName
	Printf "Calculating Statistics...\r" //Indicate on control window status of proceedure
	String BaseName 		//Create a variable for the seed string which will be the basis for all permanent names
	BaseName=ctrlName[0,strlen(ctrlName)-6]	//Initialize string to the trimmed name of the Undo  button which stores
							the value entered in the macro initialization
	String  AXwaveAdj,AYwaveAdj  //Create name strings for average posotion waves
	AXwaveAdj=BaseName+"AX"	//Create name of working AX wave
	AYwaveAdj=BaseName+"AY"	//Create name of working AY wave
	Wave AXout=$AXwaveAdj	//Create working AX wave reference
	Wave AYout=$AYwaveAdj	//Create working AY wave reference
	String  StatName 		//Create name strings for average path waves average
	StatName=BaseName+"Stats"  //Create name of average X wave
	Make /D /O /N=(10) $StatName //Make Stat wave
	Wave Statsout=$StatName	//Set average X wave reference
//CALCULATE SQUARE ROOT OF AREA ENCLOSED BY CANAL -- Statsout[0]
	Statsout[0]=abs(areaxy(AXout,AYout,0,numpnts(AXout)))^.5	//Calculate and store area enclosed
//CALCULATE PERIMETER AND CANAL LENGTH-- Statsout[1] & Statsout[2]
	Variable i 			//Declare temporary looping variable
	Statsout[1]=0 			//Reset Perimeter distance in case of failure to overwrite
		For (i=0;i<numpnts(AYout)-2;i+=1)	//Loop through the average waves
		Statsout[1]+=((AXout[i]-AXout[i+1])^2+(AYout[i]-AYout[i+1])^2)^.5		//Add distance bewteen consecutive
								points to overall distance
		endfor
	Statsout[2]=0
		For(i=0;i<PositionDistance(pcsr(B),pcsr(A),AYout);i+=1)
		Statsout[2]+=((AXout[PointCheck(pcsr(B)+i,AYout)]-
AXout[PointCheck(pcsr(B)+i+1,AYout)])^2+(AYout[PointCheck(pcsr(B)+i,AYout)]-AYout[PointCheck(pcsr(B)+i+1,AYout)])^2)^.5
		endfor
//CALCULATE MAJOR AXIS LENGTH & ANGLE-- Statsout[3] & Statsout[4]
	Variable MaxDist=0,MaxStart,MaxEnd,j,TempAngle	//Declare distance, location and secondary looping variable
		For (i=0;i<numpnts(AYout);i+=1)//Loop first point through average wave
```

```
                For (j=i+1;j<numpnts(AYout);j+=1)          //Loop second point through average wave ignoring used points
                        If(((AXout[i]-AXout[j])^2+(AYout[i]-AYout[j])^2)^.5>MaxDist)          //Compare previous maximum
                                                                distance with newly claculated distance
                        MaxDist=((AXout[i]-AXout[j])^2+(AYout[i]-AYout[j])^2)^.5 //Set new maximum distance
                        MaxStart=min(i,j)          //Store end point of new maimum distance
                        MaxEnd=max(j,i)          //Store end point of new maimum distance
                        endif
                endfor
        endfor
Statsout[3]=MaxDist                //Record Maximum distance
TempAngle=-atan2(AYout[MaxStart]-AYout[MaxEnd],AXout[MaxStart]-AXout[MaxEnd])    //Record angle of major axis
TempAngle*=(180/Pi)                //Convert angle to Degrees
        if(TempAngle>=0)          //Check if the calculated angle is positive or negative
        Statsout[4]=TempAngle //If positive, store unchanged
        else
        Statsout[4]=TempAngle+360      //If negative add 360 degrees then store
        endif
//CALCULATE MINOR AXIS LENGTH -- Statsout[5]
        Variable MinorSlope,MinSlopeDiff,MinSlopePoint,MinStart,MinEnd          //Declare point &  partial slope storage
                                                                variables
        MaxDist=0                          //Reinitialize the maximumdistance storage variable
        MinorSlope=-(AXout[MaxStart]-AXout[MaxEnd])/(AYout[MaxStart]-AYout[MaxEnd])          //Calculate slope of minor axis
                For(i=0;i<numpnts(AYout);i+=1) //Loop first point through average wave
                MinSlopeDiff=999          //Reinitialize minimum slope difference variable to impossibly large number
                        For (j=0;j<numpnts(AYout);j+=1)//Loop second point through average wave
                                if(j==i)   //If i and j are the same point
                                j+=1      //increment to the next j
                                endif
                                if(abs((AYout[i]-AYout[j])/(AXout[i]-AXout[j])-MinorSlope)<MinSlopeDiff)    //Check the differernce
                                                                between the current slope and the target slope, is it
                                                                smaller the the previous minimum difference
                                MinSlopeDiff=abs((AYout[i]-AYout[j])/(AXout[i]-AXout[j])-MinorSlope)        //Set new minimum
                                                                distance
                                MinSlopePoint=j          //Store point position
```

```
                endif
            endFor
            If(((AXout[i]-AXout[MinSlopePoint])^2+(AYout[i]-AYout[MinSlopePoint])^2)^.5>MaxDist)    //Compare
                                                    previous maximum distance with newly claculated
            MaxDist=((AXout[i]-AXout[MinSlopePoint])^2+(AYout[i]-AYout[MinSlopePoint])^2)^.5        //Set new
                                                    maximum distance
            MinStart=min(i,MinSlopePoint)
            MinEnd=max(i,MinSlopePoint)
            endif
        endfor
    Statsout[5]=MaxDist             //Record Maximum distance
//CALCULATE AVERAGE RADIUS LENGTH WITH UTRICLE -- Statsout[6]
    Variable CenterX,CenterY,RadiusTotal   //Declare temporary coordinate variables for center point and total radial
                                                    distance
    WaveStats /Q AXout              //Calculate wave stats for average X coordinate wave
    CenterX=V_avg                   //Set X coordinate of center point equal to average of X coordinates
    WaveStats /Q AYout              //Calculate wave stats for average Y coordinate wave
    CenterY=V_avg//Set Y coordinate of center point equal to average of Y coordinates
        For(i=0;i<numpnts(AYout);i+=1) //Loop thorugh average wave
        RadiusTotal+=((AXout[i]-CenterX)^2+(AYout[i]-CenterY)^2)^.5     //Compile the total of all the radial distances
        endfor
    Statsout[6]=RadiusTotal/numpnts(AYout)          //Set average equal to total distances divided by number of distances
//CALCULATE AVERAGE RADIUS LENGTH WITHOUT UTRICLE -- Statsout[7]
    RadiusTotal=0                   //Reinitialize total radius variable to 0
        For(i=min(pcsr(A),pcsr(B));i<=max(pcsr(A),pcsr(B));i+=1)//Loop thorugh average wave from one cursor to next
        RadiusTotal+=((AXout[i]-CenterX)^2+(AYout[i]-CenterY)^2)^.5     //Compile the total of all the radial distances
        endfor
    Statsout[7]=RadiusTotal/PositionDistance(pcsr(B),pcsr(A),AYout)          //Set average equl to total distances divided by
                                                    number of distances
//CALCULATE LENGTH OF AXIS PARALLEL TO UTRICLE -- Statsout[8]
    Variable UtParSlope,UtParSlopePoint     //Declare temporary point  and partial slope storage variables
    MaxDist=0                       //Reinitialize the maximumdistance storage variable
    if(abs((AYout[i]-AYout[j])/(AXout[i]-AXout[j])-UtPerpSlope)<MinSlopeDiff) //Check the differernce between the current
                                                    slope and the target slope, is it smaller the the previous
```

```
                                                                minimum difference
        UtParSlope=(AYout[pcsr(a)]-AYout[pcsr(b)])/(AXout[pcsr(a)]-AXout[pcsr(b)])        //Calculate slope of utricle
                For(i=0;i<numpnts(AYout);i+=1) //Loop first point through average wave
                MinSlopeDiff=999        //Reinitialize minimum slope difference variable to impossibly large number
                        For (j=0;j<numpnts(AYout);j+=1)//Loop second point through average wave
                                if(j==i)  //If i and j are the same point
                                j+=1      //increment to the next j
                                endif
                                if(abs((AYout[i]-AYout[j])/(AXout[i]-AXout[j])-UtParSlope)<MinSlopeDiff)   //Check the differernce
                                                                between the current slope and the target slope, is it
                                                                smaller the the previous minimum difference
                                MinSlopeDiff=abs((AYout[i]-AYout[j])/(AXout[i]-AXout[j])-UtParSlope)       //Set new minimum
                                                                distance
                                UtParSlopePoint=j        //Store point position
                                endif
                        endFor
                        If(((AXout[i]-AXout[UtParSlopePoint])^2+(AYout[i]-AYout[UtParSlopePoint])^2)^.5>MaxDist)
                                                //Compare previous maximum distance with newly claculated
                        MaxDist=((AXout[i]-AXout[UtParSlopePoint])^2+(AYout[i]-AYout[UtParSlopePoint])^2)^.5  //Set new
                                                                maximum distance
                        endif
                endfor
        Statsout[8]=MaxDist             //Record Maximum distance
//CALCULATE LENGTH OF AXIS PERPENDICULAR TO UTRICLE -- Statsout[9]
        Variable UtPerpSlope,UtPerpSlopePoint //Declare temporary point  and partial slope storage variables
        MaxDist=0                       //Reinitialize the maximumdistance storage variable
        UtPerpSlope=-(AXout[pcsr(a)]-AXout[pcsr(b)])/(AYout[pcsr(a)]-AYout[pcsr(b)])     //Calculate slope of utricle
                For(i=0;i<numpnts(AYout);i+=1) //Loop first point through average wave
                MinSlopeDiff=999        //Reinitialize minimum slope difference variable to impossibly large number
                        For (j=0;j<numpnts(AYout);j+=1)//Loop second point through average wave
                                if(j==i)  //If i and j are the same point
                                j+=1      //increment to the next j
                                Endif
```

```
                        MinSlopeDiff=abs((AYout[i]-AYout[j])/(AXout[i]-AXout[j])-UtPerpSlope)     //Set new minimum
                                                                                                  distance
                        UtPerpSlopePoint=j      //Store point position
                        endif
                    endFor
                    If(((AXout[i]-AXout[UtPerpSlopePoint])^2+(AYout[i]-AYout[UtPerpSlopePoint])^2)^.5>MaxDist)
                                        //Compare previous maximum distance with newly claculated
                    MaxDist=((AXout[i]-AXout[UtPerpSlopePoint])^2+(AYout[i]-AYout[UtPerpSlopePoint])^2)^.5          //Set
                                                                                                  new maximum distance
                    endif
                endfor
        Statsout[9]=MaxDist             //Record Maximum distance
//CALCULATE CANAL ONLY PATH WAVES
        Variable ClPathLen              //Declare variable for length of canal only path
        ClPathLen=25                    //Initialize variable to a length of 25 points
        String  AClXwaveAdj,AClYwaveAdj     //Create name strings for canal only path position waves
        AClXwaveAdj=BaseName+"Cl_AX"        //Create name of working AClX wave
        AClYwaveAdj=BaseName+"Cl_AY"        //Create name of working AClY wave
        Make /D /O /N=(ClPathLen) $AClXwaveAdj,$AClYwaveAdj         //Make waves
        Wave AClXout=$AClXwaveAdj  //Set X wave reference
        Wave AClYout=$AClYwaveAdj  //Set Y wave reference
        Make /D /O /N=(PositionDistance(pcsr(B),Pcsr(A),AYout)) XtempWave, YtempWave        //Make waves to copy original
                                                                                          points from average position waves
        XtempWave=AXout[PointCheck(p+pcsr(B),AYout)]        //Populate temporary storage wave
        YtempWave=AYout[PointCheck(p+pcsr(B),AYout)]        //Populate temporary storage wave
        Execute /Z "Interpolate /T=2 /N="+num2str(ClPathLen)+" /E=2 /Y="+AClYwaveAdj+" YtempWave"          //Cubic spline
                                                                                          interpolate canal path to set it to selected length
        Execute /Z "Interpolate /T=2 /N="+num2str(ClPathLen)+" /E=2 /Y="+AClXwaveAdj+" XtempWave"          //Cubic spline
                                                                                          interpolate canal path to set it to selected length
        if(cmpstr(nameofwave(WaveRefIndexed("",5,1)),nameofwave(AClYout))!=0 &&
cmpstr(nameofwave(WaveRefIndexed("",6,1)),nameofwave(AClYout))!=0) //Check graph status of path wave
                AppendToGraph $nameofwave(AClYout) vs $nameofwave(AClXout)      //Plot new waves on current graph
```

```
                ModifyGraph
mode($nameofwave(AClYout))=4,marker($nameofwave(AClYout))=19,rgb($nameofwave(AClYout))=(0,65280,65280)
        //Adjust wave color and style
        endif
        KillWaves YtempWave,XtempWave                   //Cleanup temporary waves
//DISPLAY OUTPUT
        Printf "\tSquare root of area enclosed - "+num2str(Statsout[0])+"\r"          //Print out results
        Printf "\tPerimeter - "+num2str(Statsout[1])+"\r"              //Print Out results
        Printf "\tCanal length - "+num2str(Statsout[2])+"\r"          //Print Out results
        Printf "\tMajor axis length - "+num2str(Statsout[3])+"  Angle - "+num2str(Statsout[4])+"\r"   //Print Out results
        Printf "\tMinor axis length - "+num2str(Statsout[5])+"\r"     //Print Out results
        Printf "\tAverage radius length - "+num2str(Statsout[6])+"\r"          //Print Out results
        Printf "\tAverage radius without utricle- "+num2str(Statsout[7])+"\r"          //Print Out results
        Printf "\tAxis parallel to utricle - "+num2str(Statsout[8])+"\r"          //Print Out results
        Printf "\tAxis perpendicular to utricle - "+num2str(Statsout[9])+"\r" //Print Out results
        Killvariables /A/Z                              //Clean up all the variables
End
```

Appendix B

Formulae for conversion to and from planar notation used in VoxBlast 3D visualization software.

VoxBlast gives:

θ – rotation about x axis (pitch) in degrees
ψ – rotation about y axis (yaw) in degrees
ρ – rotation about z axis (roll) in degrees
sp – stack position (depth) in 0.1 mms
(x,y,z) – 3D coordinates for selected points

Slice of interest defined by:

point intercept form:

$$ax + by + cz + d = 0$$

Hesian normal form:

$$\vec{n}\vec{x} = -p$$

$\vec{n}$ – unit vector perpendicular to plane

$$\vec{n} = \begin{bmatrix} \alpha \\ \beta \\ \gamma \end{bmatrix}$$

$$\vec{x} = \begin{bmatrix} x \\ y \\ z \end{bmatrix}$$

$$\alpha = \frac{a}{\sqrt{a^2 + b^2 + c^2}}$$

$$\beta = \frac{b}{\sqrt{a^2 + b^2 + c^2}}$$

$$\gamma = \frac{c}{\sqrt{a^2 + b^2 + c^2}}$$

$$p = \frac{d}{\sqrt{a^2 + b^2 + c^2}}$$

To convert from VoxBlast:

$$\alpha = \cos(\theta)\sin(\psi)\cos(\rho) + \sin(\theta)\sin(\rho)$$

$$\beta = \cos(\theta)\sin(\psi)\sin(\rho) - \sin(\theta)\cos(\rho)$$

$$\gamma = \cos(\theta)\cos(\psi)$$

When $\rho = 0$:

$$\alpha = \cos(\theta)\sin(\psi)$$

$$\beta = -\sin(\theta)$$

$$\gamma = \cos(\theta)\cos(\psi)$$

or

$$a = \begin{vmatrix} 1 & y_1 & z_1 \\ 1 & y_2 & z_2 \\ 1 & y_3 & z_3 \end{vmatrix}$$

$$b = \begin{vmatrix} x_1 & 1 & z_1 \\ x_2 & 1 & z_2 \\ x_3 & 1 & z_3 \end{vmatrix}$$

$$c = \begin{vmatrix} x_1 & y_1 & 1 \\ x_2 & y_2 & 1 \\ x_3 & y_3 & 1 \end{vmatrix}$$

$$d = \begin{vmatrix} x_1 & y_1 & z_1 \\ x_2 & y_2 & z_2 \\ x_3 & y_3 & z_3 \end{vmatrix}$$